NASA CR-175081
AVSCOM TR 86-C-8
ALLISON EDR
Report No. 12422
Copy No.

NASA

U.S. ARMY AVIATION SYSTEMS COMMAND

SMALL ENGINE COMPONENT TECHNOLOGY (SECT) STUDY FINAL REPORT

by T. R. LARKIN

ALLISON GAS TURBINE DIVISION
GENERAL MOTORS CORPORATION

Date for general release March 31, 1991

prepared for
NATIONAL AERONAUTICS AND SPACE ADMINISTRATION
Lewis Research Center
and
U.S. ARMY AVIATION RESEARCH AND TECHNOLOGY ACTIVITY
Propulsion Directorate

NASA Lewis Research Center
NAS3-24542

1. Report No.	2. Government Accession No.	3. Recipient's Catalog No.
NASA CR - 175081 AVSCOM TR - 86-C-8		

4. Title and Subtitle	5. Report Date
Small Engine Component Technology (SECT) Studies Final Report	March, 1986
	6. Performing Organization Code

7. Author(s)	8. Performing Organization Report No.
T. R. Larkin	EDR 12422
	10. Work Unit No.

9. Performing Organization Name and Address	11. Contract or Grant No.
Allison Gas Turbine Division General Motors Corporation P.O. Box 420 Indianapolis, Indiana 46206-0420	NAS 3 - 24542
	13. Type of Report and Period Covered
12. Sponsoring Agency Name and Address	Contractor Report
NASA Lewis Research Center and U.S. Army Aviation Research and Technology Activity, Propulsion Directorate, Cleveland, Ohio 44135	14. Sponsoring Agency Code 535-05-01 1L161101AH45

15. Supplementary Notes

Project Manager, Michael R. Vanco
NASA Lewis Research Center
Cleveland, Ohio 44135

16. Abstract

The objective of this Allison Gas Turbine Divison study was to identify high payoff technologies for year 2000 small gas turbine engines, and to provide a technology plan to guide research and technology efforts toward revolutionizing the small gas turbine technology base. The goal of this effort was to define the required technology to provide a 30% reduction in mission fuel burned, to reduce direct operating cost by at least 10%, and to provide increased reliabiity and durability of the gas turbine propulsion system. The baseline established to evaluate the year 2000 technology base was an eight-passenger commercial tilt-rotor aircraft powered by a current technology Allison gas turbine engine.

Three basic engine cycles were studied: the simple cycle engine, a waste heat recovery cycle, and a wave rotor engine cycle. For the simple cycle engine, two general arrangements were considered: the traditional concentric spool arrangement and a non-concentric spool arrangmeent. Both a regenerative and a recuperative cycle were studied for the waste heat recovery cycle.

An extensive cycle optimization procedure was performed for each configuration under study, using relative DOC as the figure-of-merit. This allowed for selection of the proper design max cycle temperature and cycle pressure ratio. Three of the five optimum cycles (the non-concentric, the recuperative and the regenerative engine cycles) were evaluated for a typical tilt-rotor design flight mission. Results showed that all three engines met the goal of at least 30% reduction in fuel burned relative to the defined baseline for the commercial tilt-rotor aircraft mission. In addition, the non-concentric engine provided the greatest reduction in DOC with a 16.5% improvement.

The technologies required for this substantial improvement were ranked in order of decreasing benefit.

17. Key Words (Suggested by Author(s))	18. Distribution Statement
Rotorcraft Gas turbine engines Component technologies Cycles	

19. Security Classif. (of this report)	20. Security Classif. (of this page)	21. No. of pages	22. Price*
Unclassified	Unclassified		

TABLE OF CONTENTS

TABLE OF CONTENTS (CONT)

LIST OF ILLUSTRATIONS

LIST OF ILLUSTRATIONS (CONT)

LIST OF ILLUSTRATIONS (CONT)

LIST OF ILLUSTRATIONS (CONT)

LIST OF TABLES

LIST OF TABLES (CONT)

I. SUMMARY

The goals of this effort was to define the required technology to provide a 30% reduction in mission fuel burned, to reduce direct operating cost by at least 10%, and to provide increased reliability and durability of the gas turbine propulsion system. The baseline established to evaluate the year 2000 technology base was an eight passenger commercial tilt-rotor aircraft, currently in the preliminary design phase, powered by a current state-of-the-art technology gas turbine engine.

Three basic engine cycles were studied: the simple cycle engine, a waste heat recovery cycle, and a wave rotor cycle. For the simple cycle, two general arrangements were considered: the traditional concentric spool arrangement and a nonconcentric spool arrangement. Both regenerative and recuperative cycles were studied for the waste heat recovery cycle.

An extensive cycle optimization procedure was performed for each configuration studied, using relative direct operating cost as the figure of merit. This procedure allowed for selection of the proper design maximum cycle temperature and cycle pressure ratio. Nonconcentric, recuperative, and regenerative engines were evaluated for a typical tilt-rotor design flight mission. Results showed that all three engines met the goal of at least 30% reduction in fuel burned relative to the baseline engine for the commercial tilt-rotor aircraft mission. The nonconcentric engine provided the greatest reduction in direct operating cost (DOC) with a 16.5% improvement.

Five technology areas require research effort to realize the full potential of the nonconcentric engine concept for the year 2000. In order of decreasing benefit relative to DOC reduction, the areas are ceramics, turbines, compressors, combustors, and bearings. In addition, improvements in computational fluid mechanics are essential to properly analyze the flow characteristics in small gas turbine components.

II. INTRODUCTION

Small gas turbine engines are used in a wide variety of applications. The success of the next generation of small gas turbine engines in meeting these various operational requirements will depend on development and application of new technology. This technology will provide a significant reduction in total cost of ownership by reducing fuel burned, initial acquisition cost, and maintenance costs. For example, fuel cost for small helicopter aircraft can represent as much as one half of the engine cost of ownership.

Small engine components do not achieve the same level of operational efficiency as those in larger engines, resulting in higher fuel consumption. Fuel consumption and specific power can be improved by increasing overall pressure ratio, turbine inlet temperature, and the level of component performance. As pressure ratio and turbine inlet temperature increase, sealing and cooling problems create additional parasitic losses that erode the fundamental cycle advantage. This is particularly true for small gas turbine engines where size effects make sealing and cooling more difficult.

With the threat of increasing foreign competition in the small gas turbine engine market, particularly for the 1000 horsepower class and below, aggressive research and technology programs are needed to assure continued U.S. industry competitiveness. For these reasons Allison is supportive of NASA's Small Engine Component Technology (SECT) program.

The SECT study was sponsored by the NASA Lewis Research Center and U. S. Army Aviation Research and Technology Activity-Propulsion Directorate.

The objectives of the SECT study were: (1) to identify the high payoff technologies for the year 2000 small gas turbine engine and (2) to provide a technology plan for guiding future research and technology efforts. This plan will provide the advanced technology base needed to ensure the technical advantage of U.S. manufacturers in the future small engine market.

The work performed during the study contract was divided into four basic tasks, as follows:

Task I: Select mission evaluation procedures and assumptions

Task II: Evaluate engine configurations and cycles

Task III: Conduct an engine/aircraft mission analysis to determine figures of merit to rank technology needs

Task IV: Prepare a plan to guide research and technology verification, component and systems research, and technology programs

Allison is interested in all baseline applications (rotorcraft, commuter, auxiliary power unit (APU), and cruise missile). However, a more productive program would result from studying a single application in great depth rather than several applications in lesser depth. The rotorcraft application, specifically the commercial tilt-rotor application, using a high-performance, high power/weight turboshaft engine was selected for this study. Direct operating cost (DOC) was used as the overall figure of merit. This report presents the results of this study.

III. TASK I. SELECTION OF EVALUATION PROCEDURES AND ASSUMPTIONS

The evaluation procedures and assumptions used in the Small Engine Components Technology (SECT) study are briefly described along with supporting information concerning the source or applicable background justification where appropriate. Major topics to be presented are:

- o aircraft/mission requirements
- o reference tilt-rotor aircraft characteristics
- o direct operating cost model
- o baseline engine description and scaling equations
- o baseline engine mission results and trade factors
- o environmental constraints

The SECT cycle selection and engine configuration evaluation required the definition of mission requirements, a reference aircraft, engine characteristics, and an economic model for use in obtaining cost comparisons. These items were integrated into the mission analysis computer program. Program input, major calculation routines, and output parameters for this program are generalized in the block diagram shown in Figure 1.* Mission requirements, along with airframe and engine characteristics, are used in the engine/airframe sizing or scaling routines to determine the engine/airframe size combination that will meet fixed mission requirements, i.e., "rubber engine/rubber aircraft" approach. The resultant sized aircraft along with mission fuel, distance, and time data, plus input economic criteria, are then used in the cost model to obtain direct operating cost (DOC) data. Total engine/aircraft DOC was the selected figure of merit for the SECT study.

AIRCRAFT/MISSION REQUIREMENTS

The advanced helicopter system selected for the SECT studies was based on a tilt-rotor concept developed by Bell Helicopter Textron, Inc. This concept combines the best features of the helicopter and turboprop aircraft, i.e., helicopter takeoff and landing, safety and convenience, plus the advantages of

* Figures can be found at the end of this report.

turboprop cruise speed, low noise, and vibration. All of these qualities are necessary to obtain favorable market projections for year 2000 rotorcraft applications.

The tilt-rotor mission requirements selected for this study effort are listed below:

o payload	eight passenger at 90.7 kg (200 lb) each
o range	648 km (350 nautical miles [nmi])
o cruise speed	250 knots true air speed (KTAS)
o cruise altitude	6096 m (20,000 ft)

The goal was to establish a "generic" twin engine tilt-rotor aircraft in the 4536 kg (10,000 lb) gross weight class that would be in concert with the NASA specified engine maximum power limit of 1000 shaft horsepower (shp). This vehicle class provides a spectrum of possible mission applications including corporate/executive, off-shore oil support, and medical evacuation. The Allison market projection for this class tilt-rotor is 1000 to 1200 aircraft over a ten year period. This figure is slightly higher than a Bell projection of 750 to 900 aircraft over a similar ten year period. Using 1000 aircraft as an approximate average and assuming one spare engine per aircraft provides a projected engine market of 3000 units.

The design mission profile shown in Figure 2 is consistent with air traffic control procedures, aircraft capability, and reserve definition sufficient for a rotorcraft transport concept. The operating scenario presumes that the selected tilt-rotor aircraft will be flown in the design mission during the majority of its use. The revenue mission and design mission are assumed to be identical. The engine/aircraft sizing criteria used in this study were selected to provide hover, one-engine-inoperative rate of climb, and cruise rate of climb capabilities sufficient to meet selected design operating requirements and to provide adequate margins of safety in the event of engine failure. These selected candidate sizing conditions/requirements are detailed in Table I.

TABLE I.
ENGINE/AIRCRAFT SIZING REQUIREMENTS

ENGINE/AIRCRAFT SIZING CONDITION	RATE OF CLIMB— M/MIN (FPM)	AIRCRAFT WEIGHT	ENGINE POWER SETTING	ALTITUDE M/(FT)	VELOCITY KTAS	DEGREE DAY
HOVER—OUT OF GROUND EFFECT	0 (0)	DESIGN TOGW	INTERMEDIATE POWER (AEO)	610 (2000) (1)	0	ISA + 10°C
OEI (2) RATE OF CLIMB	46 (150)	DESIGN TOGW	30 MINUTE POWER (OEI)	305 (1000)	75	ISA + 20°C
CRUISE CEILING RATE OF CLIMB	91 (300)	INITIAL CRUISE WEIGHT	MAXIMUM CONTINUOUS POWER (AEO)	6096 (20,000)	250	ISA

NOTES: (1) DEFINITION OF U.S. ARMY EUROPEAN DAY
(2) FAR PART 29/TRANSPORT CATEGORY ROTORCRAFT—TAKEOFF CATEGORY "A"

AEO—ALL ENGINES OPERATIVE
OEI—ONE ENGINE INOPERATIVE
TOGW—TAKEOFF GROSS WEIGHT

T89-4575

REFERENCE TILT-ROTOR AIRCRAFT CHARACTERISTICS

The vehicle selected for use in the SECT study effort is an eight passenger corporate/executive tilt-rotor aircraft configuration. General characteristics for this vehicle were provided to Allison Gas Turbine Division by Bell Helicopter Textron, Inc. A three view drawing of the reference aircraft is shown in Figure 3. Figure 4 shows a typical fuselage layout proposed for the eight passenger configuration along with approximate dimensions and volume data. A summary of aircraft design parameters is listed in Table II. Component or group weight breakdown is provided in Table III. Figure 5 shows the nacelle layout proposed for this vehicle and illustrates the turboshaft engine placement within the tilt-rotor nacelle. In this concept, the engine supplies power to an angle gearbox/rotor arrangement that can pivot about the conversion axis shown in Figure 5. The engine can also supply power to an interconnect driveshaft that couples the two propulsion packages through a center gearbox located in the fuselage-wing carry-through area. This driveshaft is normally unloaded and serves to synchronize thrust and rpm. However, in the event of single

TABLE II.
REFERENCE AIRCRAFT PARAMETERS

TOGW	**4772 kg (10,520 LB)**
FUSELAGE	
DIAMETER	**1.6 m (5.4 FT)**
LENGTH	**9.9 m (32.5 FT)**
ROTOR	
NUMBER OF BLADES	**3**
DIAMETER	**7.06 m (23.17 FT)**
DISK LOADING	**60.93 kg/m² (12.48 LB/FT²)**
ROTOR BLADES	
BLADE TIP SPEED (HOVER)	**13,717 M/MIN (750 FPS)**
BLADE TIP SPEED (CRUISE)	**11,120 M/MIN (608 FPS)**
MEAN BLADE CHORD	**0.36 m (1.17 FT)**
BLADE LOADING COEF	**0.1935**
WING	
SW (REFERENCE WING AREA)	**40.9 m² (134.2 FT²)**
W/SW (WING LOADING)	**382.7 kg/m² (78.4 LB/FT²)**
ASPECT RATIO	**8**
SWEEP @ L.E.	**−8° (SWEPT FWD)**
AVG THICKNESS RATIO	**24%**
TAPER RATIO	**1.00**

V986-1386

engine operation, this system transfers power to maintain continued safe operation of both rotors.

Reference tilt-rotor (helicopter mode) hover power requirements are shown in Figure 6. Cruise power requirements (airplane mode) for 3048 m (10,000 ft) and 6096 m (20,000 ft) are shown in Figures 7 and 8.

DIRECT OPERATING COST MODEL

Operating costs fall into two categories: direct cost and indirect cost. Indirect costs are basically dependent on the particular service the operator is offering, but the indirect costs may also be dependent on the airplane's characteristics. The figure of merit to assess the relative benefit of gas turbine

TABLE III.
SECT REFERENCE AIRCRAFT WEIGHT BREAKDOWN

	KILOGRAMS (POUNDS)	WEIGHT FRACTION-% (WT/TOGW-%)
•PROPULSION GROUP (INCLUDES ROTOR GROUP AND DRIVE SYSTEM)	1199 (2643)	25.1
•STRUCTURES GROUP	1100 (2425)	23.1
•FIXED EQUIPMENT	1046 (2305)	21.9
MFG EMPTY WEIGHT	3344 (7373)	70.1
•USEFUL LOAD	225 (497)	4.7
OPERATING EMPTY WEIGHT	3570 (7870)	74.8
•PAYLOAD	726 (1600)	15.2
ZERO FUEL WEIGHT	4296 (9470)	90.0
•FUEL (USABLE)	476 (1050)	10.0
TOGW	4772 (10,520)	100.0

TE86-4876

---

technologies will be based on direct operating cost which includes maintenance burden for this study. These costs are calculated as a cost per airplane nautical mile (C_{am}); however, they can be converted as follows:

$$\text{cost/seat nmi} = C_{am} \div \text{number of passenger seats}$$
$$\text{cost/block hr} = C_{am} \times V_b$$
$$\text{cost/flight hr} = C_{am} \times V_b \times t_b/t_f$$

where:

t_b = block time--hr

t_f = flight time--hr = $(T_b - T_{gm})$
V_b = block speed--knots

For the computation of block speed, the following formula based on a zero wind component was used:

$$V_b = D/(T_{gm} + T_v + T_{cl} + T_{cr})$$

where:

D = mission range or stage length in nautical miles
T_{gm} = ground maneuver time in hr (includes engine start and warm-up plus engine shutdown allowances)
T_v = vertical takeoff and landing time--hr
T_{cl} = time to climb from 762 m (2500 ft) to cruise altitude--hr
T_{cr} = time at cruise altitude and velocity--hr

Block fuel was computed from the following formula:

$$F_b = F_{gm} + F_v + F_{cl} + F_{cr}$$

where:

F_b = block fuel--lb
F_{gm} = ground maneuver fuel (fuel required for engine start and warm-up plus engine shutdown)--lb
F_v = fuel required for vertical takeoff and landing allowances--lb
F_{cl} = fuel to climb to cruise altitude--lb
F_{cr} = fuel consumed at cruise altitude and velocity--lb

The direct operating cost model used in the SECT study was based on 1967 Airline Transport Association (ATA) methodology. The cost methodologies and economic "ground rules" used in the SECT model are summarized in Table IV. The fuel cost used to obtain engine trade factors (take off gross weight [TOGW] and DOC sensitivity to changes in engine characteristics) during the Task I

TABLE IV.
DIRECT OPERATING COST MODEL (1985 ECONOMIC YEAR)

FUEL AND OIL INSURANCE COST DEPRECIATION FLIGHT CREW COST	→ 1967 ATA METHODOLOGY
ENGINE MAINTENANCE (DIRECT LABOR AND PARTS)	→ 1967 ATA EQUATION FORMAT WITH UPDATED CORRELATION FACTORS
AIRFRAME MAINTENANCE (DIRECT LABOR AND PARTS)	→ BELL HELICOPTER—EQUATION FORMAT GATE HELICOPTER WITH UPDATED CORRELATION FACTORS

GROUND RULES

•ECONOMIC BASE YEAR	1985
•FUEL COST	0.26 $/l (0.53 $l) (1.00 $/GAL [2.00 $/GAL])
•OIL COST	6.24/$l ($24/GAL)
•INSURANCE RATE	12% OF ACQ COST PER YEAR
•DEPRECIATION SCHEDULE	7 YEARS TO 25% RESIDUAL VALUE
•SPARES	AIRFRAME–10% AIRFRAME ACQ COST ENGINE—15% ENGINE ACQ COST
•UTILIZATION RATE	1000 HR/YR (2000 HR/YR)
•MAINTENANCE BURDEN	150%
•LABOR RATE	$15.00 PER MAINTENANCE MANHOURS

TE86-4877

study effort was $0.39/l ($1.50/gal.) in 1985 dollars. However, the Task III system performance evaluations were completed using $0.26/l ($1.00/gal.) and $0.53/l ($2.00/gal.) fuel cost levels.

Engine Acquisition Cost

Original equipment manufacturer (OEM) costs for the turboshaft study engines were developed using Allison material index factor methods applied to component finished weights. These costs were determined for the unity size engine (1000 shp at sea level static standard day [SLSS], intermediate rated power [IRP])

and scaled to the horsepower (hp) size necessary to meet the engine/aircraft size combination required for the design mission.

$$\text{OEM cost} = \left(\frac{\$}{shp_S}\right) \times shp_S$$

where: $\left(\frac{\$}{shp_S}\right) = \left(\frac{\$}{shp_U}\right) \times \left(\frac{shp_S}{shp_U}\right)^{-0.0125}$

shp → SLS, standard day, IRP horsepower

S → scaled engine size

U → unity engine size

Engine acquisition cost was obtained from the following relationship:

$$\text{Engine acquisition cost} = \text{OEM cost} \times 1.5$$

Aircraft Acquisition Cost

The aircraft less engine acquisition cost for the scaled aircraft/engine combination was obtained from Bell Helicopter for the reference vehicle. The cost per pound for reference vehicle is:

$$\frac{\text{aircraft cost - engine cost}}{\text{mfg empty wt - engine weight}} = \$362/\text{pound}$$

Therefore:

Aircraft cost (A/C) less eng acq cost = (mfg empty wt - engine wt) x $362/pound

Engine Direct Maintenance Cost

The ATA maintenance labor equations, which are functions of engine shaft power, required adjustment to obtain correlation with Allison maintenance labor estimates (manhours per flight hr). The adjustment factor was introduced to provide the influence of engine configuration differences, i.e., complexity, parts count, and component accessibility features on engine teardown time requirements. The ATA maintenance material equations, which are functions of engine

OEM cost, provided good correlation with Allison maintenance material cost estimates (dollars per flight hr). Therefore, no adjustments were applied to this set of equations.

Aircraft Less Engine Direct Maintenance Cost

The aircraft less engine maintenance costs were based on Bell Helicopter Textron, Inc. maintenance equations (Ref. 1) supplied to Allison during the NASA-Lewis sponsored Advanced General Aviation Turbine Engine (GATE) studies completed in 1979. These equations were developed by Bell for use in predicting conventional single rotor helicopter labor and material costs based on manufacturers empty weight less engine weight. An adjustment to these equations was required to obtain correlation with the maintenance cost level estimated by Bell for the reference tilt-rotor aircraft used in the SECT study. This adjustment or bump factor was necessary to account for the added complexity of the tilt-rotor, i.e., twin rotor/gearbox/engine propulsion packages plus the interconnect drive system, and to incorporate the effects of inflation from the 1978 to 1985 time period.

BASELINE ENGINE DESCRIPTION AND SCALING EQUATIONS

Engine Description

The baseline engine is derived from a current technology engine. This SECT baseline engine is a two-spool, front-drive, centerline-concentric, free-turbine, 1000 shp turboshaft engine. It is designed as a primary propulsion unit for advanced rotorcraft applications.

The gas generator spool is comprised of a two-stage centrifugal-flow compressor made of 6-4 titanium having an overall pressure ratio of 14:1 and driven by a two-stage, axial-flow turbine.

The first and second-stage turbine vanes are made of MAR-M509, the first-stage blades are made of MAR M246, and all are air cooled. The power turbine is comprised of two axial flow stages made of INCO 713, an output shaft made from EMS-64500, and an integral electromechanical phase displacement type torque sensor. The power turbine airfoils are not cooled.

The engine has an annular fold-back combustor having a Lamilloy®* transpiration-cooled liner and is made of INCO 718. It contains 16 airblast fuel nozzles. Fuel is mixed with air and burned in the combustor to bring the temperature of the fuel/air mixture (RIT) to 1204°C (2200°F).

The control system for this engine uses a full-authority, digital electronic control and a unitized fuel handling system. Self-contained electrical power is supplied by a high-speed permanent magnet generator that provides electrical power for ignition and electronic central functions.

An engine accessory gearbox is mounted on top of the engine and provides drive pads for the engine fuel pump, permanent magnet generator, hydraulic pump, and starter/generator system. The accessory gearbox also incorporates the self-contained engine lubrication system including the oil filter, cooler, pump, and pressure regulating system.

Figure 9 shows the general arrangement details for this engine with front and side views along with major engine envelope dimensions. It also shows an inlet air particle separator that was removed for the subject tilt-rotor installation (this unit is airframe-mounted equipment).

Basic information regarding the baseline engine is listed in Table V. The OEM's cost of $219,100 was used in Task I to develop engine/aircraft sensitivity curves or trade factors. However, this OEM cost was reevaluated during the Task III study efforts and adjusted to the cost indicated in Table V. Standard day performance plus engine cycle data summaries are listed in Table VI for SLSS, for IRP, and at 6096 m (20,000 ft)/250 KTAS, maximum cruise power conditions.

Study Engine Installation and Scaling

Installation assumptions used for the turboshaft study engines are as follows:

- o inlet recovery (PT2/PTO) = 1.00
- o aircraft bleed air requirements = 0.0

*Lamilloy is a registered trademark of the General Motors Corporation.

TABLE V.
BASELINE ENGINE (PD452-1) BASIC INFORMATION

POWER	1000 SHP AT SLSS, IRP (1204°C [2200°F] ROTOR INLET TEMPERATURE)
AIRFLOW	2.58 kg/SEC) (5.69 LB/SEC)
WEIGHT	115.67 kg (255 LB) (POWER/WEIGHT RATIO = 3.9:1)
OEM COSTS (1985 DOLLARS)	$219,100—TASK I $214,932*—TASK III

* THIS OEM COST IS BASED ON 10,000 TOTAL ENGINE BUILD AT A PRODUCTION RATE OF 80 ENGINES PER MONTH.

TE86-4878

---

o aircraft power extraction - included in the tilt-rotor power polars (Aircraft accessories are mounted in the center gearbox assembly located in the fuselage wing carry through.)

Performance, weight, and dimensions were developed for unity size (1000 shaft horsepower (shp) at SLSS, IRP) study engines. Scaling equations were then used to adjust these engine characteristics to the horsepower size necessary to meet design mission requirements. The engine scaling equations used in the SECT study are:

1)Weight

$$W_S = W_U \times \frac{shp_S}{shp_U}^{EXP}$$

where:

S → scaled engine size
U → unity engine size

TABLE VI.
BASELINE ENGINE PERFORMANCE SUMMARY

	SLSS/IRP	20K/250 KTAS/ CRUISE
SHP	1000	580
SFC kg/HR-HP (LB/HR-HP)	0.204 (0.450)	0.187 (0.412)
RIT, °C (°F)	1204 (2200)	1116 (2040)
COMPRESSOR INLET CORRECTED FLOW, $W\sqrt{\theta}/\delta$ kg/SEC (LB/SEC)	2.58 (5.69)	2.69 (5.92)
COMPRESSOR PRESSURE RATIO, R_C	14:1	14.9:1
COMPRESSOR ADIABATIC EFFICIENCY, η_C	78.4%	77.3%
GASIFIER TURBINE EFFICIENCY, η_T	85.7%	85.7%
POWER TURBINE EFFICIENCY, η_T	88.5%	88.6%
CHARGEABLE TURBINE COOLING, % OF COMPRESSOR INLET FLOW	4.8%	4.8%
LEAKAGE, % OF COMPRESSOR INLET FLOW	1.17%	1.17%
COMBUSTOR EFFICIENCY, η_B	99%	99%
COMBUSTOR Δ P/P	3.0%	3.0%
COMPRESSOR EXIT CORRECTED FLOW, $W\sqrt{\theta}/\delta$, kg/SEC (LB/SEC)	0.26 (0.57)	0.26 (.57)
GASIFIER TURBINE INLET CORRECTED FLOW $W\sqrt{\theta}\epsilon/\delta$, kg/SEC (LB/SEC)	0.43 (0.94)	.43 (0.94)
POWER TURBINE INLET CORRECTED FLOW, $W\sqrt{\theta}\epsilon/\delta$, kg/SEC (LB/SEC)	1.54 (3.4)	1.59 (3.5)
GASIFIER TURBINE $GJ\Delta h/U_m^2$	1.21	1.21
POWER TURBINE $GJ\Delta h/U_m^2$	1.66	1.66
LP RPM	29277	29277
HP RPM	48450	47123

TE86-4879

EXP = 1.05 if $shp_S/shp_U > 1.0$

EXP = 0.96 if $shp_S/shp_U < 1.0$

2)Dimensions (linear)

$$L_S = L_U \times \frac{shp_S}{shp_U}^{0.4}$$

3)Dimensions (diameters)

$$D_S = D_U \times \frac{shp_S}{shp_U}^{0.5}$$

4)Specific fuel consumption (SFC)

$SFC_S = SFC_U$ x adjustment factor (see Table VII)

TABLE VII.
ADJUSTMENT FACTOR FOR SFC SCALING VS. ENGINE SCALE FACTOR

ENGINE SCALE FACTOR (SHP_s/SHP_u)	ADJUSTMENT FACTOR	
	BASELINE ENGINE	ADVANCED TECHNOLOGY ENGINES
1.1	0.994	0.993
1.0	1.000	1.000
0.9	1.008	1.009
.0.8	1.017	1.019

TE86-4880

BASELINE ENGINE MISSION RESULTS AND TRADE FACTORS

Results from "flying" the previously presented baseline engine/reference tilt-rotor aircraft in the Allison Mission Analysis Computer Program are shown in Table VIII. This table summarizes basic information resulting from the subject engine/aircraft combination scaled to meet the SECT design mission requirements. Design TOGW, engine horsepower size at IRP, and rotor diameter are provided in Table VIII. Rate of climb capabilities are shown for each candidate sizing condition. Shown in parenthesis are the required rate of climb levels. The critical engine sizing condition is shown to be the 91.44 m/min (300 rpm) rate of climb at cruise altitude and velocity, i.e., cruise ceiling requirement.

Resultant power loading values for the PD452-1 powered tilt-rotor aircraft are compared against the Sikorsky S76 helicopter levels in Table IX for both all engines operative (AEO) and one engine operative (OEI) conditions.

Table IX shows that the tilt-rotor aircraft has a 60% higher power loading at both AEO and OEI conditions. These high power loadings, relative to the S76 helicopter, will provide the tilt-rotor aircraft with significant safety margins and capabilities for use in V/STOL and hover operations (hover and OEI rate of climb capabilities versus required levels are shown in Table VIII).

TABLE VIII.
MISSION RESULTS (PD452-1 POWERED TILT-ROTOR)

FUEL COST = $0.39/l
UTILIZATION = 1000 HRS YR

TOGW	4559 kg (10,050 LB)
SHP/ENGINE @ IRP SLSS	1010 HP
ROTOR DIAMETER	6.9 m (22.6 FT)
HOVER R OF C CAPABILITY @ 2000 FT/0 KTAS/ISA + 10°C IRP-AEO	341 M/MIN (1120 FPM) (0 M/MIN [0FPM] REQUIRED)
OEI R OF C CAPABILITY @ 1000 FT/75 KTAS/ISA + 20°C 30 MIN POWER - OEI	131 M/MIN (430 FPM) (45.7 M/MIN [150FPM] REQUIRED)
CRUISE R OF C CAPABILITY @ 20,000 FT/250 KTAS/ISA MAX. CONTINUOUS POWER	91 M/MIN (300 FPM) (ENGINE SIZING PT)
TOTAL FUEL (MISSION + RESERVES)	501 kg (1104 LB)
BLOCK FUEL	347 kg (764 LB)
TOTAL AIRCRAFT ACQ COST	$2.96 MILLION
ENGINE ACQ COST (ONE)	$331,700
DOC	1208 $/BLK HR

TE86-4881

TABLE IX.
POWER LOADING COMPARISON (SEA LEVEL STATIC, STANDARD DAY CONDITIONS)

AIRCRAFT ENGINE NO.	S76 250-C30 (2)	TILT-ROTOR PD452-1 (2)
TOGW, KG (LB)	4672 (10,300)	4559 (10,050)
SHP/ENGINE AT IRP, SLSS	650	1010
POWER LOADING = SHP TOTAL/TOGW	0.126	0.201
ΔPL (AEO CONDITION)	(BASE)	(+60%)
SHP AT OEI (30 MIN) POWER, SLSS	650	1010
POWER LOADING = SHP TOTAL/TOGW	0.063	0.100
ΔPL (OEI CONDITION)	(BASE)	(+60%)

TE86-4882

Table VIII also includes total fuel (design fuel tankage capacity) and block fuel (mission fuel burned) data along with cost data from the DOC model.

A component or group weight breakdown is shown in Table X for the scaled PD452-1/tilt-rotor aircraft combination. The total base engine weight of 234 kg (515 lb) included in the propulsion group represents only 5% of the aircraft TOGW and fuel weight of 501 kg (1104 lb) represents only 11% of the aircraft TOGW.

Mission fuel usage data is shown in Table XI on a per mission phase basis and on an engine power setting basis. These data indicate the cruise plus reserves (45 minutes of continued cruise) at an approximate maximum continuous power setting level to be the largest full usage requirement (433 kg [955 lb] or 87% of the total fuel).

A breakdown of the six direct operating cost elements is shown in Table XII with respect to aircraft and engine costs. These data indicate aircraft associated insurance and depreciation to be the two largest cost items and that only 31% of the total DOC can be associated with or influenced by engine characteristics.

TABLE X.
AIRCRAFT WEIGHT BREAKDOWN (PD452-1 POWERED TILT-ROTOR)

	KG (LB)	WEIGHT FRACTION—%
PROPULSION GROUP (INCLUDES ROTOR GROUP AND DRIVE SYSTEM)	1140 (2513)	25.0
STRUCTURES GROUP	1007 (2221)	22.1
FIXED EQUIPMENT	962 (2121)	21.1
MFG EMPTY WEIGHT	3109 (6855)	68.2
USEFUL LOAD	223 (492)	4.9
OPERATING EMPTY WEIGHT	3345 (7374)	73.1
PAYLOAD	726 (1600)	15.9
ZERO FUEL WEIGHT	4058 (8947)	89.0
FUEL (USABLE)	501 (1104)	11.0
TOGW	4559 (10,051)	100.0

TE86-4883

TABLE XI.
MISSION FUEL BREAKDOWN (PD452-1 POWERED TILT-ROTOR)

MISSION PHASE BASIS	kg(LB)	%
START AND WARM-UP ALLOWANCE	0.9 (2)	—
T.O. AND TRANSITION ALLOWANCE	14 (32)	3
CLIMB @ 180 KEAS	51 (113)	10
CRUISE @ 20K/250 KTAS	267 (588)	53
TRANSITION AND LAND ALLOWANCE	12 (27)	3
SHUT-DOWN ALLOWANCE	0.9 (2)	—
RESERVE (45 MIN)	154 (340)	31
TOTAL	501 (1104)	100%
ENGINE POWER SETTING BASIS		
INTERMEDIATE RATED POWER	66 (145)	13
~ MAX CONTINUOUS POWER	433 (955)	87
GROUND IDLE POWER	1.8 (4)	—
TOTAL	501 (1104)	100%

TE86-4884

Using the baseline engine powered tilt-rotor aircraft as the baseline, the effect of delta changes in the following engine characteristics on both TOGW and DOC was obtained:

- o engine specific fuel consumption (SFC)
- o engine weight (WT)
- o maximum engine envelope length (LE)
- o maximum engine envelope height (HE)
- o engine OEM cost ($/shp)

The results from the subject calculations are presented in the TOGW sensitivity curves shown in Figure 10 and the DOC sensitivity curves shown in Figure 11.

TABLE XII.
DOC BREAKDOWN—$/BLK HR (PD452-1 POWERED TILT-ROTOR)

FUEL COST = $0.39/l—$1.50/GALLON
UTILIZATION = 1000 HR/YR

	AIRCRAFT	+	ENGINE	→	TOTAL A/C + ENGINE
FUEL AND OIL	—		117 (10%)		117
INSURANCE	275 (23%)		80 (7%)		355
AIRCRAFT MAINT	230 (19%)		—		230
ENGINE MAINT	—		91 (8%)		91
DEPRECIATION	270 (22%)		82 (7%)		352
FLIGHT CREW	63 (5%)		—		63
TOTALS	838 (69%)	+	370 (31%)	→	1208 (100%)

TE86-4885

ENVIRONMENTAL CONSTRAINTS

Emissions Control Requirements

There are no regulations to control exhaust emissions from small aircraft gas turbines, including rotorcraft engines, and none are expected in the near future. However, the International Civil Aviation Organization recommends the control of fuel venting from all turbines regardless of size or application.

The likelihood of future emissions regulations depends on the following factors:

- o environmental politics--particularly aircraft related issues
- o size and growth of the source--size of rotorcraft fleet
- o level of emissions control technology applied by engine manufacturers

Of the three factors stated, only the level of emissions control technology can be directly influenced by the engine designs. It is important to design to the highest control levels economically practical since it is less likely that emissions control regulations will be promulgated for engines that include these designs. The next step in emission reduction becomes extremely expensive, and the cost of control, in terms of dollars per ton of pollutants removed, becomes much greater than that required to control other sources of pollution. In addition, an aircraft system that does not issue odors or visible smoke does not invite criticism and political action.

Allison has developed a high level of cost effective emissions control technology that was used in the combustion system design of the SECT engines. This technology was demonstrated on the Model 280-C1 engine that was derived from the GMA500/advanced technology demonstrator engine (ATDE) program. The emissions control techniques used were:

- o prechamber combustor
- o optimized primary zone
- o Lamilloy construction (transpiration cooling)
- o air blast fuel nozzles

The emissions goals established for the SECT program are: fuel venting emissions (none allowed), smoke (not to exceed SN = 40), and gaseous emissions. They are based on emissions testing of an engine that contained the control techniques previously stated. Table XIII gives the maximum gaseous emissions allowable as a function of engine power setting.

The units of gaseous pollutants emissions index (g/kg fuel) were chosen to be compatible with combustor component and gas generator operational parameters. These units are more independent of the final engine cycle than units expressed in specific emissions, i.e., $g/_{kW\ hr}$, or $g/_{kN}$ of thrust.

Noise

Noise constraints for gas turbine powered rotorcraft occur at two levels, regulatory and public acceptance. The regulatory constraints contained in Federal

TABLE XIII.
MAXIMUM GASEOUS EMISSIONS ALLOWABLE

ENGINE POWER SETTING	GASEOUS EMISSIONS, g/kg FUEL		
	HYDROCARBONS	CARBON MONOXIDE	NITROGEN OXIDES
MAXIMUM	0.44	0.90	18.70
INTERMEDIATE	0.46	0.96	17.60
MAXIMUM CONTINUOUS	0.47	1.10	15.80
75% MAXIMUM CONTINUOUS	0.50	1.20	12.6
25% MAXIMUM CONTINUOUS	0.63	2.90	8.40
IDLE	7.10	68.0	3.70

TE86-4886

Air Regulation (FAR) Part 36 for rotary wing aircraft are expected to remain in place in the year 2005 with a small decrement in the required noise levels. Continuing opposition at the local level to the building of new heliports, however, results in strong incentive to produce rotorcraft that are more quiet than required by FAR Part 36. The current NASA/industry cooperative rotorcraft program should produce the technology required to reduce rotor noise. Acoustic studies of helicopters in the current fleet show that the engine contributes to the aircraft noise signature and acts as a floor to limit the gains possible by rotor noise reduction. An engine noise reduction, relative to current engine levels, is required to permit the full use of the technology being developed in the NASA/industry program.

Based on Allison test experience, engines using the advanced cycles and technology embodied in the SECT program will generate noise signatures that are lower than the signatures of current engines.

IV. TASK II. ENGINE CONFIGURATION AND CYCLE EVALUATION

The procedures and assumptions identified in Task I were used to select the engine configurations and cycle conditions for Task III. The selection criteria were chosen to place priority on direct operating cost of the reference tilt-rotor aircraft as opposed to return on investment (ROI) or other economic figures of merit.

Three basic engine cycles were examined during Task II: (1) an advanced simple cycle, (2) a waste heat recovery cycle, and (3) a wave rotor cycle. For the advanced simple cycle, two types of general arrangements were examined: the traditional concentric gas turbine spool arrangement and a nonconcentric spool arrangement. For the waste heat recovery cycle, the regenerative and recuperative approaches were studied.

GAS TURBINE TECHNOLOGY PROJECTIONS FOR YEAR 2000

Special problems exist for each engine component by the small size requirement of this class of gas turbine engine. The following sections outline technology enhancements for the year 2000 for small gas turbine engine that were assumed for the cycle optimization study.

Compressor

Figure 12 shows the overall compressor polytropic efficiency as a function of exit corrected flow for the current state-of-the-art technology as well as that projected for the year 2000. Several mechanical and aerodynamic improvements are required to achieve this level of performance in small compressors, e.g., control clearances, surface roughness, manufacturing tolerance, airfoil contour, and secondary flow. Table XIV outlines these expected performance improvements for small compressors.

Turbine

Figure 13 shows the axial turbine overall total/total adiabatic efficiency as a function of inlet equivalent flow rate for both current state-of-the-art

TABLE XIV.

SMALL COMPRESSOR TECHNOLOGY ADVANCEMENTS.

- IMPROVED MANUFACTURING CAPABILITY
- IMPROVED ANALYSIS CAPABILITY
  - MULTI-ROW
  - 3-DIMENSIONAL
  - VISCOUS/QUASI-VISCOUS
- AXIAL COMPRESSOR
  - AIRFOIL CONTOUR
  - SWEEP, TILT, AND LEAN OPTIMIZATION
  - END WALL TREATMENT
- CENTRIFUGAL COMPRESSORS
  - IMPELLER AIRFOIL/PASSAGE CONTOUR
  - CLEARANCE LOSS REDUCTION
  - DIFFUSER ENTRANCE REGION OPTIMIZATION
  - SECONDARY DIFFUSER OPTIMIZATION

VS85-1106

technology as well as that projected for the year 2000. Improvements in fabrication methods, aerodynamic concepts, and analytical modeling are needed to achieve the projected level of performance in small axial turbines. Table XV outlines these expected turbine technology advancements. Figure 14 shows the radial turbine performance goals for the Small Engine Component Technology (SECT) study.

All cycle analysis assumed uncooled turbine configurations. This assumption was necessary, especially in the high pressure turbine. The size and life requirement of the high pressure (HP) turbine rotor prohibit introduction of cooling passages. Therefore ceramics were selected as the material for turbines.

TABLE XV.

TURBINE TECHNOLOGY ADVANCEMENTS.

- ADVANCED MATERIALS/FABRICATION METHODS
  - HIGHER WHEEL SPEEDS/REDUCED STAGE LANDING
  - REDUCED COOLING AIR REQUIREMENTS
  - REDUCED BLOCKAGE/HIGHER ASPECT RATIOS
  - LOWER THICKNESS/CHORD RATIO BLADING
  - UNIFORM BLADING THROATS
- ADVANCED AERODYNAMIC CONCEPTS
  - ENDWALL BOUNDARY LAYER CONTROL
  - PASSAGE MERIDIONAL CONTOURING
  - LOW REYNOLDS NUMBER BLADING
- ADVANCED ANALYTICAL MODELS
  - 3-D VANE/BLADE INTERACTION
  - 3-D VISCOUS FLOW ANALYSIS
  - OPTIMIZED AERO/HEAT TRANSFER BLADING

V505-1000

Combustor

The key technology advancement required for the combustor is the achievement of a low pattern factor to permit operation at high turbine temperatures for improved cycle efficiency. A goal pattern factor of 0.12, as defined by (T_{MAX}-rotor inlet temperature (RIT)/(RIT-CDT), has been established for year 2000 combustor technology. Other goals being addressed include low smoke and increased durability.

Materials

The main emphasis in materials development for gas turbines is toward high temperature capability, low density, low cost fabrication, and improved corrosion/erosion resistance. For the year 2000, two key materials emerge as the

requirement to significantly reduce the direct operating cost of the small gas turbine engine becomes important. First ceramic composites in the high pressure turbine rotor and stator will provide the opportunity to run the engine at higher turbine temperatures than engines in service today. A silicon carbide composite will have a 1649°C (3000°F) temperature capability by the year 2000. Secondly, to accommodate the higher compressor discharge temperatures associated with going to much higher cycle pressure ratios, titanium aluminide (Ti_3Al) will be needed for its temperature capability of 816°C (1500°F). The additional benefit of Ti_3Al is its low density (50% density reduction over superalloys) and ease of fabrication.

The selection of maximum turbine rotor inlet temperature (RIT) was based on the following:

1. For the ceramic radial HP turbine rotor, the maximum allowable surface temperature was set at 1399°C (2550°F). Based on the AGT 100 uncooled ceramic radial turbine heat transfer characteristics, the rate of $T_{M\ MAX}/T_{REL\ MAX} = 0.983$. Therefore $T_{REL\ MAX} = 1424°C$ (2595°F). Based on the SECT radial turbine designs, the ratio of $T_{REL\ MAX}/RIT = 0.927$, RIT MAX of 1538°C (2800°F) was obtained.
2. The combustor pattern factor assumed for the year 2000 technology is 0.12. For a static structure such as the HP turbine inlet vane, the maximum allowable surface temperature was set at 1649°C (3000°F). For the cycle pressure ratios considered, resulting max RIT is 1535°C (2795°F).

Therefore, maximum RIT of 1538°C (2800°F) was selected.

Recuperator/Regenerator

Recent advances in recuperator/regenerator technology make it necessary to re-examine the waste heat recovery cycle for the rotorcraft application. In the area of recuperator technology, a nitride dispersed stainless steel (NDS) is available that has an 982°C (1800°F) temperature capability. NDS recuperators can be fabricated at extremely low cost. Ceramics is another candidate material for recuperators, offering higher temperature capability (1260°C [2300°F])

than NDS. It is lighter than NDS but costs more to fabricate. This information was provided by Air Research Manufacturing Company, Torrance, California. They also provided a recuperator parametric study necessary to conduct the recuperator cycle optimization during Task II.

Regenerator technology for the year 2000 consists of using a one-piece extruded ceramic disk. This procedure minimizes cost and weight while providing high strength for higher than normal cycle pressure operation. Low leakage seals characterized by low thermal distortion are also included in the design. This design will allow the regenerative cycle to optimize at higher cycle pressure ratios than conventional regenerative cycles, such as the advanced gas turbine (AGT 100) being developed by Allison.

Wave Rotor Engine

In this concept, the conventional high pressure spool in the simple cycle engine is replaced by a wave pressure exchanger or Comprex system. The Comprex assumes the function of a turbine-driven compressor (compressor-expander) with a direct transfer of energy by impingement of the expanding gas on the air to be compressed. Figure 15 illustrates the wave rotor cycle. The Comprex rotor consists of straight axial channels that are alternately exposed to segmented ports open to the air or to the hot gases. Nonsteady flow is created by the opening and closing of the rotor channels as they pass over the ports and blocked off portions of the stator. The rotor speed and rotor length must be defined to coordinate pressure wave passage time with port opening. The Comprex system is essentially a flow switching device and is not capable of producing shaft power. It must be driven to overcome friction and windage losses. Figure 16 shows a typical wave rotor configuration for gas turbine application.

The efficiency of the energy exchange within the Comprex system is equivalent to high grade radial turbomachinery and is less sensitive to size than turbomachinery. The system is also amenable to speed changes with good efficiencies and offers instantaneous load response.

The rotor is alternately exposed to hot and cool gases and the rotor material assumes some average temperature, thereby allowing combustor outlet temperatures that are limited only by the static structure. Only a part of combustor

discharge gas is used in the Comprex system. The remainder is bypassed and diluted as required before entering the low pressure turbine.

CYCLE/CONFIGURATION EVALUATION

The methodology used to perform the cycle optimization study in Task II is shown in Figure 17. The year 2000 technology base for small gas turbine engines was used to calculate cycle performance for each engine configuration under study. Within each cycle matrix, one cycle was selected as a preliminary design point cycle to calculate engine weight, cost, and dimension. From that preliminary design point cycle, weight, cost, and dimension for the other cycles in the matrix were obtained analytically as described in Task I of this report. Using the trade factors developed during Task I, sensitivities to direct operating cost were developed for each cycle in a given matrix. This technique was used to select the cycle (RIT, R_c combination) for each configuration that gave the minimum relative direct operating cost (DOC).

Each cycle was scaled to produce 1000 shaft horsepower (shp) at sea level static (SLS) conditions. All cycle analysis assumed uncooled turbine configurations with maximum TRIT of 2800°F. Total cycle leakage was scaled as a function of cycle pressure ratio and engine flow size. Specifically:

$$\text{SECT leakage} = \text{base leakage} \times \left(\frac{R_{C\ SECT}}{R_{C\ BASE}}\right) \times \left(\frac{W_{A\ BASE}}{W_{A\ SECT}}\right)^{1/2}$$

where the base values are those from the baseline advanced technology turboshaft engine. The leakages are expressed as a percentage of total compressor inlet flow. The regenerator and recuperator systems were designed at the tiltrotor mission cruise flight condition (6096 m/250 knots true airspeed (KTAS) [20,000 ft/250 KTAS]) for optimum performance. Results of the cycle study for the concentric, nonconcentric, recuperative, regenerative, and wave rotor engine cycles are presented in the following sections.

Concentric Engine Cycle Evaluation

Cycle Evaluation

For the concentric component arrangement of the simple cycle engine, pressure ratios from 15 to 25 were investigated with turbine rotor-inlet-temperatures from 2200°F to 2800°F. Overall pressure ratios greater than 25 were not considered. Design analysis of the concentric engine indicated that the bore stress in a HP turbine was prohibitive for pressure ratios greater than 25.

Figure 18 shows the parametric cycle analysis for the concentric engine for the range of cycle parameters investigated. This chart illustrates the trends in specific fuel consumption and specific horsepower as a function of turbine temperature and pressure ratio. The weight and cost sensitivities were applied to generate the DOC trends shown in Figure 19. The minimum DOC is shown to occur at an overall pressure ratio of 25:1 and 2800°F RIT for the concentric cycle.

Engine Configuration

The concentric engine general arrangement is shown in Figure 20. The features are summarized as follows:

- o removable top-mounted accessory gearbox module
- o an aluminum inlet support
- o a four-stage axial 8.33:1 low pressure (LP) compressor
- o a gas generator incorporating with
  - a centrifugal flow 3:1 compressor (dual IMI Ti)
  - a parallel wall radial vaned diffuser (TiAl)
  - reverse flow annular combustor made from ceramic (SiC/SiC)
  - radial inflow gasifier turbine (SiC/SiC)
- o removable single-stage axial uncooled low pressure (LP) turbine (Ti_3Al)
- o removable two-stage axial uncooled free shaft power turbine (TiAl) module
- o full authority adaptive digital control
- o self-contained fuel and lubrication systems
- o engine monitoring system (EMS)

Output shaft speed is 40,000 rpm rotating counterclockwise as viewed from the aft end of the engine. The engine configuration provides an advanced design with low life cycle costs, high reliability, high survivability, and excellent maintainability for the tilt-rotor aircraft missions. A description of each component follows.

Gearbox--The accessory gearbox is designed to mount on the top of the engine for improved maintainability and can be removed with all accessories in place and without disturbing any other engine module. This module incorporates an integral oil system and provides drive pads for both engine and aircraft accessories.

Inlet support--The inlet support is cast aluminum and forms the major forward engine support case. This casting provides the flow path for engine air entering the first-stage axial LP compressor and is anti-iced with scavenge oil.

Centrifugal impeller--The compressor is designed to meet the conditions at the SLS match point. The static structure and the impeller are made from low thermal expansion titanium to maintain close clearance control. An abradable erosion resistant coating of flame sprayed aluminum-silicon applied over chromium carbide is used on the shrouds to allow tight clearances with rub protection. The compressor represents a low technical risk engine component.

Combustion system--The combustion system is a durable, high performance, reverse flow annular design that uses a machined outer casing, ceramic transition liner, and piloted air blast fuel injector. This combustor meets all requirements of the tilt-rotor aircraft mission. A reverse flow feature provides the shortest possible coupling between the compressor and the gasifier turbine with resulting benefits in shaft dynamics and engine rigidity.

Radial inflow gasifier turbine--The gasifier turbine rotor is expected to operate in a more severe thermal environment and at higher speeds than any previously tested at Allison. The analysis of this rotor is an extension of the ceramic rotor experience gained from the Advanced Gas Turbine Program.

Single-stage axial LP turbine--The LP turbine is based on a current technology turbine with slightly more severe thermal and speed operating conditions.

Blade stress and vibration characteristics are moderately above the existing engines. The material change to single crystal minimizes the required cooling flow and provides an increased temperature margin.

Power turbine--The two-stage axial power turbine is based on a current technology power turbine. The configuration incorporates advanced materials to eliminate cooling. The power turbine rotates counterclockwise when viewed from the rear and opposite the gas generator direction to provide optimum efficiency and reduced weight.

Nonconcentric Engine Cycle Evaluation

Cycle Evaluation

Moving the HP spool out in the nonconcentric type configuration eliminates the requirement to pass shafting through the center of the high pressure rotor. By eliminating the bore stress problem, overall pressure ratios up to 40:1 could be considered for this configuration. The maximum HP turbine rotor-inlet-temperature was again limited to 2800°F.

Figure 21 shows the parametric cycle analysis for the nonconcentric engine for overall pressure ratios of 25 to 40 and turbine rotor-inlet-temperatures ranging from 2200°F to 2800°F. This illustrates the trends of specific fuel consumption and specific horsepower as a function of the cycle parameters. Figure 22 illustrates the DOC trends of the nonconcentric cycle as a function of Rc and RIT. This shows the optimum cycle to be at a 30:1 overall pressure ratio and 2800°F RIT.

Engine Configuration

The nonconcentric engine is a three-spool turboshaft engine concept that offers the capability of achieving a significant reduction in specific fuel consumption (SFC) and cost and an increase in power-to-weight ratio compared to current Allison engines. The nonconcentric turbine engine achieves the reduced fuel consumption by combining high cycle pressure ratio and high turbine RIT in a three-spool configuration. The arrangement differs from the conventional two-spool engine by the addition of a third spool, which is mounted off axis

and aligned parallel to the other two spools. Advantages are improved compressor performance and surge margin, smaller diameter flow path, reduced seal and bearing diameters, elimination of bore stress problems, and a simpler accessory gear arrangement. The nonconcentric engine general arrangement, as shown in Figure 23 is a result of studies designed to meet the optimum performance constraints while minimizing the duct pressure losses and engine heat rejection. The power shaft is inside the LP shaft with the output connection located at the engine front.

Recuperator Engine Cycle Evaluation

Cycle Analysis

A comprehensive parametric study was made to select the optimum recuperator engine combination. The following parameters were considered:

- o engine
  - compression ratio, R_c--6, 10, 14
  - turbine rotor inlet temperature, RIT--1204°C, 1371°C, 1538°C (2200°F, 2500°F, 2800°F)
- o recuperator
  - effectiveness, E%--60, 70, 80
  - total pressure drop, $\Delta P/P\%$-- 6, 8, 10
  - plate and fin spacing, thickness, and offset
  - tube size, spacing, and dimpling
  - number of passes--air and gas
  - cross and counterflow
  - materials--metal and ceramic
  - number and arrangement of modules
  - size, weight, and cost

A total of 45 engine cycles were selected for analysis from the 81 possible combinations of the above parameters. Figure 24 shows a typical parametric analysis plot for the recuperative engine cycle. This trend of specific fuel consumption and specific horsepower as a function of cycle Rc and RIT is for a recuperator having a design effectiveness of 60%, and a total pressure drop of 10%.

Recuperator Configuration Analysis

Allison selected the matrix of R_c, RIT, E, and $\Delta P/P$ for investigation. AiResearch was chosen, because of their extensive experience, to select appropriate heat transfer surfaces and flow arrangements and to calculate sizes required. A description of the procedure for selecting the optimum recuperator engine combination follows.

Configuration

AiResearch selected offset rectangular heat transfer surfaces, shown in Figure 25, for all plate and fin analyses. This surface has the advantage of reducing boundary layer to zero at each fin offset and is generally acknowledged to be one of the most compact available. AiResearch had optimized this type surface for minimum core volume in a Garrett vehicular engine. AiResearch conducted the optimization based on this type of surface. A thorough optimization of the above plate and fin dimensions for DOC was not conducted. A comparison of modified plate and fin dimensions was made at 10:1 engine compression ratio and 1538°C (2800°F) RIT with a counterflow recuperator. At 60% E and 10% $\Delta P/P$ reductions of 22-25% in cost, 8-12% in weight and 3-26% in length for the same overall recuperator diameter were obtained by using slightly more fins/in. and greater plate spacing on the gas side. The study to minimize DOC was conducted with the vehicular engine dimensions that were shown to produce minimum individual core volume but not minimum overall wrap up volume. All the fin dimensions considered were acceptable from a fouling standpoint with jet fuels. For the metal cross-counterflow recuperators, AiResearch evaluated all their offset fin configurations and narrowed the selection based on weight and size. Allison made the final selection based on DOC sensitivities.

AiResearch selected 0.32 cm (1/8 in.) diameter tubing as the smallest possible, for size and weight, without encountering laminar flow that would cause poor heat transfer. Both in-line and staggered tube arrangements were evaluated along with plain, ring-dimpled, and spiral-dimpled tubes for inside boundary layer disruption. In general, in-line tubes provide smaller recuperator diameter but greater weight than staggered tubes. Dimpling provides lower weight but greater recuperator diameter. The best combination was selected for each engine condition. Ring dimples were not represented in the final selection.

AiResearch selected the following flow configuration, surface, and material combinations for comparison:

- o two-pass cross-counterflow--metal tube and shell
- o two-pass cross-counterflow--metal plate and fin
- o counterflow--metal plate and fin
- o counterflow--ceramic plate and fin

AiResearch selected an annular arrangement of six modules for all recuperator types. Figures 26 and 27 show the arrangement of the metal plate and fin two-pass cross-counterflow configuration. Six modules provide a convenient size for minimum cost of assembly, brazing, and ceramic firing operations. The annular arrangement provides a minimum weight means of channeling exhaust flow with circular shell structures.

Materials, Cost, and Size

AiResearch recuperator material development is underway and is expected to provide 982-1093°C (1800-2000°F) metal capability and 1260°C (2300°F) ceramic capability by year 2000. The metal will be nitride dispersion strengthened 300 series stainless steel and the ceramic, silicon nitride. The tilt-rotor aircraft and 648 km (350 nm) cruise mission selected would require only current day chrome-moly steel for 704°C (1300°F). This is due to the fact that the engine is sized for cruise. It has a high 90% power setting as opposed to other aircraft that might be sized for hover and cruise at 75% power. At 90% power, variable engine geometry can not be used to increase turbine outlet or recuperator inlet temperature to high levels while maintaining maximum turbine inlet temperature as could be done at 75% power. This application cannot take advantage of advanced high temperature recuperator technology. Even so, low density of the ceramic material made it a close contender.

AiResearch provided cost equations for the four types of recuperators based on (1) the number of air passage layers and plate area for the plate and fin designs and (2) tube length and number of tubes for the tube and shell designs. Allison derived sensitivity factors to describe the effect of relevant engine and recuperator parameters on the tilt-rotor aircraft DOC. Figure 11 shows

these sensitivity curves. The engine plus recuperator parameters affecting DOC and their relative weight are as follows:

o specific fuel consumption (SFC)	46%
o cost	26%
o weight	12%
o length	9%
o height (or diameter)	7%
	100%

AiResearch sized about 50 recuperators of four types for 45 selected engine thermodynamic cycles. Fifty values for one recuperator dimension were selected. The values of the other two dimensions were calculated to give the specific effectiveness and pressure drop for each cycle. Different splits between air and gas side pressure drops resulted. Allison used the sensitivity curves for weight, length, and diameter on a partial basis to select the recuperator with minimum DOC for each engine cycle. In general, the best size was a recuperator with slightly more than minimum weight, but slightly shorter and significantly less in diameter.

Selection of Recuperator Type

A recuperator type that provided minimum DOC was selected for each of the 45 engine cycles. The types considered were:

- o two-pass cross-counterflow--metal tube and shell
- o two-pass cross-counterflow--metal plate and fin
- o counterflow--metal plate and fin
- o counterflow--ceramic plate and fin

The sensitivity curves were used to determine the effect of recuperator weight, recuperator diameter (or height) engine plus recuperator length, and recuperator cost on relative DOC.

Specific fuel consumption was omitted and partial weight and cost for the recuperator were justified because comparisons of relative DOC were made for each individual engine cycle. A comparison of the four recuperator types is shown

in Table XVI for R_c of 14 and RIT of 1538°C (2800°F). Comparisons are valid line-by-line for selection of the best recuperator type because (1) partial of weight and cost was used and (2) a new datum was assumed for each line (the tube and shell ΔDOC). Lowest ΔDOCs are underlined and represented by the most negative values of ΔDOC. Two-pass cross-counterflow (metal plate and fin) configurations and counterflow (ceramic plate and fin) configurations were selected for further evaluation. The tube and shell and counterflow (metal plate and fin) configurations were not contenders and were eliminated from further consideration.

Direct Operating Cost Evaluation for Cycle Selection

The recuperative engine cycle parameters were selected to provide the minimum DOC. The sensitivity curves were used with complete values of:

- o SFC
- o cost
- o weight
- o length
- o height (or diameter)

Engine cost and weight were calculated using inhouse equations with recuperator costs from Garrett. Figures 28 through 30 show for a two pass crosscounter metallic plate and fin recuperator the effect of engine compression ratio (R_c), recuperator effectiveness (E), and recuperator total pressure drop (ΔP/P) for RIT of 1538°C (2800°F) on relative DOC. From these figures, minimum DOC is obtained at R_c = 13, E = 64%, and ΔP/P = 10%. Engine cycles with the ceramic counterflow recuperator were similarly compared and minimum DOC design was obtained at R_c = 14, E = 60%, and ΔP/P = 10%.

Table XVII compares overall DOC ratios and partial DOCs for each parameter for the best two recuperators: two-pass cross-counterflow metal plate and fin, and counterflow ceramic plate and fin. The metal recuperator has 1.4% lower overall DOC. Based on DOC considerations, a metal two-pass recuperator was selected. The ceramic recuperator excels only in weight, due to the lower density of ceramics. Therefore, the engine with two pass cross counterflow metal

TABLE XVI

1538°C (2800°F) RIT ENGINES USING PARTIAL DOCS.

		TUBE AND SHELL					CERAMIC PLATE AND FIN				
		TWO-PASS CROSS COUNTER					COUNTER				
E	ΔP/P	WEIGHT KG	HEIGHT CM	L CM	COST	ΔDOC	WEIGHT KG	HEIGHT CM	L CM	COST	ΔDOC
60	6	17.4	65.4	95.0	10,629	0.00	28.2	61.9	92.0	7,084	- 1.03
	8	17.3	57.7	95.9	10,485	0.00	23.7	62.6	87.0	5,677	- 4.37
	10	15.7	57.4	89.8	10,062	0.00	21.3	55.9	86.7	6,302	- 3.38
70	6	29.6	65.3	107.6	12,795	0.00	32.6	64.0	95.6	8,078	- 4.40
	8	28.1	63.5	107.3	12,510	0.00	31.6	64.9	90.1	6,523	- 7.02
	10	27.7	61.5	103.8	12,498	0.00	28.8	58.3	90.1	7,186	- 6.98
80	6	73.1	62.5	144.2	18,552	0.00	54.8	67.6	101.6	9,766	-10.00
	8	45.2	70.9	103.3	16,260	0.00	47.0	68.8	95.2	7,908	- 7.94
	10	41.7	64.3	104.7	15,072	0.00	42.6	69.9	91.5	6,839	- 8.32

		METALLIC PLATE AND FIN									
		TWO-PASS CROSS COUNTER					COUNTER				
E	ΔP/P	WEIGHT KG	HEIGHT CM	L CM	COST	ΔDOC	WEIGHT KG	HEIGHT CM	L CM	COST	ΔDOC
60	6	36.7	65.4	90.8	3,487	-2.53	52.0	67.5	95.8	5,811	7.26
	8	35.3	58.9	84.4	3,087	-3.79	44.3	60.9	95.9	6,342	5.24
	10	32.6	59.7	82.0	2,889	-3.42	40.3	56.3	90.4	5,573	4.25
70	6	52.8	68.1	90.3	3,495	-6.05	68.4	64.3	98.7	6,807	1.66
	8	50.4	60.6	83.1	2,857	-7.31	57.7	63.2	99.5	7,090	0.50
	10	48.3	68.9	87.3	3,110	-6.39	52.8	58.9	94.3	6,206	-1.92
80	6	95.5	67.4	86.7	3,529	-11.68	95.9	67.9	104.0	7,984	-7.41
	8	93.8	62.7	82.1	3,119	-6.10	83.4	69.4	97.4	6,494	-3.47
	10	93.9	60.0	79.3	2,911	-4.80	75.5	68.6	99.5	7,064	-2.53

		TUBE AND SHELL					CERAMIC PLATE AND FIN				
		TWO-PASS CROSSCOUNTER					COUNTER				
E	ΔP/P	WEIGHT LB	HEIGHT IN.	L IN.	COST	ΔDOC	WEIGHT LB	HEIGHT IN.	L IN.	COST	ΔDOC
60	6	38.4	25.76	37.39	10,629	0.00	62.2	24.39	36.23	7,084	- 1.03
	8	38.1	22.71	37.77	10,485	0.00	52.3	24.64	34.24	5,677	- 4.37
	10	34.6	22.60	35.34	10,062	0.00	47.0	22.00	34.12	6,302	- 3.38
70	6	65.3	25.70	42.37	12,795	0.00	71.8	25.20	37.65	8,078	- 4.40
	8	61.9	25.00	42.26	12,510	0.00	69.6	25.54	35.48	6,523	- 7.02
	10	61.1	24.20	40.86	12,498	0.00	63.4	22.96	35.47	7,186	- 6.98
80	6	161.2	24.6	56.77	18,552	0.00	120.9	26.62	39.99	9,766	-10.00
	8	99.7	27.9	40.69	16,260	0.00	103.6	27.09	37.49	7,908	- 7.94
	10	91.9	25.3	41.21	15,072	0.00	93.9	27.53	36.04	6,839	- 8.32

		METALLIC PLATE AND FIN									
		TWO-PASS CROSSCOUNTER					COUNTER				
E	ΔP/P	WEIGHT LB	HEIGHT IN.	L IN.	COST	ΔDOC	WEIGHT LB	HEIGHT IN.	L IN.	COST	ΔDOC
60	6	81.0	25.76	35.75	3,487	-2.53	114.6	26.57	37.70	5,811	7.26
	8	77.9	23.17	33.24	3,087	-3.79	97.7	23.98	37.74	6,342	5.24
	10	71.9	23.51	32.29	2,889	-3.42	88.9	22.17	35.59	5,573	4.25
70	6	116.4	26.83	35.56	3,495	-6.05	150.7	25.31	38.87	6,807	1.66
	8	111.2	23.84	32.73	2,857	-7.31	127.2	24.88	39.16	7,090	0.50
	10	106.4	27.12	34.39	3,110	-6.39	116.3	23.17	37.12	6,206	-1.92
80	6	210.5	26.55	34.15	3,529	-11.68	211.4	26.73	40.96	7,984	-7.41
	8	206.7	24.68	32.33	3,119	-6.10	183.8	27.34	38.33	6,494	-3.47
	10	207.1	23.63	31.24	2,911	-4.80	166.5	26.99	39.18	7,064	-2.53

TABLE XVII.

RECUPERATIVE ENGINE COMPARISON—PLATE AND FIN RECUPERATORS.

	CERAMIC COUNTERFLOW		METAL TWO-PASS CROSS-COUNTERFLOW
PARTIAL ΔDOCS			
SFC	1.41	(EQUAL)	1.41
COST—$	−1.24		−2.04 (BEST)
WEIGHT—KG (LB)	−0.72 (−1.58) (BEST)		−0.56 (−1.23)
LENGTH—CM (IN.)	0.69 (−0.27)		−1.83 (−0.72) (BEST)
DIAMETER—CM (IN)	−1.32 (−0.52)		−2.39 (−0.94) (BEST)
TOTAL Δ DOC	−2.20		−3.52 (BEST)
OVERALL DOC/DOC*	0.9780		0.9648 (BEST)

TE86-4895

plate and fin recuperator was selected. The general engine outline is shown in Figure 31.

All recuperator and engine performance had been calculated and compared for the cruise condition (6096 m [20,000 ft] altitude 250 knot) where the majority of mission fuel is burned. It was necessary to calculate sea level performance for the best engine and recuperator combination so that a mission analysis could be made to calculate DOC. Allison supplied sea level engine cycle data to AiResearch, which they used to calculate sea level recuperator performance. Table XVIII shows the sea level and altitude performance details for the selected two-pass cross-counterflow metal plate and fin recuperator. Sea level effectiveness and pressure drop are significantly lower because of increased Reynolds number; however, only a small portion of mission fuel is burned at sea level conditions.

Engine Configuration

The recuperative engine that is shown in Figure 31 employs a six module metal two pass cross-counterflow recuperator. The core of each module is 28 cm (11.1 in.) long x 15 cm (6.1 in.) wide x 5 cm (2 in.) thick. Manifolding increases overall length to 38 cm (15.1 in.). The six modules are arranged so that the 15 cm (6.1 in.) sides form a hexagon with 27 cm (10.8 in.) inside diameter and are surrounded by a 49 cm (19.4 in.) diameter exhaust duct. Total recuperator

TABLE XVIII.

SEA LEVEL AND ALTITUDE RECUPERATOR PERFORMANCE TWO-PASS CROSS-COUNTERFLOW—METAL PLATE AND FIN.

INLET PRESSURE KG/CM² (PSIA)	AIRFLOW EACH OF 6 MODULES KG/SEC (LB/SEC)	INLET TEMPERATURE °C (°F)	OUTLET TEMPERATURE °C (°F)	EFFEC-TIVENESS %	ABSOLUTE PRESSURE DROP KG/CM² (PSI)	PRESSURE DROP RATIO ΔP/P
6096m (20,000 FT)						
AIR 7.03 (100.0)	0.135 (0.2979)	324 (616)	549 (1021)	60	0.31 (4.38)	0.0438 CORE
GAS 0.53 (7.54)	0.141 (0.3098)	699 (1290)	497 (926)		0.14 (1.98)	0.0263 CORE
						0.0303 MANIFOLDS
						0.1004 TOTAL
SEA LEVEL						
AIR 13.7 (194.2)	0.256 (0.5641)	393 (740)	631 (1168)	52.9	0.57 (8.04)	0.0414 CORE
GAS 1.17 (16.68)	0.258 (0.5693)	842 (1548)	632 (1169)		0.02 (0.25)	0.0151 CORE
						0.0129 MAINFOLDS
						0.0694 TOTAL

TE86-4896

weight including ducting is 35 kg (77 lb.). Material is modified nitride dispersed type 321 stainless steel convoluted and brazed with 982°C (1800°F) capability. The cores consist of 20 air passage layers and 21 gas passage layers interspersed. Exhaust gas makes one pass through the 5 cm (2 in.) dimension while compressor discharge air makes two passes through the 28 cm (11.1 in.) dimension. This recuperator provides a thermal effectiveness of 60% and a pressure drop of 10% at cruise.

The advanced technology recuperative engine features a two-shaft arrangement that permits considerable freedom in the matching of loads of differing torque versus speed characteristics to the same engine.

The engine, which has modular construction, incorporates a radial inlet housing integral with the accessory gearbox, a two-stage axial compressor with variable geometry, an impeller with radial diffuser, a single can combustor, a single-stage axial gasifier turbine, a two-stage axial free power turbine, a six module metal two pass cross-counterflow recuperator, and an electronic fuel control system.

In summary, inlet air passes through a radial inlet to the axial-impeller compressor. There it passes through variable inlet guide vanes, which can be used

to change engine airflow, and to an axial compressor and an impeller, where it is compressed. The compressed air passes from the impeller through a parallel wall radial vaned diffuser and is collected by a TiAl scroll. The compressor discharge air makes two passes through the 28 cm (11.1 in.) dimension of the recuperator core, where it is heated, and exhaust gas makes one pass through the 5 cm (2 in.) core. From the recuperator, the air flows through an H-188 Lamilloy®* combustor.

Fuel is mixed with the air and burned in the combustor to bring the temperature of the fuel/air mixture to 1538°C (2800°F). The hot gases are collected by an inlet scroll where the vanes direct the flow to the gasifier turbine. Sufficient power is extracted at this location to meet the requirements of the HP compressor and the oil pump system.

The discharge from the gasifier turbine is directed through an interturbine duct and vane arrangement at the power turbine. The vanes direct the gas flow

to the power turbine where power output is extracted for various applications. The flow from the power turbine is directed through the recuperator to the exhaust.

Regenerative Engine Cycle Evaluation

Cycle Analysis

A comprehensive parametric study was made to select the optimum regenerator-engine combination. Regenerator, as used here, refers to a rotating periodic-type heat exchanger. The following parameters were considered:

- o engine
  - o compression ratio, Rc--6, 8, 10, 12
  - o turbine rotor inlet temperature, RIT--1204°C, 1371°C, 1538°C (2200°F, 2500°F, 2800°F)

*Lamilloy is a registered trademark of the General Motors Corporation.

- o regenerator
  - o effectiveness, E%--60, 65, 70, 75, 80
  - o total pressure drop, $\Delta P/P$%-- 6, 8, 9, 10, 11, 12, 13, 14, 17, 20
  - o passage shape and size (hydraulic diameter--D_H)
  - o parameters--number of passages/in.^{2} (N), surface area/unit volume (ß), passage hydraulic diameter (D_H), wall thickness (S), and open area fraction (σ) all interrelated
  - o flow length (disk thickness)
  - o disk flow area and seal blockage area
  - o gas to airflow area split
  - o disk rotational speed
  - o heat transfer and friction coefficients
  - o number and arrangement of disks
  - o disk and seal materials
  - o size, weight, and cost

A total of 126 engine cycles were evaluated. Figure 32 shows a typical parametric analysis plot for the regenerative engine cycle. This trend of specific fuel consumption and specific horsepower as a function of cycle Rc and RIT is for a regenerator having a design effectiveness of 70%, and a total pressure drop of 13%. A description of the procedure for selecting the optimum regenerator engine combination follows.

Regenerator Configuration Analysis

Configuration

Allison selected an extruded ceramic heat transfer matrix with equilateral triangular passages formed by three sets of parallel walls intersecting at common points. Figure 33 is a photo of a similar matrix. This triangular matrix provides the strength required to resist radially inward pressure loads. An open area fraction of 0.715 was selected based on previous stress analysis that showed that such a matrix would withstand the pressure loads (Ref 2). Once the open area fraction has been selected, the relationship of four additional matrix variables is fixed, as shown in Table XIX.

TABLE XIX.

HEAT TRANSFER MATRIX PROPERTIES FOR EQUILATERAL TRIANGULAR PASSAGES WITH OPEN AREA FRACTION OF 0.715.

SURFACE VOLUME $b-FT^2/FT^3$	HYDRAULIC DIAMETER D_H—IN.	PASSAGES $IN.^2$ N	WALL THICKNESS σ—IN.
800	0.0429	299	0.0079
900	0.0381	379	0.0070
956*	0.0359	427	0.0066
1000	0.0343	468	0.0063
1800**	0.0190	1500	0.0035

* SELECTED FOR TILT ROTOR AIRCRAFT MINIMUM DOC

** TYPICAL SELECTION FOR GROUND APPLICATION FOR MINIMUM SPECIFIC FUEL CONSUMPTION (SFC)

TE86-4897

Surface-to-volume ratio was used as a primary variable in the heat transfer calculations. Analytical values of the dimensionless Colburn heat transfer factor (J) and Fanning friction factor (f), were used (Ref 3). These analytical values are judged to be representative of the experimental values that have been reported. As a function of Reynolds number (Re) for fully developed laminar flow, they are:

$$J \times Re = 3.51 = \text{constant}$$
$$f \times Re = 13.333 = \text{constant}$$

The regenerator disk parameters were fixed based on prior experience. Open area fraction was limited to a maximum of 0.715 for strength requirements. A minimum workable disk flow length or thickness of 7.6 cm (3 in.) was chosen because minimum length produces minimum disk volume and weight for a given effectiveness and pressure drop. Higher values of surface-area-to-volume ratio (β) compensate for shorter flow length. Gas-to-airflow area ratio was set at 1.2 to provide minimum specific fuel consumption. Disk rotational speed is 12 rpm.

With the disk parameters fixed, regenerator sizing involved finding the combination of surface-to-volume ratio (ß) and disk diameter (D) required to obtain the thermal effectiveness and pressure drop selected for each engine cycle. Higher surface area increases effectiveness and pressure drop while larger disk diameter increases effectiveness and decreases pressure drop. An allowance of 1% for engine internal duct pressure losses was included, based on experience. Regenerators were sized for the 6096 m (20,000 ft) altitude, 250 knot cruise condition since most mission fuel was burned at that condition. Reynolds number effects at altitude conditions required lower values of surface area to volume ratio and larger hydraulic diameter passages than those for sea level applications, as shown in Table XIX.

Rotating regenerators employ double-sided seals on both sides of the disks with a rubbing face seal on one side and a static leaf seal on the other. The seals are exposed to full engine pressure ratio. Allowance for seal leakage must be made in engine performance calculations. A seal leakage scaling equation, based on an established engine leakage data base, was used. This equation is scaled based on disk diameter, engine pressure ratio, disk speed, and disk thickness. The equation treats the rubbing wearface, static leaves, and carryover due to disk rotation separately. The equation is as follows:

$$L_2 = 0.3L_1 \frac{R_{c_2}}{R_{c_1}} \frac{D_2}{D_1} + 0.3L_1 \frac{R_{c_2}}{R_{c_1}} + 0.1L_1 \frac{R_{c_2}}{R_{c_1}} \frac{D_2}{D_1} + 0.3L_1 \frac{R_{c_2}}{R_{c_1}} \left(\frac{D_2}{D_1}\right)^2 \frac{N_2}{N_1} \frac{W_2}{W_1}$$

wearface leaf joints leaves carryover

where

- L = absolute leakage
- D = disk diameter
- R_c = compression ratio
- N = disk speed
- W = disk thickness
- 1 = base conditions
- 2 = new conditions

Two regenerator disks were selected to minimize engine length and height. Figure 34 shows how the disks contribute to engine length and height, yet provide

a compact package. Smaller disk diameters, provided by the use of two disks, allow the capability for a one piece extrusion eliminating cement joints. Two disks have the disadvantages of higher leakage, weight, and cost, which are important factors and would merit further study in a detailed design.

Materials and Cost

Current regenerator materials are adequate for the cruise-sized tilt-rotor aircraft because this application does not allow use of high regenerator inlet temperature. Regenerator inlet temperature is 769°C (1417°F) at the operating cruise condition. The regenerator disk would be extruded aluminum silicate, which is rated for 1093°C (2000°F) steady-state operation. The cold side seal would use a 0.06 thick 430SS platform with attached impregnated graphite wearfacing and Inco X750 seal leaves. The hot side seal would use an 0.08 thick Inco 625 platform with impregnated graphite rim wearface and plasma sprayed nickel oxide-calcium fluoride crossarm wearface with L605 cobalt alloy seal leaves. Regenerators with these materials have demonstrated good durability at 982°C (1800°F) and 4:1 pressure ratio in ground applications and are expected to be adequate for the selected cruise temperature of 769°C (1417°F) and 10:1 pressure ratio.

Cost estimates for several regenerator diameters were obtained from the disk and seal vendors supplying current parts for Allison engines. Curves were obtained from the cost data to provide costs for all sizes evaluated. Allowance was made for the proposed production rates. The sensitivity factors derived in Task I describe the effect of relevant engine and regenerator parameters on the tilt-rotor aircraft DOC. Figure 11 shows these sensitivity curves. The engine and regenerator parameters affecting DOC and their relative weights are as follows:

o SFC	46%
o cost	26%
o weight	12%
o length	9%
o height (or diameter)	7%
	100%

Direct Operating Cost Evaluation for Cycle Selection

The engine cycle was selected to provide minimum DOC at the cruise condition. The DOC sensitivity curves were used to obtain the separate factors for:

- o SFC
- o cost
- o weight
- o length
- o height (or diameter)

These separate factors were summed to obtain an overall DOC factor for each engine. Engine cost, weight, and length were calculated using inhouse equations for turbomachinery, gearbox, and accessories with regenerator values added. Regenerator weight and cost included values for covers, drives, and ducting. Figures 35 through 37 show plots of DOC versus engine R_c, regenerator effectiveness (E), and regenerator $\Delta P/P$. These plots show that minimum DOC is obtained when $R_c = 9.5$, $E = 69\%$, and $\Delta P/P = 13\%$. Calculations were extended to $\Delta P/P = 20\%$ but showed no tendency to optimize. Reductions in regenerator weight with increasing pressure drop were greater than the increases in engine size and weight necessary to maintain the required power. These results merit further study. It was decided to limit the regenerator pressure drop to 13% because the resulting axial disk loads act against the cold side seal and result in greater seal wear. The regenerator disks for the selected engine were 15.72 in. in diameter. The size of their cases relative to the engine is shown in Figure 34. Based on these considerations, the regenerative engine with $R_c = 10$, $E = 70\%$, and $\Delta P/P = 13\%$ was selected.

All regenerator and engine performances had been calculated and compared for the cruise condition (6096 m [20,000 ft] altitude, 250 knots) where the majority of mission fuel is burned. It was necessary to calculate sea level performance for the selected engine and regenerator combination so that a mission analysis could be made to determine actual DOC. Table XX shows both the sea level and altitude performance data for the selected regenerator. Sea level effectiveness and pressure drop are lower than at altitude because of increased Reynolds number. However, only a small portion of mission fuel is burned at sea level conditions. The Reynolds number effect also accounts for the selec-

tion of passages with larger hydraulic diameter for altitude conditions as opposed to ground applications as depicted in Table XIX. Leakages of 5.2% at 6096 m (20,000 ft) cruise and 5.5% at sea level 100% were calculated for the selected regenerator-engine combination.

Engine Configuration

The regenerative engine shown in Figure 34 is a two shaft engine. Air passes through a conventional inlet housing through variable inlet guide vanes and then through an axial/centrifugal rotor, where it is compressed. The compressed air passes from the impeller through a parallel wall radial vaned diffuser and is collected by a TiAl scroll. The compressor discharge air then passes through the high pressure side of either rotating ceramic regenerator disk where it is heated. From the regenerators, the air flows through an H-188 Lamilloy combustor.

Fuel is mixed with the air and burned in the combustor to bring the temperature of the fuel/air mixture to 1538°C (2800°F). The hot gases are discharged into a scroll where the vanes direct the flow to the gasifier turbine. Sufficient power is extracted at this point by the gasifier turbine to meet the requirements of the HP compressor and the engine and aircraft accessories.

The discharge from the single-stage gasifier turbine is directed through an interturbine duct and vane arrangement to the two-stage power turbine. The vanes direct the flow to the power turbine where the power output for various applications is extracted. The flow from the power turbine goes through the low pressure side of each of the regenerators to the exhaust.

The regenerative engine employs two rotating ceramic regenerator disks 40 cm (15.7 in.) in diameter and 8 cm (3 in.) thick. The disks are extruded aluminum silicate with 426 equilateral triangular holes per square inch and 0.02 cm (0.0066 in.) thick walls, resulting in 0.715 open area. Each hole has a 0.09 cm (0.036 in.) hydraulic diameter (inscribed circle). Regenerators optimized for altitude operation require larger holes than those for sea level operation where 0.05 cm (0.019 in.) hydraulic diameter is common. Each disk weighs 5.6 kg (12.4 lb).

TABLE XX.

SEA LEVEL AND ALTITUDE REGENERATOR PERFORMANCE CERAMIC TRIANGULAR PASSAGE MATRIX.

	INLET PRESSURE KG/CM² (PSIA)	AIRFLOW EACH OF 2 DISKS (LB/SEC)	INLET TEMPERATURE °C (°F)	OUTLET TEMPERATURE °C (°F)	EFFEC-TIVENESS %	ABSOLUTE PRESSURE DROP KG/M² (PSI)	PRESSURE DROP RATIO ΔP/P
6096m (20,000 FT)							
AIR	5.16 (73.4)	0.47 (1.027)	259 (499)	617 (1142)	70.0	54.56 (0.0776)	0.0011
GAS	0.58 (8.24)	0.48 (1.0598)	769 (1417)	447 (836)		604.95 (0.9116)	0.1189
							0.0100 DUCTS
							0.130 TOTAL
SEA LEVEL—MAXIMUM							
AIR	10.02 (142.6)	0.85 (1.8811)	322 (611)	653 (1207)	55.2	60.40 (0.0859)	0.0006
GAS	1.24 (17.7)	0.88 (1.9463)	921 (1690)	629 (1165)		755.13 (1.0740)	0.0681
							0.0100 DUCTS
							0.0787 TOTAL

TE86-4898

Compressor discharge flow is directed through one sector of the disk and turbine outflow through the remaining sector. The disk matrix absorbs heat from the turbine outflow, carries it to the other sector by rotation, and gives it up to the compressor discharge flow. The two flows are directed through the disk and kept separated by seals running against the disk faces.

The seals have sheet metal substrates with attached graphite and metal oxide wear facings sealing against the rotating disk and metal foil static sealing leaves sealing against the engine casing. A regenerator leakage of 5.2% at cruise was used for the selected design. The disk is driven by a surrounding ring gear joined to its outer diameter by a cast-in-place elastomer.

The entire regenerator system including a portion of engine case weight assignable to the regenerator is 30.6 kg (67.4 lb). The system provides a thermal effectiveness of 70% and pressure drop of 13% at cruise.

Wave Rotor Engine Cycle Selection

For the wave rotor engine cycle, cycle pressure ratios from 15 to 45 were studied along with turbine rotor-inlet-temperatures from 2200°F to 2800°F. Figure 38 shows the parametric cycle analysis trends of specific fuel consumption and specific horsepower for the range of cycle parameters invesitaged. The optimum wave rotor cycle occurs at Rc = 38 and RIT = 2800°F, as shown in Figure 39.

A possible arrangement of a wave rotor in-line engine using the Comprex system is shown schematically in Figure 40 and shown mechanically in Figure 41. The wave rotor in-line configuration provides an engine envelope that is streamlined and similar to an existing engine but somewhat longer and heavier with the addition of the wave rotor components. Because of the asymmetric inlet and outlet ducting of the wave rotor, the in-line configuration is best suited to centrifugal compressors and turbines where the swirl of the gases can be used to extract the mass flow at discrete locations around the periphery of the rotating components in ducts that can be matched to similar ducts on the wave rotor. Locations of the two combustors within a streamlined envelope configuration may be difficult because of the need to reroute air and combustion gas around the wave rotor. In order to keep the Comprex system into a compact configuration, the following techniques have been employed:

- o the two combustors are placed on the top and bottom of the Comprex system to maintain relative short duct connections
- o vaned diffusers are used as the main technique for rapid diffusion of existing flows to low velocities in order to shorten the connecting ducts
- o the use of short turning distances permits compact ducting arrangements for the wave rotor including the upstream and downstream inlets

The mechanical arrangement shows that air passes through the low pressure compressor (axial and centrifugal made from rapid solidification technology (RST) Al and TiAl forging, respectively) and the Comprex rotor (made from oxide dispersioned strengthened (ODS) Ni) before entering into the two combustors D_0 and D_1 at station 3. The combustor D_0 discharge gas (station 4) passes through the Comprex and from there to the power turbine (made from TiAl). The combustor D_1 exit gas at station 5 (with dilution if required) passes through

the low pressure turbine made from Ni_3Al (station 6) and is mixed with the Comprex discharge gas (station 7) before the power turbine (station 8).

The wave rotor engine is unique because the single stage LP turbine does not produce enough energy to drive the LP compressor under all operating conditions. A special gearbox located at the engine front is designed to transfer energy from the three-stage power turbine to the LP turbine for driving the LP compressor.

ENGINE CYCLE/CONFIGURATION SELECTION

Table XXI compares the optimum cycles for each of the 5 configurations investigated. Each of these cycles was optimized using relative direct operating cost as the figure of merit. A preliminary analysis was conducted to establish the feasibility of these five configurations.

TABLE XXI.
SECT OPTIMUM CYCLE COMPARISON.

	BASELINE	CONCENTRIC	NONCONCENTRIC	RECUPERATIVE	REGENERATIVE	WAVE ROTOR
R_c	14	25	30	13	10	36
RIT—°C (°F)	1204 (2200)	1538 (2800)	1538 (2800)	1538 (2800)	1538 (2800)	1538 (2800)
$W\sqrt{\theta}/\delta$	5.7	3.2	3.5	3.4	3.8	3.2
CRUISE SFC	0.412	0.330	0.327	0.306	0.306	0.33
WEIGHT—KG (LB)	116 (256)	56 (124)	63 (139)	105 (232)	102 (224)	85 (187)
OEM COST $	214,932	111,651	123,788	125,606	160,486	154,060
Δ DOC – %	BASE	16.8	15.3	14	11.6	11.6

TE86-4899

The design analysis of the concentric engine indicated that the bore stress in the ceramic HP turbine was prohibitive. Moving the HP spool out in the nonconcentric type configuration eliminated the requirement to pass shafting through the center of the high presure rotor, thus eliminating the bore stress problem.

A thorough analysis of the wave rotor type engine was not complete at the end of Task II. The initial investigation into the wave rotor indicated that the shaft power output type was unsuitable for gas turbine applications because of inherent low efficiency as compared to projected compressor efficiency for year 2000. On the other hand, the pressure exchanger type wave rotor (no shaft power output) is mechanically complex due to the required flow split ahead of the high pressure turbine. However, recent wave rotor analysis indicates that the shaft power output device can be made at least as efficient as that projected for year 2000 compressors, as illustrated in Figure 42. This figure shows that for corrected exit flows less than 0.41 kg/sec (0.9 lb/sec), the efficiency potential of the wave rotor exceeds that of the compressor efficiency assessment for year 2000. At least an additional 1% reduction in DOC would be realized based on the projected improvement in wave rotor performance. A more detailed study is required to fully assess the potential of wave rotors for year 2000 gas turbine applications.

Based on these analyses, the nonconcentric engine, recuperative engine, and regenerative engine were selected for system performance evaluation. The performance, component selection, dimensional data, for each selected configuration and reference engine are presented in Table XXII. Table XXIIA gives a detailed weight and cost breakdown of these three selected configurations. The engine cost and appropriate regenerator or recuperator costs are also tabulated in Table XXIIA.

TABLE XXII.
TASK III STUDY ENGINES—DEFINITION AND DATA SUMMARY

	BASELINE ENGINE	ADVANCED TECHNOLOGY ENGINES		
ENGINE IDENTIFICATION	CONCENTRIC CYCLE ENGINE	RECUPERATIVE CYCLE ENGINE	REGENERATIVE CYCLE ENGINE	NONCONCENTRIC CYCLE ENGINE
NO. SPOOLS L.P. COMPRESSOR H.P. COMPRESSOR H.P. TURBINE L.P. TURBINE POWER TURBINE	1 — CENTRIFUGAL AXIAL — AXIAL	1 — AXIAL/CENTRIF AXIAL — AXIAL	1 — AXIAL/CENTRIF AXIAL — AXIAL	2 AXIAL/CENTRIF CENTRIFUGAL RADIAL RADIAL AXIAL
IRP AT SLSS • R_s • RIT, °C (°F) • Wa, Kg/SEC (LB/SEC) • SHP, HP 6.1 KM (20000')	14 1204 (2200) 2.59 (5.7) 1000	13 1538 (2800) 1.54 (3.4) 1000	10 1538 (2800) 1.72 (3.8) 1000	30 1538 (2800) 1.59 (3.5) 1000
MAX CRUISE AT 463 Km/HR TAS (250 KTAS) • SHP • SFC (Δ SFC%)	582 0.412 (BASE)	580 0.306 (–25.7%)	580 0.306 (25.7%)	580 0.327 (–20.6%)
WEIGHT, Kg (LB) (Δ WEIGHT, %)	115.67 (255.0) (BASE)	105.05 (231.6) (–9.2%)	101.42 (223.6) (–12.3%)	62.91 (138.7) (–45.6%)
MAX LENGTH, CM (IN.) MAX HEIGHT, CM (IN.) TURB EXIT DIA, CM (IN.)	87.22 (34.34) 58.17 (22.90) 33.07 (13.02)	80.01 (31.50) 50.80 (20.00) 23.01 (9.06)	68.07 (26.80) 58.42 (23.00) 23.22 (9.14)	50.16 (19.75) 40.13 (15.80) 23.37 (9.20)
OEM COST, 1985 $ (Δ COST, %)	214,900 (BASE)	125,600 (–41.6%)	160,500 (–25.3%)	123,800 (–42.4%)
LP COMPRESSOR $W\sqrt{\theta}/\delta$ IN $W\sqrt{\theta}/\delta$ OUT RC ηAD	— — — —	— — — —	— — — —	3.5 0.7 7.0 0.870
HP COMPRESSOR $W\sqrt{\theta}/\delta$ IN $W\sqrt{\theta}/\delta$ OUT RC ηAD	5.69 0.57 14.0 0.784	3.4 0.36 13 0.835	3.8 0.54 10 0.858	0.7 0.2 4.7 0.802
HP TURBINE $W\sqrt{\theta}/\delta$ ηAD RPM Re	0.94 0.857 48450 4.01	0.67 0.90 61000 2.56	1.0 0.903 49900 2.17	0.3 0.89 72500 2.4
LP TURBINE $W\sqrt{\theta}/\delta$ ηAD RPM Re	— — — —	— — — —	— — — —	0.7 0.903 47500 2.0
POWER TURBINE $W\sqrt{\theta}/\delta$ ηAD RPM Re	3.45 0.885 29277 3.21	1.57 0.909 43900 4.49	2.0 0.912 38900 3.80	1.3 0.907 44550 5.5

TE86-4870

TABLE XXII A
ADVANCED ENGINES WEIGHT BREAKDOWN

ENGINE: Section	NONCONCENTRIC Wt-Lb	RECUPERATIVE Wt-Lb	REGENERATIVE Wt-Lb
Inlet/Fwd Support	7.12	3.66	4.34
LPC Rotor	6.81	—	—
LPC Housing	1.21	—	—
Scroll & Diff-LPC	12.14	—	—
HPC Rotor	1.64	6.77	7.44
HPC Housing	1.87	8.07	8.87
Scroll/Diffuser	2.98	6.37	8.67
Combustor & Hsg	7.38	24.32	17.21
HPT Rotor	1.06	5.08	6.31
HPT Housing	1.31	1.87	2.33
Interm. Turb Spt	—	5.02	5.41
LPT Rotor	1.88	—	—
LPT Housing	3.79	—	—
Power T Rotor	7.46	8.50	9.15
Power T Housing	9.88	6.65	7.16
Rear Brg Support	5.57	—	—
Block (½)	—	—	9.42
Regenerators (2) (with ½ block)	—	—	67.35
Recuperator	—	77.00	—
Exhaust Duct(s)	—	17.50	6.04
Controls	37.76	34.81	36.49
Acc Dr Gearbox	28.82	26.02	27.37
TOTAL WEIGHT	138.86	231.64	223.56
TOTAL MANUFACTURING COST	$123,788	$125,608	$160,486
RECUPERATOR/ REGENERATOR COST	—	$ 8,370	$ 30,280

V. TASK III. SYSTEM PERFORMANCE EVALUATION

The purpose of the Task III effort was to provide a system performance evaluation of the Task II selected advanced technology engine configurations against the Task I selected baseline or state-of-the-art engine.

The nonconcentric, recuperative, and regenerative engines were evaluated using the Allison mission analysis procedures and ground rules established in Task I. Each study engine/tilt-rotor aircraft combination was sized to meet the specified design mission. All engines were sized for the cruise rate of climb requirement. The unity size engines have the same shaft horsepower (shp) at this cruise sizing condition so the critical weight per unit horsepower characteristic for each engine will trend the weight number shown in Table XXII. The mission analysis provided the following:

- o aircraft weight, mission fuel, and DOC breakdowns
- o engine/aircraft sizing information
- o aircraft acquisition cost, fuel burned, and TOGW comparisons
- o DOC comparisons (primary figure of merit)

MISSION FUEL

Reductions in mission fuel burned are shown relative to the baseline engine powered tilt-rotor aircraft in Figure 43. The fuel burn reductions shown in Figure 43 are a result of the maximum cruise power specific fuel consumption (SFC) characteristics summarized in Table XXII. Table XXIII shows that 86% of the mission fuel is consumed at a power setting that is approximate to maximum cruise at the cruise altitude and velocity. The fuel burn reductions indicated in Figure 43 are 30.7% for recuperator, 30.5% for regenerator, and 30.1% for nonconcentric. All three advanced technology engines achieved the fuel burn reduction goal of 30%.

AIRCRAFT WEIGHT

Aircraft weight breakdown for each study engine/tilt rotor aircraft is shown in Table XXIV. The advanced engine weight varies from 2.8% for the nonconcentric engine to 4.7% for the recuperative engine whereas the baseline engine

TABLE XXIII.
MISSION FUEL BREAKDOWN COMPARISON

ENGINE I.D.	BASELINE ENGINE		RECUPERATIVE CYCLE ENGINE		REGENERATIVE CYCLE ENGINE		NONCONCENTRIC CYCLE ENGINE	
	Kg (LB)	%	Kg (LB)	%	Kg (LB)	%	Kg (LB)	%
I. MISSION PHASE								
START AND WARM-UP ALLOWANCE	1.36 (3)	0.3	0.91 (2)	0.2	0.91 (2)	0.2	0.91 (2)	0.2
•TAKEOFF AND TRANSITION ALLOWANCE	15 (32)	2.9	10 (22)	2.8	10 (23)	2.9	10 (22)	2.8
•CLIMB @ 333.3 Km/HR EAS (180 KEAS)	52 (115)	10.2	38 (84)	10.7	39 (87)	11.1	36 (80)	10.1
•CRUISE @ 6.1 Km/463 Km/HR TAS (20,000 FT/250 KTAS)	273 (602)	53.2	186 (411)	52.6	185 (408)	52.2	191 (423)	53.4
•TRANSITION AND LAND ALLOWANCES	12 (27)	2.4	9 (20)	2.6	10 (21)	2.7	8 (18)	2.3
SHUT-DOWN ALLOWANCES	0.91 (2)	0.2	0.45 (1)	0.1	0.45 (1)	0.1	0.45 (1)	0.1
FUEL BURNED	354 (781)	69.2	245 (540)	69.0	246 (542)	69.1	247 (546)	68.9
•RESERVES	157 (347)	30.8	110 (242)	31.0	109 (241)	30.8	112 (246)	31.1
TOTAL FUEL	511 (1128)	100.0	355 (782)	100.0	355 (783)	100.0	359 (792)	100.0
II. ENGINE POWER								
INTERMEDIATE RATED POWER	67 (148)	13.1	48 (106)	13.6	50 (110)	14.0	46 (102)	12.9
MAX CONTINUOUS (APPROX)	442 (975)	86.4	305 (673)	86.0	304 (670)	85.6	312 (687)	86.7
GROUND IDLE	2.27 (5)	0.5	1.36 (3)	0.4	1.36 (3)	0.4	1.36 (3)	0.4
TOTAL	512 (1128)	100.0	355 (782)	100.0	355 (783)	100.0	359 (792)	100.0

TE86-4873

weight is 5.2%. The fuel weight is in the range of 8.3% to 8.8% for the advanced engines and 11.1% for the baseline engine. Figure 44 shows reductions in TOGW of 7.7% for the recuperative engine, 8.0% for regenerative engine, and 11.5% for the nonconcentric engine compared to the baseline engine. The nonconcentric engine has the largest reduction in TOGW because it has the lowest engine weight of the advanced engines. For this mission, all three advanced engines had fuel burn reductions of ≈ 30%.

COST COMPARISONS

With the fuel and TOGW trend variations established for the advanced engines, aircraft acquisition cost trends shown in Figure 45 will track with the engine original equipment manufacturer (OEM) cost characteristics listed in Table XXII. Aircraft cost equals airframe plus engine acquisition cost, where airframe cost is a function of airframe weight. The reductions in direct

TABLE XXIV.
AIRCRAFT WEIGHT BREAKDOWN COMPARISON

ENGINE I.D.	BASELINE ENGINE			RECUPERATIVE CYCLE ENGINE			REGENERATIVE CYCLE ENGINE			NONCONCENTRIC CYCLE ENGINE		
	Kg	(LB)	%	Kg	(LB)	%	Kg	(LB)	%	Kg	(LB)	%
BARE ENGINE WEIGHT	239	(528)	5.2	200	(442)	4.7	193	(426)	4.5	114	(252)	2.8
PROPULSION GROUP (LESS ENGINE WEIGHT)	936	(2063)	20.3	853	(1880)	20.0	847	(1868)	19.9	793	(1748)	19.4
STRUCTURE GROUP	1014	(2236)	21.9	973	(2144)	22.8	971	(2140)	22.9	952	(2098)	23.3
FIXED EQUIPMENT	967	(2131)	20.9	939	(2070)	22.1	937	(2066)	22.1	925	(2040)	22.6
•MFG EMPTY WEIGHT	3156	(6958)	68.3	2965	(6536)	69.6	2948	(6500)	69.4	2784	(6138)	68.1
USEFUL LOAD	224	(494)	4.9	219	(482)	5.1	219	(482)	5.1	218	(480)	5.3
•OPERATING EMPTY WEIGHT	3380	(7452)		3184	(7018)		3167	(6982)		3002	(6618)	
PAYLOAD (8 PASS. @ 91 KG (200 LB) EA	726	(1600)	15.7	726	(1600)	17.0	726	(1600)	17.1	726	(1600)	17.8
•ZERO FUEL WEIGHT	4106	(9052)		3910	(8618)		3893	(8582)		3728	(8218)	
FUEL (USABLE)	512	(1128)	11.1	355	(782)	8.3	355	(783)	8.4	359	(792)	8.8
•TOGW	4618	(10,180)	100.0	4265	(9400)	100.0	4248	(9365)	100.0	4087	(9010)	100.0

TE86-4874

operating cost (DOC) for the advanced engines are shown in Figure 46 for $1/gal and $2/gal fuel cost. The direct operating cost (DOC) trends shown in Figure 46 track with the aircraft acquisition cost trends. This conclusion is confirmed by examination of the DOC cost breakdown comparison tabulated in Table XXV. The fuel and oil effect on ΔDOC for this mission is -2% for all advanced engines. The two largest cost components, insurance and depreciation, are direct functions of aircraft acquisition cost. A more detailed breakdown for DOC is shown in Table XXVI for the baseline and nonconcentric engine. Only 22% of the advanced engine/tilt rotor aircraft DOC was influenced by engine characteristics.

ENGINE SELECTION

Table XXVII presents a summary of the mission results. The nonconcentric engine was selected because it has the greatest reduction in DOC relative to the baseline. The reduction in DOC is 16.5% for $1/gal fuel cost and 17.4% for $2/gal fuel cost. Figure 47 shows a general arrangement of the nonconcentric engine. Table XXVIII provides a cycle summary of this engine at sea level and at the 20,000 ft altitude cruise condition.

TABLE XXV.
DOC COMPARISON—$/BLK HR

DOC @ 0.26 $/L (1.00 $/GAL) AND 1000 HR/YEAR

ENGINE ID	BASELINE	RECUPERATIVE CYCLE ENGINE	REGENERATIVE CYCLE ENGINE	NONCONCENTRIC CYCLE ENGINE
FUEL AND OIL	80	56	56	56
INSURANCE	359	308	319	296
A/C MAINTENANCE	235	215	214	203
ENGINE MAINTENANCE	91	87	89	78
DEPRECIATION	357	304	315	293
FLIGHT CREW	63	63	63	63
TOTAL =	1185	1033	1056	989
(Δ DOC, %)	(BASE)	(−12.8%)	(−10.9%)	(−16.5%)

TE86-4872

TABLE XXVI
DOC BREAKDOWN—$/BLK HR

0.26$/L (1.00 $/GAL) AND 1000 HR UTILIZATION

	BASELINE POWERED TILT-ROTOR			NONCONCENTRIC POWERED TILT-ROTOR		
	AIRCRAFT +	ENGINE →	TOTAL A/C + ENG	AIRCRAFT +	ENGINE →	TOTAL A/C + ENG
FUEL AND OIL	—	79.77 (6.7%)	79.77	—	56.06 (5.7%)	56.06
INSURANCE	279.36 (23.6%)	79.87 (6.7%)	359.23	255.57 (25.8%)	40.25 (4.1%)	295.82
AIRCRAFT MAINTENANCE	235.32 (19.8%)	—	235.32	203.14 (20.5%)	—	203.14
ENGINE MAINTENANCE	—	91.31 (7.8%)	91.31	—	78.41 (7.9%)	78.41
DEPRECIATION	274.37 (23.2%)	82.01 (6.9%)	356.38	251.00 (25.4%)	41.34 (4.2%)	292.34
FLIGHT CREW	63.00 (5.3%)	—	63.00	63.00 (6.4%)	—	63.00
TOTALS =	852.05	332.96	1185.01	772.71	216.06	988.77
(%TOTAL DOC)	(71.9%)	(28.1%)	(100%)	(78.1%)	(21.9%)	(100%)

VS85-1297

TABLE XXVII
TASK III SUMMARY OF MISSION RESULTS

ENGINE IDENTIFICATION	BASELINE ENGINE	RECUPERATIVE CYCLE ENGINE		REGENERATIVE CYCLE ENGINE		NONCONCENTRIC CYCLE ENGINE	
TOGW SHP/ENGINE @ IRP SLSS ROTOR DIAMETER	4618 Kg (10,180 LB) 1035 HP 6.95M (22.8 FT)	4264 (9400) 955 6.67 (21.9)	(−7.7%)	4248 (9365) 950 6.64 (21.8)	(−8.0%)	4087 (9010) 900 6.52 (21.4)	(−11.5%)
•HOVER R OF C CAPABILITY @ 0.61 Km/0 KM/HR TAS/ISA +10°C IRP-AEO (2000 FT/0 KTAS/ISA + 50°F IRP-AEO)	357 M/MIN (1170 FPM) (0 FPM REQ'D)	360 (1180)		347 (1140)		326 (1070)	
•OEI R OF C CAPABILITY @ 0.30 Km/138.9 Km/HR TAS/ISA +20°C (1000 FT/75 KTAS/ISA +68°F) 30 MIN POWER - OEI	140 M/MIN (460 FPM) (150 FPM REQ'D)	145 (480)		140 (460)		113 (370)	
•CRUISE R OF C CAPABILITY @ 6.1 Km/463 Km/HR TAS/ISA (20,000 FT/250 KTAS/ISA) MAX CONTINUOUS POWER	91 M/MIN (300 FPM) (ENGINE SIZING PT)	91 (300)		91 (300)		91 (300)	
TOTAL FUEL (MISSION + RESERVES) BLOCK FUEL	512 KG (1128 LB) 354 KG (781 LB)	355 (782) 245 (541)	(−30.7%)	355 (783) 246 (543)	(−30.5%)	359 (791) 248 (546)	(−30.1%)
ENGINE ACQ COST (ONE) TOTAL AIRCRAFT ACQ COST	$332,800 $2.99 MILLION	179,700 2.56	(−14.4%)	228,600 2.66	(−11.0%)	167,700 2.46	(−17.7%)
DOC @ 0.26 $/LITER (1.00 $/GAL) AND 1000 HR	1185 $/BLK HR	1033	(−12.8%)	1056	(−10.9%)	989	(−16.5%)
DOC @ 0.53 $/LITER (2.00 $/GAL) AND 1000 HR	1264 $/BLK HR	1087	(−14.0%)	1111	(−12.1%)	1044	(−17.4%)

TE86-4871

For the nonconcentric engine, the effects of SFC, weight, maximum envelope length, maximum envelope height, and OEM cost on TOGW and DOC was determined. Figure 48 indicates engine specific fuel consumption (SFC) to have the largest effect on direct operating cost (DOC) followed by original equipment manufacturer (OEM) cost. Changes in envelope dimension are shown to have a relatively small effect on DOC with respect to a 10% change in either length or height requirements. The TOGW and DOC sensitivity levels developed for the advanced technology engine in Task III are significantly lower (30 to 60%) than those obtained from the baseline or current technology engine in Task I (see Figures 11 and 12).

In addition to the sensitivities developed with respect to changes in engine characteristics, DOC sensitivity to variations in fuel cost and aircraft utilization rate is shown in Figure 49 for the nonconcentric engine powered tiltrotor. These data indicate significant reductions in DOC for the increased utilization rate (1000 to 2000 hr/year) and a much larger influence on DOC for increased fuel cost at the higher utilization level.

TABLE XXVIII.
NONCONCENTRIC ENGINE CYCLE SUMMARY

	SEA LEVEL STATIC, STANDARD DAY	20,000 FT/250 KTAS MAXIMUM CRUISE
OVERALL		
SHP	1000	580
SFC	0.352	0.327
RIT (°F)	2800	2600
$Ro/_A$	30	32.6
LP COMPRESSOR		
$W\sqrt{\theta}/\delta$	3.5	3.7
Rc	7.0	7.4
ηAD	0.870	0.861
HP COMPRESSOR		
$W\sqrt{\theta}/\delta$	0.7	0.7
Rc	4.7	4.8
ηAD	0.802	0.802
HP TURBINE		
$W\sqrt{\theta}/\delta$	0.3	0.3
Re	2.4	2.4
ηAD	0.890	0.89
LP TURBINE		
$W\sqrt{\theta}/\delta$	0.7	0.7
Re	2.0	2.0
ηAD	0.903	0.903
POWER TURBINE		
$W\sqrt{\theta}/\delta$	1.3	1.3
Re	5.5	6.5
ηAD	0.907	0.904
TOTAL CHARGEABLE COOLING & LEAKAGE	5.3%	5.3%
TOTAL PRESSURE DROP LOSS	15.9%	16.8%

TE86-6560

VI. TASK IV. SMALL ENGINE COMPONENT TECHNOLOGY PLAN

The main objective of Task IV was to identify the technology requirements and provide a technology plan for year 2000 advanced small engine components. This section describes a technology plan for the selected advanced non-concentric engine, as shown in Figure 47. This engine achieves significantly reduced specific fuel consumption (SFC) levels by combining high cycle pressure ratio and high turbine inlet temperature in a three-spool configuration. The engine configuration offers advantages with regard to aerodynamics, flow path dimensions, bore stresses, a simple accessory arrangement, and reduced seal and bearing diameters.

Based on the Task III trade-off study, a list of the key technology requirements for the nonconcentric engine is given in Table XXIX, along with its direct operating cost (DOC) payoff. The nonmetallic structure results in a 7.0% reduction in DOC because it allows the turbine to operate at 1538°C (2800°F) rotor inlet temperature (RIT). A 2.5% improvement in DOC occurs due to the use of the uncooled turbine. Advanced aerodynamics required for year 2000 in order of priority are turbine, compressor, and combustor. Bearings technology is required for increased reliability and durability. Technology plans for each of these areas will be described in this section.

TABLE XXIX.
NONCONCENTRIC ENGINE ADVANCED TECHNOLOGY REQUIREMENTS.

	REQUIREMENT	DOC PAYOFF
CERAMICS	2800°F	7.0%
	UNCOOLED TURBINES	2.5%
TURBINE	YEAR 2000 EFFICIENCY	2.8%
COMPRESSOR	YEAR 2000 EFFICIENCY	2.3%
COMBUSTOR	IMPROVE PATTERN FACTOR FROM 0.2 TO 0.12	1.5%
BEARINGS	INCREASED RELIABILITY	
	INCREASED DURABILITY	—

CERAMICS TECHNOLOGY PLAN

Significant improvements in the performance characteristics of advanced gas turbine engines are directly related to the development of high temperature materials and components. Current Ni based superalloys used in rotating and static high temperature structures have limitations due to high fabrication cost, low strength at elevated temperatures, high strategic materials content (cobalt and chromium), and added complexity for required air cooling. Extensive work is being performed on the development of advanced structural ceramics that offer numerous potential benefits (high temperature strength, low density, and no strategic materials content). While the potential advantages offered by the incorporation of ceramics in advanced gas turbine engines are attractive in a variety of components, including ceramic combustors, regenerators, plenums, vanes, and insulating members, the maximum benefits are realized in the high pressure (HP) radial turbine rotor. The use of advanced ceramic materials in the HP radial turbine rotor application offer significant improvements in performance and fuel consumption by allowing uncooled operation at turbine inlet temperatures of 2800°F and anticipated life capability in excess of 1000 hrs. However, this also is the highest risk component due to the severe mechanical and thermal operating environment. While considerable progress has been achieved on the use of structural ceramic components in gas turbine engines, a significant effort is required for successful application of ceramics to the HP rotor in the SECT engine. The objectives of the proposed program include definition and evolution of ceramic material systems and rotor fabrication techniques capable of high speed operation at temperatures of 2800°F, which demonstrate improved toughness/impact resistance, reduced property variability, increased reliability, and life capability in excess of 1000 hrs. The approaches required to achieve these objectives include material and component evolution/characterization, ceramic/ceramic and ceramic/metal interface and compatibility definition, nondestructive flaw detection techniques development, and component rig/engine environment testing and evaluation. The ceramic technology programs are shown in Figure 50.

Material Development and Characterization

The primary candidate monolithic ceramic materials for use in advanced heat engines are silicon carbide (SiC), silicon nitrade (Si_3N_4), and partially

stabilized zirconia (PSZ). The fracture strength of these materials as a function of temperature is shown in Figure 51. While the PSZ and Si_3N_4 materials have higher room temperature strengths than SiC, PSZ and Si_3N_4 suffer degradations in strength and susceptibility to oxidation at temperatures above 1000-1200°C. The SiC retains its room temperature properties to approximately 1500°C.

A number of ceramic suppliers are actively pursuing the development of sintered Si_3N_4, which features improved elevated temperature strength characteristics. Kyocera has a developmental Si_3N_4 material (SN-270), currently available only in test bar form, that maintains a strength of 100 $lb/in.^2$ (ksi) at a temperature of 1400°C. SiC and Si_3N_4 are considered prime monolithic ceramic material candidates for application in the severe operating environment (2800°F uncooled) of the HP rotor in the SECT engine. Allison has had extensive experience and successful test results with both SiC and Si_3N_4 complex geometry components produced by a variety of fabrication techniques (injection molding, slip-casting, and isostatic pressing) for the CATE and advanced gas turbine (AGT) 100 programs.

However, current monolithic ceramics have a major limitation-inherent brittleness that can lead to catastrophic failure. This limitation is a major concern for high speed rotating components, particularly for application to manrated advanced gas turbine engines.

To address the material limitations of both metallic superalloys and monolithic ceramics, a variety of composite materials systems are being evaluated. These materials (e.g., carbon/carbon, SiC/SiC, and SiC/glass-ceramic) have demonstrated improvements in fracture strength, thermal shock resistance, fracture roughness, and strain tolerance. Carbon/carbon materials, while attractive for extremely high temperature applications, are limited by a lack of oxidation resistance and are totally dependent on advanced protective coatings. Since these coatings consist of a thick monolithic ceramic (e.g., SiC), this material system as applied to many component structures suffers the same short-comings as silicon-based monolithic ceramics. The most attractive composite materials are ceramic/ceramic systems that use silicon carbide as a reinforcing fiber.

During the last decade, an extensive ceramic composite materials development effort has been conducted using high-modules SiC Nicalon continuous fiber in low modulus glass or glass-ceramic matrices. The first generation of these materials was developed using borosilicate glass matrix. Subsequently, a family of more refractory composite materials was developed based on Corning lithium-aluminosilicate (LAS) glass-ceramic matrix. Both United Technology Research Center (UTRC) and Corning Glass Works (CGW) have been actively developing SiC fiber reinforced/LAS composite systems. However, refractory glass-ceramic composites experience rapid increases in the matrix viscosity at temperatures in excess of 1250°C, resulting in the fiber/matrix debonding and loss of component structural integrity. This temperature limitation of current SiC/glass-ceramic materials restricts the maximum component temperature to approximately 1200-1300°C, precluding the application of this material to the extreme thermal conditions that are required of the SECT HP turbine rotor.

SiC/SiC composites are commercially available from Amercom in the USA and SEP (Societe Europeenne de Propulsion) in France. Amercom is in a preliminary stage of development of these composites while SEP is currently marketing both one-dimensional and multidimensional composites. This material uses Nicalon SiC fiber reinforced in SiC matrix. The fibers are coated with up to four layers of chemical vapor deposition (CVD) SiC coating. The material is toughened by developing a weak interfacial bond between the SiC fiber and the first SVD SiC layer. The room temperature strength of the 0/0 orientation SEP CERASEP SiC/SiC material is about 62,000 lb/in.^{2}, which decreased to 35,000 lb/in.^{2} at temperatures of 1250-1500°C. This behavior is consistent with the expected behavior of Nicalon fiber, whose properties are thought to degrade approximately 1250°C. Unlike SiC/borium magnesium aluminosilicate (BMAS) ceramic composite where the matrix viscosity increases rapidly over 1250°C, SiC/SiC composites appear to retain reasonable strength levels up to 1500°C. The room temperature strength of 0/0 orientation after 100 hrs of isothermal exposure in air at 1500°C was 33,000 lb/in.^{2}.

The Nicalon SiC fibers are thought to consist of microcrystalline beta silicon carbide, graphite, and amorphous silica, but they may also have homogeneous structure. Upon heating above 1250°C, the fibers lose carbon monoxide and undergo coarsening of the silicon carbide grains. This quickly leads to brittleness and loss of strength.

To address this temperature limitation, Defense Advanced Research Projects Agency (DARPA) is conducting the advanced ceramics based on polymer processing program at Dow Corning. The goal of this program is the development of an economical, improved SiC fiber from a domestic supplier with higher strengths, fewer impurities, and a higher temperature capability than current fibers. While these fibers are currently under development and not commercially available, it is anticipated that future ceramic/ceramic composites will feature significant improvements in strength, toughness, and maximum use temperature.

A complete characterization of the mechanical, physical, and chemical properties of candidate ceramic materials is required to obtain structurally sound ceramic turbine components. This program consists of five subtasks:

- o generation of material properties, including thermal expansion, thermal conductivity, specific heat, elastic modulus, Poisson's ratio, and strength characteristics, required to employ a linear elastic probabilistic approach to structural design.
- o generation of time dependent properties, including thermal fatigue, creep, and crack propagation characteristics, with emphasis on the probabilistic nature of these properties.
- o evaluation of environmental effects, including oxidation, hot corrosion, and erosion, that could cause property degradation of candidate materials during long-term use.
- o development of the relationship between material structure and mechanical properties with special emphasis on establishing the size, type, and distribution of strength limiting defects.
- o development of a high resolution inspection technique to detect critical size defects in candidate ceramic materials.

Ceramic/Ceramic and Ceramic/Metal Interactions and Compatibility

A critical element required for the successful application of ceramics and ceramic composites is an understanding of the compatibility of ceramic/ceramic and ceramic/metal interfaces and the possible interations between these materials. While little published literature exists on this phenomenon pertaining strictly to ceramic composites, this class of materials will exhibit

much of the same behavior and problem areas associated with monolithic structural ceramics. The high temperature operation of the ceramic components required to use full material capability can result in wear, adhesion, and interactions with adjacent structures, both metallic and nonmetallic. Garrett in the Ceramic Gas Turbine Engine Program used both compliant layers (HS-25) and lubricants (CoO) to minimize contact loading and reactions between reaction-bonded silicon nitride and other materials. Allison has successfully used both compliant layers (L605) and high temperature lubricants (boron nitride) in the CATE program for the attachment between the SiC turbine blade and the turbine wheel. The L605-BN combination demonstrated uniform loading and prevented reactions during spin testing to 2500 cycles. The high temperature of the ceramic may also create problems for secondary metal components. The temperature of the ceramic often exceeds the temperature capability of the metal, and the close proximity of the hot ceramic can cause unacceptable thermal gradients. Thermal barrier materials will be used at strategic locations, both for ceramic/ceramic and ceramic/metal interfaces. Candidate thermal barrier materials need to have low thermal conductivity, adequate strength, compatible thermal expansion, and the capability of being produced in proper sizes and shapes. Thermal barrier materials currently being developed and used are zirconia, zircon, mullite, and cordierite.

One of the configurations that will be considered for the HP turbine rotor involves the use of a monolithic ceramic hub section for strength and fabricability and a ceramic composite blade section for increased fracture toughness and impact resistance. Considerable effort is required to identify and characterize the optimum joining technique for attaching the monolithic hub to the composite blade structure. Various methods suitable for this attachment include brazing, high temperature glass bending, diffusion bonding, and hot isostatic pressing. Evaluation of the attachment joint would include specimen testing, subcomponent element testing, and characterization and spin testing of the full scale hardware.

Nondestructive Evaluation

Since ceramic materials are highly probabilistic in nature, design stresses are very sensitive to material property variability. An extensive quality

assurance program is therefore essential to the successful use of ceramic material in gas turbine engines. This program has two primary objectives:

- o reduction of property variability
- o early rejection of defective components

There are two distinct types of microstructural defects that control ceramic component performance in high reliability applications. The first type of defect is small in degree but very large in extent, i.e. variations in chemistry, grain size, and density. Such defects significantly affect both thermal and elastic properties as well as strength-related characteristics. The second type of defect is large in degree but very small in extent i.e., cracks, pores, and inclusions in the size range below 100 microns. Such defects primarily control material strength. In view of (1) the limitations associated with available quality assurance measures and (2) the high levels of reliability required in a commercial 1000 hr gas turbine engine, it is clear that more sensitive nondestructive evaluation (NDE) techniques are required.

Normal nondestructive techniques can be used to find gross cracks, voids, and inclusions. The techniques used are well known and require little adaptation for use with ceramic materials. However, the resolution limits of these techniques are above the critical flaw size (10-100 microns) for ceramic materials. Therefore, inspection techniques with increased resolution are required. The following NDE techniques will be investigated: ultrasonic velocity, reflective ultrasound, scanning photoacoustic microscopy, and X-ray microradiography.

Rig/Engine Environment Testing

For the successful application of ceramic components in advanced gas turbine engines, particularly in the severe operating conditions of the SECT HP turbine rotor, testing must be conducted on components that represent a production manufacturing process and a corresponding design for which analysis predicts an acceptable reliability level. However, defects as small as 20 microns can control the material critical strength. No existing NDE technique can reliably detect such flaws. Therefore, proof testing is required to identify flawed components and to qualify rotors for subsequent engine testing until advanced

methods are available. For the SECT HP rotor, the following rig qualification tests will be conducted:

- o spin testing at room and elevated temperature
- o cold flow rig testing
- o hot flow rig testing
- o vibration bench testing
- o thermal shock testing (fluidized bed)

Engine testing and evaluation will be conducted on the SECT HP rotors to characterize performance, fuel consumption, component efficiency, reliability, life characteristics, and verification of design/analysis methodology. An engine test program with incrementally increasing turbine inlet temperature will be conducted to capitalize on current ceramic materials technology and to advance the state of the art with ceramic components. This approach permits early introduction of ceramic components into the baseline program and yields an improved gas turbine engine capability in the latter part of the program.

AXIAL TURBINE TECHNOLOGY PLAN

The inlet equivalent flow rates of the small axial flow turbines, indentified from the SECT trade studies, ranged from 0.7 to 2.4 lbm/sec. Axial flow turbines of this physical size exhibit degraded efficiency levels when compared to their larger counterparts. This characteristic is shown by Figure 52, which shows a simple correlation of current state-of-the-art overall turbine efficiencies in terms of inlet equivalent flow rate. This performance trend can be attributed to the inability to affect a true aero/mechanical scale in these smaller machines. This trend is due in part to fabrication constraints and manufacturing tolerances in addition to lower Reynolds numbers and absence of advanced analysis tools that accurately model the more sophisticated flow fields in these small blade rows.

The turbine efficiency goals established for the SECT program are also presented in Figure 52. This efficiency trend curve denotes the placement of the axial flow power turbine incorporated in the optimum nonconcentric engine configuration. The year 2000 turbine aero technology curve reflects a substantial improvement in the efficiency characteristic as the turbine inlet equivalent

flow rate (physical size) was reduced. The SECT program aero goal reflects a 3.3% increase in efficiency for the power turbine as compared to current state-of-the-art technology. The achievement of the SECT turbine efficiency goal will be realized through a variety of technology advancements. A major portion will be achieved through significant advancements in the area of turbine aerodynamics. Other performance improvements will be derived from technology areas such as computational fluid mechanics, material science, casting technology, ceramics, and innovative mechanical design concepts.

A brief aerodynamic description of the two stage axial flow power turbine for nonconcentric engine configuration, discussion of the various technology areas that will contribute toward the achievement of the SECT year 2000 turbine efficiency goals, and a description of the various turbine aero key technology programs are presented in the following sections.

Power Turbine Description

The power turbine for the selected SECT engine is a two stage axial flow design. The aerodynamic design point for the power turbine is tabulated below:

o inlet equivalent flow rate, $W\sqrt{\theta_{cr}}\varepsilon/\delta$	1.31 lbm/sec
o total/total expansion ratio, R_{eTT}	5.5
o overall equivalent work, $\Delta h/\theta_{cr}$	45.6 Btu/lbm
o rotational speed, N	44550 rpm
o total/total efficiency, n_{TT}	90.7%

The power turbine has an average stage load coefficient ($gJ\Delta h/U_m 2$) of 1.62 and an average flow coefficient (V_x/U_m) of 0.44, at aero design point conditions. At this same match point, the power turbine has an exit Mach number of 0.42 and 19 degrees of exit swirl (measured from axial) in a direction opposite to rotation. The last blade has an exit AN^2 (annulus area x rotational speed squared) value of 5.6×10^{10} $in.^2$ rpm^2 and hub/tip diameter ratio of 0.66. The power split ratio between the power turbine first and second stage is 51/49.

Technology Areas

The efficiency levels demonstrated for large axial flow turbines cannot be maintained for the small size turbines identified in the SECT program. This is due to the inability to maintain aerodynamic similarity in such parameters as inlet turbulence level, endwall boundary layer thicknesses, and Reynolds number. Fabrication constraints and manufacturing tolerances prohibit the scaling of physical parameters such as airfoil thickness/chord ratio, trailing edge thickness, fillet radii, blade tip clearances, and surface roughness. As a consequence, small axial flow turbine blading generally has higher trailing edge blockages, lower aspect ratios, higher maximum thickness/chord ratios, and higher rip clearance/blade height ratios than larger counterparts.

In order to identify the areas of technology that will provide the higher payoffs, an assessment of the various sources of loss was analytically determined for the baseline SECT power turbine assuming current state-of-the-art design technology. This study was conducted using the performance model of Kacker and Okapuu. A breakdown of the turbine losses is illustrated in Figure 53. The predominate source of aerodynamic inefficiency arises from secondary flow losses (45%), followed by profile losses (25%) and shrouded blade tip clearance (22%) losses. The magnitude of the various losses in terms of a total pressure loss coefficient (ω) is shown in Figure 54. The cross-hatched area denotes the goal reduction in the various loss mechanisms to be achieved by the SECT key technology programs. The attainment of these loss reductions will enable the small axial flow power turbine to meet the SECT goal efficiency.

Approach/Technology Plan

The proposed technology programs for the axial turbine are shown in Figure 55. This series of programs includes both experimental and analytical efforts. These programs systematically address aero design concepts that offer high potential for the reduction of secondary, profile, and tip clearance losses. In addition, certain tasks will provide data for the critical verification of 3-D viscous flow analysis tools. A discussion of each program follows.

Vane Tip Endwall Mechanical Sculpturing

Stator endwall contour geometries that are axisymmetric about the engine centerline have been experimentally shown to be an effective method of reducing stator secondary flow losses. Stator tip contours of this description are widely used in modern HP turbines. This experimental program is designed to assess the benefits of stator tip endwall contours in the meridional direction that are not surfaces of revolution.

The approach involves five basic phases including the following:

1. analytical
2. design and fabrication
3. stator annular cascade test
4. full stage test
5. data reduction and analysis

During the analytical phase, a currently available 3-D inviscid code will be revised to handle the passage flow analysis for a stator whose endwalls are not surfaces of revolution. This model will be employed to evaluate candidate contour configurations. The selected tip endwall contour will be incorporated in the stator assembly of an existing small turbine rig.

The initial test phase will involve the aero evaluation of this concept using a full annular cascade. The test plan will consist of radial/circumferential (r,θ) surveys over a broad range of expansion ratios. On completion of the cascade test, the rotor assembly will be installed and complete stage performance mapping will be conducted. In addition, rotor exit (r,θ) surveys will be performed at selected overall expansion ratios. The data reduction and analysis phase includes comparing the annular cascade and full stage aero data with available data featuring the use of conventional stator endwall contours that are surfaces of revolution. This analysis procedure will involve comparing stator exit loss contours and overall stage performance maps.

Endwall Boundary Layer Control

Efficiency improvement is expected to result from stator endwall boundary layer control. The work of Stewart and Wong (reported in NASA RME55E11 entitled "Removal of Secondary-Flow Accommodations in a Two-Dimensional Turbine Nozzle Passage by Boundary Layer Bleed") shows that the removal of endwall secondary flow produces an extremely clean flow field into the downstream rotor. This will have a favorable impact on the vane blade interation losses and allow the rotor to operate more efficiently.

This experimental program is designed to determine the aero losses associated with the vane secondary flows by altering the character of the end-wall boundary layer using bleed and blowing at selected locations. The approach to be used in this program consists of five basic phases, including:

1. 2-D cascade evaluation of candidate endwall boundary layer bleed and blow concepts
2. full annular cascade tests of boundary layer control geometries selected from Phase 1
3. single stage turbine test to assess benefits of stator endwall bleed
4. two stage turbine test to measure performance improvement using first stage vane bleed in combination with second vane blowing
5. data reduction and analysis

In each of the test phases, a complete aerodynamic evaluation will be performed including the development of loss contour maps and turbine performance maps, wherever appropriate. The two stage turbine rig test will use the first vane low momentum endwall bleed as a source of air to energize the second vane endwall boundary layer. This unique concept will provide a more uniform flow field into both rotors.

Optimized 3-D Blading

The availability of the 3-D viscous airfoil passage flow analysis will provide the turbine aero designer with the ability to analytically assess the benefits of nonconventional blading exhibiting extensive 3-D passage geometries. Furthermore, this analysis model will lead to the optimum definition of the

radial distributions of such aero parameters of stage work, reaction, and turning distribution. This approach is contrasted with the current turbine design methodology where the velocity diagrams are first generated and then airfoil contours are designed to provide the defined vane/blade exit flow field.

This experimental program is structured to demonstrate the efficiency improvement that will be provided using a 3-D viscous flow analysis to define the complete vane and blade passage geometry for a small turbine rig. The approach is to employ an existing small turbine rig that was designed using conventional 2-D design analysis tools as a baseline. The turbine rig will be redesigned using 3-D viscous analysis tools to define the optimum vane and blade passage (radial distribution of airfoil throats and 3-D stacking). The redesigned turbine will maintain the baseline turbine overall stage work and reaction. This turbine will be fabricated and tested and its performance compared to the baseline design.

The major thrust of this program is to demonstrate the performance that will be provided by the availability of an advanced 3-D viscous flow analysis model. The improved understanding of the viscous flow losses in a small axial flow turbine will be paramount to the achievement of SECT performance goals.

3-D Viscous Flow Model Verification Tests

Bench mark experimental data will be required for the verification and upgrading of the subsonic and transonic 3-D viscous flow analysis. This effort is an extension of the work conducted at NASA Lewis by Seaholtz and Goldman, which employed a constant section annular stator assembly with constant diameter hub and tip endwalls. The program approach involves the design and fabrication of a stator annular cascade that establishes a strong 3-D flow field (nonconstant section airfoil, 3-D stack, and tip endwall contouring). The test procedure will involve detailed static pressure mapping along the vane and endwall surfaces. Vane-to-vane flow field velocity measurements will be conducted at near hub, mean, and tip spanwise locations for a series of selected chordal positions. This program will provide a valuable experimental data base for the critical verification of the airfoil passage 3-D, viscous flow analysis model.

Surface Finish/Reynolds Number Effects

This effort is structured to experimentally evaluate the effects of rotor blade surface finish and Reynolds number on the small axial flow turbine stage efficiency. This program complements, and is a logical extension of, the work conducted by Avco Lycoming (ref 17). It is anticipated that the results reported for the stator will be altered due to the different character of the boundary layer in this airfoil row. The test program will employ an existing small axial turbine rig to assess the effects of rotor surface finish over a broad range of inlet Reynolds numbers and overall expansion ratios. The proposed test plan will evaluate a total of three surface finishes. Performance mapping will be generated for each of four inlet Reynolds numbers. These results will provide a valuable insight relative to the effects of surface finish on the reduction of small rotor blade profile loss and how it is altered by Reynolds number.

Optimized Vane and Blade Aero Loading Distributions

This program involves the analytical assessment of the impact of inlet turbulence level and Reynolds number on the optimum vane and blade surface velocity distributions. This task is an analytical extension of the work conducted experimentally under the NASA funded E^3 effort (ref 18). The turbine airfoil optimization program combines the following design modules with an optimization algorithm:

- o airfoil section generator
- o 2-D inviscid blade-to-blade code
- o airfoil surface boundary layer analysis
- o airfoil profile loss model

In general, the optimization procedure minimizes (maximizes) an objective payoff function to a number of constraints. These constraints are formulated so that the airfoil maintains the velocity triangles and meets certain design criteria. The relevent criteria employed in this investigation will be the minimization of the airfoil fully mixed profile loss coefficient. The airfoil optimization model will be exercised over a broad range of inlet Reynolds numbers and turbulence levels characteristic of those encountered in small axial

flow turbine stages. It is anticipated these variables will have a significant impact on the airfoil optimum aerodynamic loading distribution and will complement the work conducted under NASA E^3 (ref 18), which addressed higher Reynolds numbers and lower inlet turbulence levels.

Turbine Rig Technology

This program will verify the SECT efficiency goals for the two stage power turbine to be incorporated in the selected nonconcentric engine. The technologies, derived from the above key technology programs, will be employed in the aero design of this advanced small axial flow turbine. The turbine will be tested in an engine environment and will feature the use of a continuous, free floating ceramic blade shroud, and ceramic vanes and blades.

Summary

The achievement of the SECT axial turbine efficiency goals will be realized through a variety of technology advancements. A major portion of this efficiency gain will be achieved through improved aerodynamics, as provided by key technology programs, along with the advanced analytical techniques. Advancements in other areas, such as material science, casting technology, and ceramics, in conjunction with innovative mechanical design concepts, will contribute toward meeting year 2000 efficiency goals.

RADIAL TURBINE TECHNOLOGY PLAN

The low flow capacity requirements of a small high pressure ratio engine with acceptable speed requirements and corresponding stress levels lead to the selection of radial inflow turbines. The radial turbine's high work per stage capability and reduced sensitivity to clearance effects, relative to a comparable designed axial stage gives this configuration the potential for superior efficiency characteristics. In terms of aerodynamic considerations, reduced passage widths (small blade heights) are a strong driver for the selection of a radial turbine.

Current technology in radial turbine design yields adiabatic efficiency levels shown in Figure 56. Goals set for technology programs are shown for both the

low and high pressure turbines and reflect an efficiency improvement of 3.0% over current technology.

The results of a loss breakdown study for the design point of the high pressure radial turbine is shown in Figure 57. The aerodynamic losses within the stages may be broken down into six categories: vaneless space friction (wall between vane and rotor), rotor incidence, windage (on hub), rotor clearance, rotor, and vane. Rotor and vane losses comprise the two greatest losses and are due to two major phenomenon: profile loss (or friction drag) and secondary losses (due to secondary flows in passages). Rotor clearance losses are targeted for a 0.3% point reduction by the advancements in clearance reduction resulting from use of ceramics and improved design concepts.

Approach/Technology Plan

The technology plan designed to achieve these efficiency goals is outlined in Figure 58 and targets both aspects of the vane and rotor loss mechanisms. For the purpose of technology advancement in the area of vane design, four design parameters have been selected for assessment of their loss reducing potential. Two parameters address profile losses and two parameters address secondary losses. Within the rotor, flow loss contributors are less easily delineated. In this case, each of three programs will assess the loss reduction potential of improved analysis tools and selected design changes. Verification of this improved design concept will be accomplished in a ceramic rotor and vane rig test. The technology programs are discussed in the following sections.

Vane Loss

The vane loss reduction programs have been structured as follows. An experimental program will examine the effects of vane aspect ratio (passage width/vane chord) and corner fillet radii on vane row loss levels. A set of rig adapted hardware will be designed and fabricated to test at three passage widths and three fillet radii separately and simultaneously. Use of available rig hardware is the preferred approach. The potential for improved efficiency is 0.6 percentage points. Design philosophy based on ceramic technology will be used in establishing feasibility of the range of radii and widths to be examined.

The second vane loss reduction program uses hardware of the first program with additional components added to modulate inlet turbulence levels. In addition, vane surface finish will be varied to determine proper design tradeoff relationships between losses and vane design. Three surface finish values and three turbulence levels will be examined. Potential loss reduction is anticipated to be 0.4 percentage points.

Rotor Loss

The rotor loss reduction program uses two analytical studies, each backed by experimental verification. Flow path contouring and 3-D flow analysis comprise the two areas of emphasis. The flow path contouring or rotor hub sculpturing study is aimed at analytically defining a hub contour that improves predicted rotor aerodynamic performance with a simultaneous improvement in rotor life. Quasi-3-D flow predictions will be made on three hub contures showing promise in tailoring blade velocity profiles to exhibit low loss characteristics. Rotor life predictions will be made for each design as well. Based on these results, a fourth design will be assembled and similar predictions made. The potential loss reduction is anticipated to be 0.9 percentage points.

The second program will experimentally evaluate the aerodynamic performance of the final design as determined in the previous program. This program, as well as the previous program, will be targeted to use the NASA Lewis Research Center (LeRC) radial turbine rig under development. A pressure instrumented test rotor will be fabricated. Test data will be analyzed and compared to predicted values. Information derived will be available to formulate advanced rotor design methodology.

The third rotor loss reduction program applies an advanced 3-D viscous flow analysis tool to a radial turbine rotor. The 3-D method is currently being developed in-house. Verification of predictions made using this tool will be greatly facilitated by using the data from the high temperature radial turbine program funded by NASA LeRC Contract NAS3-24230. Aero rig data from the highly instrumented but uncooled rotor fabricated in this program will be used to verify predictions. Performance benefits derivable by the subsequent use of this code as a design tool are estimated at 0.8 percentage points.

Completion of the radial turbine technology programs will result in the ability to design an advanced turbine using the resulting data bases and analytical tools and will realize the goal efficiencies as identified in the effort reported herein. The ceramic turbine verification program will include the design, fabrication, and hot rig test in an existing test rig. The rig is anticipated to be one presently used in the ongoing AGT 100 program.

COMPRESSOR TECHNOLOGY PLAN

The inherent problem in small engine compressors is performance. The inability of this class of small compressors to demonstrate the loading and efficiency levels of larger compressors can be directly attributed to the nonscalability of physical size and the relative lack of sophistication in analytical techniques to identify and quantify associated losses. However, the introduction of advanced design concepts, improved computational analysis, and modern materials/processes in the design and fabrication of small compressors is a key to bridging this performance gap.

An overview of the trends in compressor technology portraying Allison Gas Turbine state-of-the-art technology is shown in Figure 59, where polytropic efficiency is plotted against corrected exit flow. Since mass flow rate and pressure ratio determine the physical size of the rear compressor section, exit flow is a logical parameter to represent size.

Figure 59 comprises a sampling of axial, centrifugal, axial-centrifugal and dual centrifugal compression systems. The larger axial compressors have demonstrated polytropic efficiencies 1.5-15% higher than advanced axial-centrifugals and 2-3% higher than centrifugal compressors. This can be attributed to the larger flow size and considerable experience and research investment in axial compressors. Axial compressors have been limited to larger flow size applications (above 1 lbm/sec exit flow versus 0.1-0.3 lbm/sec for centrifugals) to avoid severe efficiency penalties associated with small exit blade heights. A recent analytical study was conducted to investigate the areas of concern and to determine the projections for efficiency potential in both large and small compressors for the year 2000. The results are presented in Figure 60.

The improvements (aerodynamic and mechanical) for small and large compressors are approximately 4.5% and 2% respectively. The results of this study are further presented in Figure 59 where the year 2000 technology assessment is compared to current state-of-the-art technology. The scope of the SECT compressor program is to demonstrate an increase in polytropic efficiency of 4-4.5% from current levels in small engine compressors. The SECT goals will be achieved by identifying high payoff technologies for year 2000 small gas turbine engine applications and by providing the appropriate technology plan.

SECT Compressor Design

For the current SECT study, based on mission studies for the representative tilt-rotor application, the aerodynamic design point for the compressor is given below:

corrected airflow lbm/sec	3.487
pressure ratio, Rc_{t-t}	30:1
adiabatic efficiency, n_{tt}%	78.7
polytropic efficiency, $n_{p\ t-t}$%	86.3
exit Mach number	0.30

To meet these goals--very high pressure ratio at a relatively low airflow rate and high efficiency levels--a four stage axial coupled to a single stage centrifugal was selected as the best configuration. The axial/centrifugal compressor takes advantage of the higher efficiency potential in the axial and alleviates the penalties due to reduced aft stage blade heights by employing a centrifugal compressor. Table XXX summarizes some of the salient aerodynamic and geometric design features for the axial compressor. These features are compared to two advanced axial compressors designed and experimentally tested within the last three years. The SECT compressor is designed to produce a pressure ratio of 7:1 and an efficiency of 85.1%, with adequate surge margin at design and slow speeds. The goal of this design is to evaluate loading levels (diffusion factor) and inlet tip speeds that are reflective of bigger flow size compressors, while reducing the losses normally associated with lower airflow rates and blade heights. This will be achieved with low aspect ratio blading technology for added loading/efficiency capability, improved analytical techniques, and advanced design concepts.

TABLE XXX.
SECT-COMPRESSOR TECHNOLOGY
CURRENT DEMONSTRATED AXIAL COMPRESSOR TECHNOLOGY.

	CURRENT TECHNOLOGY		
	LARGE	SMALL	DESIGN GOAL
CORRECTED AIR FLOW LBM INLET	26.24	3.91	3.487
SEC EXIT	4.57	1.424	0.682
PRESSURE RATIO	8.05	3.35	7.00
PRESSURE RATIO STAGE			1.627 + (15-20%)
NO. STAGES	6.0	4.0	4.0
ηT-T	84.4	84.6	85.1
η POLY	88.2	87.0	88.5
AVERAGE DIFFUSION FACTOR			0.440
COMP EXIT M_N			0.450
INLET TIP SPEED—FT/SEC	1410.0	1180.0	1436.0
EXIT ROTOR HEIGHT—IN.	0.875	0.552	0.270
AVERAGE ASPECT RATIO	1.228	1.027	0.750

The aerodynamic and geometric design features of the SECT centrifugal compressor are presented in Table XXXI. These features are compared to two experimentally verified centrifugal compressors, large current technology, and small (AGT) compressors. The SECT centrifugal is designed to produce a pressure ratio of 4.7 at 82.1% efficiency. The pressure ratio split between the axial and centrifugal compressors, dictated by axial loading levels, and impeller tip speeds and stress levels has indicated that for optimizing the specific speed (for increased exit blade height) and performance potential of the centrifugal compressor, increased rotational speed was desired. However, the increased speed resulted in excessive bore stress levels for the high pressure turbine rotor at 2800°F RIT. Therefore, the desire for increased speed and reduced turbine stress levels directed the SECT compressor to a nonconcentric configuration. From Table XXXI, it can be observed that the SECT goals require a 1.5% improvement in efficiency with a 24% reduction in exit blade height, 26% increase in tip speed and 70% increase in discharge temperature (all deterrents to performance) relative to the AGT. Improved analytical methods and design concepts will be vital for improving the performance potential of small centrifugal compressors. The following paragraphs examine the areas of technology required for small engine compressors for the year 2000.

TABLE XXXI.
SECT-COMPRESSOR TECHNOLOGY
CURRENT DEMONSTRATED CENTRIFUGAL COMPRESSOR TECHNOLOGY.

	CURRENT TECHNOLOGY	AGT	DESIGN GOAL
CORRECTED AIR FLOW LBM INLET / SEC EXIT	3.60 / 1.096	0.774 / 0.190	0.703 / 0.183
PRESSURE RATIO	4.136	5.477	4.700
ηT-T	85.6	80.70	82.10
η POLY	88.1	84.70	85.6
COMP EXIT M_N		0.242	0.300
SPECIFIC SPEED, N_S		80.0	71.01
INLET HT		0.450	0.541
EXIT TIP SPEED—FT/SEC		1800.0	2260.0
CDT—°R		920.0	1568
EXIT AXIAL BLADE HEIGHT	0.406	0.218	0.165
BACK CURVATURE—DEG	50.0	50.0	47.5

Technology Areas

The major areas of concern contributing to small engine compressors not achieving the performance levels demonstrated by large flow compressors are small physical size, innadequate analytical skills to identify the loss mechanisms, and the lack of experience and experimental date. This is partly due to earlier efforts in small compressors being directed primarily toward the development of economical and rugged units, without much consideration for improving efficiency/loading potential. This discrepancy in performance can be further explained by the following: for a reduction in airflow rate, the speed should be increased and all other physical parameters reduced by the square root of the change in airflow rate to maintain aerodynamic similarity. However, because of manufacturing and structural limitations, it is not possible to scale certain physical parameters--thickness, leading edge radius (LER), and clearance--appropriately. Small size compressors are designed with higher thickness/chord (T/C), leading edge radius/chord (LER/c), and Mach number to T/C ratios. The Mach number levels in the compressor are maintained by scaling up the rotational speed. Clearance and tolerance levels to blade contour and surface roughness are not scalable and remain similar to levels of larger compressors. This combination results in increased losses in the passage and blade-row due to shock, profile, end-wall, boundary layer and clearance. While it may be possible to reduce the losses due to the above factors

with improved mechanical design and manufacturing techniques, small engine compressors have the inherent problem of low Reynolds number flows. Improvements in this area can be achieved by understanding the phenomena of low Reynolds number flow in a turbo-machinery blade row and developing analytical tools for implementation with advanced design concepts. Some concepts considered likely candidates are:

- o airfoil sweep and lean optimization to reduce shock losses
- o airfoil contouring to design velocity/diffusion controlled blading to minimize shock losses and suction surface flow separation
- o casing treatment--endwall treatment to energize boundary layer and enhance part speed flow/efficiency lapse rates for improved stability
- o design of 3-D diffuser vanes to account for highly sheared flows at diffuser entrance region
- o bleed/blow feature at diffuser throat for improved efficiency and stability at slow speed
- o clearance control/minimization over operating range of compressor by improved mechanical design

Axial Compressor Technology Plan

A discussion of the various component test programs shown in Figure 61 follows. The approach was conceived as a systematic method to experimentally investigate the factors contributing to reduced loading capability and efficiency levels of small engine compressors. This series of tests will also create the data base and experience necessary for the evaluation of analytical techniques and design of high performance axial compressors. The acquired information will not be restricted to small compressor designs, but will also be beneficial for improving the performance of large compressors.

Performance Evaluation of True Axial Compressor Scaling

Since certain physical parameters limit the scaling down of a compressor to achieve aerodynamic similarity, this program proposes to test two aerodynamically similar compressors by photographically scaling up a small size compressor. The experimental data from the two compressors will deliver a direct correlation of compressor performance versus Reynolds number changes.

The approach taken will be to test an advanced small compressor with relatively high loadings. This compressor will be scaled up to a higher flow size and performance data obtained. This will give data comparison due to Reynolds number changes associated with the two sets of hardware. Further testing will be conducted to evaluate the performance of large-flow hardware at small-flow Reynolds number to give Reynolds number effects on the same hardware. Advanced experimental techniques and instrumentation--laser velocimetry--will be used to fully evaluate the flow fields and quantify losses associated with low Reynolds number compressors.

These tests will provide a data base for scaling effects in an axial compressor for small axial design. These data will be an asset in calculating the effect of compressor performances as a result of Reynolds number changes.

Cascade Testing Related to Small Size Axial Compressors

Cascade tests have been directed at developing optimum blade shapes and blade design more applicable to large engine compressors. Recent requirements of small compressors to sustain increased loading at increased tip speeds and Mach numbers have necessitated the need for high thickness blading for high Mach number applications.

The proposed cascade test will be conducted on the scaled up hardware of a small compressor cascade to evaluate the optimum blade design to minimize losses due to shock and associated blade profile losses. Velocity controlled (controlled diffusion)blading and leading edge sweep effects will be investigated to control shock structure and reduce such inefficiencies as boundary layer growth, suction surface separation, and endwall secondary flow effects. The tests, conducted in large hardware, will ease the use of laser velocimetry to investigate the flow field and assess performance. By testing both large and small hardware, data for Reynolds number, roughness, and tolerance effects can be obtained and included in analytical predictive models.

The major thrust of this program will be to establish the improvements necessary in analytical predictive techniques to account for the various factors affecting the performance of high thickness/chord, LER/chord blading in a high

Mach number environment. This will set the basis for a viable design method for improving compressor performance.

Aerodynamics Concept Evaluation on Rotating Single Stage Axle Rig.

From previous experience, performance calculated from an isolated blade row, as in a cascade, proved different when a similar blade row was in a rotating stage environment. It is essential that the validity of the findings from prior testing be obtained on a rotating stage where blade row interaction effects can be included. The objective of this program will be to investigate the effects of blade shape, surface roughness, and sweep effects on compressor performance.

The approach taken would be to scale an existing small stage up in flow size and conduct experimental test on the large hardware to evaluate the influence of intrastage reaction--due to nonuniform inlet pressure and temperature profiles, wakes, and boundary layer blockage. The designs will include the concepts contributing to improved performance as determined from previous experimental cascade data. The resulting benefits from the large hardware will be verified on the small stage.

This program will set a valid basis for selection of advanced design concepts, blade shapes, and surface roughness for small size compressor design. The data obtained from these tests will also establish the required guidelines in computational techniques for the design of highly loaded small axial compressors to verify efficiency and pressure ratio capabilities reflective of larger flow size compressors.

Multistage Axial Compressor Test Bed

A multistage axial compressor test bed will be used to verify aerodynamic design concepts and validate analytic techniques before initiating the design of the actual SECT axial compressor. This will set the basis for a logical and proven design methodology using advanced design concepts and detailed analyses for high performance multistage compressors reflective of year 2000 technology.

The approach taken in this program will be to use components of an existing advanced multistage axial compressor. Potential improvements in performance will be investigated by perturbing the design to evaluate the individual effects of low aspect ratio airfoils and endwall blading modifications-sweep, end bends. Based on in-house experience, low aspect ratio blading has been employed to enhance the performance of both large and small compressors. Low aspect ratio airfoils have in addition, contributed to improved stability at design and part speeds. These trends warrant the investigation of low aspect ratio airfoils as a viable candidate in the design of the SECT axial compressor.

Earlier analyses on compressors have revealed that losses associated with secondary flow are substantial and that work to reduce this phenomena is vital for future compressor design. This is especially true in small flow compressors that operate at much higher clearance/blade span ratios. This results in more intense leakage flow patterns, endwall vorticities, and boundary layer (blockage) growth. It is reasonable to assume that there are potential gains to be made by desensitizing the design to these mechanisms. Casing (tip) treatment over rotors has been a successful ploy to energize the boundary layer and enhance surge margin potential at slow speed. This has, however, been achieved at the expense of compressor efficiency as it was used purely as diagnostic confirmation for redesign. By proper selection of the geometry of tip treatment (slots versus holes, blade angled slots versus circumferential, etc.), the surge margin improvements can be made with minimal efficiency reduction.

The multistage test bed will also be used to verify the benefits of airfoil sweep and end-bends as an effective way of reducing losses associated with the endwall region. Airfoil sweep has shown potential for reducing 3-D shock losses in high speed rotor flows. Stator end-bends, achieved by resetting the stator airfoil closed in the vicinity of the endwalls, result in unloading the endwall region with attendant reduction in losses associated with the boundary layer. End-bends also serve to reduce the incidence levels and enhance surge margin potential.

The results obtained from this program will be accounted for by the analytical model and directly applied to the design of the SECT axial compressor.

Radial Compressor Technology Plan

The proposed technology program for centrifugal compressors are shown in Figure 62. A discussion of each program follows.

Flow Size Effects on Small Centrifugal Compressors

The main objective of this program is to study low flow sizes--i.e. 0.1 lb/sec - 0.5 lb/sec - to evaluate compressor performance and evolve/verify computational techniques directly applicable for the design of the SECT centrifugal compressor.

Based on previous experience, centrifugal compressors in different flow size regimes demonstrate performance levels not consistent with Reynolds number changes. This can be partly explained by the different configurations not being designed to consistent blade thicknesses and running clearances. The approach in this program will be to eliminate such inconsistencies by designing two sets of hardware encompassing large and small flow regimes, testing of both sets of hardware with advanced experimental techniques--customized two-spot velocimetry. The derived data base will provide for improvements in computational methods. Testing would include the effects of clearance and shroud surface finish on compressor performance. The fully instrumented rig allows investigation of the entire flow field and nonscalability effects on performance to be included in the development of analytical models. This will be the key to improved performance potential in centrifugal compressors in both large and small flow sizes.

Reynolds Number Effect on Small Centrifugal Compressor Performance

The objective of this program is to evaluate pure Reynolds number effect on small flow size compressors consistent with the flow size study. This can be easily conducted as a continuation of the previous program.

The approach is to quantify Reynolds number effects on small size hardware from flow size scale study by adapting inlet ram capability to identify the resulting changes in loss mechanisms. Based upon the data, the necessary modifi-

cations can be effected in analytical techniques, and similar tests on big hardware determined. Testing will be conducted with extensive instrumentation.

The results of this program will allow the proper assessment of Reynolds number in analytical models for the design of high performance small centrifugal compressors. The models evolved from this program would not be confined to small compressors, but centrifugal compressor design in general.

Impeller Leading Edge Blade Shape on Centrifugal Compressor Performance

Design of centrifugal impellers has been confined to vertical leading edge impellers employing straight element sections. Recent work on swept-back leading edges has revealed improvements in range for larger flow size compressors. In axial compressors, velocity controlled airfoils have been designed to contain shock structures, enhancing performance potential. The objective in this program is to investigate the possibility of improved range and efficiency on small compressors by incorporating advance design concepts.

The approach would be to design and experimentally evaluate a conventional impeller and advanced impeller of equivalent work to investigate the potential benefits of leading edge sweep and contoured blades. Improved instrumentation and experimental techniques--advanced laser velocimetry--will be employed to calculate and understand the complex flow field within the blade row for inclusion of these concepts in analytical/computational models. The benefits realized from leading edge and impeller blade shapes may be vital to the future design of high performance centrifugal compressors requiring improved range and efficiency.

Investigate Passage Contouring for Improved Centrifugal Compressor Performance and Clearance Tolerance

The design of centrifugal passages has been axisymmetrix and surfaces of revolution. Since small size compressor performance is substantially affected by running clearance, the objective is to employ centrifugal passages of non-axisymmetry and nonsurfaces of revolution to enhance efficiency and reduce clearance sensitivity. This would involve the development of supporting

analytical capability to design geometries and verification through experimental evaluation. Any potential payoff associated with determining the optimum controur of these surfaces would bridge the gap in performance (in small compressors) and result in improved analytical/predictive techniques for the design of centrifugal compressors.

Advanced Diffuser System

The flow characteristics of the entrance region of the centrifugal compressor is of vital importance to the overall performance and stability at design and off-design speeds. The flow is highly sheared and viscous and enters the diffuser leading edge with uneven pressure and temperature gradients. In spite of this complex 3-D flow phenomena, the design of radial diffusers has been 2-D wedge-shaped vanes with no consideration given to the nonuniformities. Since the selection of diffuser throat area--by accounting for aerodynamic blockage due to the presence of boundary layers--and leading edge incidence determines high speed flow capacity and slow speed stability, respectively, potential benefits in the design of 3-D vanes were customized for the inlet flow conditions. The incorporation of bleed/blow capability for performance enhancement, as evidenced in the improvements in range/flow regulation of higher pressure ratio impellers by the Allison patented system of inducer bleed, may be a desirable feature.

The approach in this program involves thorough investigation of the vaneless space/diffuser entry region of a design, including features such as 3-D vanes and bleed/blow capability to quantify any potential payoffs. The data obtained by using advanced laser velocimetry would create the data base for comparisons against similar conventional diffuser designs, give a better understanding of the flow phenomena, and qualify emloying advanced design techniques. This program would set the basis for the design of centrifugal compression systems with good slow speed flow/efficiency lapse rates without requiring the attendant compromises in design performance.

Verification of Small Compressor Technology

The SECT compressor technology plan has been conceived as a systematic means of elevating the performance levels of small engine compressors as has been

shown in Figures 61 and 62. The knowledge acquired from the compressor technology programs will be used to design and fabricate the SECT nonconcentric compressor. This program will experimentally verify the design techniques and goals of the program. In summary, the outcome of this program will result in the evolution of an advanced and viable design methodology for high performance compressors satisfying the requirements of year 2000+ technology.

COMPUTATIONAL FLUID MECHANICS

The flow in small gas turbine engine compressors and turbines is dominated by performance limiting 3-D viscous flow phenomena. Those phenomena include rapidly growing endwall boundary layers, secondary flows driven by strong cross-stream pressure gradients, and significant tip/leakage flows. In low aspect ratio axial turbomachines, these flow features occupy a significant portion of the airfoil span and, therefore, account for a major part of the overall total pressure loss in these machines. In high pressure ratio centrifugal compressors, performance can be further reduced by separated flow in the exducer.

In addition to the concern over the viscous flow phenomena and the impact on performance, there has emerged over the last few years considerable interest and concern about the unsteady flow interaction between rotating and stationary blade rows and its effect on the time mean aerodynamic and thermal characteristics. These unsteady phenomena include potential flow interactions giving rise to significant pressure fluctuations on the airfoil surfaces and viscous interactions resulting from the downstream row cutting the wakes shed from the upstream row. Experimental studies have shown that these time unsteady vane blade interaction effects are large and the resulting time mean aerodynamic and heat transfer characteristics are considerably different from those of isolated vane and blade rows. In small turbomachines, it is likely that these interactive effects are magnified because of the increased importance of endwall viscous flow phenomena.

Proposed Advanced Technology Effort

A series of three advanced technology programs that address the development and qualification of improved flow models for small compressors and turbines is proposed. These programs are directed at the development of analyses with

P.156

NASA CR-175081
AVSCOM TR 86-C-8
ALLISON EDR
Report No. 12422
Copy No.

SMALL ENGINE COMPONENT TECHNOLOGY (SECT) STUDY FINAL REPORT

by T. R. LARKIN

ALLISON GAS TURBINE DIVISION
GENERAL MOTORS CORPORATION

Date for general release March 31, 1991

prepared for
NATIONAL AERONAUTICS AND SPACE ADMINISTRATION
Lewis Research Center
and
U.S. ARMY AVIATION RESEARCH AND TECHNOLOGY ACTIVITY
Propulsion Directorate

NASA Lewis Research Center
NAS3-24542

1. Report No.	2. Government Accession No.	3. Recipient's Catalog No.
NASA CR - 175081 AVSCOM TR - 86-C-8		

4. Title and Subtitle	5. Report Date
Small Engine Component Technology (SECT) Studies Final Report	March, 1986
	6. Performing Organization Code

7. Author(s)	8. Performing Organization Report No.
T. R. Larkin	EDR 12422
	10. Work Unit No.

9. Performing Organization Name and Address	11. Contract or Grant No.
Allison Gas Turbine Division General Motors Corporation P.O. Box 420 Indianapolis, Indiana 46206-0420	NAS 3 - 24542
	13. Type of Report and Period Covered
12. Sponsoring Agency Name and Address	Contractor Report
NASA Lewis Research Center and U.S. Army Aviation Research and Technology Activity, Propulsion Directorate, Cleveland, Ohio 44135	14. Sponsoring Agency Code 535-05-01 1L161101AH45

15. Supplementary Notes

Project Manager, Michael R. Vanco
NASA Lewis Research Center
Cleveland, Ohio 44135

16. Abstract

The objective of this Allison Gas Turbine Divison study was to identify high payoff technologies for year 2000 small gas turbine engines, and to provide a technology plan to guide research and technology efforts toward revolutionizing the small gas turbine technology base. The goal of this effort was to define the required technology to provide a 30% reduction in mission fuel burned, to reduce direct operating cost by at least 10%, and to provide increased reliabiity and durability of the gas turbine propulsion system. The baseline established to evaluate the year 2000 technology base was an eight-passenger commercial tilt-rotor aircraft powered by a current technology Allison gas turbine engine.

Three basic engine cycles were studied: the simple cycle engine, a waste heat recovery cycle, and a wave rotor engine cycle. For the simple cycle engine, two general arrangements were considered: the traditional concentric spool arrangement and a non-concentric spool arrangmeent. Both a regenerative and a recuperative cycle were studied for the waste heat recovery cycle.

An extensive cycle optimization procedure was performed for each configuration under study, using relative DOC as the figure-of-merit. This allowed for selection of the proper design max cycle temperature and cycle pressure ratio. Three of the five optimum cycles (the non-concentric, the recuperative and the regenerative engine cycles) were evaluated for a typical tilt-rotor design flight mission. Results showed that all three engines met the goal of at least 30% reduction in fuel burned relative to the defined baseline for the commercial tilt-rotor aircraft mission. In addition, the non-concentric engine provided the greatest reduction in DOC with a 16.5% improvement.

The technologies required for this substantial improvement were ranked in order of decreasing benefit.

17. Key Words (Suggested by Author(s))	18. Distribution Statement
Rotorcraft Gas turbine engines Component technologies Cycles	

19. Security Classif. (of this report)	20. Security Classif. (of this page)	21. No. of pages	22. Price*
Unclassified	Unclassified		

TABLE OF CONTENTS

TABLE OF CONTENTS (CONT)

LIST OF ILLUSTRATIONS

LIST OF ILLUSTRATIONS (CONT)

LIST OF ILLUSTRATIONS (CONT)

LIST OF ILLUSTRATIONS (CONT)

LIST OF TABLES

LIST OF TABLES (CONT)

I. SUMMARY

The goals of this effort was to define the required technology to provide a 30% reduction in mission fuel burned, to reduce direct operating cost by at least 10%, and to provide increased reliability and durability of the gas turbine propulsion system. The baseline established to evaluate the year 2000 technology base was an eight passenger commercial tilt-rotor aircraft, currently in the preliminary design phase, powered by a current state-of-the-art technology gas turbine engine.

Three basic engine cycles were studied: the simple cycle engine, a waste heat recovery cycle, and a wave rotor cycle. For the simple cycle, two general arrangements were considered: the traditional concentric spool arrangement and a nonconcentric spool arrangement. Both regenerative and recuperative cycles were studied for the waste heat recovery cycle.

An extensive cycle optimization procedure was performed for each configuration studied, using relative direct operating cost as the figure of merit. This procedure allowed for selection of the proper design maximum cycle temperature and cycle pressure ratio. Nonconcentric, recuperative, and regenerative engines were evaluated for a typical tilt-rotor design flight mission. Results showed that all three engines met the goal of at least 30% reduction in fuel burned relative to the baseline engine for the commercial tilt-rotor aircraft mission. The nonconcentric engine provided the greatest reduction in direct operating cost (DOC) with a 16.5% improvement.

Five technology areas require research effort to realize the full potential of the nonconcentric engine concept for the year 2000. In order of decreasing benefit relative to DOC reduction, the areas are ceramics, turbines, compressors, combustors, and bearings. In addition, improvements in computational fluid mechanics are essential to properly analyze the flow characteristics in small gas turbine components.

II. INTRODUCTION

Small gas turbine engines are used in a wide variety of applications. The success of the next generation of small gas turbine engines in meeting these various operational requirements will depend on development and application of new technology. This technology will provide a significant reduction in total cost of ownership by reducing fuel burned, initial acquisition cost, and maintenance costs. For example, fuel cost for small helicopter aircraft can represent as much as one half of the engine cost of ownership.

Small engine components do not achieve the same level of operational efficiency as those in larger engines, resulting in higher fuel consumption. Fuel consumption and specific power can be improved by increasing overall pressure ratio, turbine inlet temperature, and the level of component performance. As pressure ratio and turbine inlet temperature increase, sealing and cooling problems create additional parasitic losses that erode the fundamental cycle advantage. This is particularly true for small gas turbine engines where size effects make sealing and cooling more difficult.

With the threat of increasing foreign competition in the small gas turbine engine market, particularly for the 1000 horsepower class and below, aggressive research and technology programs are needed to assure continued U.S. industry competitiveness. For these reasons Allison is supportive of NASA's Small Engine Component Technology (SECT) program.

The SECT study was sponsored by the NASA Lewis Research Center and U. S. Army Aviation Research and Technology Activity-Propulsion Directorate.

The objectives of the SECT study were: (1) to identify the high payoff technologies for the year 2000 small gas turbine engine and (2) to provide a technology plan for guiding future research and technology efforts. This plan will provide the advanced technology base needed to ensure the technical advantage of U.S. manufacturers in the future small engine market.

The work performed during the study contract was divided into four basic tasks, as follows:

Task I: Select mission evaluation procedures and assumptions

Task II: Evaluate engine configurations and cycles

Task III: Conduct an engine/aircraft mission analysis to determine figures of merit to rank technology needs

Task IV: Prepare a plan to guide research and technology verification, component and systems research, and technology programs

Allison is interested in all baseline applications (rotorcraft, commuter, auxiliary power unit (APU), and cruise missile). However, a more productive program would result from studying a single application in great depth rather than several applications in lesser depth. The rotorcraft application, specifically the commercial tilt-rotor application, using a high-performance, high power/weight turboshaft engine was selected for this study. Direct operating cost (DOC) was used as the overall figure of merit. This report presents the results of this study.

III. TASK I. SELECTION OF EVALUATION PROCEDURES AND ASSUMPTIONS

The evaluation procedures and assumptions used in the Small Engine Components Technology (SECT) study are briefly described along with supporting information concerning the source or applicable background justification where appropriate. Major topics to be presented are:

- o aircraft/mission requirements
- o reference tilt-rotor aircraft characteristics
- o direct operating cost model
- o baseline engine description and scaling equations
- o baseline engine mission results and trade factors
- o environmental constraints

The SECT cycle selection and engine configuration evaluation required the definition of mission requirements, a reference aircraft, engine characteristics, and an economic model for use in obtaining cost comparisons. These items were integrated into the mission analysis computer program. Program input, major calculation routines, and output parameters for this program are generalized in the block diagram shown in Figure 1.* Mission requirements, along with airframe and engine characteristics, are used in the engine/airframe sizing or scaling routines to determine the engine/airframe size combination that will meet fixed mission requirements, i.e., "rubber engine/rubber aircraft" approach. The resultant sized aircraft along with mission fuel, distance, and time data, plus input economic criteria, are then used in the cost model to obtain direct operating cost (DOC) data. Total engine/aircraft DOC was the selected figure of merit for the SECT study.

AIRCRAFT/MISSION REQUIREMENTS

The advanced helicopter system selected for the SECT studies was based on a tilt-rotor concept developed by Bell Helicopter Textron, Inc. This concept combines the best features of the helicopter and turboprop aircraft, i.e., helicopter takeoff and landing, safety and convenience, plus the advantages of

* Figures can be found at the end of this report.

turboprop cruise speed, low noise, and vibration. All of these qualities are necessary to obtain favorable market projections for year 2000 rotorcraft applications.

The tilt-rotor mission requirements selected for this study effort are listed below:

o payload	eight passenger at 90.7 kg (200 lb) each
o range	648 km (350 nautical miles [nmi])
o cruise speed	250 knots true air speed (KTAS)
o cruise altitude	6096 m (20,000 ft)

The goal was to establish a "generic" twin engine tilt-rotor aircraft in the 4536 kg (10,000 lb) gross weight class that would be in concert with the NASA specified engine maximum power limit of 1000 shaft horsepower (shp). This vehicle class provides a spectrum of possible mission applications including corporate/executive, off-shore oil support, and medical evacuation. The Allison market projection for this class tilt-rotor is 1000 to 1200 aircraft over a ten year period. This figure is slightly higher than a Bell projection of 750 to 900 aircraft over a similar ten year period. Using 1000 aircraft as an approximate average and assuming one spare engine per aircraft provides a projected engine market of 3000 units.

The design mission profile shown in Figure 2 is consistent with air traffic control procedures, aircraft capability, and reserve definition sufficient for a rotorcraft transport concept. The operating scenario presumes that the selected tilt-rotor aircraft will be flown in the design mission during the majority of its use. The revenue mission and design mission are assumed to be identical. The engine/aircraft sizing criteria used in this study were selected to provide hover, one-engine-inoperative rate of climb, and cruise rate of climb capabilities sufficient to meet selected design operating requirements and to provide adequate margins of safety in the event of engine failure. These selected candidate sizing conditions/requirements are detailed in Table I.

TABLE I.
ENGINE/AIRCRAFT SIZING REQUIREMENTS

ENGINE/AIRCRAFT SIZING CONDITION	RATE OF CLIMB— M/MIN (FPM)	AIRCRAFT WEIGHT	ENGINE POWER SETTING	ALTITUDE M/(FT)	VELOCITY KTAS	DEGREE DAY
HOVER–OUT OF GROUND EFFECT	0 (0)	DESIGN TOGW	INTERMEDIATE POWER (AEO)	610 (2000) (1)	0	ISA + 10°C
OEI (2) RATE OF CLIMB	46 (150)	DESIGN TOGW	30 MINUTE POWER (OEI)	305 (1000)	75	ISA + 20°C
CRUISE CEILING RATE OF CLIMB	91 (300)	INITIAL CRUISE WEIGHT	MAXIMUM CONTINUOUS POWER (AEO)	6096 (20,000)	250	ISA

NOTES: (1) DEFINITION OF U.S. ARMY EUROPEAN DAY
(2) FAR PART 29/TRANSPORT CATEGORY ROTORCRAFT—TAKEOFF CATEGORY "A"

AEO—ALL ENGINES OPERATIVE
OEI—ONE ENGINE INOPERATIVE
TOGW—TAKEOFF GROSS WEIGHT

T880-4675

REFERENCE TILT-ROTOR AIRCRAFT CHARACTERISTICS

The vehicle selected for use in the SECT study effort is an eight passenger corporate/executive tilt-rotor aircraft configuration. General characteristics for this vehicle were provided to Allison Gas Turbine Division by Bell Helicopter Textron, Inc. A three view drawing of the reference aircraft is shown in Figure 3. Figure 4 shows a typical fuselage layout proposed for the eight passenger configuration along with approximate dimensions and volume data. A summary of aircraft design parameters is listed in Table II. Component or group weight breakdown is provided in Table III. Figure 5 shows the nacelle layout proposed for this vehicle and illustrates the turboshaft engine placement within the tilt-rotor nacelle. In this concept, the engine supplies power to an angle gearbox/rotor arrangement that can pivot about the conversion axis shown in Figure 5. The engine can also supply power to an interconnect driveshaft that couples the two propulsion packages through a center gearbox located in the fuselage-wing carry-through area. This driveshaft is normally unloaded and serves to synchronize thrust and rpm. However, in the event of single

TABLE II.
REFERENCE AIRCRAFT PARAMETERS

TOGW	**4772 kg (10,520 LB)**
FUSELAGE	
DIAMETER	**1.6 m (5.4 FT)**
LENGTH	**9.9 m (32.5 FT)**
ROTOR	
NUMBER OF BLADES	**3**
DIAMETER	**7.06 m (23.17 FT)**
DISK LOADING	**60.93 kg/m² (12.48 LB/FT²)**
ROTOR BLADES	
BLADE TIP SPEED (HOVER)	**13,717 M/MIN (750 FPS)**
BLADE TIP SPEED (CRUISE)	**11,120 M/MIN (608 FPS)**
MEAN BLADE CHORD	**0.36 m (1.17 FT)**
BLADE LOADING COEF	**0.1935**
WING	
SW (REFERENCE WING AREA)	**40.9 m² (134.2 FT²)**
W/SW (WING LOADING)	**382.7 kg/m² (78.4 LB/FT²)**
ASPECT RATIO	**8**
SWEEP @ L.E.	**−8° (SWEPT FWD)**
AVG THICKNESS RATIO	**24%**
TAPER RATIO	**1.00**

V986-1286

engine operation, this system transfers power to maintain continued safe operation of both rotors.

Reference tilt-rotor (helicopter mode) hover power requirements are shown in Figure 6. Cruise power requirements (airplane mode) for 3048 m (10,000 ft) and 6096 m (20,000 ft) are shown in Figures 7 and 8.

DIRECT OPERATING COST MODEL

Operating costs fall into two categories: direct cost and indirect cost. Indirect costs are basically dependent on the particular service the operator is offering, but the indirect costs may also be dependent on the airplane's characteristics. The figure of merit to assess the relative benefit of gas turbine

TABLE III.
SECT REFERENCE AIRCRAFT WEIGHT BREAKDOWN

	KILOGRAMS (POUNDS)	WEIGHT FRACTION-% (WT/TOGW-%)
•PROPULSION GROUP (INCLUDES ROTOR GROUP AND DRIVE SYSTEM)	1199 (2643)	25.1
•STRUCTURES GROUP	1100 (2425)	23.1
•FIXED EQUIPMENT	1046 (2305)	21.9
MFG EMPTY WEIGHT	3344 (7373)	70.1
•USEFUL LOAD	225 (497)	4.7
OPERATING EMPTY WEIGHT	3570 (7870)	74.8
•PAYLOAD	726 (1600)	15.2
ZERO FUEL WEIGHT	4296 (9470)	90.0
•FUEL (USABLE)	476 (1050)	10.0
TOGW	4772 (10,520)	100.0

TE86-4876

---

technologies will be based on direct operating cost which includes maintenance burden for this study. These costs are calculated as a cost per airplane nautical mile (C_{am}); however, they can be converted as follows:

$$\text{cost/seat nmi} = C_{am} \div \text{number of passenger seats}$$
$$\text{cost/block hr} = C_{am} \times V_b$$
$$\text{cost/flight hr} = C_{am} \times V_b \times t_b/t_f$$

where:

t_b = block time--hr

t_f = flight time--hr = $(T_b - T_{gm})$
V_b = block speed--knots

For the computation of block speed, the following formula based on a zero wind component was used:

$$V_b = D/(T_{gm} + T_v + T_{cl} + T_{cr})$$

where:

D = mission range or stage length in nautical miles
T_{gm} = ground maneuver time in hr (includes engine start and warm-up plus engine shutdown allowances)
T_v = vertical takeoff and landing time--hr
T_{cl} = time to climb from 762 m (2500 ft) to cruise altitude--hr
T_{cr} = time at cruise altitude and velocity--hr

Block fuel was computed from the following formula:

$$F_b = F_{gm} + F_v + F_{cl} + F_{cr}$$

where:

F_b = block fuel--lb
F_{gm} = ground maneuver fuel (fuel required for engine start and warm-up plus engine shutdown)--lb
F_v = fuel required for vertical takeoff and landing allowances--lb
F_{cl} = fuel to climb to cruise altitude--lb
F_{cr} = fuel consumed at cruise altitude and velocity--lb

The direct operating cost model used in the SECT study was based on 1967 Airline Transport Association (ATA) methodology. The cost methodologies and economic "ground rules" used in the SECT model are summarized in Table IV. The fuel cost used to obtain engine trade factors (take off gross weight [TOGW] and DOC sensitivity to changes in engine characteristics) during the Task I

TABLE IV.
DIRECT OPERATING COST MODEL (1985 ECONOMIC YEAR)

FUEL AND OIL INSURANCE COST DEPRECIATION FLIGHT CREW COST	→ 1967 ATA METHODOLOGY
ENGINE MAINTENANCE (DIRECT LABOR AND PARTS)	→ 1967 ATA EQUATION FORMAT WITH UPDATED CORRELATION FACTORS
AIRFRAME MAINTENANCE (DIRECT LABOR AND PARTS)	→ BELL HELICOPTER—EQUATION FORMAT GATE HELICOPTER WITH UPDATED CORRELATION FACTORS

GROUND RULES

•ECONOMIC BASE YEAR	1985
•FUEL COST	0.26 $/l (0.53 $l) (1.00 $/GAL [2.00 $/GAL])
•OIL COST	6.24/$l ($24/GAL)
•INSURANCE RATE	12% OF ACQ COST PER YEAR
•DEPRECIATION SCHEDULE	7 YEARS TO 25% RESIDUAL VALUE
•SPARES	AIRFRAME–10% AIRFRAME ACQ COST ENGINE—15% ENGINE ACQ COST
•UTILIZATION RATE	1000 HR/YR (2000 HR/YR)
•MAINTENANCE BURDEN	150%
•LABOR RATE	$15.00 PER MAINTENANCE MANHOURS

TE86-4877

study effort was $0.39/l ($1.50/gal.) in 1985 dollars. However, the Task III system performance evaluations were completed using $0.26/l ($1.00/gal.) and $0.53/l ($2.00/gal.) fuel cost levels.

Engine Acquisition Cost

Original equipment manufacturer (OEM) costs for the turboshaft study engines were developed using Allison material index factor methods applied to component finished weights. These costs were determined for the unity size engine (1000 shp at sea level static standard day [SLSS], intermediate rated power [IRP])

and scaled to the horsepower (hp) size necessary to meet the engine/aircraft size combination required for the design mission.

$$\text{OEM cost} = \left(\frac{\$}{shp_S}\right) \times shp_S$$

where: $\left(\frac{\$}{shp_S}\right) = \left(\frac{\$}{shp_U}\right) \times \left(\frac{shp_S}{shp_U}\right)^{-0.0125}$

shp → SLS, standard day, IRP horsepower

S → scaled engine size

U → unity engine size

Engine acquisition cost was obtained from the following relationship:

Engine acquisition cost = OEM cost x 1.5

Aircraft Acquisition Cost

The aircraft less engine acquisition cost for the scaled aircraft/engine combination was obtained from Bell Helicopter for the reference vehicle. The cost per pound for reference vehicle is:

$$\frac{\text{aircraft cost - engine cost}}{\text{mfg empty wt - engine weight}} = \$362/\text{pound}$$

Therefore:

Aircraft cost (A/C) less eng acq cost = (mfg empty wt - engine wt) x $362/pound

Engine Direct Maintenance Cost

The ATA maintenance labor equations, which are functions of engine shaft power, required adjustment to obtain correlation with Allison maintenance labor estimates (manhours per flight hr). The adjustment factor was introduced to provide the influence of engine configuration differences, i.e., complexity, parts count, and component accessibility features on engine teardown time requirements. The ATA maintenance material equations, which are functions of engine

OEM cost, provided good correlation with Allison maintenance material cost estimates (dollars per flight hr). Therefore, no adjustments were applied to this set of equations.

Aircraft Less Engine Direct Maintenance Cost

The aircraft less engine maintenance costs were based on Bell Helicopter Textron, Inc. maintenance equations (Ref. 1) supplied to Allison during the NASA-Lewis sponsored Advanced General Aviation Turbine Engine (GATE) studies completed in 1979. These equations were developed by Bell for use in predicting conventional single rotor helicopter labor and material costs based on manufacturers empty weight less engine weight. An adjustment to these equations was required to obtain correlation with the maintenance cost level estimated by Bell for the reference tilt-rotor aircraft used in the SECT study. This adjustment or bump factor was necessary to account for the added complexity of the tilt-rotor, i.e., twin rotor/gearbox/engine propulsion packages plus the interconnect drive system, and to incorporate the effects of inflation from the 1978 to 1985 time period.

BASELINE ENGINE DESCRIPTION AND SCALING EQUATIONS

Engine Description

The baseline engine is derived from a current technology engine. This SECT baseline engine is a two-spool, front-drive, centerline-concentric, free-turbine, 1000 shp turboshaft engine. It is designed as a primary propulsion unit for advanced rotorcraft applications.

The gas generator spool is comprised of a two-stage centrifugal-flow compressor made of 6-4 titanium having an overall pressure ratio of 14:1 and driven by a two-stage, axial-flow turbine.

The first and second-stage turbine vanes are made of MAR-M509, the first-stage blades are made of MAR M246, and all are air cooled. The power turbine is comprised of two axial flow stages made of INCO 713, an output shaft made from EMS-64500, and an integral electromechanical phase displacement type torque sensor. The power turbine airfoils are not cooled.

The engine has an annular fold-back combustor having a Lamilloy®* transpiration-cooled liner and is made of INCO 718. It contains 16 airblast fuel nozzles. Fuel is mixed with air and burned in the combustor to bring the temperature of the fuel/air mixture (RIT) to 1204°C (2200°F).

The control system for this engine uses a full-authority, digital electronic control and a unitized fuel handling system. Self-contained electrical power is supplied by a high-speed permanent magnet generator that provides electrical power for ignition and electronic central functions.

An engine accessory gearbox is mounted on top of the engine and provides drive pads for the engine fuel pump, permanent magnet generator, hydraulic pump, and starter/generator system. The accessory gearbox also incorporates the self-contained engine lubrication system including the oil filter, cooler, pump, and pressure regulating system.

Figure 9 shows the general arrangement details for this engine with front and side views along with major engine envelope dimensions. It also shows an inlet air particle separator that was removed for the subject tilt-rotor installation (this unit is airframe-mounted equipment).

Basic information regarding the baseline engine is listed in Table V. The OEM's cost of $219,100 was used in Task I to develop engine/aircraft sensitivity curves or trade factors. However, this OEM cost was reevaluated during the Task III study efforts and adjusted to the cost indicated in Table V. Standard day performance plus engine cycle data summaries are listed in Table VI for SLSS, for IRP, and at 6096 m (20,000 ft)/250 KTAS, maximum cruise power conditions.

Study Engine Installation and Scaling

Installation assumptions used for the turboshaft study engines are as follows:

- o inlet recovery (PT2/PT0) = 1.00
- o aircraft bleed air requirements = 0.0

*Lamilloy is a registered trademark of the General Motors Corporation.

TABLE V.
BASELINE ENGINE (PD452-1) BASIC INFORMATION

POWER	1000 SHP AT SLSS, IRP (1204°C [2200°F] ROTOR INLET TEMPERATURE)
AIRFLOW	2.58 kg/SEC) (5.69 LB/SEC)
WEIGHT	115.67 kg (255 LB) (POWER/WEIGHT RATIO = 3.9:1)
OEM COSTS (1985 DOLLARS)	$219,100—TASK I $214,932*—TASK III

* THIS OEM COST IS BASED ON 10,000 TOTAL ENGINE BUILD AT A PRODUCTION RATE OF 80 ENGINES PER MONTH.

TE86-4878

---

o aircraft power extraction - included in the tilt-rotor power polars (Aircraft accessories are mounted in the center gearbox assembly located in the fuselage wing carry through.)

Performance, weight, and dimensions were developed for unity size (1000 shaft horsepower (shp) at SLSS, IRP) study engines. Scaling equations were then used to adjust these engine characteristics to the horsepower size necessary to meet design mission requirements. The engine scaling equations used in the SECT study are:

1)Weight

$$W_S = W_U \times \frac{shp_S}{shp_U}^{EXP}$$

where:

S → scaled engine size
U → unity engine size

TABLE VI.
BASELINE ENGINE PERFORMANCE SUMMARY

	SLSS/IRP	20K/250 KTAS/ CRUISE
SHP	1000	580
SFC kg/HR-HP (LB/HR-HP)	0.204 (0.450)	0.187 (0.412)
RIT, °C (°F)	1204 (2200)	1116 (2040)
COMPRESSOR INLET CORRECTED FLOW, $W\sqrt{\theta}/\delta$ kg/SEC (LB/SEC)	2.58 (5.69)	2.69 (5.92)
COMPRESSOR PRESSURE RATIO, R_c	14:1	14.9:1
COMPRESSOR ADIABATIC EFFICIENCY, η_c	78.4%	77.3%
GASIFIER TURBINE EFFICIENCY, η_T	85.7%	85.7%
POWER TURBINE EFFICIENCY, η_T	88.5%	88.6%
CHARGEABLE TURBINE COOLING, % OF COMPRESSOR INLET FLOW	4.8%	4.8%
LEAKAGE, % OF COMPRESSOR INLET FLOW	1.17%	1.17%
COMBUSTOR EFFICIENCY, η_B	99%	99%
COMBUSTOR Δ P/P	3.0%	3.0%
COMPRESSOR EXIT CORRECTED FLOW, $W\sqrt{\theta}/\delta$, kg/SEC (LB/SEC)	0.26 (0.57)	0.26 (.57)
GASIFIER TURBINE INLET CORRECTED FLOW $W\sqrt{\theta}\epsilon/\delta$, kg/SEC (LB/SEC)	0.43 (0.94)	.43 (0.94)
POWER TURBINE INLET CORRECTED FLOW, $W\sqrt{\theta}\epsilon/\delta$, kg/SEC (LB/SEC)	1.54 (3.4)	1.59 (3.5)
GASIFIER TURBINE $GJ\Delta h/U_m^2$	1.21	1.21
POWER TURBINE $GJ\Delta h/U_m^2$	1.66	1.66
LP RPM	29277	29277
HP RPM	48450	47123

TE86-4879

EXP = 1.05 if $shp_S/shp_U > 1.0$

EXP = 0.96 if $shp_S/shp_U < 1.0$

2)Dimensions (linear)

$$L_S = L_U \times \frac{shp_S}{shp_U}^{0.4}$$

3)Dimensions (diameters)

$$D_S = D_U \times \frac{shp_S}{shp_U}^{0.5}$$

4)Specific fuel consumption (SFC)

$SFC_S = SFC_U$ x adjustment factor (see Table VII)

TABLE VII.
ADJUSTMENT FACTOR FOR SFC SCALING VS. ENGINE SCALE FACTOR

ENGINE SCALE FACTOR (SHP_s/SHP_u)	ADJUSTMENT FACTOR	
	BASELINE ENGINE	ADVANCED TECHNOLOGY ENGINES
1.1	0.994	0.993
1.0	1.000	1.000
0.9	1.008	1.009
.0.8	1.017	1.019

TE86-4880

BASELINE ENGINE MISSION RESULTS AND TRADE FACTORS

Results from "flying" the previously presented baseline engine/reference tilt-rotor aircraft in the Allison Mission Analysis Computer Program are shown in Table VIII. This table summarizes basic information resulting from the subject engine/aircraft combination scaled to meet the SECT design mission requirements. Design TOGW, engine horsepower size at IRP, and rotor diameter are provided in Table VIII. Rate of climb capabilities are shown for each candidate sizing condition. Shown in parenthesis are the required rate of climb levels. The critical engine sizing condition is shown to be the 91.44 m/min (300 rpm) rate of climb at cruise altitude and velocity, i.e., cruise ceiling requirement.

Resultant power loading values for the PD452-1 powered tilt-rotor aircraft are compared against the Sikorsky S76 helicopter levels in Table IX for both all engines operative (AEO) and one engine operative (OEI) conditions.

Table IX shows that the tilt-rotor aircraft has a 60% higher power loading at both AEO and OEI conditions. These high power loadings, relative to the S76 helicopter, will provide the tilt-rotor aircraft with significant safety margins and capabilities for use in V/STOL and hover operations (hover and OEI rate of climb capabilities versus required levels are shown in Table VIII).

TABLE VIII.
MISSION RESULTS (PD452-1 POWERED TILT-ROTOR)

FUEL COST = $0.39/l
UTILIZATION = 1000 HRS YR

TOGW	4559 kg (10,050 LB)
SHP/ENGINE @ IRP SLSS	1010 HP
ROTOR DIAMETER	6.9 m (22.6 FT)
HOVER R OF C CAPABILITY @ 2000 FT/0 KTAS/ISA + 10°C IRP-AEO	341 M/MIN (1120 FPM) (0 M/MIN [0FPM] REQUIRED)
OEI R OF C CAPABILITY @ 1000 FT/75 KTAS/ISA + 20°C 30 MIN POWER - OEI	131 M/MIN (430 FPM) (45.7 M/MIN [150FPM] REQUIRED)
CRUISE R OF C CAPABILITY @ 20,000 FT/250 KTAS/ISA MAX. CONTINUOUS POWER	91 M/MIN (300 FPM) (ENGINE SIZING PT)
TOTAL FUEL (MISSION + RESERVES)	501 kg (1104 LB)
BLOCK FUEL	347 kg (764 LB)
TOTAL AIRCRAFT ACQ COST	$2.96 MILLION
ENGINE ACQ COST (ONE)	$331,700
DOC	1208 $/BLK HR

TE86-4881

TABLE IX.
POWER LOADING COMPARISON (SEA LEVEL STATIC, STANDARD DAY CONDITIONS)

AIRCRAFT ENGINE NO.	S76 250-C30 (2)	TILT-ROTOR PD452-1 (2)
TOGW, KG (LB)	4672 (10,300)	4559 (10,050)
SHP/ENGINE AT IRP, SLSS	650	1010
POWER LOADING = SHP TOTAL/TOGW	0.126	0.201
ΔPL (AEO CONDITION)	(BASE)	(+60%)
SHP AT OEI (30 MIN) POWER, SLSS	650	1010
POWER LOADING = SHP TOTAL/TOGW	0.063	0.100
ΔPL (OEI CONDITION)	(BASE)	(+60%)

TE86-4882

Table VIII also includes total fuel (design fuel tankage capacity) and block fuel (mission fuel burned) data along with cost data from the DOC model.

A component or group weight breakdown is shown in Table X for the scaled PD452-1/tilt-rotor aircraft combination. The total base engine weight of 234 kg (515 lb) included in the propulsion group represents only 5% of the aircraft TOGW and fuel weight of 501 kg (1104 lb) represents only 11% of the aircraft TOGW.

Mission fuel usage data is shown in Table XI on a per mission phase basis and on an engine power setting basis. These data indicate the cruise plus reserves (45 minutes of continued cruise) at an approximate maximum continuous power setting level to be the largest full usage requirement (433 kg [955 lb] or 87% of the total fuel).

A breakdown of the six direct operating cost elements is shown in Table XII with respect to aircraft and engine costs. These data indicate aircraft associated insurance and depreciation to be the two largest cost items and that only 31% of the total DOC can be associated with or influenced by engine characteristics.

TABLE X.
AIRCRAFT WEIGHT BREAKDOWN (PD452-1 POWERED TILT-ROTOR)

	KG (LB)	WEIGHT FRACTION—%
PROPULSION GROUP (INCLUDES ROTOR GROUP AND DRIVE SYSTEM)	1140 (2513)	25.0
STRUCTURES GROUP	1007 (2221)	22.1
FIXED EQUIPMENT	962 (2121)	21.1
MFG EMPTY WEIGHT	3109 (6855)	68.2
USEFUL LOAD	223 (492)	4.9
OPERATING EMPTY WEIGHT	3345 (7374)	73.1
PAYLOAD	726 (1600)	15.9
ZERO FUEL WEIGHT	4058 (8947)	89.0
FUEL (USABLE)	501 (1104)	11.0
TOGW	4559 (10,051)	100.0

TE86-4883

TABLE XI.
MISSION FUEL BREAKDOWN (PD452-1 POWERED TILT-ROTOR)

MISSION PHASE BASIS	kg(LB)	%
START AND WARM-UP ALLOWANCE	0.9 (2)	—
T.O. AND TRANSITION ALLOWANCE	14 (32)	3
CLIMB @ 180 KEAS	51 (113)	10
CRUISE @ 20K/250 KTAS	267 (588)	53
TRANSITION AND LAND ALLOWANCE	12 (27)	3
SHUT-DOWN ALLOWANCE	0.9 (2)	—
RESERVE (45 MIN)	154 (340)	31
TOTAL	501 (1104)	100%
ENGINE POWER SETTING BASIS		
INTERMEDIATE RATED POWER	66 (145)	13
~ MAX CONTINUOUS POWER	433 (955)	87
GROUND IDLE POWER	1.8 (4)	—
TOTAL	501 (1104)	100%

TE86-4884

Using the baseline engine powered tilt-rotor aircraft as the baseline, the effect of delta changes in the following engine characteristics on both TOGW and DOC was obtained:

- o engine specific fuel consumption (SFC)
- o engine weight (WT)
- o maximum engine envelope length (LE)
- o maximum engine envelope height (HE)
- o engine OEM cost ($/shp)

The results from the subject calculations are presented in the TOGW sensitivity curves shown in Figure 10 and the DOC sensitivity curves shown in Figure 11.

TABLE XII.
DOC BREAKDOWN—$/BLK HR (PD452-1 POWERED TILT-ROTOR)

FUEL COST = $0.39/l—$1.50/GALLON
UTILIZATION = 1000 HR/YR

	AIRCRAFT	+	ENGINE	→	TOTAL A/C + ENGINE
FUEL AND OIL	—		117 (10%)		117
INSURANCE	275 (23%)		80 (7%)		355
AIRCRAFT MAINT	230 (19%)		—		230
ENGINE MAINT	—		91 (8%)		91
DEPRECIATION	270 (22%)		82 (7%)		352
FLIGHT CREW	63 (5%)		—		63
TOTALS	838 (69%)	+	370 (31%)	→	1208 (100%)

TE86-4885

ENVIRONMENTAL CONSTRAINTS

Emissions Control Requirements

There are no regulations to control exhaust emissions from small aircraft gas turbines, including rotorcraft engines, and none are expected in the near future. However, the International Civil Aviation Organization recommends the control of fuel venting from all turbines regardless of size or application.

The likelihood of future emissions regulations depends on the following factors:

- o environmental politics--particularly aircraft related issues
- o size and growth of the source--size of rotorcraft fleet
- o level of emissions control technology applied by engine manufacturers

Of the three factors stated, only the level of emissions control technology can be directly influenced by the engine designs. It is important to design to the highest control levels economically practical since it is less likely that emissions control regulations will be promulgated for engines that include these designs. The next step in emission reduction becomes extremely expensive, and the cost of control, in terms of dollars per ton of pollutants removed, becomes much greater than that required to control other sources of pollution. In addition, an aircraft system that does not issue odors or visible smoke does not invite criticism and political action.

Allison has developed a high level of cost effective emissions control technology that was used in the combustion system design of the SECT engines. This technology was demonstrated on the Model 280-C1 engine that was derived from the GMA500/advanced technology demonstrator engine (ATDE) program. The emissions control techniques used were:

- o prechamber combustor
- o optimized primary zone
- o Lamilloy construction (transpiration cooling)
- o air blast fuel nozzles

The emissions goals established for the SECT program are: fuel venting emissions (none allowed), smoke (not to exceed SN = 40), and gaseous emissions. They are based on emissions testing of an engine that contained the control techniques previously stated. Table XIII gives the maximum gaseous emissions allowable as a function of engine power setting.

The units of gaseous pollutants emissions index (g/kg fuel) were chosen to be compatible with combustor component and gas generator operational parameters. These units are more independent of the final engine cycle than units expressed in specific emissions, i.e., $g/_{kW\ hr}$, or $g/_{kN}$ of thrust.

Noise

Noise constraints for gas turbine powered rotorcraft occur at two levels, regulatory and public acceptance. The regulatory constraints contained in Federal

TABLE XIII.
MAXIMUM GASEOUS EMISSIONS ALLOWABLE

ENGINE POWER SETTING	GASEOUS EMISSIONS, g/kg FUEL		
	HYDROCARBONS	CARBON MONOXIDE	NITROGEN OXIDES
MAXIMUM	0.44	0.90	18.70
INTERMEDIATE	0.46	0.96	17.60
MAXIMUM CONTINUOUS	0.47	1.10	15.80
75% MAXIMUM CONTINUOUS	0.50	1.20	12.6
25% MAXIMUM CONTINUOUS	0.63	2.90	8.40
IDLE	7.10	68.0	3.70

TE86-4886

Air Regulation (FAR) Part 36 for rotary wing aircraft are expected to remain in place in the year 2005 with a small decrement in the required noise levels. Continuing opposition at the local level to the building of new heliports, however, results in strong incentive to produce rotorcraft that are more quiet than required by FAR Part 36. The current NASA/industry cooperative rotorcraft program should produce the technology required to reduce rotor noise. Acoustic studies of helicopters in the current fleet show that the engine contributes to the aircraft noise signature and acts as a floor to limit the gains possible by rotor noise reduction. An engine noise reduction, relative to current engine levels, is required to permit the full use of the technology being developed in the NASA/industry program.

Based on Allison test experience, engines using the advanced cycles and technology embodied in the SECT program will generate noise signatures that are lower than the signatures of current engines.

IV. TASK II. ENGINE CONFIGURATION AND CYCLE EVALUATION

The procedures and assumptions identified in Task I were used to select the engine configurations and cycle conditions for Task III. The selection criteria were chosen to place priority on direct operating cost of the reference tilt-rotor aircraft as opposed to return on investment (ROI) or other economic figures of merit.

Three basic engine cycles were examined during Task II: (1) an advanced simple cycle, (2) a waste heat recovery cycle, and (3) a wave rotor cycle. For the advanced simple cycle, two types of general arrangements were examined: the traditional concentric gas turbine spool arrangement and a nonconcentric spool arrangement. For the waste heat recovery cycle, the regenerative and recuperative approaches were studied.

GAS TURBINE TECHNOLOGY PROJECTIONS FOR YEAR 2000

Special problems exist for each engine component by the small size requirement of this class of gas turbine engine. The following sections outline technology enhancements for the year 2000 for small gas turbine engine that were assumed for the cycle optimization study.

Compressor

Figure 12 shows the overall compressor polytropic efficiency as a function of exit corrected flow for the current state-of-the-art technology as well as that projected for the year 2000. Several mechanical and aerodynamic improvements are required to achieve this level of performance in small compressors, e.g., control clearances, surface roughness, manufacturing tolerance, airfoil contour, and secondary flow. Table XIV outlines these expected performance improvements for small compressors.

Turbine

Figure 13 shows the axial turbine overall total/total adiabatic efficiency as a function of inlet equivalent flow rate for both current state-of-the-art

TABLE XIV.

SMALL COMPRESSOR TECHNOLOGY ADVANCEMENTS.

- IMPROVED MANUFACTURING CAPABILITY
- IMPROVED ANALYSIS CAPABILITY
  - MULTI-ROW
  - 3-DIMENSIONAL
  - VISCOUS/QUASI-VISCOUS
- AXIAL COMPRESSOR
  - AIRFOIL CONTOUR
  - SWEEP, TILT, AND LEAN OPTIMIZATION
  - END WALL TREATMENT
- CENTRIFUGAL COMPRESSORS
  - IMPELLER AIRFOIL/PASSAGE CONTOUR
  - CLEARANCE LOSS REDUCTION
  - DIFFUSER ENTRANCE REGION OPTIMIZATION
  - SECONDARY DIFFUSER OPTIMIZATION

VS85-1106

technology as well as that projected for the year 2000. Improvements in fabrication methods, aerodynamic concepts, and analytical modeling are needed to achieve the projected level of performance in small axial turbines. Table XV outlines these expected turbine technology advancements. Figure 14 shows the radial turbine performance goals for the Small Engine Component Technology (SECT) study.

All cycle analysis assumed uncooled turbine configurations. This assumption was necessary, especially in the high pressure turbine. The size and life requirement of the high pressure (HP) turbine rotor prohibit introduction of cooling passages. Therefore ceramics were selected as the material for turbines.

TABLE XV.

TURBINE TECHNOLOGY ADVANCEMENTS.

- ADVANCED MATERIALS/FABRICATION METHODS
  - HIGHER WHEEL SPEEDS/REDUCED STAGE LANDING
  - REDUCED COOLING AIR REQUIREMENTS
  - REDUCED BLOCKAGE/HIGHER ASPECT RATIOS
  - LOWER THICKNESS/CHORD RATIO BLADING
  - UNIFORM BLADING THROATS
- ADVANCED AERODYNAMIC CONCEPTS
  - ENDWALL BOUNDARY LAYER CONTROL
  - PASSAGE MERIDIONAL CONTOURING
  - LOW REYNOLDS NUMBER BLADING
- ADVANCED ANALYTICAL MODELS
  - 3-D VANE/BLADE INTERACTION
  - 3-D VISCOUS FLOW ANALYSIS
  - OPTIMIZED AERO/HEAT TRANSFER BLADING

V305-1986

Combustor

The key technology advancement required for the combustor is the achievement of a low pattern factor to permit operation at high turbine temperatures for improved cycle efficiency. A goal pattern factor of 0.12, as defined by (T_{MAX}-rotor inlet temperature (RIT)/(RIT-CDT), has been established for year 2000 combustor technology. Other goals being addressed include low smoke and increased durability.

Materials

The main emphasis in materials development for gas turbines is toward high temperature capability, low density, low cost fabrication, and improved corrosion/erosion resistance. For the year 2000, two key materials emerge as the

requirement to significantly reduce the direct operating cost of the small gas turbine engine becomes important. First ceramic composites in the high pressure turbine rotor and stator will provide the opportunity to run the engine at higher turbine temperatures than engines in service today. A silicon carbide composite will have a 1649°C (3000°F) temperature capability by the year 2000. Secondly, to accommodate the higher compressor discharge temperatures associated with going to much higher cycle pressure ratios, titanium aluminide (Ti_3Al) will be needed for its temperature capability of 816°C (1500°F). The additional benefit of Ti_3Al is its low density (50% density reduction over superalloys) and ease of fabrication.

The selection of maximum turbine rotor inlet temperature (RIT) was based on the following:

1. For the ceramic radial HP turbine rotor, the maximum allowable surface temperature was set at 1399°C (2550°F). Based on the AGT 100 uncooled ceramic radial turbine heat transfer characteristics, the rate of $T_{M\ MAX}/T_{REL\ MAX} = 0.983$. Therefore $T_{REL\ MAX} = 1424°C$ (2595°F). Based on the SECT radial turbine designs, the ratio of $T_{REL\ MAX}/RIT = 0.927$, RIT MAX of 1538°C (2800°F) was obtained.
2. The combustor pattern factor assumed for the year 2000 technology is 0.12. For a static structure such as the HP turbine inlet vane, the maximum allowable surface temperature was set at 1649°C (3000°F). For the cycle pressure ratios considered, resulting max RIT is 1535°C (2795°F).

Therefore, maximum RIT of 1538°C (2800°F) was selected.

Recuperator/Regenerator

Recent advances in recuperator/regenerator technology make it necessary to re-examine the waste heat recovery cycle for the rotorcraft application. In the area of recuperator technology, a nitride dispersed stainless steel (NDS) is available that has an 982°C (1800°F) temperature capability. NDS recuperators can be fabricated at extremely low cost. Ceramics is another candidate material for recuperators, offering higher temperature capability (1260°C [2300°F])

than NDS. It is lighter than NDS but costs more to fabricate. This information was provided by Air Research Manufacturing Company, Torrance, California. They also provided a recuperator parametric study necessary to conduct the recuperator cycle optimization during Task II.

Regenerator technology for the year 2000 consists of using a one-piece extruded ceramic disk. This procedure minimizes cost and weight while providing high strength for higher than normal cycle pressure operation. Low leakage seals characterized by low thermal distortion are also included in the design. This design will allow the regenerative cycle to optimize at higher cycle pressure ratios than conventional regenerative cycles, such as the advanced gas turbine (AGT 100) being developed by Allison.

Wave Rotor Engine

In this concept, the conventional high pressure spool in the simple cycle engine is replaced by a wave pressure exchanger or Comprex system. The Comprex assumes the function of a turbine-driven compressor (compressor-expander) with a direct transfer of energy by impingement of the expanding gas on the air to be compressed. Figure 15 illustrates the wave rotor cycle. The Comprex rotor consists of straight axial channels that are alternately exposed to segmented ports open to the air or to the hot gases. Nonsteady flow is created by the opening and closing of the rotor channels as they pass over the ports and blocked off portions of the stator. The rotor speed and rotor length must be defined to coordinate pressure wave passage time with port opening. The Comprex system is essentially a flow switching device and is not capable of producing shaft power. It must be driven to overcome friction and windage losses. Figure 16 shows a typical wave rotor configuration for gas turbine application.

The efficiency of the energy exchange within the Comprex system is equivalent to high grade radial turbomachinery and is less sensitive to size than turbomachinery. The system is also amenable to speed changes with good efficiencies and offers instantaneous load response.

The rotor is alternately exposed to hot and cool gases and the rotor material assumes some average temperature, thereby allowing combustor outlet temperatures that are limited only by the static structure. Only a part of combustor

discharge gas is used in the Comprex system. The remainder is bypassed and diluted as required before entering the low pressure turbine.

CYCLE/CONFIGURATION EVALUATION

The methodology used to perform the cycle optimization study in Task II is shown in Figure 17. The year 2000 technology base for small gas turbine engines was used to calculate cycle performance for each engine configuration under study. Within each cycle matrix, one cycle was selected as a preliminary design point cycle to calculate engine weight, cost, and dimension. From that preliminary design point cycle, weight, cost, and dimension for the other cycles in the matrix were obtained analytically as described in Task I of this report. Using the trade factors developed during Task I, sensitivities to direct operating cost were developed for each cycle in a given matrix. This technique was used to select the cycle (RIT, R_c combination) for each configuration that gave the minimum relative direct operating cost (DOC).

Each cycle was scaled to produce 1000 shaft horsepower (shp) at sea level static (SLS) conditions. All cycle analysis assumed uncooled turbine configurations with maximum TRIT of 2800°F. Total cycle leakage was scaled as a function of cycle pressure ratio and engine flow size. Specifically:

$$\text{SECT leakage} = \text{base leakage} \times \left(\frac{R_{C\ SECT}}{R_{C\ BASE}}\right) \times \left(\frac{W_{A\ BASE}}{W_{A\ SECT}}\right)^{1/2}$$

where the base values are those from the baseline advanced technology turboshaft engine. The leakages are expressed as a percentage of total compressor inlet flow. The regenerator and recuperator systems were designed at the tiltrotor mission cruise flight condition (6096 m/250 knots true airspeed (KTAS) [20,000 ft/250 KTAS]) for optimum performance. Results of the cycle study for the concentric, nonconcentric, recuperative, regenerative, and wave rotor engine cycles are presented in the following sections.

Concentric Engine Cycle Evaluation

Cycle Evaluation

For the concentric component arrangement of the simple cycle engine, pressure ratios from 15 to 25 were investigated with turbine rotor-inlet-temperatures from 2200°F to 2800°F. Overall pressure ratios greater than 25 were not considered. Design analysis of the concentric engine indicated that the bore stress in a HP turbine was prohibitive for pressure ratios greater than 25.

Figure 18 shows the parametric cycle analysis for the concentric engine for the range of cycle parameters investigated. This chart illustrates the trends in specific fuel consumption and specific horsepower as a function of turbine temperature and pressure ratio. The weight and cost sensitivities were applied to generate the DOC trends shown in Figure 19. The minimum DOC is shown to occur at an overall pressure ratio of 25:1 and 2800°F RIT for the concentric cycle.

Engine Configuration

The concentric engine general arrangement is shown in Figure 20. The features are summarized as follows:

- o removable top-mounted accessory gearbox module
- o an aluminum inlet support
- o a four-stage axial 8.33:1 low pressure (LP) compressor
- o a gas generator incorporating with
  - a centrifugal flow 3:1 compressor (dual IMI Ti)
  - a parallel wall radial vaned diffuser (TiAl)
  - reverse flow annular combustor made from ceramic (SiC/SiC)
  - radial inflow gasifier turbine (SiC/SiC)
- o removable single-stage axial uncooled low pressure (LP) turbine (Ti_3Al)
- o removable two-stage axial uncooled free shaft power turbine (TiAl) module
- o full authority adaptive digital control
- o self-contained fuel and lubrication systems
- o engine monitoring system (EMS)

Output shaft speed is 40,000 rpm rotating counterclockwise as viewed from the aft end of the engine. The engine configuration provides an advanced design with low life cycle costs, high reliability, high survivability, and excellent maintainability for the tilt-rotor aircraft missions. A description of each component follows.

Gearbox--The accessory gearbox is designed to mount on the top of the engine for improved maintainability and can be removed with all accessories in place and without disturbing any other engine module. This module incorporates an integral oil system and provides drive pads for both engine and aircraft accessories.

Inlet support--The inlet support is cast aluminum and forms the major forward engine support case. This casting provides the flow path for engine air entering the first-stage axial LP compressor and is anti-iced with scavenge oil.

Centrifugal impeller--The compressor is designed to meet the conditions at the SLS match point. The static structure and the impeller are made from low thermal expansion titanium to maintain close clearance control. An abradable erosion resistant coating of flame sprayed aluminum-silicon applied over chromium carbide is used on the shrouds to allow tight clearances with rub protection. The compressor represents a low technical risk engine component.

Combustion system--The combustion system is a durable, high performance, reverse flow annular design that uses a machined outer casing, ceramic transition liner, and piloted air blast fuel injector. This combustor meets all requirements of the tilt-rotor aircraft mission. A reverse flow feature provides the shortest possible coupling between the compressor and the gasifier turbine with resulting benefits in shaft dynamics and engine rigidity.

Radial inflow gasifier turbine--The gasifier turbine rotor is expected to operate in a more severe thermal environment and at higher speeds than any previously tested at Allison. The analysis of this rotor is an extension of the ceramic rotor experience gained from the Advanced Gas Turbine Program.

Single-stage axial LP turbine--The LP turbine is based on a current technology turbine with slightly more severe thermal and speed operating conditions.

Blade stress and vibration characteristics are moderately above the existing engines. The material change to single crystal minimizes the required cooling flow and provides an increased temperature margin.

Power turbine--The two-stage axial power turbine is based on a current technology power turbine. The configuration incorporates advanced materials to eliminate cooling. The power turbine rotates counterclockwise when viewed from the rear and opposite the gas generator direction to provide optimum efficiency and reduced weight.

Nonconcentric Engine Cycle Evaluation

Cycle Evaluation

Moving the HP spool out in the nonconcentric type configuration eliminates the requirement to pass shafting through the center of the high pressure rotor. By eliminating the bore stress problem, overall pressure ratios up to 40:1 could be considered for this configuration. The maximum HP turbine rotor-inlet-temperature was again limited to 2800°F.

Figure 21 shows the parametric cycle analysis for the nonconcentric engine for overall pressure ratios of 25 to 40 and turbine rotor-inlet-temperatures ranging from 2200°F to 2800°F. This illustrates the trends of specific fuel consumption and specific horsepower as a function of the cycle parameters. Figure 22 illustrates the DOC trends of the nonconcentric cycle as a function of Rc and RIT. This shows the optimum cycle to be at a 30:1 overall pressure ratio and 2800°F RIT.

Engine Configuration

The nonconcentric engine is a three-spool turboshaft engine concept that offers the capability of achieving a significant reduction in specific fuel consumption (SFC) and cost and an increase in power-to-weight ratio compared to current Allison engines. The nonconcentric turbine engine achieves the reduced fuel consumption by combining high cycle pressure ratio and high turbine RIT in a three-spool configuration. The arrangement differs from the conventional two-spool engine by the addition of a third spool, which is mounted off axis

and aligned parallel to the other two spools. Advantages are improved compressor performance and surge margin, smaller diameter flow path, reduced seal and bearing diameters, elimination of bore stress problems, and a simpler accessory gear arrangement. The nonconcentric engine general arrangement, as shown in Figure 23 is a result of studies designed to meet the optimum performance constraints while minimizing the duct pressure losses and engine heat rejection. The power shaft is inside the LP shaft with the output connection located at the engine front.

Recuperator Engine Cycle Evaluation

Cycle Analysis

A comprehensive parametric study was made to select the optimum recuperator engine combination. The following parameters were considered:

- o engine
  - compression ratio, R_c--6, 10, 14
  - turbine rotor inlet temperature, RIT--1204°C, 1371°C, 1538°C (2200°F, 2500°F, 2800°F)
- o recuperator
  - effectiveness, E%--60, 70, 80
  - total pressure drop, ΔP/P%-- 6, 8, 10
  - plate and fin spacing, thickness, and offset
  - tube size, spacing, and dimpling
  - number of passes--air and gas
  - cross and counterflow
  - materials--metal and ceramic
  - number and arrangement of modules
  - size, weight, and cost

A total of 45 engine cycles were selected for analysis from the 81 possible combinations of the above parameters. Figure 24 shows a typical parametric analysis plot for the recuperative engine cycle. This trend of specific fuel consumption and specific horsepower as a function of cycle Rc and RIT is for a recuperator having a design effectiveness of 60%, and a total pressure drop of 10%.

Recuperator Configuration Analysis

Allison selected the matrix of R_c, RIT, E, and ΔP/P for investigation. AiResearch was chosen, because of their extensive experience, to select appropriate heat transfer surfaces and flow arrangements and to calculate sizes required. A description of the procedure for selecting the optimum recuperator engine combination follows.

Configuration

AiResearch selected offset rectangular heat transfer surfaces, shown in Figure 25, for all plate and fin analyses. This surface has the advantage of reducing boundary layer to zero at each fin offset and is generally acknowledged to be one of the most compact available. AiResearch had optimized this type surface for minimum core volume in a Garrett vehicular engine. AiResearch conducted the optimization based on this type of surface. A thorough optimization of the above plate and fin dimensions for DOC was not conducted. A comparison of modified plate and fin dimensions was made at 10:1 engine compression ratio and 1538°C (2800°F) RIT with a counterflow recuperator. At 60% E and 10% ΔP/P reductions of 22-25% in cost, 8-12% in weight and 3-26% in length for the same overall recuperator diameter were obtained by using slightly more fins/in. and greater plate spacing on the gas side. The study to minimize DOC was conducted with the vehicular engine dimensions that were shown to produce minimum individual core volume but not minimum overall wrap up volume. All the fin dimensions considered were acceptable from a fouling standpoint with jet fuels. For the metal cross-counterflow recuperators, AiResearch evaluated all their offset fin configurations and narrowed the selection based on weight and size. Allison made the final selection based on DOC sensitivities.

AiResearch selected 0.32 cm (1/8 in.) diameter tubing as the smallest possible, for size and weight, without encountering laminar flow that would cause poor heat transfer. Both in-line and staggered tube arrangements were evaluated along with plain, ring-dimpled, and spiral-dimpled tubes for inside boundary layer disruption. In general, in-line tubes provide smaller recuperator diameter but greater weight than staggered tubes. Dimpling provides lower weight but greater recuperator diameter. The best combination was selected for each engine condition. Ring dimples were not represented in the final selection.

AiResearch selected the following flow configuration, surface, and material combinations for comparison:

- o two-pass cross-counterflow--metal tube and shell
- o two-pass cross-counterflow--metal plate and fin
- o counterflow--metal plate and fin
- o counterflow--ceramic plate and fin

AiResearch selected an annular arrangement of six modules for all recuperator types. Figures 26 and 27 show the arrangement of the metal plate and fin two-pass cross-counterflow configuration. Six modules provide a convenient size for minimum cost of assembly, brazing, and ceramic firing operations. The annular arrangement provides a minimum weight means of channeling exhaust flow with circular shell structures.

Materials, Cost, and Size

AiResearch recuperator material development is underway and is expected to provide 982-1093°C (1800-2000°F) metal capability and 1260°C (2300°F) ceramic capability by year 2000. The metal will be nitride dispersion strengthened 300 series stainless steel and the ceramic, silicon nitride. The tilt-rotor aircraft and 648 km (350 nm) cruise mission selected would require only current day chrome-moly steel for 704°C (1300°F). This is due to the fact that the engine is sized for cruise. It has a high 90% power setting as opposed to other aircraft that might be sized for hover and cruise at 75% power. At 90% power, variable engine geometry can not be used to increase turbine outlet or recuperator inlet temperature to high levels while maintaining maximum turbine inlet temperature as could be done at 75% power. This application cannot take advantage of advanced high temperature recuperator technology. Even so, low density of the ceramic material made it a close contender.

AiResearch provided cost equations for the four types of recuperators based on (1) the number of air passage layers and plate area for the plate and fin designs and (2) tube length and number of tubes for the tube and shell designs. Allison derived sensitivity factors to describe the effect of relevant engine and recuperator parameters on the tilt-rotor aircraft DOC. Figure 11 shows

these sensitivity curves. The engine plus recuperator parameters affecting DOC and their relative weight are as follows:

o specific fuel consumption (SFC)	46%
o cost	26%
o weight	12%
o length	9%
o height (or diameter)	7%
	100%

AiResearch sized about 50 recuperators of four types for 45 selected engine thermodynamic cycles. Fifty values for one recuperator dimension were selected. The values of the other two dimensions were calculated to give the specific effectiveness and pressure drop for each cycle. Different splits between air and gas side pressure drops resulted. Allison used the sensitivity curves for weight, length, and diameter on a partial basis to select the recuperator with minimum DOC for each engine cycle. In general, the best size was a recuperator with slightly more than minimum weight, but slightly shorter and significantly less in diameter.

Selection of Recuperator Type

A recuperator type that provided minimum DOC was selected for each of the 45 engine cycles. The types considered were:

- o two-pass cross-counterflow--metal tube and shell
- o two-pass cross-counterflow--metal plate and fin
- o counterflow--metal plate and fin
- o counterflow--ceramic plate and fin

The sensitivity curves were used to determine the effect of recuperator weight, recuperator diameter (or height) engine plus recuperator length, and recuperator cost on relative DOC.

Specific fuel consumption was omitted and partial weight and cost for the recuperator were justified because comparisons of relative DOC were made for each individual engine cycle. A comparison of the four recuperator types is shown

in Table XVI for R_c of 14 and RIT of 1538°C (2800°F). Comparisons are valid line-by-line for selection of the best recuperator type because (1) partial of weight and cost was used and (2) a new datum was assumed for each line (the tube and shell ΔDOC). Lowest ΔDOCs are underlined and represented by the most negative values of ΔDOC. Two-pass cross-counterflow (metal plate and fin) configurations and counterflow (ceramic plate and fin) configurations were selected for further evaluation. The tube and shell and counterflow (metal plate and fin) configurations were not contenders and were eliminated from further consideration.

Direct Operating Cost Evaluation for Cycle Selection

The recuperative engine cycle parameters were selected to provide the minimum DOC. The sensitivity curves were used with complete values of:

- o SFC
- o cost
- o weight
- o length
- o height (or diameter)

Engine cost and weight were calculated using inhouse equations with recuperator costs from Garrett. Figures 28 through 30 show for a two pass crosscounter metallic plate and fin recuperator the effect of engine compression ratio (R_c), recuperator effectiveness (E), and recuperator total pressure drop ($\Delta P/P$) for RIT of 1538°C (2800°F) on relative DOC. From these figures, minimum DOC is obtained at R_c = 13, E = 64%, and $\Delta P/P$ = 10%. Engine cycles with the ceramic counterflow recuperator were similarly compared and minimum DOC design was obtained at R_c = 14, E = 60%, and $\Delta P/P$ = 10%.

Table XVII compares overall DOC ratios and partial DOCs for each parameter for the best two recuperators: two-pass cross-counterflow metal plate and fin, and counterflow ceramic plate and fin. The metal recuperator has 1.4% lower overall DOC. Based on DOC considerations, a metal two-pass recuperator was selected. The ceramic recuperator excels only in weight, due to the lower density of ceramics. Therefore, the engine with two pass cross counterflow metal

TABLE XVI

1538°C (2800°F) RIT ENGINES USING PARTIAL DOCS.

		TUBE AND SHELL					CERAMIC PLATE AND FIN				
		TWO-PASS CROSS COUNTER					COUNTER				
E	ΔP/P	WEIGHT KG	HEIGHT CM	L CM	COST	ΔDOC	WEIGHT KG	HEIGHT CM	L CM	COST	ΔDOC
60	6	17.4	65.4	95.0	10,629	0.00	28.2	61.9	92.0	7,084	- 1.03
	8	17.3	57.7	95.9	10,485	0.00	23.7	62.6	87.0	5,677	- 4.37
	10	15.7	57.4	89.8	10,062	0.00	21.3	55.9	86.7	6,302	- 3.38
70	6	29.6	65.3	107.6	12,795	0.00	32.6	64.0	95.6	8,078	- 4.40
	8	28.1	63.5	107.3	12,510	0.00	31.6	64.9	90.1	6,523	- 7.02
	10	27.7	61.5	103.8	12,498	0.00	28.8	58.3	90.1	7,186	- 6.98
80	6	73.1	62.5	144.2	18,552	0.00	54.8	67.6	101.6	9,766	-10.00
	8	45.2	70.9	103.3	16,260	0.00	47.0	68.8	95.2	7,908	- 7.94
	10	41.7	64.3	104.7	15,072	0.00	42.6	69.9	91.5	6,839	- 8.32

		METALLIC PLATE AND FIN									
		TWO-PASS CROSS COUNTER					COUNTER				
E	ΔP/P	WEIGHT KG	HEIGHT CM	L CM	COST	ΔDOC	WEIGHT KG	HEIGHT CM	L CM	COST	ΔDOC
60	6	36.7	65.4	90.8	3,487	-2.53	52.0	67.5	95.8	5,811	7.26
	8	35.3	58.9	84.4	3,087	-3.79	44.3	60.9	95.9	6,342	5.24
	10	32.6	59.7	82.0	2,889	-3.42	40.3	56.3	90.4	5,573	4.25
70	6	52.8	68.1	90.3	3,495	-6.05	68.4	64.3	98.7	6,807	1.66
	8	50.4	60.6	83.1	2,857	-7.31	57.7	63.2	99.5	7,090	0.50
	10	48.3	68.9	87.3	3,110	-6.39	52.8	58.9	94.3	6,206	-1.92
80	6	95.5	67.4	86.7	3,529	-11.68	95.9	67.9	104.0	7,984	-7.41
	8	93.8	62.7	82.1	3,119	-6.10	83.4	69.4	97.4	6,494	-3.47
	10	93.9	60.0	79.3	2,911	-4.80	75.5	68.6	99.5	7,064	-2.53

		TUBE AND SHELL					CERAMIC PLATE AND FIN				
		TWO-PASS CROSSCOUNTER					COUNTER				
E	ΔP/P	WEIGHT LB	HEIGHT IN.	L IN.	COST	ΔDOC	WEIGHT LB	HEIGHT IN.	L IN.	COST	ΔDOC
60	6	38.4	25.76	37.39	10,629	0.00	62.2	24.39	36.23	7,084	- 1.03
	8	38.1	22.71	37.77	10,485	0.00	52.3	24.64	34.24	5,677	- 4.37
	10	34.6	22.60	35.34	10,062	0.00	47.0	22.00	34.12	6,302	- 3.38
70	6	65.3	25.70	42.37	12,795	0.00	71.8	25.20	37.65	8,078	- 4.40
	8	61.9	25.00	42.26	12,510	0.00	69.6	25.54	35.48	6,523	- 7.02
	10	61.1	24.20	40.86	12,498	0.00	63.4	22.96	35.47	7,186	- 6.98
80	6	161.2	24.6	56.77	18,552	0.00	120.9	26.62	39.99	9,766	-10.00
	8	99.7	27.9	40.69	16,260	0.00	103.6	27.09	37.49	7,908	- 7.94
	10	91.9	25.3	41.21	15,072	0.00	93.9	27.53	36.04	6,839	- 8.32

		METALLIC PLATE AND FIN									
		TWO-PASS CROSSCOUNTER					COUNTER				
E	ΔP/P	WEIGHT LB	HEIGHT IN.	L IN.	COST	ΔDOC	WEIGHT LB	HEIGHT IN.	L IN.	COST	ΔDOC
60	6	81.0	25.76	35.75	3,487	-2.53	114.6	26.57	37.70	5,811	7.26
	8	77.9	23.17	33.24	3,087	-3.79	97.7	23.98	37.74	6,342	5.24
	10	71.9	23.51	32.29	2,889	-3.42	88.9	22.17	35.59	5,573	4.25
70	6	116.4	26.83	35.56	3,495	-6.05	150.7	25.31	38.87	6,807	1.66
	8	111.2	23.84	32.73	2,857	-7.31	127.2	24.88	39.16	7,090	0.50
	10	106.4	27.12	34.39	3,110	-6.39	116.3	23.17	37.12	6,206	-1.92
80	6	210.5	26.55	34.15	3,529	-11.68	211.4	26.73	40.96	7,984	-7.41
	8	206.7	24.68	32.33	3,119	-6.10	183.8	27.34	38.33	6,494	-3.47
	10	207.1	23.63	31.24	2,911	-4.80	166.5	26.99	39.18	7,064	-2.53

TABLE XVII.

RECUPERATIVE ENGINE COMPARISON—PLATE AND FIN RECUPERATORS.

	CERAMIC COUNTERFLOW		METAL TWO-PASS CROSS-COUNTERFLOW
PARTIAL ΔDOCS			
SFC	1.41	(EQUAL)	1.41
COST—$	−1.24		−2.04 (BEST)
WEIGHT—KG (LB)	−0.72 (−1.58) (BEST)		−0.56 (−1.23)
LENGTH—CM (IN.)	0.69 (−0.27)		−1.83 (−0.72) (BEST)
DIAMETER—CM (IN)	−1.32 (−0.52)		−2.39 (−0.94) (BEST)
TOTAL Δ DOC	−2.20		−3.52 (BEST)
OVERALL DOC/DOC*	0.9780		0.9648 (BEST)

TE86-4895

plate and fin recuperator was selected. The general engine outline is shown in Figure 31.

All recuperator and engine performance had been calculated and compared for the cruise condition (6096 m [20,000 ft] altitude 250 knot) where the majority of mission fuel is burned. It was necessary to calculate sea level performance for the best engine and recuperator combination so that a mission analysis could be made to calculate DOC. Allison supplied sea level engine cycle data to AiResearch, which they used to calculate sea level recuperator performance. Table XVIII shows the sea level and altitude performance details for the selected two-pass cross-counterflow metal plate and fin recuperator. Sea level effectiveness and pressure drop are significantly lower because of increased Reynolds number; however, only a small portion of mission fuel is burned at sea level conditions.

Engine Configuration

The recuperative engine that is shown in Figure 31 employs a six module metal two pass cross-counterflow recuperator. The core of each module is 28 cm (11.1 in.) long x 15 cm (6.1 in.) wide x 5 cm (2 in.) thick. Manifolding increases overall length to 38 cm (15.1 in.). The six modules are arranged so that the 15 cm (6.1 in.) sides form a hexagon with 27 cm (10.8 in.) inside diameter and are surrounded by a 49 cm (19.4 in.) diameter exhaust duct. Total recuperator

TABLE XVIII.

SEA LEVEL AND ALTITUDE RECUPERATOR PERFORMANCE TWO-PASS CROSS-COUNTERFLOW—METAL PLATE AND FIN.

INLET PRESSURE KG/CM² (PSIA)	AIRFLOW EACH OF 6 MODULES KG/SEC (LB/SEC)	INLET TEMPERATURE °C (°F)	OUTLET TEMPERATURE °C (°F)	EFFEC-TIVENESS %	ABSOLUTE PRESSURE DROP KG/CM² (PSI)	PRESSURE DROP RATIO ΔP/P
6096m (20,000 FT)						
AIR 7.03 (100.0)	0.135 (0.2979)	324 (616)	549 (1021)	60	0.31 (4.38)	0.0438 CORE
GAS 0.53 (7.54)	0.141 (0.3098)	699 (1290)	497 (926)		0.14 (1.98)	0.0263 CORE
						0.0303 MANIFOLDS
						0.1004 TOTAL
SEA LEVEL						
AIR 13.7 (194.2)	0.256 (0.5641)	393 (740)	631 (1168)	52.9	0.57 (8.04)	0.0414 CORE
GAS 1.17 (16.68)	0.258 (0.5693)	842 (1548)	632 (1169)		0.02 (0.25)	0.0151 CORE
						0.0129 MAINFOLDS
						0.0694 TOTAL

TE86-4896

weight including ducting is 35 kg (77 lb.). Material is modified nitride dispersed type 321 stainless steel convoluted and brazed with 982°C (1800°F) capability. The cores consist of 20 air passage layers and 21 gas passage layers interspersed. Exhaust gas makes one pass through the 5 cm (2 in.) dimension while compressor discharge air makes two passes through the 28 cm (11.1 in.) dimension. This recuperator provides a thermal effectiveness of 60% and a pressure drop of 10% at cruise.

The advanced technology recuperative engine features a two-shaft arrangement that permits considerable freedom in the matching of loads of differing torque versus speed characteristics to the same engine.

The engine, which has modular construction, incorporates a radial inlet housing integral with the accessory gearbox, a two-stage axial compressor with variable geometry, an impeller with radial diffuser, a single can combustor, a single-stage axial gasifier turbine, a two-stage axial free power turbine, a six module metal two pass cross-counterflow recuperator, and an electronic fuel control system.

In summary, inlet air passes through a radial inlet to the axial-impeller compressor. There it passes through variable inlet guide vanes, which can be used

to change engine airflow, and to an axial compressor and an impeller, where it is compressed. The compressed air passes from the impeller through a parallel wall radial vaned diffuser and is collected by a TiAl scroll. The compressor discharge air makes two passes through the 28 cm (11.1 in.) dimension of the recuperator core, where it is heated, and exhaust gas makes one pass through the 5 cm (2 in.) core. From the recuperator, the air flows through an H-188 Lamilloy®* combustor.

Fuel is mixed with the air and burned in the combustor to bring the temperature of the fuel/air mixture to 1538°C (2800°F). The hot gases are collected by an inlet scroll where the vanes direct the flow to the gasifier turbine. Sufficient power is extracted at this location to meet the requirements of the HP compressor and the oil pump system.

The discharge from the gasifier turbine is directed through an interturbine duct and vane arrangement at the power turbine. The vanes direct the gas flow

to the power turbine where power output is extracted for various applications. The flow from the power turbine is directed through the recuperator to the exhaust.

Regenerative Engine Cycle Evaluation

Cycle Analysis

A comprehensive parametric study was made to select the optimum regenerator-engine combination. Regenerator, as used here, refers to a rotating periodic-type heat exchanger. The following parameters were considered:

- o engine
  - o compression ratio, Rc--6, 8, 10, 12
  - o turbine rotor inlet temperature, RIT--1204°C, 1371°C, 1538°C (2200°F, 2500°F, 2800°F)

*Lamilloy is a registered trademark of the General Motors Corporation.

- o regenerator
  - o effectiveness, E%--60, 65, 70, 75, 80
  - o total pressure drop, $\Delta P/P$%-- 6, 8, 9, 10, 11, 12, 13, 14, 17, 20
  - o passage shape and size (hydraulic diameter--D_H)
  - o parameters--number of passages/in.^{2} (N), surface area/unit volume (β), passage hydraulic diameter (D_H), wall thickness (S), and open area fraction (σ) all interrelated
  - o flow length (disk thickness)
  - o disk flow area and seal blockage area
  - o gas to airflow area split
  - o disk rotational speed
  - o heat transfer and friction coefficients
  - o number and arrangement of disks
  - o disk and seal materials
  - o size, weight, and cost

A total of 126 engine cycles were evaluated. Figure 32 shows a typical parametric analysis plot for the regenerative engine cycle. This trend of specific fuel consumption and specific horsepower as a function of cycle Rc and RIT is for a regenerator having a design effectiveness of 70%, and a total pressure drop of 13%. A description of the procedure for selecting the optimum regenerator engine combination follows.

Regenerator Configuration Analysis

Configuration

Allison selected an extruded ceramic heat transfer matrix with equilateral triangular passages formed by three sets of parallel walls intersecting at common points. Figure 33 is a photo of a similar matrix. This triangular matrix provides the strength required to resist radially inward pressure loads. An open area fraction of 0.715 was selected based on previous stress analysis that showed that such a matrix would withstand the pressure loads (Ref 2). Once the open area fraction has been selected, the relationship of four additional matrix variables is fixed, as shown in Table XIX.

TABLE XIX.

HEAT TRANSFER MATRIX PROPERTIES FOR EQUILATERAL TRIANGULAR PASSAGES WITH OPEN AREA FRACTION OF 0.715.

SURFACE VOLUME b–FT²/FT³	HYDRAULIC DIAMETER D_H—IN.	PASSAGES IN.² N	WALL THICKNESS σ—IN.
800	0.0429	299	0.0079
900	0.0381	379	0.0070
956*	0.0359	427	0.0066
1000	0.0343	468	0.0063
1800*	0.0190	1500	0.0035

* SELECTED FOR TILT ROTOR AIRCRAFT MINIMUM DOC

** TYPICAL SELECTION FOR GROUND APPLICATION FOR MINIMUM SPECIFIC FUEL CONSUMPTION (SFC)

TE86-4897

Surface-to-volume ratio was used as a primary variable in the heat transfer calculations. Analytical values of the dimensionless Colburn heat transfer factor (J) and Fanning friction factor (f), were used (Ref 3). These analytical values are judged to be representative of the experimental values that have been reported. As a function of Reynolds number (Re) for fully developed laminar flow, they are:

$$J \times Re = 3.51 = \text{constant}$$
$$f \times Re = 13.333 = \text{constant}$$

The regenerator disk parameters were fixed based on prior experience. Open area fraction was limited to a maximum of 0.715 for strength requirements. A minimum workable disk flow length or thickness of 7.6 cm (3 in.) was chosen because minimum length produces minimum disk volume and weight for a given effectiveness and pressure drop. Higher values of surface-area-to-volume ratio (ß) compensate for shorter flow length. Gas-to-airflow area ratio was set at 1.2 to provide minimum specific fuel consumption. Disk rotational speed is 12 rpm.

With the disk parameters fixed, regenerator sizing involved finding the combination of surface-to-volume ratio (ß) and disk diameter (D) required to obtain the thermal effectiveness and pressure drop selected for each engine cycle. Higher surface area increases effectiveness and pressure drop while larger disk diameter increases effectiveness and decreases pressure drop. An allowance of 1% for engine internal duct pressure losses was included, based on experience. Regenerators were sized for the 6096 m (20,000 ft) altitude, 250 knot cruise condition since most mission fuel was burned at that condition. Reynolds number effects at altitude conditions required lower values of surface area to volume ratio and larger hydraulic diameter passages than those for sea level applications, as shown in Table XIX.

Rotating regenerators employ double-sided seals on both sides of the disks with a rubbing face seal on one side and a static leaf seal on the other. The seals are exposed to full engine pressure ratio. Allowance for seal leakage must be made in engine performance calculations. A seal leakage scaling equation, based on an established engine leakage data base, was used. This equation is scaled based on disk diameter, engine pressure ratio, disk speed, and disk thickness. The equation treats the rubbing wearface, static leaves, and carryover due to disk rotation separately. The equation is as follows:

$$L_2 = \underbrace{0.3L_1 \frac{R_{c_2}}{R_{c_1}} \frac{D_2}{D_1}}_{\text{wearface}} + \underbrace{0.3L_1 \frac{R_{c_2}}{R_{c_1}}}_{\text{leaf joints}} + \underbrace{0.1L_1 \frac{R_{c_2}}{R_{c_1}} \frac{D_2}{D_1}}_{\text{leaves}} + \underbrace{0.3L_1 \frac{R_{c_2}}{R_{c_1}} \left(\frac{D_2}{D_1}\right)^2 \frac{N_2}{N_1} \frac{W_2}{W_1}}_{\text{carryover}}$$

where

- L = absolute leakage
- D = disk diameter
- R_c = compression ratio
- N = disk speed
- W = disk thickness
- 1 = base conditions
- 2 = new conditions

Two regenerator disks were selected to minimize engine length and height. Figure 34 shows how the disks contribute to engine length and height, yet provide

a compact package. Smaller disk diameters, provided by the use of two disks, allow the capability for a one piece extrusion eliminating cement joints. Two disks have the disadvantages of higher leakage, weight, and cost, which are important factors and would merit further study in a detailed design.

Materials and Cost

Current regenerator materials are adequate for the cruise-sized tilt-rotor aircraft because this application does not allow use of high regenerator inlet temperature. Regenerator inlet temperature is 769°C (1417°F) at the operating cruise condition. The regenerator disk would be extruded aluminum silicate, which is rated for 1093°C (2000°F) steady-state operation. The cold side seal would use a 0.06 thick 430SS platform with attached impregnated graphite wearfacing and Inco X750 seal leaves. The hot side seal would use an 0.08 thick Inco 625 platform with impregnated graphite rim wearface and plasma sprayed nickel oxide-calcium fluoride crossarm wearface with L605 cobalt alloy seal leaves. Regenerators with these materials have demonstrated good durability at 982°C (1800°F) and 4:1 pressure ratio in ground applications and are expected to be adequate for the selected cruise temperature of 769°C (1417°F) and 10:1 pressure ratio.

Cost estimates for several regenerator diameters were obtained from the disk and seal vendors supplying current parts for Allison engines. Curves were obtained from the cost data to provide costs for all sizes evaluated. Allowance was made for the proposed production rates. The sensitivity factors derived in Task I describe the effect of relevant engine and regenerator parameters on the tilt-rotor aircraft DOC. Figure 11 shows these sensitivity curves. The engine and regenerator parameters affecting DOC and their relative weights are as follows:

o SFC	46%
o cost	26%
o weight	12%
o length	9%
o height (or diameter)	7%
	100%

Direct Operating Cost Evaluation for Cycle Selection

The engine cycle was selected to provide minimum DOC at the cruise condition. The DOC sensitivity curves were used to obtain the separate factors for:

- o SFC
- o cost
- o weight
- o length
- o height (or diameter)

These separate factors were summed to obtain an overall DOC factor for each engine. Engine cost, weight, and length were calculated using inhouse equations for turbomachinery, gearbox, and accessories with regenerator values added. Regenerator weight and cost included values for covers, drives, and ducting. Figures 35 through 37 show plots of DOC versus engine R_c, regenerator effectiveness (E), and regenerator $\Delta P/P$. These plots show that minimum DOC is obtained when $R_c = 9.5$, $E = 69\%$, and $\Delta P/P = 13\%$. Calculations were extended to $\Delta P/P = 20\%$ but showed no tendency to optimize. Reductions in regenerator weight with increasing pressure drop were greater than the increases in engine size and weight necessary to maintain the required power. These results merit further study. It was decided to limit the regenerator pressure drop to 13% because the resulting axial disk loads act against the cold side seal and result in greater seal wear. The regenerator disks for the selected engine were 15.72 in. in diameter. The size of their cases relative to the engine is shown in Figure 34. Based on these considerations, the regenerative engine with $R_c = 10$, $E = 70\%$, and $\Delta P/P = 13\%$ was selected.

All regenerator and engine performances had been calculated and compared for the cruise condition (6096 m [20,000 ft] altitude, 250 knots) where the majority of mission fuel is burned. It was necessary to calculate sea level performance for the selected engine and regenerator combination so that a mission analysis could be made to determine actual DOC. Table XX shows both the sea level and altitude performance data for the selected regenerator. Sea level effectiveness and pressure drop are lower than at altitude because of increased Reynolds number. However, only a small portion of mission fuel is burned at sea level conditions. The Reynolds number effect also accounts for the selec-

tion of passages with larger hydraulic diameter for altitude conditions as opposed to ground applications as depicted in Table XIX. Leakages of 5.2% at 6096 m (20,000 ft) cruise and 5.5% at sea level 100% were calculated for the selected regenerator-engine combination.

Engine Configuration

The regenerative engine shown in Figure 34 is a two shaft engine. Air passes through a conventional inlet housing through variable inlet guide vanes and then through an axial/centrifugal rotor, where it is compressed. The compressed air passes from the impeller through a parallel wall radial vaned diffuser and is collected by a TiAl scroll. The compressor discharge air then passes through the high pressure side of either rotating ceramic regenerator disk where it is heated. From the regenerators, the air flows through an H-188 Lamilloy combustor.

Fuel is mixed with the air and burned in the combustor to bring the temperature of the fuel/air mixture to 1538°C (2800°F). The hot gases are discharged into a scroll where the vanes direct the flow to the gasifier turbine. Sufficient power is extracted at this point by the gasifier turbine to meet the requirements of the HP compressor and the engine and aircraft accessories.

The discharge from the single-stage gasifier turbine is directed through an interturbine duct and vane arrangement to the two-stage power turbine. The vanes direct the flow to the power turbine where the power output for various applications is extracted. The flow from the power turbine goes through the low pressure side of each of the regenerators to the exhaust.

The regenerative engine employs two rotating ceramic regenerator disks 40 cm (15.7 in.) in diameter and 8 cm (3 in.) thick. The disks are extruded aluminum silicate with 426 equilateral triangular holes per square inch and 0.02 cm (0.0066 in.) thick walls, resulting in 0.715 open area. Each hole has a 0.09 cm (0.036 in.) hydraulic diameter (inscribed circle). Regenerators optimized for altitude operation require larger holes than those for sea level operation where 0.05 cm (0.019 in.) hydraulic diameter is common. Each disk weighs 5.6 kg (12.4 lb).

TABLE XX.

SEA LEVEL AND ALTITUDE REGENERATOR PERFORMANCE CERAMIC TRIANGULAR PASSAGE MATRIX.

	INLET PRESSURE KG/CM² (PSIA)	AIRFLOW EACH OF 2 DISKS (LB/SEC)	INLET TEMPERATURE °C (°F)	OUTLET TEMPERATURE °C (°F)	EFFEC-TIVENESS %	ABSOLUTE PRESSURE DROP KG/M² (PSI)	PRESSURE DROP RATIO ΔP/P
6096m (20,000 FT)							
AIR	5.16 (73.4)	0.47 (1.027)	259 (499)	617 (1142)	70.0	54.56 (0.0776)	0.0011
GAS	0.58 (8.24)	0.48 (1.0598)	769 (1417)	447 (836)		604.95 (0.9116)	0.1189
							0.0100 DUCTS
							0.130 TOTAL
SEA LEVEL—MAXIMUM							
AIR	10.02 (142.6)	0.85 (1.8811)	322 (611)	653 (1207)	55.2	60.40 (0.0859)	0.0006
GAS	1.24 (17.7)	0.88 (1.9463)	921 (1690)	629 (1165)		755.13 (1.0740)	0.0681
							0.0100 DUCTS
							0.0787 TOTAL

TE86-4898

Compressor discharge flow is directed through one sector of the disk and turbine outflow through the remaining sector. The disk matrix absorbs heat from the turbine outflow, carries it to the other sector by rotation, and gives it up to the compressor discharge flow. The two flows are directed through the disk and kept separated by seals running against the disk faces.

The seals have sheet metal substrates with attached graphite and metal oxide wear facings sealing against the rotating disk and metal foil static sealing leaves sealing against the engine casing. A regenerator leakage of 5.2% at cruise was used for the selected design. The disk is driven by a surrounding ring gear joined to its outer diameter by a cast-in-place elastomer.

The entire regenerator system including a portion of engine case weight assignable to the regenerator is 30.6 kg (67.4 lb). The system provides a thermal effectiveness of 70% and pressure drop of 13% at cruise.

Wave Rotor Engine Cycle Selection

For the wave rotor engine cycle, cycle pressure ratios from 15 to 45 were studied along with turbine rotor-inlet-temperatures from 2200°F to 2800°F. Figure 38 shows the parametric cycle analysis trends of specific fuel consumption and specific horsepower for the range of cycle parameters invesitaged. The optimum wave rotor cycle occurs at Rc = 38 and RIT = 2800°F, as shown in Figure 39.

A possible arrangement of a wave rotor in-line engine using the Comprex system is shown schematically in Figure 40 and shown mechanically in Figure 41. The wave rotor in-line configuration provides an engine envelope that is streamlined and similar to an existing engine but somewhat longer and heavier with the addition of the wave rotor components. Because of the asymmetric inlet and outlet ducting of the wave rotor, the in-line configuration is best suited to centrifugal compressors and turbines where the swirl of the gases can be used to extract the mass flow at discrete locations around the periphery of the rotating components in ducts that can be matched to similar ducts on the wave rotor. Locations of the two combustors within a streamlined envelope configuration may be difficult because of the need to reroute air and combustion gas around the wave rotor. In order to keep the Comprex system into a compact configuration, the following techniques have been employed:

- o the two combustors are placed on the top and bottom of the Comprex system to maintain relative short duct connections
- o vaned diffusers are used as the main technique for rapid diffusion of existing flows to low velocities in order to shorten the connecting ducts
- o the use of short turning distances permits compact ducting arrangements for the wave rotor including the upstream and downstream inlets

The mechanical arrangement shows that air passes through the low pressure compressor (axial and centrifugal made from rapid solidification technology (RST) Al and TiAl forging, respectively) and the Comprex rotor (made from oxide dispersioned strengthened (ODS) Ni) before entering into the two combustors D_0 and D_1 at station 3. The combustor D_0 discharge gas (station 4) passes through the Comprex and from there to the power turbine (made from TiAl). The combustor D_1 exit gas at station 5 (with dilution if required) passes through

the low pressure turbine made from Ni_3Al (station 6) and is mixed with the Comprex discharge gas (station 7) before the power turbine (station 8).

The wave rotor engine is unique because the single stage LP turbine does not produce enough energy to drive the LP compressor under all operating conditions. A special gearbox located at the engine front is designed to transfer energy from the three-stage power turbine to the LP turbine for driving the LP compressor.

ENGINE CYCLE/CONFIGURATION SELECTION

Table XXI compares the optimum cycles for each of the 5 configurations investigated. Each of these cycles was optimized using relative direct operating cost as the figure of merit. A preliminary analysis was conducted to establish the feasibility of these five configurations.

TABLE XXI.
SECT OPTIMUM CYCLE COMPARISON.

	BASELINE	CONCENTRIC	NONCONCENTRIC	RECUPERATIVE	REGENERATIVE	WAVE ROTOR
R_c	14	25	30	13	10	36
RIT—°C (°F)	1204 (2200)	1538 (2800)	1538 (2800)	1538 (2800)	1538 (2800)	1538 (2800)
$W\sqrt{\theta}/\delta$	5.7	3.2	3.5	3.4	3.8	3.2
CRUISE SFC	0.412	0.330	0.327	0.306	0.306	0.33
WEIGHT—KG (LB)	116 (255)	56 (124)	63 (139)	105 (232)	102 (224)	86 (187)
OEM COST $	214,932	111,651	123,788	125,608	160,486	154,060
Δ DOC - %	BASE	16.8	15.3	14	11.6	11.6

TE86-4899

The design analysis of the concentric engine indicated that the bore stress in the ceramic HP turbine was prohibitive. Moving the HP spool out in the nonconcentric type configuration eliminated the requirement to pass shafting through the center of the high presure rotor, thus eliminating the bore stress problem.

A thorough analysis of the wave rotor type engine was not complete at the end of Task II. The initial investigation into the wave rotor indicated that the shaft power output type was unsuitable for gas turbine applications because of inherent low efficiency as compared to projected compressor efficiency for year 2000. On the other hand, the pressure exchanger type wave rotor (no shaft power output) is mechanically complex due to the required flow split ahead of the high pressure turbine. However, recent wave rotor analysis indicates that the shaft power output device can be made at least as efficient as that projected for year 2000 compressors, as illustrated in Figure 42. This figure shows that for corrected exit flows less than 0.41 kg/sec (0.9 lb/sec), the efficiency potential of the wave rotor exceeds that of the compressor efficiency assessment for year 2000. At least an additional 1% reduction in DOC would be realized based on the projected improvement in wave rotor performance. A more detailed study is required to fully assess the potential of wave rotors for year 2000 gas turbine applications.

Based on these analyses, the nonconcentric engine, recuperative engine, and regenerative engine were selected for system performance evaluation. The performance, component selection, dimensional data, for each selected configuration and reference engine are presented in Table XXII. Table XXIIA gives a detailed weight and cost breakdown of these three selected configurations. The engine cost and appropriate regenerator or recuperator costs are also tabulated in Table XXIIA.

TABLE XXII.
TASK III STUDY ENGINES—DEFINITION AND DATA SUMMARY

	BASELINE ENGINE	ADVANCED TECHNOLOGY ENGINES		
ENGINE IDENTIFICATION	CONCENTRIC CYCLE ENGINE	RECUPERATIVE CYCLE ENGINE	REGENERATIVE CYCLE ENGINE	NONCONCENTRIC CYCLE ENGINE
NO. SPOOLS L.P. COMPRESSOR H.P. COMPRESSOR H.P. TURBINE L.P. TURBINE POWER TURBINE	1 — CENTRIFUGAL AXIAL — AXIAL	1 — AXIAL/CENTRIF AXIAL — AXIAL	1 — AXIAL/CENTRIF AXIAL — AXIAL	2 AXIAL/CENTRIF CENTRIFUGAL RADIAL RADIAL AXIAL
IRP AT SLSS • R_s • RIT, °C (°F) • Ws, Kg/SEC (LB/SEC) • SHP, HP 6.1 KM (20000')	14 1204 (2200) 2.59 (5.7) 1000	13 1538 (2800) 1.54 (3.4) 1000	10 1538 (2800) 1.72 (3.8) 1000	30 1538 (2800) 1.59 (3.5) 1000
MAX CRUISE AT 463 Km/HR TAS (250 KTAS) • SHP • SFC (Δ SFC%)	 582 0.412 (BASE)	 580 0.306 (–25.7%)	 580 0.306 (25.7%)	 580 0.327 (–20.6%)
WEIGHT, Kg (LB) (Δ WEIGHT, %)	115.67 (255.0) (BASE)	105.05 (231.6) (–9.2%)	101.42 (223.6) (–12.3%)	62.91 (138.7) (–45.6%)
MAX LENGTH, CM (IN.) MAX HEIGHT, CM (IN.) TURB EXIT DIA, CM (IN.)	87.22 (34.34) 58.17 (22.90) 33.07 (13.02)	80.01 (31.50) 50.80 (20.00) 23.01 (9.06)	68.07 (26.80) 58.42 (23.00) 23.22 (9.14)	50.16 (19.75) 40.13 (15.80) 23.37 (9.20)
OEM COST, 1985 $ (Δ COST, %)	214,900 (BASE)	125,600 (–41.6%)	160,500 (–25.3%)	123,800 (–42.4%)
LP COMPRESSOR $W\sqrt{\theta}/\delta$ IN $W\sqrt{\theta}/\delta$ OUT RC ηAD	 — — — —	 — — — —	 — — — —	 3.5 0.7 7.0 0.870
HP COMPRESSOR $W\sqrt{\theta}/\delta$ IN $W\sqrt{\theta}/\delta$ OUT RC ηAD	 5.69 0.57 14.0 0.784	 3.4 0.36 13 0.835	 3.8 0.54 10 0.858	 0.7 0.2 4.7 0.802
HP TURBINE $W\sqrt{\theta}/\delta$ ηAD RPM Re	 0.94 0.857 48450 4.01	 0.67 0.90 61000 2.56	 1.0 0.903 49900 2.17	 0.3 0.89 72500 2.4
LP TURBINE $W\sqrt{\theta}/\delta$ ηAD RPM Re	 — — — —	 — — — —	 — — — —	 0.7 0.903 47500 2.0
POWER TURBINE $W\sqrt{\theta}/\delta$ ηAD RPM Re	 3.45 0.885 29277 3.21	 1.57 0.909 43900 4.49	 2.0 0.912 38900 3.80	 1.3 0.907 44550 5.5

TE86-4870

TABLE XXII A
ADVANCED ENGINES WEIGHT BREAKDOWN

ENGINE: Section	NONCONCENTRIC Wt-Lb	RECUPERATIVE Wt-Lb	REGENERATIVE Wt-Lb
Inlet/Fwd Support	7.12	3.66	4.34
LPC Rotor	6.81	—	—
LPC Housing	1.21	—	—
Scroll & Diff-LPC	12.14	—	—
HPC Rotor	1.64	6.77	7.44
HPC Housing	1.87	8.07	8.87
Scroll/Diffuser	2.98	6.37	8.67
Combustor & Hsg	7.38	24.32	17.21
HPT Rotor	1.06	5.08	6.31
HPT Housing	1.31	1.87	2.33
Interm. Turb Spt	—	5.02	5.41
LPT Rotor	1.88	—	—
LPT Housing	3.79	—	—
Power T Rotor	7.46	8.50	9.15
Power T Housing	9.88	6.65	7.16
Rear Brg Support	5.57	—	—
Block (½)	—	—	9.42
Regenerators (2) (with ½ block)	—	—	67.35
Recuperator	—	77.00	—
Exhaust Duct(s)	—	17.50	6.04
Controls	37.76	34.81	36.49
Acc Dr Gearbox	28.82	26.02	27.37
TOTAL WEIGHT	138.86	231.64	223.56
TOTAL MANUFACTURING COST	$123,788	$125,608	$160,486
RECUPERATOR/ REGENERATOR COST	—	$ 8,370	$ 30,280

V. TASK III. SYSTEM PERFORMANCE EVALUATION

The purpose of the Task III effort was to provide a system performance evaluation of the Task II selected advanced technology engine configurations against the Task I selected baseline or state-of-the-art engine.

The nonconcentric, recuperative, and regenerative engines were evaluated using the Allison mission analysis procedures and ground rules established in Task I. Each study engine/tilt-rotor aircraft combination was sized to meet the specified design mission. All engines were sized for the cruise rate of climb requirement. The unity size engines have the same shaft horsepower (shp) at this cruise sizing condition so the critical weight per unit horsepower characteristic for each engine will trend the weight number shown in Table XXII. The mission analysis provided the following:

- o aircraft weight, mission fuel, and DOC breakdowns
- o engine/aircraft sizing information
- o aircraft acquisition cost, fuel burned, and TOGW comparisons
- o DOC comparisons (primary figure of merit)

MISSION FUEL

Reductions in mission fuel burned are shown relative to the baseline engine powered tilt-rotor aircraft in Figure 43. The fuel burn reductions shown in Figure 43 are a result of the maximum cruise power specific fuel consumption (SFC) characteristics summarized in Table XXII. Table XXIII shows that 86% of the mission fuel is consumed at a power setting that is approximate to maximum cruise at the cruise altitude and velocity. The fuel burn reductions indicated in Figure 43 are 30.7% for recuperator, 30.5% for regenerator, and 30.1% for nonconcentric. All three advanced technology engines achieved the fuel burn reduction goal of 30%.

AIRCRAFT WEIGHT

Aircraft weight breakdown for each study engine/tilt rotor aircraft is shown in Table XXIV. The advanced engine weight varies from 2.8% for the nonconcentric engine to 4.7% for the recuperative engine whereas the baseline engine

TABLE XXIII.
MISSION FUEL BREAKDOWN COMPARISON

ENGINE I.D.	BASELINE ENGINE			RECUPERATIVE CYCLE ENGINE			REGENERATIVE CYCLE ENGINE			NONCONCENTRIC CYCLE ENGINE		
	Kg	(LB)	%	Kg	(LB)	%	Kg	(LB)	%	Kg	(LB)	%
I. MISSION PHASE												
START AND WARM-UP ALLOWANCE	1.36	(3)	0.3	0.91	(2)	0.2	0.91	(2)	0.2	0.91	(2)	0.2
•TAKEOFF AND TRANSITION ALLOWANCE	15	(32)	2.9	10	(22)	2.8	10	(23)	2.9	10	(22)	2.8
•CLIMB @ 333.3 Km/HR EAS (180 KEAS)	52	(115)	10.2	38	(84)	10.7	39	(87)	11.1	36	(80)	10.1
•CRUISE @ 6.1 Km/463 Km/HR TAS (20,000 FT/250 KTAS)	273	(602)	53.2	186	(411)	52.6	185	(408)	52.2	191	(423)	53.4
•TRANSITION AND LAND ALLOWANCES	12	(27)	2.4	9	(20)	2.6	10	(21)	2.7	8	(18)	2.3
SHUT-DOWN ALLOWANCES	0.91	(2)	0.2	0.45	(1)	0.1	0.45	(1)	0.1	0.45	(1)	0.1
FUEL BURNED	354	(781)	69.2	245	(540)	69.0	246	(542)	69.1	247	(546)	68.9
•RESERVES	157	(347)	30.8	110	(242)	31.0	109	(241)	30.8	112	(246)	31.1
TOTAL FUEL	511	(1128)	100.0	355	(782)	100.0	355	(783)	100.0	359	(792)	100.0
II. ENGINE POWER												
INTERMEDIATE RATED POWER	67	(148)	13.1	48	(106)	13.6	50	(110)	14.0	46	(102)	12.9
MAX CONTINUOUS (APPROX)	442	(975)	86.4	305	(673)	86.0	304	(670)	85.6	312	(687)	86.7
GROUND IDLE	2.27	(5)	0.5	1.36	(3)	0.4	1.36	(3)	0.4	1.36	(3)	0.4
TOTAL	512	(1128)	100.0	355	(782)	100.0	355	(783)	100.0	359	(792)	100.0

TE86-4873

weight is 5.2%. The fuel weight is in the range of 8.3% to 8.8% for the advanced engines and 11.1% for the baseline engine. Figure 44 shows reductions in TOGW of 7.7% for the recuperative engine, 8.0% for regenerative engine, and 11.5% for the nonconcentric engine compared to the baseline engine. The nonconcentric engine has the largest reduction in TOGW because it has the lowest engine weight of the advanced engines. For this mission, all three advanced engines had fuel burn reductions of ≈ 30%.

COST COMPARISONS

With the fuel and TOGW trend variations established for the advanced engines, aircraft acquisition cost trends shown in Figure 45 will track with the engine original equipment manufacturer (OEM) cost characteristics listed in Table XXII. Aircraft cost equals airframe plus engine acquisition cost, where airframe cost is a function of airframe weight. The reductions in direct

TABLE XXIV.
AIRCRAFT WEIGHT BREAKDOWN COMPARISON

ENGINE I.D.	BASELINE ENGINE			RECUPERATIVE CYCLE ENGINE			REGENERATIVE CYCLE ENGINE			NONCONCENTRIC CYCLE ENGINE		
	Kg	(LB)	%	Kg	(LB)	%	Kg	(LB)	%	Kg	(LB)	%
BARE ENGINE WEIGHT	239	(528)	5.2	200	(442)	4.7	193	(426)	4.5	114	(252)	2.8
PROPULSION GROUP (LESS ENGINE WEIGHT)	936	(2063)	20.3	853	(1880)	20.0	847	(1868)	19.9	793	(1748)	19.4
STRUCTURE GROUP	1014	(2236)	21.9	973	(2144)	22.8	971	(2140)	22.9	952	(2098)	23.3
FIXED EQUIPMENT	967	(2131)	20.9	939	(2070)	22.1	937	(2066)	22.1	925	(2040)	22.6
•MFG EMPTY WEIGHT	3156	(6958)	68.3	2965	(6536)	69.6	2948	(6500)	69.4	2784	(6138)	68.1
USEFUL LOAD	224	(494)	4.9	219	(482)	5.1	219	(482)	5.1	218	(480)	5.3
•OPERATING EMPTY WEIGHT	3380	(7452)		3184	(7018)		3167	(6982)		3002	(6618)	
PAYLOAD (8 PASS. @ 91 KG (200 LB) EA	726	(1600)	15.7	726	(1600)	17.0	726	(1600)	17.1	726	(1600)	17.8
•ZERO FUEL WEIGHT	4106	(9052)		3910	(8618)		3893	(8582)		3728	(8218)	
FUEL (USABLE)	512	(1128)	11.1	355	(782)	8.3	355	(783)	8.4	359	(792)	8.8
•TOGW	4618	(10,180)	100.0	4265	(9400)	100.0	4248	(9365)	100.0	4087	(9010)	100.0

TE86-4874

operating cost (DOC) for the advanced engines are shown in Figure 46 for $1/gal and $2/gal fuel cost. The direct operating cost (DOC) trends shown in Figure 46 track with the aircraft acquisition cost trends. This conclusion is confirmed by examination of the DOC cost breakdown comparison tabulated in Table XXV. The fuel and oil effect on ΔDOC for this mission is -2% for all advanced engines. The two largest cost components, insurance and depreciation, are direct functions of aircraft acquisition cost. A more detailed breakdown for DOC is shown in Table XXVI for the baseline and nonconcentric engine. Only 22% of the advanced engine/tilt rotor aircraft DOC was influenced by engine characteristics.

ENGINE SELECTION

Table XXVII presents a summary of the mission results. The nonconcentric engine was selected because it has the greatest reduction in DOC relative to the baseline. The reduction in DOC is 16.5% for $1/gal fuel cost and 17.4% for $2/gal fuel cost. Figure 47 shows a general arrangement of the nonconcentric engine. Table XXVIII provides a cycle summary of this engine at sea level and at the 20,000 ft altitude cruise condition.

TABLE XXV.
DOC COMPARISON—$/BLK HR

DOC @ 0.26 $/L (1.00 $/GAL) AND 1000 HR/YEAR

ENGINE ID	BASELINE	RECUPERATIVE CYCLE ENGINE	REGENERATIVE CYCLE ENGINE	NONCONCENTRIC CYCLE ENGINE
FUEL AND OIL	80	56	56	56
INSURANCE	359	308	319	296
A/C MAINTENANCE	235	215	214	203
ENGINE MAINTENANCE	91	87	89	78
DEPRECIATION	357	304	315	293
FLIGHT CREW	63	63	63	63
TOTAL =	1185	1033	1056	989
(Δ DOC, %)	(BASE)	(−12.8%)	(−10.9%)	(−16.5%)

TE86-4872

TABLE XXVI
DOC BREAKDOWN—$/BLK HR

0.26$/L (1.00 $/GAL) AND 1000 HR UTILIZATION

	BASELINE POWERED TILT-ROTOR			NONCONCENTRIC POWERED TILT-ROTOR		
	AIRCRAFT	+ ENGINE →	TOTAL A/C + ENG	AIRCRAFT	+ ENGINE →	TOTAL A/C + ENG
FUEL AND OIL	—	79.77 (6.7%)	79.77	—	56.06 (5.7%)	56.06
INSURANCE	279.36 (23.6%)	79.87 (6.7%)	359.23	255.57 (25.8%)	40.25 (4.1%)	295.82
AIRCRAFT MAINTENANCE	235.32 (19.8%)	—	235.32	203.14 (20.5%)	—	203.14
ENGINE MAINTENANCE	—	91.31 (7.8%)	91.31	—	78.41 (7.9%)	78.41
DEPRECIATION	274.37 (23.2%)	82.01 (6.9%)	356.38	251.00 (25.4%)	41.34 (4.2%)	292.34
FLIGHT CREW	63.00 (5.3%)	—	63.00	63.00 (6.4%)	—	63.00
TOTALS =	852.05	332.96	1185.01	772.71	216.06	988.77
(%TOTAL DOC)	(71.9%)	(28.1%)	(100%)	(78.1%)	(21.9%)	(100%)

VS85-1297

TABLE XXVII
TASK III SUMMARY OF MISSION RESULTS

ENGINE IDENTIFICATION	BASELINE ENGINE	RECUPERATIVE CYCLE ENGINE		REGENERATIVE CYCLE ENGINE		NONCONCENTRIC CYCLE ENGINE	
TOGW	4618 Kg (10,180 LB)	4264 (9400)	(−7.7%)	4248 (9365)	(−8.0%)	4087 (9010)	(−11.5%)
SHP/ENGINE @ IRP SLSS	4035 HP	955		950		900	
ROTOR DIAMETER	6.95M (22.8 FT)	6.67 (21.9)		6.64 (21.8)		6.52 (21.4)	
•HOVER R OF C CAPABILITY @ 0.61 Km/0 KM/HR TAS/ISA +10°C IRP-AEO (2000 FT/0 KTAS/ISA + 50°F IRP-AEO)	357 M/MIN (1170 FPM) (0 FPM REQ'D)	360 (1180)		347 (1140)		326 (1070) →	
•OEI R OF C CAPABILITY @ 0.30 Km/138.9 Km/HR TAS/ISA +20°C (1000 FT/75 KTAS/ISA +68°F) 30 MIN POWER - OEI	140 M/MIN (460 FPM) (150 FPM REQ'D)	145 (480)		140 (460)		113 (370) →	
•CRUISE R OF C CAPABILITY @ 6.1 Km/463 Km/HR TAS/ISA (20,000 FT/250 KTAS/ISA) MAX CONTINUOUS POWER	91 M/MIN (300 FPM) (ENGINE SIZING PT)	91 (300)		91 (300)		91 (300) →	
TOTAL FUEL (MISSION + RESERVES)	512 KG (1128 LB)	355 (782)		355 (783)		359 (791)	
BLOCK FUEL	354 KG (781 LB)	245 (541)	(−30.7%)	246 (543)	(−30.5%)	248 (546)	(−30.1%)
ENGINE ACQ COST (ONE)	$332,800	179,700		228,600		167,700	
TOTAL AIRCRAFT ACQ COST	$2.99 MILLION	2.56	(−14.4%)	2.86	(−11.0%)	2.46	(−17.7%)
DOC @ 0.26 $/LITER (1.00 $/GAL) AND 1000 HR	1185 $/BLK HR	1033	(−12.8%)	1056	(−10.9%)	989	(−16.5%)
DOC @ 0.53 $/LITER (2.00 $/GAL) AND 1000 HR	1264 $/BLK HR	1087	(−14.0%)	1111	(−12.1%)	1044	(−17.4%)

TE86-4871

For the nonconcentric engine, the effects of SFC, weight, maximum envelope length, maximum envelope height, and OEM cost on TOGW and DOC was determined. Figure 48 indicates engine specific fuel consumption (SFC) to have the largest effect on direct operating cost (DOC) followed by original equipment manufacturer (OEM) cost. Changes in envelope dimension are shown to have a relatively small effect on DOC with respect to a 10% change in either length or height requirements. The TOGW and DOC sensitivity levels developed for the advanced technology engine in Task III are significantly lower (30 to 60%) than those obtained from the baseline or current technology engine in Task I (see Figures 11 and 12).

In addition to the sensitivities developed with respect to changes in engine characteristics, DOC sensitivity to variations in fuel cost and aircraft utilization rate is shown in Figure 49 for the nonconcentric engine powered tiltrotor. These data indicate significant reductions in DOC for the increased utilization rate (1000 to 2000 hr/year) and a much larger influence on DOC for increased fuel cost at the higher utilization level.

TABLE XXVIII.
NONCONCENTRIC ENGINE CYCLE SUMMARY

	SEA LEVEL STATIC, STANDARD DAY	20,000 FT/250 KTAS MAXIMUM CRUISE
OVERALL		
SHP	1000	580
SFC	0.352	0.327
RIT (°F)	2800	2600
Ro/A	30	32.6
LP COMPRESSOR		
$W\sqrt{\theta}/\delta$	3.5	3.7
Rc	7.0	7.4
η_{AD}	0.870	0.861
HP COMPRESSOR		
$W\sqrt{\theta}/\delta$	0.7	0.7
Rc	4.7	4.8
η_{AD}	0.802	0.802
HP TURBINE		
$W\sqrt{\theta}/\delta$	0.3	0.3
Re	2.4	2.4
η_{AD}	0.890	0.89
LP TURBINE		
$W\sqrt{\theta}/\delta$	0.7	0.7
Re	2.0	2.0
η_{AD}	0.903	0.903
POWER TURBINE		
$W\sqrt{\theta}/\delta$	1.3	1.3
Re	5.5	6.5
η_{AD}	0.907	0.904
TOTAL CHARGEABLE COOLING & LEAKAGE	5.3%	5.3%
TOTAL PRESSURE DROP LOSS	15.9%	16.8%

TE86-6550

VI. TASK IV. SMALL ENGINE COMPONENT TECHNOLOGY PLAN

The main objective of Task IV was to identify the technology requirements and provide a technology plan for year 2000 advanced small engine components. This section describes a technology plan for the selected advanced non-concentric engine, as shown in Figure 47. This engine achieves significantly reduced specific fuel consumption (SFC) levels by combining high cycle pressure ratio and high turbine inlet temperature in a three-spool configuration. The engine configuration offers advantages with regard to aerodynamics, flow path dimensions, bore stresses, a simple accessory arrangement, and reduced seal and bearing diameters.

Based on the Task III trade-off study, a list of the key technology requirements for the nonconcentric engine is given in Table XXIX, along with its direct operating cost (DOC) payoff. The nonmetallic structure results in a 7.0% reduction in DOC because it allows the turbine to operate at 1538°C (2800°F) rotor inlet temperature (RIT). A 2.5% improvement in DOC occurs due to the use of the uncooled turbine. Advanced aerodynamics required for year 2000 in order of priority are turbine, compressor, and combustor. Bearings technology is required for increased reliability and durability. Technology plans for each of these areas will be described in this section.

TABLE XXIX.
NONCONCENTRIC ENGINE ADVANCED TECHNOLOGY REQUIREMENTS.

	REQUIREMENT	DOC PAYOFF
CERAMICS	2800°F	7.0%
	UNCOOLED TURBINES	2.5%
TURBINE	YEAR 2000 EFFICIENCY	2.8%
COMPRESSOR	YEAR 2000 EFFICIENCY	2.3%
COMBUSTOR	IMPROVE PATTERN FACTOR FROM 0.2 TO 0.12	1.5%
BEARINGS	INCREASED RELIABILITY	
	INCREASED DURABILITY	—

CERAMICS TECHNOLOGY PLAN

Significant improvements in the performance characteristics of advanced gas turbine engines are directly related to the development of high temperature materials and components. Current Ni based superalloys used in rotating and static high temperature structures have limitations due to high fabrication cost, low strength at elevated temperatures, high strategic materials content (cobalt and chromium), and added complexity for required air cooling. Extensive work is being performed on the development of advanced structural ceramics that offer numerous potential benefits (high temperature strength, low density, and no strategic materials content). While the potential advantages offered by the incorporation of ceramics in advanced gas turbine engines are attractive in a variety of components, including ceramic combustors, regenerators, plenums, vanes, and insulating members, the maximum benefits are realized in the high pressure (HP) radial turbine rotor. The use of advanced ceramic materials in the HP radial turbine rotor application offer significant improvements in performance and fuel consumption by allowing uncooled operation at turbine inlet temperatures of 2800°F and anticipated life capability in excess of 1000 hrs. However, this also is the highest risk component due to the severe mechanical and thermal operating environment. While considerable progress has been achieved on the use of structural ceramic components in gas turbine engines, a significant effort is required for successful application of ceramics to the HP rotor in the SECT engine. The objectives of the proposed program include definition and evolution of ceramic material systems and rotor fabrication techniques capable of high speed operation at temperatures of 2800°F, which demonstrate improved toughness/impact resistance, reduced property variability, increased reliability, and life capability in excess of 1000 hrs. The approaches required to achieve these objectives include material and component evolution/characterization, ceramic/ceramic and ceramic/metal interface and compatibility definition, nondestructive flaw detection techniques development, and component rig/engine environment testing and evaluation. The ceramic technology programs are shown in Figure 50.

Material Development and Characterization

The primary candidate monolithic ceramic materials for use in advanced heat engines are silicon carbide (SiC), silicon nitrade (Si_3N_4), and partially

stabilized zirconia (PSZ). The fracture strength of these materials as a function of temperature is shown in Figure 51. While the PSZ and Si_3N_4 materials have higher room temperature strengths than SiC, PSZ and Si_3N_4 suffer degradations in strength and susceptibility to oxidation at temperatures above 1000-1200°C. The SiC retains its room temperature properties to approximately 1500°C.

A number of ceramic suppliers are actively pursuing the development of sintered Si_3N_4, which features improved elevated temperature strength characteristics. Kyocera has a developmental Si_3N_4 material (SN-270), currently available only in test bar form, that maintains a strength of 100 $lb/in.^2$ (ksi) at a temperature of 1400°C. SiC and Si_3N_4 are considered prime monolithic ceramic material candidates for application in the severe operating environment (2800°F uncooled) of the HP rotor in the SECT engine. Allison has had extensive experience and successful test results with both SiC and Si_3N_4 complex geometry components produced by a variety of fabrication techniques (injection molding, slip-casting, and isostatic pressing) for the CATE and advanced gas turbine (AGT) 100 programs.

However, current monolithic ceramics have a major limitation-inherent brittleness that can lead to catastrophic failure. This limitation is a major concern for high speed rotating components, particularly for application to manrated advanced gas turbine engines.

To address the material limitations of both metallic superalloys and monolithic ceramics, a variety of composite materials systems are being evaluated. These materials (e.g., carbon/carbon, SiC/SiC, and SiC/glass-ceramic) have demonstrated improvements in fracture strength, thermal shock resistance, fracture roughness, and strain tolerance. Carbon/carbon materials, while attractive for extremely high temperature applications, are limited by a lack of oxidation resistance and are totally dependent on advanced protective coatings. Since these coatings consist of a thick monolithic ceramic (e.g., SiC), this material system as applied to many component structures suffers the same short-comings as silicon-based monolithic ceramics. The most attractive composite materials are ceramic/ceramic systems that use silicon carbide as a reinforcing fiber.

During the last decade, an extensive ceramic composite materials development effort has been conducted using high-modules SiC Nicalon continuous fiber in low modulus glass or glass-ceramic matrices. The first generation of these materials was developed using borosilicate glass matrix. Subsequently, a family of more refractory composite materials was developed based on Corning lithium-aluminosilicate (LAS) glass-ceramic matrix. Both United Technology Research Center (UTRC) and Corning Glass Works (CGW) have been actively developing SiC fiber reinforced/LAS composite systems. However, refractory glass-ceramic composites experience rapid increases in the matrix viscosity at temperatures in excess of 1250°C, resulting in the fiber/matrix debonding and loss of component structural integrity. This temperature limitation of current SiC/glass-ceramic materials restricts the maximum component temperature to approximately 1200-1300°C, precluding the application of this material to the extreme thermal conditions that are required of the SECT HP turbine rotor.

SiC/SiC composites are commercially available from Amercom in the USA and SEP (Societe Europeenne de Propulsion) in France. Amercom is in a preliminary stage of development of these composites while SEP is currently marketing both one-dimensional and multidimensional composites. This material uses Nicalon SiC fiber reinforced in SiC matrix. The fibers are coated with up to four layers of chemical vapor deposition (CVD) SiC coating. The material is toughened by developing a weak interfacial bond between the SiC fiber and the first SVD SiC layer. The room temperature strength of the 0/0 orientation SEP CERASEP SiC/SiC material is about 62,000 lb/in.^{2}, which decreased to 35,000 lb/in.^{2} at temperatures of 1250-1500°C. This behavior is consistent with the expected behavior of Nicalon fiber, whose properties are thought to degrade approximately 1250°C. Unlike SiC/borium magnesium aluminosilicate (BMAS) ceramic composite where the matrix viscosity increases rapidly over 1250°C, SiC/SiC composites appear to retain reasonable strength levels up to 1500°C. The room temperature strength of 0/0 orientation after 100 hrs of isothermal exposure in air at 1500°C was 33,000 lb/in.^{2}.

The Nicalon SiC fibers are thought to consist of microcrystalline beta silicon carbide, graphite, and amorphous silica, but they may also have homogeneous structure. Upon heating above 1250°C, the fibers lose carbon monoxide and undergo coarsening of the silicon carbide grains. This quickly leads to brittleness and loss of strength.

To address this temperature limitation, Defense Advanced Research Projects Agency (DARPA) is conducting the advanced ceramics based on polymer processing program at Dow Corning. The goal of this program is the development of an economical, improved SiC fiber from a domestic supplier with higher strengths, fewer impurities, and a higher temperature capability than current fibers. While these fibers are currently under development and not commercially available, it is anticipated that future ceramic/ceramic composites will feature significant improvements in strength, toughness, and maximum use temperature.

A complete characterization of the mechanical, physical, and chemical properties of candidate ceramic materials is required to obtain structurally sound ceramic turbine components. This program consists of five subtasks:

- o generation of material properties, including thermal expansion, thermal conductivity, specific heat, elastic modulus, Poisson's ratio, and strength characteristics, required to employ a linear elastic probabilistic approach to structural design.
- o generation of time dependent properties, including thermal fatigue, creep, and crack propagation characteristics, with emphasis on the probabilistic nature of these properties.
- o evaluation of environmental effects, including oxidation, hot corrosion, and erosion, that could cause property degradation of candidate materials during long-term use.
- o development of the relationship between material structure and mechanical properties with special emphasis on establishing the size, type, and distribution of strength limiting defects.
- o development of a high resolution inspection technique to detect critical size defects in candidate ceramic materials.

Ceramic/Ceramic and Ceramic/Metal Interactions and Compatibility

A critical element required for the successful application of ceramics and ceramic composites is an understanding of the compatibility of ceramic/ceramic and ceramic/metal interfaces and the possible interations between these materials. While little published literature exists on this phenomenon pertaining strictly to ceramic composites, this class of materials will exhibit

much of the same behavior and problem areas associated with monolithic structural ceramics. The high temperature operation of the ceramic components required to use full material capability can result in wear, adhesion, and interactions with adjacent structures, both metallic and nonmetallic. Garrett in the Ceramic Gas Turbine Engine Program used both compliant layers (HS-25) and lubricants (CoO) to minimize contact loading and reactions between reaction-bonded silicon nitride and other materials. Allison has successfully used both compliant layers (L605) and high temperature lubricants (boron nitride) in the CATE program for the attachment between the SiC turbine blade and the turbine wheel. The L605-BN combination demonstrated uniform loading and prevented reactions during spin testing to 2500 cycles. The high temperature of the ceramic may also create problems for secondary metal components. The temperature of the ceramic often exceeds the temperature capability of the metal, and the close proximity of the hot ceramic can cause unacceptable thermal gradients. Thermal barrier materials will be used at strategic locations, both for ceramic/ceramic and ceramic/metal interfaces. Candidate thermal barrier materials need to have low thermal conductivity, adequate strength, compatible thermal expansion, and the capability of being produced in proper sizes and shapes. Thermal barrier materials currently being developed and used are zirconia, zircon, mullite, and cordierite.

One of the configurations that will be considered for the HP turbine rotor involves the use of a monolithic ceramic hub section for strength and fabricability and a ceramic composite blade section for increased fracture toughness and impact resistance. Considerable effort is required to identify and characterize the optimum joining technique for attaching the monolithic hub to the composite blade structure. Various methods suitable for this attachment include brazing, high temperature glass bending, diffusion bonding, and hot isostatic pressing. Evaluation of the attachment joint would include specimen testing, subcomponent element testing, and characterization and spin testing of the full scale hardware.

Nondestructive Evaluation

Since ceramic materials are highly probabilistic in nature, design stresses are very sensitive to material property variability. An extensive quality

assurance program is therefore essential to the successful use of ceramic material in gas turbine engines. This program has two primary objectives:

- o reduction of property variability
- o early rejection of defective components

There are two distinct types of microstructural defects that control ceramic component performance in high reliability applications. The first type of defect is small in degree but very large in extent, i.e. variations in chemistry, grain size, and density. Such defects significantly affect both thermal and elastic properties as well as strength-related characteristics. The second type of defect is large in degree but very small in extent i.e., cracks, pores, and inclusions in the size range below 100 microns. Such defects primarily control material strength. In view of (1) the limitations associated with available quality assurance measures and (2) the high levels of reliability required in a commercial 1000 hr gas turbine engine, it is clear that more sensitive nondestructive evaluation (NDE) techniques are required.

Normal nondestructive techniques can be used to find gross cracks, voids, and inclusions. The techniques used are well known and require little adaptation for use with ceramic materials. However, the resolution limits of these techniques are above the critical flaw size (10-100 microns) for ceramic materials. Therefore, inspection techniques with increased resolution are required. The following NDE techniques will be investigated: ultrasonic velocity, reflective ultrasound, scanning photoacoustic microscopy, and X-ray microradiography.

Rig/Engine Environment Testing

For the successful application of ceramic components in advanced gas turbine engines, particularly in the severe operating conditions of the SECT HP turbine rotor, testing must be conducted on components that represent a production manufacturing process and a corresponding design for which analysis predicts an acceptable reliability level. However, defects as small as 20 microns can control the material critical strength. No existing NDE technique can reliably detect such flaws. Therefore, proof testing is required to identify flawed components and to qualify rotors for subsequent engine testing until advanced

methods are available. For the SECT HP rotor, the following rig qualification tests will be conducted:

- o spin testing at room and elevated temperature
- o cold flow rig testing
- o hot flow rig testing
- o vibration bench testing
- o thermal shock testing (fluidized bed)

Engine testing and evaluation will be conducted on the SECT HP rotors to characterize performance, fuel consumption, component efficiency, reliability, life characteristics, and verification of design/analysis methodology. An engine test program with incrementally increasing turbine inlet temperature will be conducted to capitalize on current ceramic materials technology and to advance the state of the art with ceramic components. This approach permits early introduction of ceramic components into the baseline program and yields an improved gas turbine engine capability in the latter part of the program.

AXIAL TURBINE TECHNOLOGY PLAN

The inlet equivalent flow rates of the small axial flow turbines, indentified from the SECT trade studies, ranged from 0.7 to 2.4 lbm/sec. Axial flow turbines of this physical size exhibit degraded efficiency levels when compared to their larger counterparts. This characteristic is shown by Figure 52, which shows a simple correlation of current state-of-the-art overall turbine efficiencies in terms of inlet equivalent flow rate. This performance trend can be attributed to the inability to affect a true aero/mechanical scale in these smaller machines. This trend is due in part to fabrication constraints and manufacturing tolerances in addition to lower Reynolds numbers and absence of advanced analysis tools that accurately model the more sophisticated flow fields in these small blade rows.

The turbine efficiency goals established for the SECT program are also presented in Figure 52. This efficiency trend curve denotes the placement of the axial flow power turbine incorporated in the optimum nonconcentric engine configuration. The year 2000 turbine aero technology curve reflects a substantial improvement in the efficiency characteristic as the turbine inlet equivalent

flow rate (physical size) was reduced. The SECT program aero goal reflects a 3.3% increase in efficiency for the power turbine as compared to current state-of-the-art technology. The achievement of the SECT turbine efficiency goal will be realized through a variety of technology advancements. A major portion will be achieved through significant advancements in the area of turbine aerodynamics. Other performance improvements will be derived from technology areas such as computational fluid mechanics, material science, casting technology, ceramics, and innovative mechanical design concepts.

A brief aerodynamic description of the two stage axial flow power turbine for nonconcentric engine configuration, discussion of the various technology areas that will contribute toward the achievement of the SECT year 2000 turbine efficiency goals, and a description of the various turbine aero key technology programs are presented in the following sections.

Power Turbine Description

The power turbine for the selected SECT engine is a two stage axial flow design. The aerodynamic design point for the power turbine is tabulated below:

o inlet equivalent flow rate, $W\sqrt{\theta_{cr}}\varepsilon/\delta$	1.31 lbm/sec
o total/total expansion ratio, R_{eTT}	5.5
o overall equivalent work, $\Delta h/\theta_{cr}$	45.6 Btu/lbm
o rotational speed, N	44550 rpm
o total/total efficiency, η_{TT}	90.7%

The power turbine has an average stage load coefficient ($gJ\Delta h/U_m^2$) of 1.62 and an average flow coefficient (V_x/U_m) of 0.44, at aero design point conditions. At this same match point, the power turbine has an exit Mach number of 0.42 and 19 degrees of exit swirl (measured from axial) in a direction opposite to rotation. The last blade has an exit AN^2 (annulus area x rotational speed squared) value of 5.6×10^{10} in.^{2} rpm^2 and hub/tip diameter ratio of 0.66. The power split ratio between the power turbine first and second stage is 51/49.

Technology Areas

The efficiency levels demonstrated for large axial flow turbines cannot be maintained for the small size turbines identified in the SECT program. This is due to the inability to maintain aerodynamic similarity in such parameters as inlet turbulence level, endwall boundary layer thicknesses, and Reynolds number. Fabrication constraints and manufacturing tolerances prohibit the scaling of physical parameters such as airfoil thickness/chord ratio, trailing edge thickness, fillet radii, blade tip clearances, and surface roughness. As a consequence, small axial flow turbine blading generally has higher trailing edge blockages, lower aspect ratios, higher maximum thickness/chord ratios, and higher rip clearance/blade height ratios than larger counterparts.

In order to identify the areas of technology that will provide the higher pay-offs, an assessment of the various sources of loss was analytically determined for the baseline SECT power turbine assuming current state-of-the-art design technology. This study was conducted using the performance model of Kacker and Okapuu. A breakdown of the turbine losses is illustrated in Figure 53. The predominate source of aerodynamic inefficiency arises from secondary flow losses (45%), followed by profile losses (25%) and shrouded blade tip clearance (22%) losses. The magnitude of the various losses in terms of a total pressure loss coefficient (ω) is shown in Figure 54. The cross-hatched area denotes the goal reduction in the various loss mechanisms to be achieved by the SECT key technology programs. The attainment of these loss reductions will enable the small axial flow power turbine to meet the SECT goal efficiency.

Approach/Technology Plan

The proposed technology programs for the axial turbine are shown in Figure 55. This series of programs includes both experimental and analytical efforts. These programs systematically address aero design concepts that offer high potential for the reduction of secondary, profile, and tip clearance losses. In addition, certain tasks will provide data for the critical verification of 3-D viscous flow analysis tools. A discussion of each program follows.

Vane Tip Endwall Mechanical Sculpturing

Stator endwall contour geometries that are axisymmetric about the engine centerline have been experimentally shown to be an effective method of reducing stator secondary flow losses. Stator tip contours of this description are widely used in modern HP turbines. This experimental program is designed to assess the benefits of stator tip endwall contours in the meridional direction that are not surfaces of revolution.

The approach involves five basic phases including the following:

1. analytical
2. design and fabrication
3. stator annular cascade test
4. full stage test
5. data reduction and analysis

During the analytical phase, a currently available 3-D inviscid code will be revised to handle the passage flow analysis for a stator whose endwalls are not surfaces of revolution. This model will be employed to evaluate candidate contour configurations. The selected tip endwall contour will be incorporated in the stator assembly of an existing small turbine rig.

The initial test phase will involve the aero evaluation of this concept using a full annular cascade. The test plan will consist of radial/circumferential (r,θ) surveys over a broad range of expansion ratios. On completion of the cascade test, the rotor assembly will be installed and complete stage performance mapping will be conducted. In addition, rotor exit (r,θ) surveys will be performed at selected overall expansion ratios. The data reduction and analysis phase includes comparing the annular cascade and full stage aero data with available data featuring the use of conventional stator endwall contours that are surfaces of revolution. This analysis procedure will involve comparing stator exit loss contours and overall stage performance maps.

Endwall Boundary Layer Control

Efficiency improvement is expected to result from stator endwall boundary layer control. The work of Stewart and Wong (reported in NASA RME55E11 entitled "Removal of Secondary-Flow Accommodations in a Two-Dimensional Turbine Nozzle Passage by Boundary Layer Bleed") shows that the removal of endwall secondary flow produces an extremely clean flow field into the downstream rotor. This will have a favorable impact on the vane blade interation losses and allow the rotor to operate more efficiently.

This experimental program is designed to determine the aero losses associated with the vane secondary flows by altering the character of the end-wall boundary layer using bleed and blowing at selected locations. The approach to be used in this program consists of five basic phases, including:

1. 2-D cascade evaluation of candidate endwall boundary layer bleed and blow concepts
2. full annular cascade tests of boundary layer control geometries selected from Phase 1
3. single stage turbine test to assess benefits of stator endwall bleed
4. two stage turbine test to measure performance improvement using first stage vane bleed in combination with second vane blowing
5. data reduction and analysis

In each of the test phases, a complete aerodynamic evaluation will be performed including the development of loss contour maps and turbine performance maps, wherever appropriate. The two stage turbine rig test will use the first vane low momentum endwall bleed as a source of air to energize the second vane endwall boundary layer. This unique concept will provide a more uniform flow field into both rotors.

Optimized 3-D Blading

The availability of the 3-D viscous airfoil passage flow analysis will provide the turbine aero designer with the ability to analytically assess the benefits of nonconventional blading exhibiting extensive 3-D passage geometries. Furthermore, this analysis model will lead to the optimum definition of the

radial distributions of such aero parameters of stage work, reaction, and turning distribution. This approach is contrasted with the current turbine design methodology where the velocity diagrams are first generated and then airfoil contours are designed to provide the defined vane/blade exit flow field.

This experimental program is structured to demonstrate the efficiency improvement that will be provided using a 3-D viscous flow analysis to define the complete vane and blade passage geometry for a small turbine rig. The approach is to employ an existing small turbine rig that was designed using conventional 2-D design analysis tools as a baseline. The turbine rig will be redesigned using 3-D viscous analysis tools to define the optimum vane and blade passage (radial distribution of airfoil throats and 3-D stacking). The redesigned turbine will maintain the baseline turbine overall stage work and reaction. This turbine will be fabricated and tested and its performance compared to the baseline design.

The major thrust of this program is to demonstrate the performance that will be provided by the availability of an advanced 3-D viscous flow analysis model. The improved understanding of the viscous flow losses in a small axial flow turbine will be paramount to the achievement of SECT performance goals.

3-D Viscous Flow Model Verification Tests

Bench mark experimental data will be required for the verification and upgrading of the subsonic and transonic 3-D viscous flow analysis. This effort is an extension of the work conducted at NASA Lewis by Seaholtz and Goldman, which employed a constant section annular stator assembly with constant diameter hub and tip endwalls. The program approach involves the design and fabrication of a stator annular cascade that establishes a strong 3-D flow field (nonconstant section airfoil, 3-D stack, and tip endwall contouring). The test procedure will involve detailed static pressure mapping along the vane and endwall surfaces. Vane-to-vane flow field velocity measurements will be conducted at near hub, mean, and tip spanwise locations for a series of selected chordal positions. This program will provide a valuable experimental data base for the critical verification of the airfoil passage 3-D, viscous flow analysis model.

Surface Finish/Reynolds Number Effects

This effort is structured to experimentally evaluate the effects of rotor blade surface finish and Reynolds number on the small axial flow turbine stage efficiency. This program complements, and is a logical extension of, the work conducted by Avco Lycoming (ref 17). It is anticipated that the results reported for the stator will be altered due to the different character of the boundary layer in this airfoil row. The test program will employ an existing small axial turbine rig to assess the effects of rotor surface finish over a broad range of inlet Reynolds numbers and overall expansion ratios. The proposed test plan will evaluate a total of three surface finishes. Performance mapping will be generated for each of four inlet Reynolds numbers. These results will provide a valuable insight relative to the effects of surface finish on the reduction of small rotor blade profile loss and how it is altered by Reynolds number.

Optimized Vane and Blade Aero Loading Distributions

This program involves the analytical assessment of the impact of inlet turbulence level and Reynolds number on the optimum vane and blade surface velocity distributions. This task is an analytical extension of the work conducted experimentally under the NASA funded E^3 effort (ref 18). The turbine airfoil optimization program combines the following design modules with an optimization algorithm:

- o airfoil section generator
- o 2-D inviscid blade-to-blade code
- o airfoil surface boundary layer analysis
- o airfoil profile loss model

In general, the optimization procedure minimizes (maximizes) an objective payoff function to a number of constraints. These constraints are formulated so that the airfoil maintains the velocity triangles and meets certain design criteria. The relevent criteria employed in this investigation will be the minimization of the airfoil fully mixed profile loss coefficient. The airfoil optimization model will be exercised over a broad range of inlet Reynolds numbers and turbulence levels characteristic of those encountered in small axial

flow turbine stages. It is anticipated these variables will have a significant impact on the airfoil optimum aerodynamic loading distribution and will complement the work conducted under NASA E^3 (ref 18), which addressed higher Reynolds numbers and lower inlet turbulence levels.

Turbine Rig Technology

This program will verify the SECT efficiency goals for the two stage power turbine to be incorporated in the selected nonconcentric engine. The technologies, derived from the above key technology programs, will be employed in the aero design of this advanced small axial flow turbine. The turbine will be tested in an engine environment and will feature the use of a continuous, free floating ceramic blade shroud, and ceramic vanes and blades.

Summary

The achievement of the SECT axial turbine efficiency goals will be realized through a variety of technology advancements. A major portion of this efficiency gain will be achieved through improved aerodynamics, as provided by key technology programs, along with the advanced analytical techniques. Advancements in other areas, such as material science, casting technology, and ceramics, in conjunction with innovative mechanical design concepts, will contribute toward meeting year 2000 efficiency goals.

RADIAL TURBINE TECHNOLOGY PLAN

The low flow capacity requirements of a small high pressure ratio engine with acceptable speed requirements and corresponding stress levels lead to the selection of radial inflow turbines. The radial turbine's high work per stage capability and reduced sensitivity to clearance effects, relative to a comparable designed axial stage gives this configuration the potential for superior efficiency characteristics. In terms of aerodynamic considerations, reduced passage widths (small blade heights) are a strong driver for the selection of a radial turbine.

Current technology in radial turbine design yields adiabatic efficiency levels shown in Figure 56. Goals set for technology programs are shown for both the

low and high pressure turbines and reflect an efficiency improvement of 3.0% over current technology.

The results of a loss breakdown study for the design point of the high pressure radial turbine is shown in Figure 57. The aerodynamic losses within the stages may be broken down into six categories: vaneless space friction (wall between vane and rotor), rotor incidence, windage (on hub), rotor clearance, rotor, and vane. Rotor and vane losses comprise the two greatest losses and are due to two major phenomenon: profile loss (or friction drag) and secondary losses (due to secondary flows in passages). Rotor clearance losses are targeted for a 0.3% point reduction by the advancements in clearance reduction resulting from use of ceramics and improved design concepts.

Approach/Technology Plan

The technology plan designed to achieve these efficiency goals is outlined in Figure 58 and targets both aspects of the vane and rotor loss mechanisms. For the purpose of technology advancement in the area of vane design, four design parameters have been selected for assessment of their loss reducing potential. Two parameters address profile losses and two parameters address secondary losses. Within the rotor, flow loss contributors are less easily delineated. In this case, each of three programs will assess the loss reduction potential of improved analysis tools and selected design changes. Verification of this improved design concept will be accomplished in a ceramic rotor and vane rig test. The technology programs are discussed in the following sections.

Vane Loss

The vane loss reduction programs have been structured as follows. An experimental program will examine the effects of vane aspect ratio (passage width/vane chord) and corner fillet radii on vane row loss levels. A set of rig adapted hardware will be designed and fabricated to test at three passage widths and three fillet radii separately and simultaneously. Use of available rig hardware is the preferred approach. The potential for improved efficiency is 0.6 percentage points. Design philosophy based on ceramic technology will be used in establishing feasibility of the range of radii and widths to be examined.

The second vane loss reduction program uses hardware of the first program with additional components added to modulate inlet turbulence levels. In addition, vane surface finish will be varied to determine proper design tradeoff relationships between losses and vane design. Three surface finish values and three turbulence levels will be examined. Potential loss reduction is anticipated to be 0.4 percentage points.

Rotor Loss

The rotor loss reduction program uses two analytical studies, each backed by experimental verification. Flow path contouring and 3-D flow analysis comprise the two areas of emphasis. The flow path contouring or rotor hub sculpturing study is aimed at analytically defining a hub contour that improves predicted rotor aerodynamic performance with a simultaneous improvement in rotor life. Quasi-3-D flow predictions will be made on three hub contures showing promise in tailoring blade velocity profiles to exhibit low loss characteristics. Rotor life predictions will be made for each design as well. Based on these results, a fourth design will be assembled and similar predictions made. The potential loss reduction is anticipated to be 0.9 percentage points.

The second program will experimentally evaluate the aerodynamic performance of the final design as determined in the previous program. This program, as well as the previous program, will be targeted to use the NASA Lewis Research Center (LeRC) radial turbine rig under development. A pressure instrumented test rotor will be fabricated. Test data will be analyzed and compared to predicted values. Information derived will be available to formulate advanced rotor design methodology.

The third rotor loss reduction program applies an advanced 3-D viscous flow analysis tool to a radial turbine rotor. The 3-D method is currently being developed in-house. Verification of predictions made using this tool will be greatly facilitated by using the data from the high temperature radial turbine program funded by NASA LeRC Contract NAS3-24230. Aero rig data from the highly instrumented but uncooled rotor fabricated in this program will be used to verify predictions. Performance benefits derivable by the subsequent use of this code as a design tool are estimated at 0.8 percentage points.

Completion of the radial turbine technology programs will result in the ability to design an advanced turbine using the resulting data bases and analytical tools and will realize the goal efficiencies as identified in the effort reported herein. The ceramic turbine verification program will include the design, fabrication, and hot rig test in an existing test rig. The rig is anticipated to be one presently used in the ongoing AGT 100 program.

COMPRESSOR TECHNOLOGY PLAN

The inherent problem in small engine compressors is performance. The inability of this class of small compressors to demonstrate the loading and efficiency levels of larger compressors can be directly attributed to the nonscalability of physical size and the relative lack of sophistication in analytical techniques to identify and quantify associated losses. However, the introduction of advanced design concepts, improved computational analysis, and modern materials/processes in the design and fabrication of small compressors is a key to bridging this performance gap.

An overview of the trends in compressor technology portraying Allison Gas Turbine state-of-the-art technology is shown in Figure 59, where polytropic efficiency is plotted against corrected exit flow. Since mass flow rate and pressure ratio determine the physical size of the rear compressor section, exit flow is a logical parameter to represent size.

Figure 59 comprises a sampling of axial, centrifugal, axial-centrifugal and dual centrifugal compression systems. The larger axial compressors have demonstrated polytropic efficiencies 1.5-15% higher than advanced axial-centrifugals and 2-3% higher than centrifugal compressors. This can be attributed to the larger flow size and considerable experience and research investment in axial compressors. Axial compressors have been limited to larger flow size applications (above 1 lbm/sec exit flow versus 0.1-0.3 lbm/sec for centrifugals) to avoid severe efficiency penalties associated with small exit blade heights. A recent analytical study was conducted to investigate the areas of concern and to determine the projections for efficiency potential in both large and small compressors for the year 2000. The results are presented in Figure 60.

The improvements (aerodynamic and mechanical) for small and large compressors are approximately 4.5% and 2% respectively. The results of this study are further presented in Figure 59 where the year 2000 technology assessment is compared to current state-of-the-art technology. The scope of the SECT compressor program is to demonstrate an increase in polytropic efficiency of 4-4.5% from current levels in small engine compressors. The SECT goals will be achieved by identifying high payoff technologies for year 2000 small gas turbine engine applications and by providing the appropriate technology plan.

SECT Compressor Design

For the current SECT study, based on mission studies for the representative tilt-rotor application, the aerodynamic design point for the compressor is given below:

corrected airflow lbm/sec	3.487
pressure ratio, Rc_{t-t}	30:1
adiabatic efficiency, n_{tt}%	78.7
polytropic efficiency, $n_{p\ t-t}$%	86.3
exit Mach number	0.30

To meet these goals--very high pressure ratio at a relatively low airflow rate and high efficiency levels--a four stage axial coupled to a single stage centrifugal was selected as the best configuration. The axial/centrifugal compressor takes advantage of the higher efficiency potential in the axial and alleviates the penalties due to reduced aft stage blade heights by employing a centrifugal compressor. Table XXX summarizes some of the salient aerodynamic and geometric design features for the axial compressor. These features are compared to two advanced axial compressors designed and experimentally tested within the last three years. The SECT compressor is designed to produce a pressure ratio of 7:1 and an efficiency of 85.1%, with adequate surge margin at design and slow speeds. The goal of this design is to evaluate loading levels (diffusion factor) and inlet tip speeds that are reflective of bigger flow size compressors, while reducing the losses normally associated with lower airflow rates and blade heights. This will be achieved with low aspect ratio blading technology for added loading/efficiency capability, improved analytical techniques, and advanced design concepts.

TABLE XXX.
SECT-COMPRESSOR TECHNOLOGY
CURRENT DEMONSTRATED AXIAL COMPRESSOR TECHNOLOGY.

	CURRENT TECHNOLOGY		
	LARGE	SMALL	DESIGN GOAL
CORRECTED AIR FLOW LBM INLET / SEC EXIT	26.24 / 4.57	3.91 / 1.424	3.487 / 0.682
PRESSURE RATIO	8.05	3.35	7.00
PRESSURE RATIO STAGE			1.627 + (15-20%)
NO. STAGES	6.0	4.0	4.0
ηT-T	84.4	84.6	85.1
η POLY	88.2	87.0	88.5
AVERAGE DIFFUSION FACTOR			0.440
COMP EXIT M_N			0.450
INLET TIP SPEED—FT/SEC	1410.0	1180.0	1436.0
EXIT ROTOR HEIGHT—IN.	0.875	0.552	0.270
AVERAGE ASPECT RATIO	1.228	1.027	0.750

The aerodynamic and geometric design features of the SECT centrifugal compressor are presented in Table XXXI. These features are compared to two experimentally verified centrifugal compressors, large current technology, and small (AGT) compressors. The SECT centrifugal is designed to produce a pressure ratio of 4.7 at 82.1% efficiency. The pressure ratio split between the axial and centrifugal compressors, dictated by axial loading levels, and impeller tip speeds and stress levels has indicated that for optimizing the specific speed (for increased exit blade height) and performance potential of the centrifugal compressor, increased rotational speed was desired. However, the increased speed resulted in excessive bore stress levels for the high pressure turbine rotor at 2800°F RIT. Therefore, the desire for increased speed and reduced turbine stress levels directed the SECT compressor to a nonconcentric configuration. From Table XXXI, it can be observed that the SECT goals require a 1.5% improvement in efficiency with a 24% reduction in exit blade height, 26% increase in tip speed and 70% increase in discharge temperature (all deterrents to performance) relative to the AGT. Improved analytical methods and design concepts will be vital for improving the performance potential of small centrifugal compressors. The following paragraphs examine the areas of technology required for small engine compressors for the year 2000.

TABLE XXXI.
SECT-COMPRESSOR TECHNOLOGY
CURRENT DEMONSTRATED CENTRIFUGAL COMPRESSOR TECHNOLOGY.

	CURRENT TECHNOLOGY	AGT	DESIGN GOAL
CORRECTED AIR FLOW LBM INLET	3.60	0.774	0.703
SEC EXIT	1.096	0.190	0.183
PRESSURE RATIO	4.136	5.477	4.700
ηT-T	85.6	80.70	82.10
η POLY	88.1	84.70	85.6
COMP EXIT M_N		0.242	0.300
SPECIFIC SPEED, N_s		80.0	71.01
INLET HT		0.450	0.541
EXIT TIP SPEED—FT/SEC		1800.0	2260.0
CDT—°R		920.0	1568
EXIT AXIAL BLADE HEIGHT	0.406	0.218	0.165
BACK CURVATURE—DEG	50.0	50.0	47.5

Technology Areas

The major areas of concern contributing to small engine compressors not achieving the performance levels demonstrated by large flow compressors are small physical size, innadequate analytical skills to identify the loss mechanisms, and the lack of experience and experimental date. This is partly due to earlier efforts in small compressors being directed primarily toward the development of economical and rugged units, without much consideration for improving efficiency/loading potential. This discrepancy in performance can be further explained by the following: for a reduction in airflow rate, the speed should be increased and all other physical parameters reduced by the square root of the change in airflow rate to maintain aerodynamic similarity. However, because of manufacturing and structural limitations, it is not possible to scale certain physical parameters--thickness, leading edge radius (LER), and clearanee--appropriately. Small size compressors are designed with higher thickness/chord (T/C), leading edge radius/chord (LER/c), and Mach number to T/C ratios. The Mach number levels in the compressor are maintained by scaling up the rotational speed. Clearance and tolerance levels to blade contour and surface roughness are not scalable and remain similar to levels of larger compressors. This combination results in increased losses in the passage and blade-row due to shock, profile, end-wall, boundary layer and clearance. While it may be possible to reduce the losses due to the above factors

with improved mechanical design and manufacturing techniques, small engine compressors have the inherent problem of low Reynolds number flows. Improvements in this area can be achieved by understanding the phenomena of low Reynolds number flow in a turbo-machinery blade row and developing analytical tools for implementation with advanced design concepts. Some concepts considered likely candidates are:

- o airfoil sweep and lean optimization to reduce shock losses
- o airfoil contouring to design velocity/diffusion controlled blading to minimize shock losses and suction surface flow separation
- o casing treatment--endwall treatment to energize boundary layer and enhance part speed flow/efficiency lapse rates for improved stability
- o design of 3-D diffuser vanes to account for highly sheared flows at diffuser entrance region
- o bleed/blow feature at diffuser throat for improved efficiency and stability at slow speed
- o clearance control/minimization over operating range of compressor by improved mechanical design

Axial Compressor Technology Plan

A discussion of the various component test programs shown in Figure 61 follows. The approach was conceived as a systematic method to experimentally investigate the factors contributing to reduced loading capability and efficiency levels of small engine compressors. This series of tests will also create the data base and experience necessary for the evaluation of analytical techniques and design of high performance axial compressors. The acquired information will not be restricted to small compressor designs, but will also be beneficial for improving the performance of large compressors.

Performance Evaluation of True Axial Compressor Scaling

Since certain physical parameters limit the scaling down of a compressor to achieve aerodynamic similarity, this program proposes to test two aerodynamically similar compressors by photographically scaling up a small size compressor. The experimental data from the two compressors will deliver a direct correlation of compressor performance versus Reynolds number changes.

The approach taken will be to test an advanced small compressor with relatively high loadings. This compressor will be scaled up to a higher flow size and performance data obtained. This will give data comparison due to Reynolds number changes associated with the two sets of hardware. Further testing will be conducted to evaluate the performance of large-flow hardware at small-flow Reynolds number to give Reynolds number effects on the same hardware. Advanced experimental techniques and instrumentation--laser velocimetry--will be used to fully evaluate the flow fields and quantify losses associated with low Reynolds number compressors.

These tests will provide a data base for scaling effects in an axial compressor for small axial design. These data will be an asset in calculating the effect of compressor performances as a result of Reynolds number changes.

Cascade Testing Related to Small Size Axial Compressors

Cascade tests have been directed at developing optimum blade shapes and blade design more applicable to large engine compressors. Recent requirements of small compressors to sustain increased loading at increased tip speeds and Mach numbers have necessitated the need for high thickness blading for high Mach number applications.

The proposed cascade test will be conducted on the scaled up hardware of a small compressor cascade to evaluate the optimum blade design to minimize losses due to shock and associated blade profile losses. Velocity controlled (controlled diffusion)blading and leading edge sweep effects will be investigated to control shock structure and reduce such inefficiencies as boundary layer growth, suction surface separation, and endwall secondary flow effects. The tests, conducted in large hardware, will ease the use of laser velocimetry to investigate the flow field and assess performance. By testing both large and small hardware, data for Reynolds number, roughness, and tolerance effects can be obtained and included in analytical predictive models.

The major thrust of this program will be to establish the improvements necessary in analytical predictive techniques to account for the various factors affecting the performance of high thickness/chord, LER/chord blading in a high

Mach number environment. This will set the basis for a viable design method for improving compressor performance.

Aerodynamics Concept Evaluation on Rotating Single Stage Axle Rig.

From previous experience, performance calculated from an isolated blade row, as in a cascade, proved different when a similar blade row was in a rotating stage environment. It is essential that the validity of the findings from prior testing be obtained on a rotating stage where blade row interaction effects can be included. The objective of this program will be to investigate the effects of blade shape, surface roughness, and sweep effects on compressor performance.

The approach taken would be to scale an existing small stage up in flow size and conduct experimental test on the large hardware to evaluate the influence of intrastage reaction--due to nonuniform inlet pressure and temperature profiles, wakes, and boundary layer blockage. The designs will include the concepts contributing to improved performance as determined from previous experimental cascade data. The resulting benefits from the large hardware will be verified on the small stage.

This program will set a valid basis for selection of advanced design concepts, blade shapes, and surface roughness for small size compressor design. The data obtained from these tests will also establish the required guidelines in computational techniques for the design of highly loaded small axial compressors to verify efficiency and pressure ratio capabilities reflective of larger flow size compressors.

Multistage Axial Compressor Test Bed

A multistage axial compressor test bed will be used to verify aerodynamic design concepts and validate analytic techniques before initiating the design of the actual SECT axial compressor. This will set the basis for a logical and proven design methodology using advanced design concepts and detailed analyses for high performance multistage compressors reflective of year 2000 technology.

The approach taken in this program will be to use components of an existing advanced multistage axial compressor. Potential improvements in performance will be investigated by perturbing the design to evaluate the individual effects of low aspect ratio airfoils and endwall blading modifications-sweep, end bends. Based on in-house experience, low aspect ratio blading has been employed to enhance the performance of both large and small compressors. Low aspect ratio airfoils have in addition, contributed to improved stability at design and part speeds. These trends warrant the investigation of low aspect ratio airfoils as a viable candidate in the design of the SECT axial compressor.

Earlier analyses on compressors have revealed that losses associated with secondary flow are substantial and that work to reduce this phenomena is vital for future compressor design. This is especially true in small flow compressors that operate at much higher clearance/blade span ratios. This results in more intense leakage flow patterns, endwall vorticities, and boundary layer (blockage) growth. It is reasonable to assume that there are potential gains to be made by desensitizing the design to these mechanisms. Casing (tip) treatment over rotors has been a successful ploy to energize the boundary layer and enhance surge margin potential at slow speed. This has, however, been achieved at the expense of compressor efficiency as it was used purely as diagnostic confirmation for redesign. By proper selection of the geometry of tip treatment (slots versus holes, blade angled slots versus circumferential, etc.), the surge margin improvements can be made with minimal efficiency reduction.

The multistage test bed will also be used to verify the benefits of airfoil sweep and end-bends as an effective way of reducing losses associated with the endwall region. Airfoil sweep has shown potential for reducing 3-D shock losses in high speed rotor flows. Stator end-bends, achieved by resetting the stator airfoil closed in the vicinity of the endwalls, result in unloading the endwall region with attendant reduction in losses associated with the boundary layer. End-bends also serve to reduce the incidence levels and enhance surge margin potential.

The results obtained from this program will be accounted for by the analytical model and directly applied to the design of the SECT axial compressor.

Radial Compressor Technology Plan

The proposed technology program for centrifugal compressors are shown in Figure 62. A discussion of each program follows.

Flow Size Effects on Small Centrifugal Compressors

The main objective of this program is to study low flow sizes--i.e. 0.1 lb/sec - 0.5 lb/sec - to evaluate compressor performance and evolve/verify computational techniques directly applicable for the design of the SECT centrifugal compressor.

Based on previous experience, centrifugal compressors in different flow size regimes demonstrate performance levels not consistent with Reynolds number changes. This can be partly explained by the different configurations not being designed to consistent blade thicknesses and running clearances. The approach in this program will be to eliminate such inconsistencies by designing two sets of hardware encompassing large and small flow regimes, testing of both sets of hardware with advanced experimental techniques--customized two-spot velocimetry. The derived data base will provide for improvements in computational methods. Testing would include the effects of clearance and shroud surface finish on compressor performance. The fully instrumented rig allows investigation of the entire flow field and nonscalability effects on performance to be included in the development of analytical models. This will be the key to improved performance potential in centrifugal compressors in both large and small flow sizes.

Reynolds Number Effect on Small Centrifugal Compressor Performance

The objective of this program is to evaluate pure Reynolds number effect on small flow size compressors consistent with the flow size study. This can be easily conducted as a continuation of the previous program.

The approach is to quantify Reynolds number effects on small size hardware from flow size scale study by adapting inlet ram capability to identify the resulting changes in loss mechanisms. Based upon the data, the necessary modifi-

cations can be effected in analytical techniques, and similar tests on big hardware determined. Testing will be conducted with extensive instrumentation.

The results of this program will allow the proper assessment of Reynolds number in analytical models for the design of high performance small centrifugal compressors. The models evolved from this program would not be confined to small compressors, but centrifugal compressor design in general.

Impeller Leading Edge Blade Shape on Centrifugal Compressor Performance

Design of centrifugal impellers has been confined to vertical leading edge impellers employing straight element sections. Recent work on swept-back leading edges has revealed improvements in range for larger flow size compressors. In axial compressors, velocity controlled airfoils have been designed to contain shock structures, enhancing performance potential. The objective in this program is to investigate the possibility of improved range and efficiency on small compressors by incorporating advance design concepts.

The approach would be to design and experimentally evaluate a conventional impeller and advanced impeller of equivalent work to investigate the potential benefits of leading edge sweep and contoured blades. Improved instrumentation and experimental techniques--advanced laser velocimetry--will be employed to calculate and understand the complex flow field within the blade row for inclusion of these concepts in analytical/computational models. The benefits realized from leading edge and impeller blade shapes may be vital to the future design of high performance centrifugal compressors requiring improved range and efficiency.

Investigate Passage Contouring for Improved Centrifugal Compressor Performance and Clearance Tolerance

The design of centrifugal passages has been axisymmetrix and surfaces of revolution. Since small size compressor performance is substantially affected by running clearance, the objective is to employ centrifugal passages of nonaxisymmetry and nonsurfaces of revolution to enhance efficiency and reduce clearance sensitivity. This would involve the development of supporting

analytical capability to design geometries and verification through experimental evaluation. Any potential payoff associated with determining the optimum controur of these surfaces would bridge the gap in performance (in small compressors) and result in improved analytical/predictive techniques for the design of centrifugal compressors.

Advanced Diffuser System

The flow characteristics of the entrance region of the centrifugal compressor is of vital importance to the overall performance and stability at design and off-design speeds. The flow is highly sheared and viscous and enters the diffuser leading edge with uneven pressure and temperature gradients. In spite of this complex 3-D flow phenomena, the design of radial diffusers has been 2-D wedge-shaped vanes with no consideration given to the nonuniformities. Since the selection of diffuser throat area--by accounting for aerodynamic blockage due to the presence of boundary layers--and leading edge incidence determines high speed flow capacity and slow speed stability, respectively, potential benefits in the design of 3-D vanes were customized for the inlet flow conditions. The incorporation of bleed/blow capability for performance enhancement, as evidenced in the improvements in range/flow regulation of higher pressure ratio impellers by the Allison patented system of inducer bleed, may be a desirable feature.

The approach in this program involves thorough investigation of the vaneless space/diffuser entry region of a design, including features such as 3-D vanes and bleed/blow capability to quantify any potential payoffs. The data obtained by using advanced laser velocimetry would create the data base for comparisons against similar conventional diffuser designs, give a better understanding of the flow phenomena, and qualify emloying advanced design techniques. This program would set the basis for the design of centrifugal compression systems with good slow speed flow/efficiency lapse rates without requiring the attendant compromises in design performance.

Verification of Small Compressor Technology

The SECT compressor technology plan has been conceived as a systematic means of elevating the performance levels of small engine compressors as has been

shown in Figures 61 and 62. The knowledge acquired from the compressor technology programs will be used to design and fabricate the SECT nonconcentric compressor. This program will experimentally verify the design techniques and goals of the program. In summary, the outcome of this program will result in the evolution of an advanced and viable design methodology for high performance compressors satisfying the requirements of year 2000+ technology.

COMPUTATIONAL FLUID MECHANICS

The flow in small gas turbine engine compressors and turbines is dominated by performance limiting 3-D viscous flow phenomena. Those phenomena include rapidly growing endwall boundary layers, secondary flows driven by strong cross-stream pressure gradients, and significant tip/leakage flows. In low aspect ratio axial turbomachines, these flow features occupy a significant portion of the airfoil span and, therefore, account for a major part of the overall total pressure loss in these machines. In high pressure ratio centrifugal compressors, performance can be further reduced by separated flow in the exducer.

In addition to the concern over the viscous flow phenomena and the impact on performance, there has emerged over the last few years considerable interest and concern about the unsteady flow interaction between rotating and stationary blade rows and its effect on the time mean aerodynamic and thermal characteristics. These unsteady phenomena include potential flow interactions giving rise to significant pressure fluctuations on the airfoil surfaces and viscous interactions resulting from the downstream row cutting the wakes shed from the upstream row. Experimental studies have shown that these time unsteady vane blade interaction effects are large and the resulting time mean aerodynamic and heat transfer characteristics are considerably different from those of isolated vane and blade rows. In small turbomachines, it is likely that these interactive effects are magnified because of the increased importance of endwall viscous flow phenomena.

Proposed Advanced Technology Effort

A series of three advanced technology programs that address the development and qualification of improved flow models for small compressors and turbines is proposed. These programs are directed at the development of analyses with

capability to predict important 3-D viscous and unsteady flow phenomena. The proposed programs shown in Figure 63 are as follows:

- o 3-D Viscous Centrifugal Compressor Analysis
- o 3-D Viscous Axial Turbomachinery Analysis
- o 3-D Viscous Unsteady Stage Analysis

All of these programs involve extensions of proven techniques incorporated into existing turbomachinery flow models developed at Allison. Details of each of these programs are given in the following subsections.

3-D Viscous Centrifugal Compressor Analysis

The impeller analysis to be developed under this program will be based on Allison's 3-D viscous flow model. This code, currently operational for a variety of applications, incorporates a partially parabolic Navier-Stokes (N-S) solver that neglects streamwise diffusion in the primary flow direction. This solver employs finite volume procedures to integrate the parabolic N-S equations written in arbitrary curvilinear coordinates. A solution is achieved using a multiple-pass forward-marching integration scheme coupled with a pressure correction procedure to enforce local and global mass conservation. Turbulence is modeled using the two-equation K-ε model.

Results for a radial impeller tested by Eckardt, Figures 64 and 65, demonstrate the current capability for modeling impeller flows. Figure 64 presents a schematic representation of the blade-conforming sheared coordinate system employed in the computations. A coordinate stretching procedure was used to cluster points in the high gradient near-wall and blade-tip regions. Comparison of experimental and computed primary velocity components on a series of cross-stream planes in the exducer are presented in Figure 65. Good qualitative agreement is shown between the results on all planes. Clearly shown is the formation of the jet and wake structure characteristic of impeller flows. The wake results from a vortex formed by the blade tip leakage flows.

The proposed development effort will concentrate on extending the current impeller analysis to treat high pressure ratio machines. Specifically, the tasks to be performed are as follows:

- o add splitter modeling capability
- o modify numerical scheme to treat transonic flows

The splitters will be modeled using the same procedures currently in place for treating the primary impeller blades. The same primary blade tip gap model based on clustering grid points in that region will also be incorporated with the splitter blade model. For ease of enforcing the splitter blade surface boundary conditions, the grid will be made to conform to the splitter blade surface.

The planned approach to treating transonic flows will involve investigating both locally elliptic and globally elliptic procedures in combination with or in place of the current partially parabolic scheme. Such elliptic procedures are required to model supersonic entrance region flows near the tip section of impellers.

3-D Viscous Axial Turbomachinery Analysis

This analysis will build on an extensive background in time-marching Euler/Navier-Stokes solvers and advanced body-conforming grid systems. Specifically, this analysis will incorporate a 3-D O-type grid, shown in Figure 66, and a rapid, robust, second-order accurate hopscotch algorithm. This grid system and numerical scheme are presently incorporated into the Allison 3-D Euler code, which has been extensively tested for axial flow turbine rotors and stators.

Predicted airfoil surface Mach number distributions from the Euler code for a flared endwall rectilinear cascade are presented in Figures 67 and 68 for 8.28% and 48.9% span, respectively, where spanwise distance is measured from the flared endwall. Also presented in these figures for comparison are the experimental data and results from the Denton code.

The work under this program will center on modifying the O-type grid generator to cluster mesh points near the high-gradient near-wall regions, modifying the

hopscotch scheme for N-S calculations and implementing a suitable turbulence model. The required grid packing scheme will redistribute points after a uniformly spaced grid has been generated. The changes to the hopscotch algorithm to treat the N-S equations have already been programmed and tested in an Allison-developed 2-D nozzle code. These modifications have been tested in combination with the two equation K-ε turbulence model to analyze 2-D vectored and thrust-reversing nozzle configurations. Results from those tests, reported in a recent AIAA paper (Ref 4), show excellent agreement with experimental measurements.

3-D Viscous Unsteady Stage Analysis

The 3-D stage analysis effort will draw on efforts from the 3-D Viscous Axial Turbomachinery Analysis program and the Air Force Vane-Blade Interaction (VBI) program. The final produce will be a full 3-D viscous unsteady stage analysis with the capability to predict all viscous and transient flow phenomena in an axial turbine stage.

The techniques required to couple the vane and blade row solutions are being developed under the Air Force VBI for a 2-D blade-to-blade flow model. The development efforts are broken down as follows:

- o grid modifications
- o radiation boundary condition implementation
- o phase-lagged periodic boundary point treatment
- o vane and blade row coupling procedures

The proposed O-type grid system, shown in Figure 69, incorporates an end cap to allow for specification of a single axial location for the inflow and outflow boundary points and the point density along the boundaries. The grid generation scheme incorporates techniques to allow for user control over the field point distribution.

Radiation boundary conditions along the stage inflow and outflow boundaries and required to allow radiating waves to pass through the boundaries without reflection. The boundary point calculations will be based on a Riemann invariant method of characteristics currently incorporated in the VBI analysis.

To treat vane-blade interacting flows with unequal numbers of airfoils in each row, special procedures are needed to calculate the spatially periodic boundary points. With unequal numbers of vanes and blades, the flow along these boundaries is time periodic but not spatially periodic. A scheme to treat these boundaries has been devised under the VBI program and will be implemented into the 3-D stage analysis.

The most difficult task for the stage analysis is the formulation of procedures to couple the vane and blade row solutions. The proposed scheme will be based on the overlapped grid arrangement shown in Figure 69 and will involve interpolating field data from one blade row solution to establish boundary data for the other solution.

COMBUSTOR TECHNOLOGY PLAN

Depending on the selected engine configuration, an annular or can combustor could be used for the proposed application. The nonconcentric engine with high cycle pressure ratio (30), high combustor discharge temperature (approximately 3000°F), and low combustor inlet correction flow (0.2 lb/sec) poses a number of combustion technical challenges, including the following:

- o combustion system durability
- o combustor exhaust temperature quality
- o wider fuel turndown ratio
- o idle combustion efficiency
- o exhaust smoke characteristics
- o ignition and lean flame stability characteristics
- o nozzle and liner carboning

Combustion system durability characteristics are severely affected due to low corrected flow rate, high inlet air pressure and temperature levels, and high burner temperature rise. Innovative cooling designs need to be developed for annular combustors to simultaneously satisfy both life and DOC design objectives.

To facilitate the use of uncooled ceramics for gasifier vanes, burner outlet radial profile should be controlled and circumferential pattern factor reduced

to 0.12. This along with high temperature rise places exacting design requirements on obtaining an optimum combustor/injector system.

The required fuel injection system needs to operate over a much wider fuel turndown ratio and should give better spray quality than current injectors to obtain high idle efficiency.

The proposed engine will operate over a wide range of combustor airflow and fuel flow conditions requiring improvements in ignition and flame stability characteristics. In addition, the burner fuel-air mixing should be enhanced to minimize exhaust smoke emissions.

Better combustor design techniques should be evolved in order to achieve an optimum combustion system with minimum hardware modifications and test iterations.

Proposed Advanced Technology

The following technology programs are proposed for the SECT application with the overall schedule shown in Figure 70:

1. durability enhancement
2. low-cost advanced design atomizer
3. low smoke research
4. prechamber combustor research
5. analytical model development

Combustion system durability can be improved in a number of ways. Combustor heat intensity should be increased with attendant reduction in the required combustion volume and liner surface area. Radiation and convective heat loading on the liner walls can be reduced by improving fuel-air mixing and achieving velocity distribution that minimizes the cooling film mixing rate with the main combustion air.

A number of cooling schemes can be analytically evaluated to select the most promising concepts for further investigation. The candidate cooling schemes include stacked or machined rings (baseline), Lamilloy, effusion, impingement/

convection, and composite matrix. Nonmetallic materials including monolithic ceramics (silicon nitride and silicon carbide) and ceramic composites should also be included in this initial investigation to select the most promising schemes, identify the technology gaps, and prepare a test plan.

Comparison between the various cooling schemes should be made in simulated combustor rigs where control can be exercised over hot-side and cold-side boundary conditions. The rig data will be used for model validation and evolution of advanced liner cooling design methodology.

The main objectives of the proposed low cost advanced atomizer program are to improve atomization quality and start performance, solve the gumming and plugging problems associated with small injectors, and develop low cost design concepts. Based on an in-depth review of available fuel injection design concepts, including airblast, injectors with oval spray, spill-return atomizers, and alternate injection schemes, selection can be made of the most promising design concepts for preliminary design and bench scale testing. These models can be upgraded and should be used for detailed analysis of the best selected configuration.

The empirical data base should be used along with analytical models to design an optimum combustor/injector system that addresses the main design and problems of small high temperature rise combustors.

The allowable smoke emission levels of small propulsion engines have been high compared to large engines due to small exhaust plume with attendant high threshold of visible smoke. Many of the low smoke reduction techniques used in large engines are not directly applicable to small engines. A technology program is therefore proposed to further reduce exhaust smoke emissions of small engines. Innovative combustor internal aerothermal design features will be investigated using analytical models complimented by bench scale testing. Conflicting design requirements of low smoke, high combustion intensity (with attendant effect on durability), lean flame stability, altitude relight, and burner exit temperature quality will be addressed in the proposed program.

Allison has successfully developed small helicopter combustion systems where prechamber designs are used to solve the conflicting design requirements of

high fuel turndown ratio, high idle efficiency, good start characteristics, and low smoke. The prechamber design technology needs further improvement for application in the proposed advanced helicopter engine.

During the last ten years, a number of analytical combustor design procedures have been proposed, and these have been successfully used to help design advanced combustion concepts. In order to further improve model prediction accuracy, significant advances are needed in many areas including numerical scheme, physical submodels of turbulence, turbulence/chemistry interaction, spray evaporation/combustion, soot, and radiation. A sustained technical effort must be maintained in evaluating and applying analytical models for small gas turbine combustors.

BEARING TECHNOLOGY PLAN

Bearings in small gas turbine engines have unique problems when compared to those in larger engines. Centrifugal force effects have been shown (Ref 2) to be relatively more severe in small bearings when DN (diameter of bore in mm x speed in rpm) is kept constant (as in a scaled reduction of a base engine design). Bearing heat generation is likely to be more severe. In addition, the environment temperature is usually higher in small engines at the same cycle temperatures since the bearing is located closer to the heat source. Normal cooling air practices will be less effective. Small engines and airframes are affected more by inefficiency such as bearing oil churning/windage losses and air/oil cooler drag losses, which prompt use of minimum oil flows and maximum acceptable bearing operating temperature. All these conditions tend to reduce elastohydrodynamic oil film thickness. This results in lower fatigue life, increased wear, possible separator failure, and lubricant deterioration problems.

The small engine bearing also has less tolerance for unforeseen loads, load combinations, and transient operating conditions not normally analyzed or evaluated. These conditions include accelerations, hot starts after shutdown and soakback, and abusive engine/aircraft operation. New application and mission profiles frequently contain severe operating conditions not considered in

the mission mix of the original design/development. The severe operating conditions cause thermal distress and separator distress that can lead to complete and rapid bearing failure.

In addition to these problems, the small engine is usually expected to carry a price tag comparable to its relative weight or power. While the bearing cost may be less due to the lower material volume used, other manufacturing, inspection, and engineering costs do not scale down.

The key bearing needs are as follows:

- o higher temperature capability
- o higher speed capability
- o improved efficiency
- o increased life potential
- o reduced or equivalent cost

This program objective is to develop a bearing system capable of operating reliably in the high speed, high temperature environment of an advanced small gas turbine engine. The goal is to arrive at a bearing system design that will not place constraints on engine design, causing performance to be compromised.

Proposed Advanced Technology

Air bearings have already demonstrated their ability to operate under conditions similar to those expected in an advanced, small gas turbine engine. However, the bearing size that would be required appears to preclude their use in supporting thrust loads. For example, an air lubricated bearing to support 200-300 lb axial load would be about six inches in diameter. Actual thrust loads anticipated could easily be five to ten times that high. Nevertheless, since radial loading is normally quite light, the air bearing seems to be a viable option for those positions with radial load only. Moreover, it is usually possible to locate the thrust bearings in the forward part of the engine where lower temperatures permit the use of liquid lubricated rolling element bearings. The air lubricated radial bearings are required only in the aft hot section of the engine. A possible arrangement for the gas generator for such an engine is shown in Figure 71. Remaining goals for an air bearing technology

program would be to demonstrate satisfactory durability as well as capacity to provide adequate rotor dynamic stability margins during excursions from design conditions.

For the rolling element bearing, a more conventional design approach using advanced materials is proposed. In order to reduce the high centrifugal forces resulting from high speed, ceramic rolling elements (silicon nitride) will be used. The marked difference in physical properties between ceramics and steel (see Table XXXII) necessitates some additional design considerations. The different thermal expansion characteristics make it extremely difficult to fit ceramic inner and outer rings properly to ferrous or other metallic shafts and housings. Consequently, it is expected that ceramics will be confined to the rolling elements, and an advanced ferrous material, most likely M-50NiL, will be used for the rings. The difference in elastic properties (modulus of elasticity and Poissons ratio) necessitates some changes in raceway contact geometry as compared to current all metal bearings. The improved fracture toughness of the M-50NiL will also provide adequate margins against catastrophic failures. In addition, early results (Ref 5) suggest that this materials may provide improved fatigue life as well.

The proposed materials address the problems of low fatigue life and catastrophic failure of the rolling contact components. These materials also provide temperature capability beyond the limits of current, conventional liquid lubricants. Another problem to be addressed is that of retainer wear failures. Retainer distress is a common failure made in current high speed rolling bearings (over 1 million DN). One of the major factors contributing to this distress is the high dynamic forces that result from minor imbalance. Since it is not possible to balance all retainers perfectly, the next approach would be to use a low mass density material. Strides have been made in the development of modable polymeric materials that are useable in the 500-600°F temperature range. These materials include polyether etherketone (PEEK) and poly(amide-imide) with glass or carbon fiber reinforcement for strength and stiffness. Injection molded cages of engineered polymeric materials have been in use in ball and roller bearings for more conventional applications for two decades. The most commonly used material has been glass-fiber-reinforced nylon 6/6, which is suitable for temperatures below 300°F. Within this temperature limit, such cages have demonstrated superiority over conventional steel cages under

TABLE XXXII

SELECTED PHYSICAL AND THERMAL PROPERTIES OF SILICON NITRIDE AND M50 STEEL (REF.11)

PROPERTY	SILICON NITRIDE	M50 STEEL
HARDNESS, R_C AT 20°C	78	64
MAXIMUM USEFUL TEMPERATURE* °C (°F)	1200 (2192)	320 (61)
DENSITY, G/CM^3	3.2	7.6
ELASTIC MODULES AT 20°C (68°F) GPA (10^6 mPa)	310 (45)	190 (28)
POISSON'S RATIO	0.26	0.28
THERMAL CONDUCTIVITY AT 20°C CAL/S M °C	7.3	13.4
COEFFICIENT OF THERMAL EXPANSION, 10^{-6}/°C	2.9	12.3

* MAXIMUM OPERATING TEMPERATURE WHEN USED FOR ROLLING BEARINGS BASED ON A MINIMUM HOT HARDNESS OF R_C 57 AFTER LONG-TERM SOAKING AT TEMPERATURE, COMPARED TO A MAXIMUM TEMPERATURE OF 180°C (356°F) FOR 52100 STEEL

TE86-4887

conditions of significant misalignment and interrupted lubrication. This superiority is attributed to the greater flexibility of the polymeric and its porosity, which allows it to absorb liquid lubricant for later release when the primary supply is cut off. These proven characteristics, together with the higher temperature capability of the advanced materials, are worthy of investigation for their applicability to small turbine engine bearings.

The remaining area of concern to be addressed is that of lubrication of the rolling element bearings for extended periods of time at high speed and high temperature. Because of the design philosophy, the operating temperatures can be kept within the capabilities of current or advanced liquid lubricants (Ref 6). However, some work will still be required to accommodate specific properties of the advanced fluids and to establish optimum design criteria for the bearing components, with respect to the lubricant and method of application.

Approach/Technology Plan

Since the proposed approach to advanced small engine design involves air bearings for radial loads in the hot section and rolling element bearings for thrust loads in the cold section, the technology plan will be discussed in two parts.

Air Bearings

This portion of the program will be undertaken with an outside partner, such as Mechanical Technology Incorporated, Latham, New York. Several bearing designs will be analyzed with consideration given to system rotor dynamics characteristics as well as bearing performance. After several iterations, during which engine operating conditions as well as bearing design will be refined, one configuration will be selected for rig testing. Subsequent to rig testing, a final design will be prepared and fabricated for testing in an engine. The time table for this program is shown in Figure 72.

Rolling Element Bearings

The rolling element bearing program is to be conducted primarily in-house, although outside consultation on materials is anticipated along with vendor coordination for purchased items. The elements of the plan are shown in Figure 73.

The program will begin with indepth research to determine the most promising materials to be used. Extensive computer analysis will be done including full dynamic analysis using ADORE (Ref 2) and finite element analysis of cage designs using an in-house developed technique, as well as older programs such as SHABERTH (Ref 7). Many ideas and concepts can be tested by making minor modifications to existing bearings. It is proposed that test rig design and procurement begin early, so that development testing can be performed on such bearings in a timely manner. It is expected that lubrication techniques necessary for the high speeds encountered will be for the most part empirically determined during this stage. Goals will be to optimize lubrication, cooling, and power loss. Pertinent bearing parameters evolved for the rolling element bearings will be used in the system rotor dynamics studies mentioned for air bearings. A final prototype bearing design will be fabricated for further performance testing in the rig under a full spectrum of simulated operating conditions. Improvements discovered in this test series will be incorporated in a final design that will be procured for performance testing in an engine, along with the air bearings. Longer term endurance testing will be performed in the rig rather than in an engine.

Summary

The particular problems associated with advanced, small gas turbine engine bearings are high temperature and high dynamic forces leading to short life, cage distress, catastrophic failure, and excessive power loss. Advanced concepts to mitigate these problems were reviewed against the background of current practice. The most promising approach for future small engine bearing systems was suggested to be air bearings for radial loads positioned in the hot section of the engine and liquid lubricated rolling element bearings for axial loads located in the cold section. A four year program, consisting of design analysis, rig testing and engine testing, to sort out remaining needs, was proposed. Completion of the proposed program should result in a proven bearing system for small gas turbine engines that will be useful into the next century.

VII. CONCLUSIONS

This study was conducted to provide identification of the high payoff technologies for future small gas turbine engines and to provide a plan to make these technologies available by the year 2000. These objectives were accomplished, and conclusions regarding the study results are as follows:

1. Engine design--The nonconcentric engine configuration provided the greatest reduction in direct operating cost for the commercial tilt-rotor aircraft mission under study. This general arrangement is a result of studies to produce the optimum reduction in direct operating cost for the advanced simple cycle engine. This configuration has a turbine inlet temperature of 1538°C (2800°F) and a 30:1 overall pressure ratio. The nonconcentric engine configuration achieves a 30% reduction in fuel burned while reducing direct operating cost by 16.5%.

2. Key technologies--The five technology areas that require research to be incorporated in the year 2000 small gas turbine engine are ceramics, compressors, combustors, turbines, and bearings. In addition, improvements in computational fluid mechanics are essential to analyze the flow phenomena in small turbomachinery components. Because of the high risk nature of these programs, Government sponsorship of these component technology programs is needed. Without the research effort, it is unlikely the U.S. can remain competitive in the worldwide small gas turbine engine market.

APPENDIX A - SYMBOLS AND ACRONYMS

$\Delta P/P$	total pressure drop
ΔT	temperature rises
ε	regenerator effectiveness
σ	open area fraction
γ	density ratio Q/P*
$/shp	engine OEM cost per shaft horsepower
A/C	aircraft
AEO	all engines operative
AN^2	annulus area x rotational speed squared
APU	auxiliary power unit
ATA	Airline Transport Association
ß	surface area/unit volume
B	surface-area-to-volume ratio
BMAS	barium magnesium aluminosilicate
BOT	burner outlet temperature
BRG	bearing
C_{am}	cost per airplane nautical mile
CDT	compressor discharge temperature
CGW	Corning Glass Works
CPU	central processing unit
CVD	chemical vapor disposition
D	mission range or stage length in nautical miles
DARPA	Defense Advanced Research Projects Agency
D_H	hydraulic diameter
DN	diameter of bearing bore in mm x speed in rpm
DOC	direct operating cost
DOC*	reference or baseline DOC level
E	effectiveness
EMS	engine monitoring system
f	Fanning friction factor
FAR	federal air regulation
Fb	block fuel
F_{cl}	fuel to climb to cruise altitude
F_{ar}	fuel consumed at cruise altitude and velocity

F_{gm}	ground maneuver fuel
fpm	feet per minute
fps	feet per second
F_v	fuel required for vertical takeoff and landing allowances
GATE	General Aviation Turbine Engine
GW	gross weight
HE	maximum engine envelope height
hp	horsepower
HP	high pressure
IRP	intermediate rated power
ISA	international standard atmosphere
J	Colburn heat transfer factor
KEAS	knots equivalent air speed
KTAS	knots true air speed
L	absolute leakage
LAS	lithium aluminosilicate
LDV	laser Doppler velocimeter
LE	maximum engine envelope length
LER	leading edge radius
LeRC	Lewis Research Center
LER/C	leading edge radius/chord
MDN	million diameter of bore (m/m) speed-rpm
N	disk speed, rpm
NDE	nondestructive evaluation
NDS	nitride dispersed stainless steel
N-S	Navier-Stokes
nmi	nautical mile
ODS	oxide dispersioned strengthened
OEI	one engine inoperative
OEM	original equipment manufacturer
PEEK	polyether etherketone
PSZ	partially stabilized zirconia
R_c	compression ratio
Re	turbine expansion ratio
RIT	rotor inlet temperature

Ro/A	overall pressure ratio
R of C	rate of climb
ROI	return on investment
RST	rapid solidication technology
S	wall thickness
SFC	specific fuel consumption
SHP	shaft horsepower
SiC	silicon carbide
Si_3N_4	silicon nitride
SLS	sea level static
SLSS	sea level static standard day
SOA	state-of-the-art
SP	specific power
t_b	block time
T/C	thickness chord
T_{cl}	time to climb
T_{cr}	time at cruise altitude and velocity
t_f	flight time
T_{gm}	ground maneuver time in hours
T_{max}	maximum surface temperature
T_v	vertical takeoff and landing time
TOGW	takeoff gross weight
U	unity engine size
UTRC	United Tecbnology Research Center
V_b	block speed
VBI	Vane-Blade Interaction
W	disk thickness
Wa	airflow rate
wt	engine weight

APPENDIX B--REFERENCES

1. GATE Final Report (NASA CR-159558); Allison Gas Turbine Division, GMC (EDR 9528) April 10, 1979; page 125 and Reference No. 14.
2. U.S. Army TACOM R&D Center Technical Report No. 13087 (Allison EDR 11999), December 1984.
3. Shah and London, NR-090-342, Stanford University TR No. 75, November 1971.
4. O. K. Kwon and R. A. Delaney, "Navier-Stokes Solution Procedure for Analysis of Steady Two-Dimensional Transonic Nozzle Flows," AIAA Paper No. 85-1587, 1985.
5. P. K. Gupta, Advanced Dynamics of Rolling Elements, Springer-Verlag, New York, 1984.
6. S. N. Bamberger, B. L. Avergach, and P. K. Person, "Improved Fracture Toughness Bearings," Report No. AFWAL-TR-84-2103, AFWAL?POSL, Wright-Patterson Air Force Base, Ohio, January 1985.
7. M. A. Ragen, et. al., Reserch Report-User Mnaual for Computer Program AT81Y003 SHABERTH, Report No. NASA CR No. 165365, Lewis Research Center, 1981 (COSMIC Program No. LEW-12761).
8. D. N. Buckley, "Tribological Systems as Applied to Aircraft Engines," NASA Technical Memorandum 86965, Lewis Research Center, 1985.
9. J. F. Dill and M. J. Cronin, "Assessment of Advanced Powder/Non-Metal Materials for Advanced Rolling Element Bearing Applications," AFWAL-TR-85-2048, AFWAL/POSL, Wright Patterson Air Force Base, Ohio, July 1985.
10. S. Gray and P. D. Gupta, "Friction and Wear of Solid Lubricated Contact in Gas Turbine Engine Bearings," AFWAL-TR-84-4143, November 1984.
11. "High Temperature Self-Lubricating Coatins for Air Lubricated Foil Bearings for the Automotive Gas Turbine," MTI-79TR76.
12. L. B. Sibley, "Silicon Nitride Bearing Elements for High Speed, High Temperature Applications," Problems in Bearings and Lubrication, AGARD Confernece Proceedings No. 323, 1982.
13. "Solid Lubrication Methodology," NASA-CR--174690, 1984.
14. "Solid Lubricated Rolling Element Bearings," AFWAL-TR-83-4129, Vol I-VII, August 1984.

15. F. J. Suriano, "Advanced SPS/APV Foil Bearing Development Program," NAPC-PE-91C, March 2, 1984.
16. Stewart and Wong, "Removal of Secondary-Flow Accommodations in a Two-Dimensional Turbine Nozzle Passage by Boundary layer Bleed," NASA RM E55E11.
17. Avco Lycoming, "Small Axial Turbine Stator Technology Program", Contract (NAS3-22109).
18. W. B. Gardner "Energy Efficient Engine Low-Pressure Turbine Boundary Layer Program Technology Report," NASA CR-165338, Lewis Research Center, April 1981.

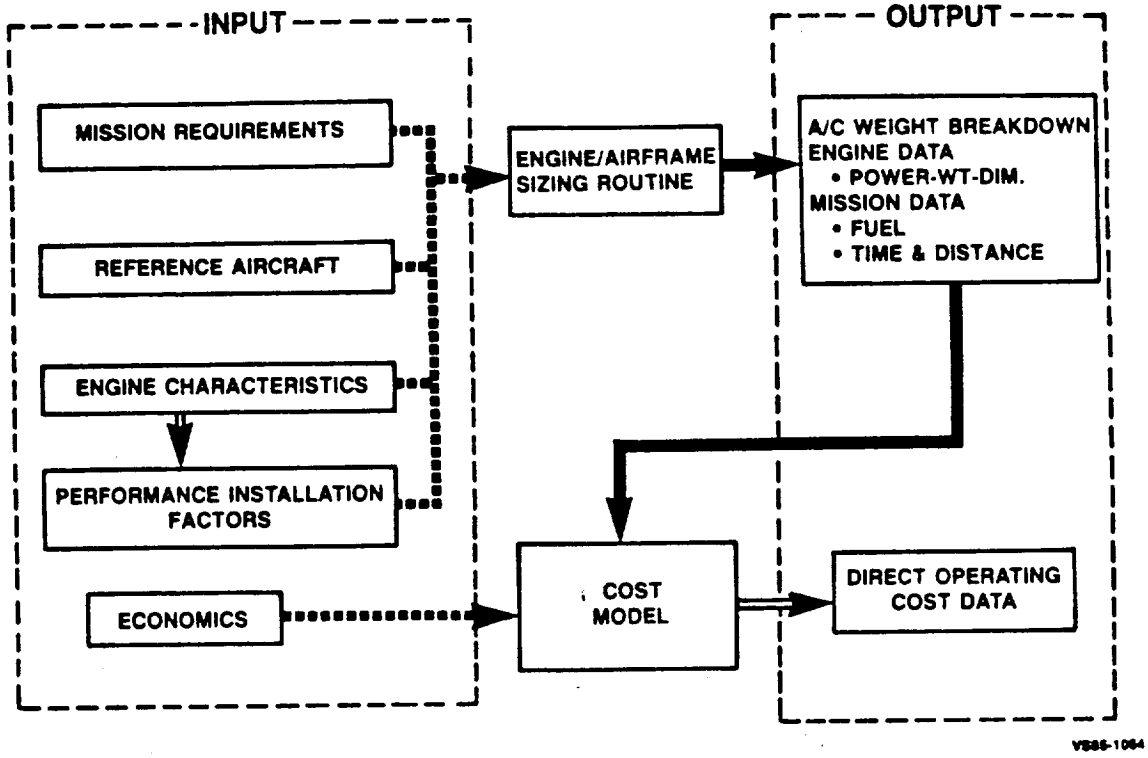

Figure 1. SECT mission analysis procedure.

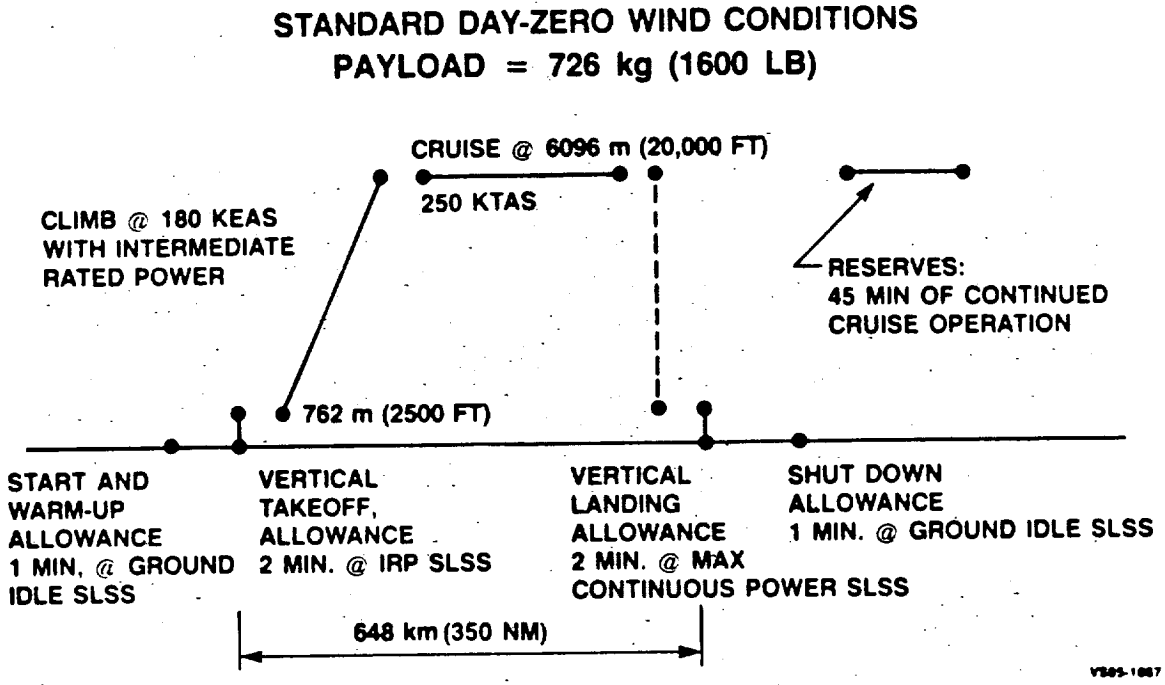

Figure 2. Reference tilt-rotor mission profile.

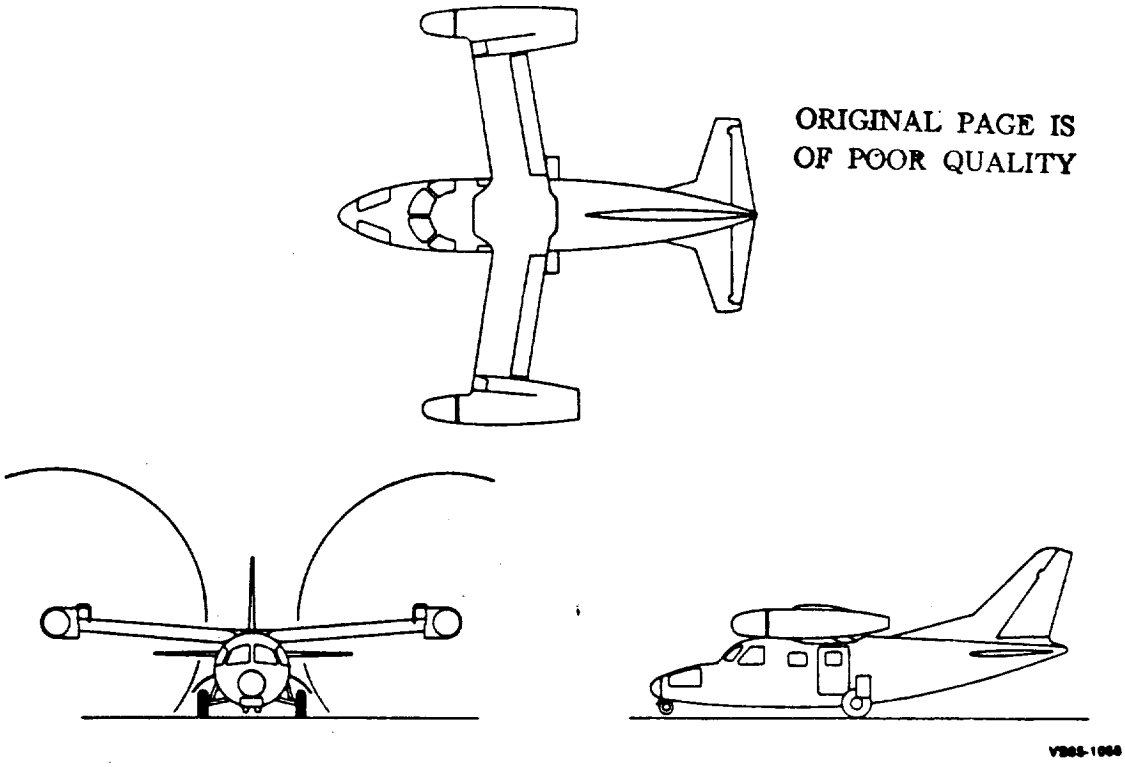

Figure 3. Three-view drawing of reference tilt-rotor aircraft.

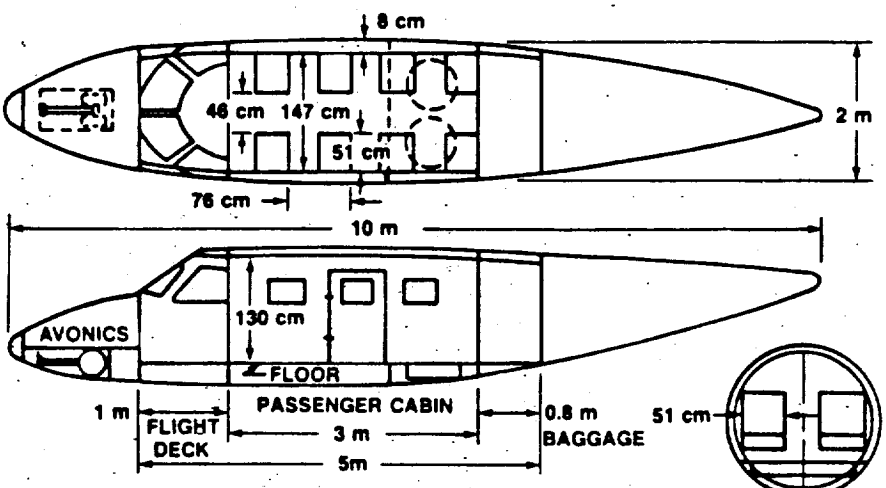

	VOLUME m³
AVONICS	0.5
FLIGHT DECK	1.8
PASSENGER CABIN	6.4
BAGGAGE	1.4
MAIN GEAR BAY	0.5
NOSE GEAR BAY	0.2
FUSELAGE	13.2

FUSELAGE WETTED AREA 39 m²

Figure 4. Approximate fusilage layout--eight passengers.

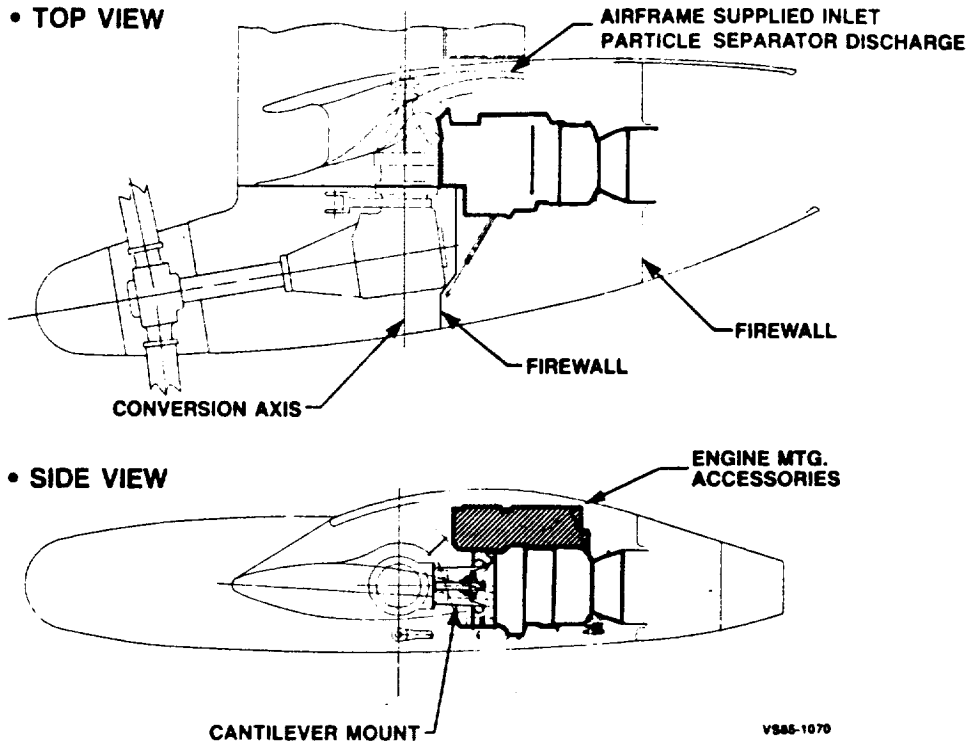

Figure 5. Nacelle layout.

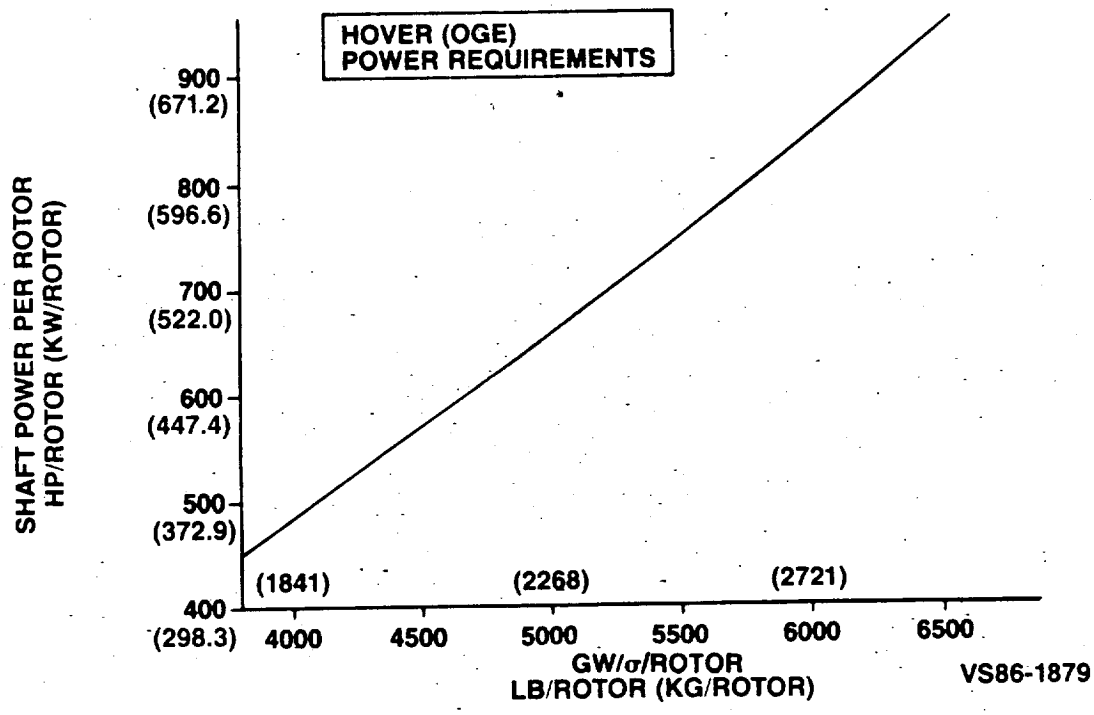

Figure 6. SECT baseline tilt-rotor lower power requirements (helicopter mode).

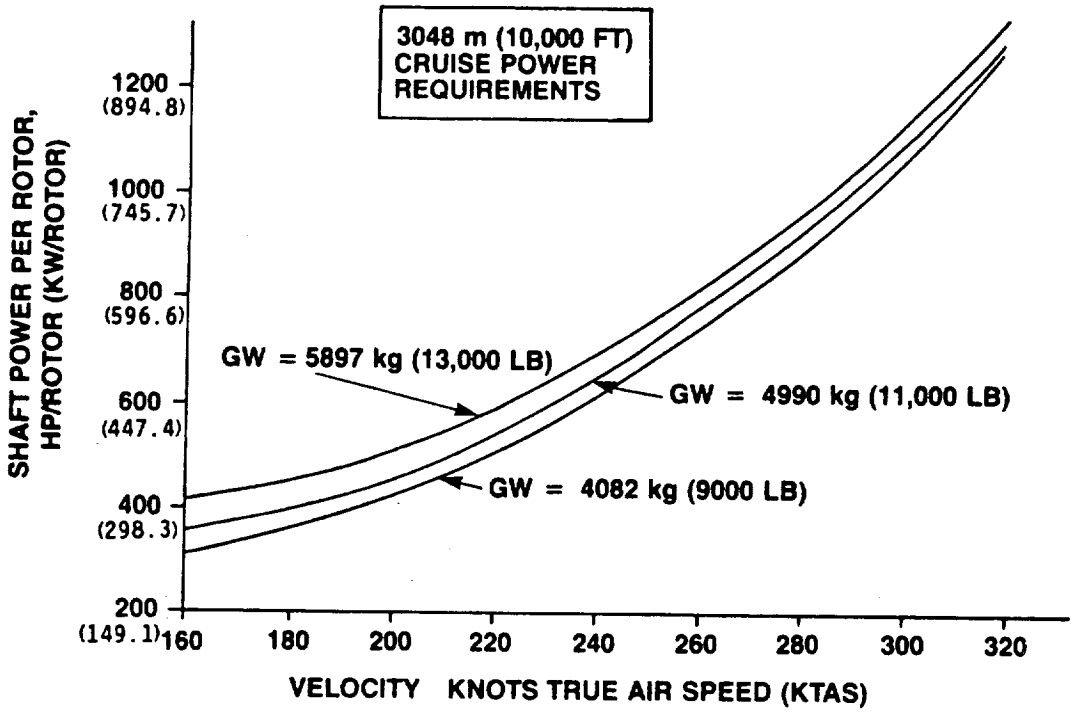

Figure 7. SECT baseline tilt-rotor cruise power requirements (10,000 ft airplane mode).

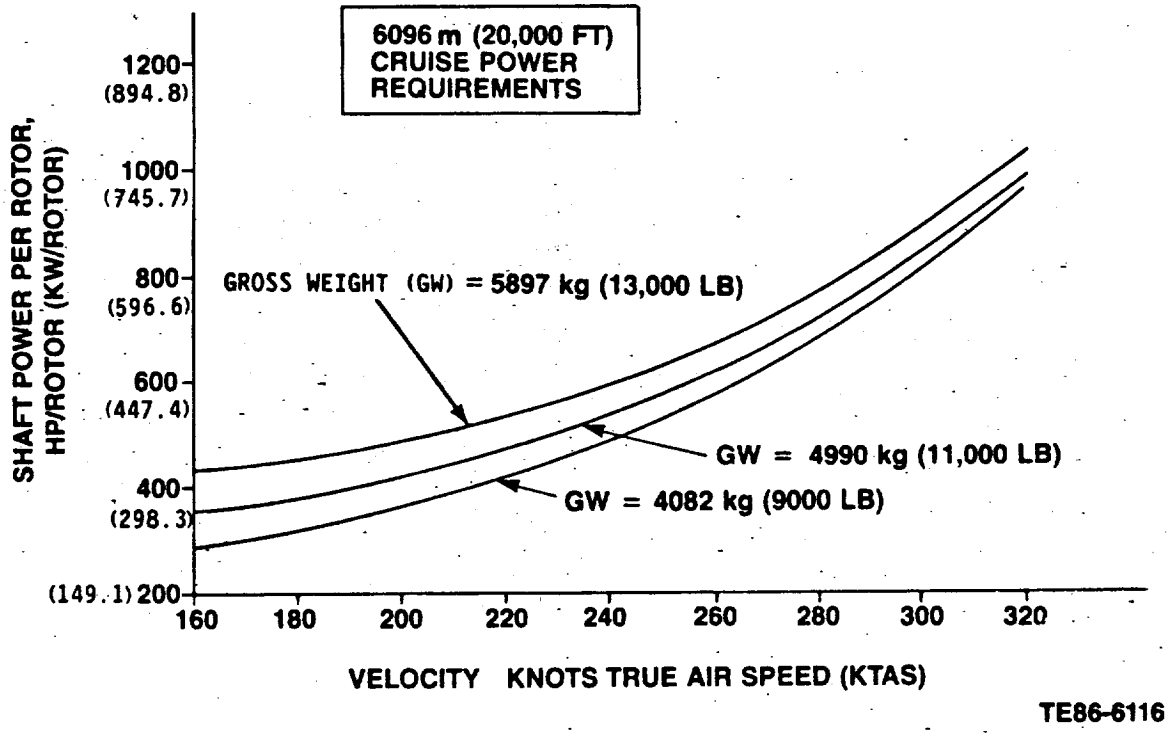

Figure 8. SECT baseline tilt-rotor cruise power requirements (20,000 ft airplane mode).

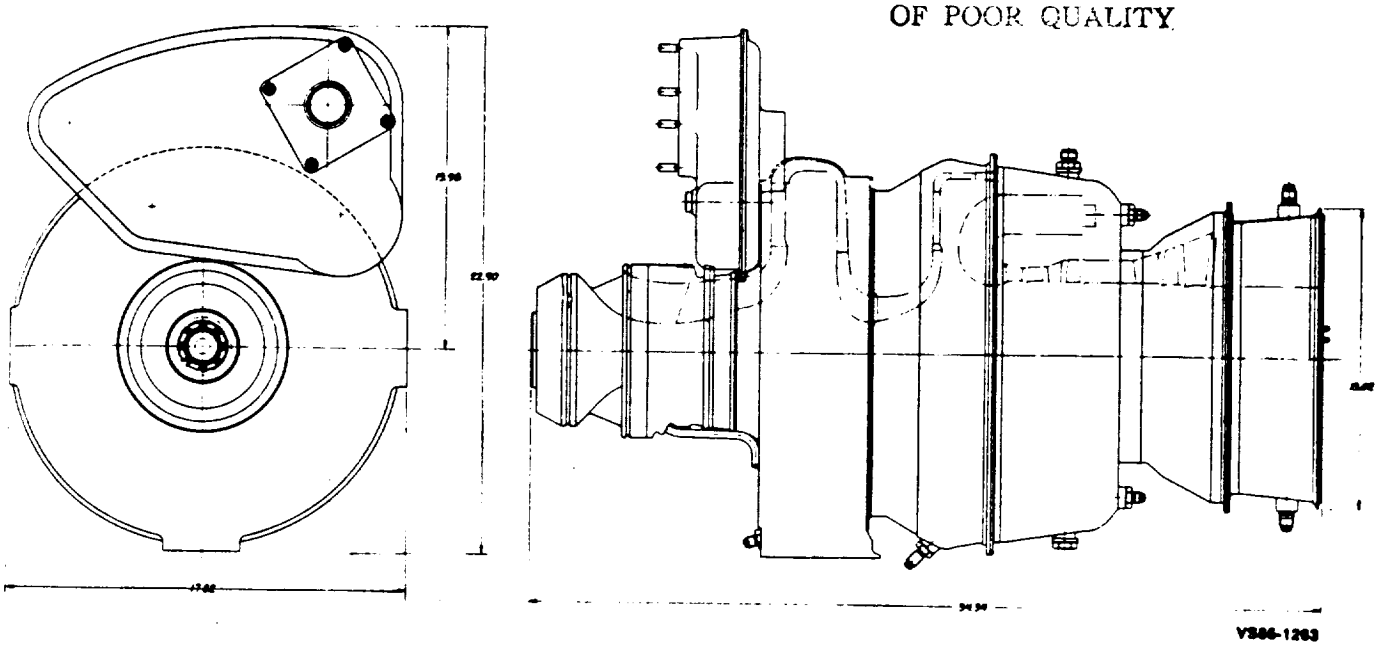

Figure 9. Baseline engine general outline.

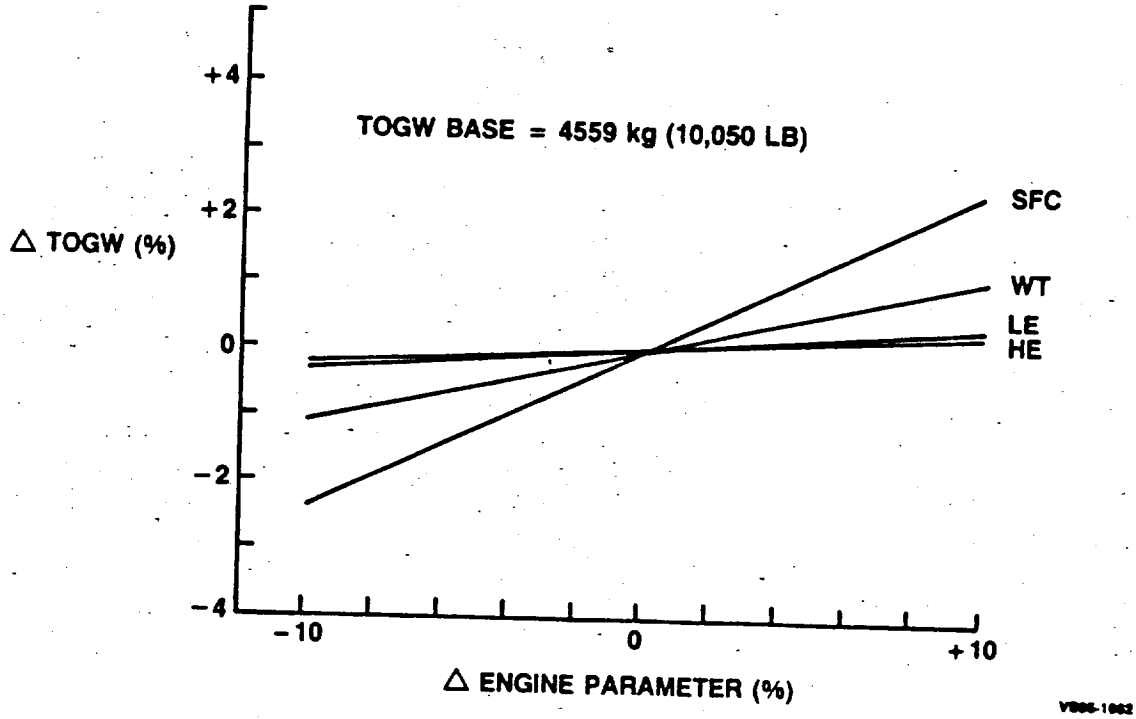

Figure 10. TOGW sensitivity curves (baseline engine).

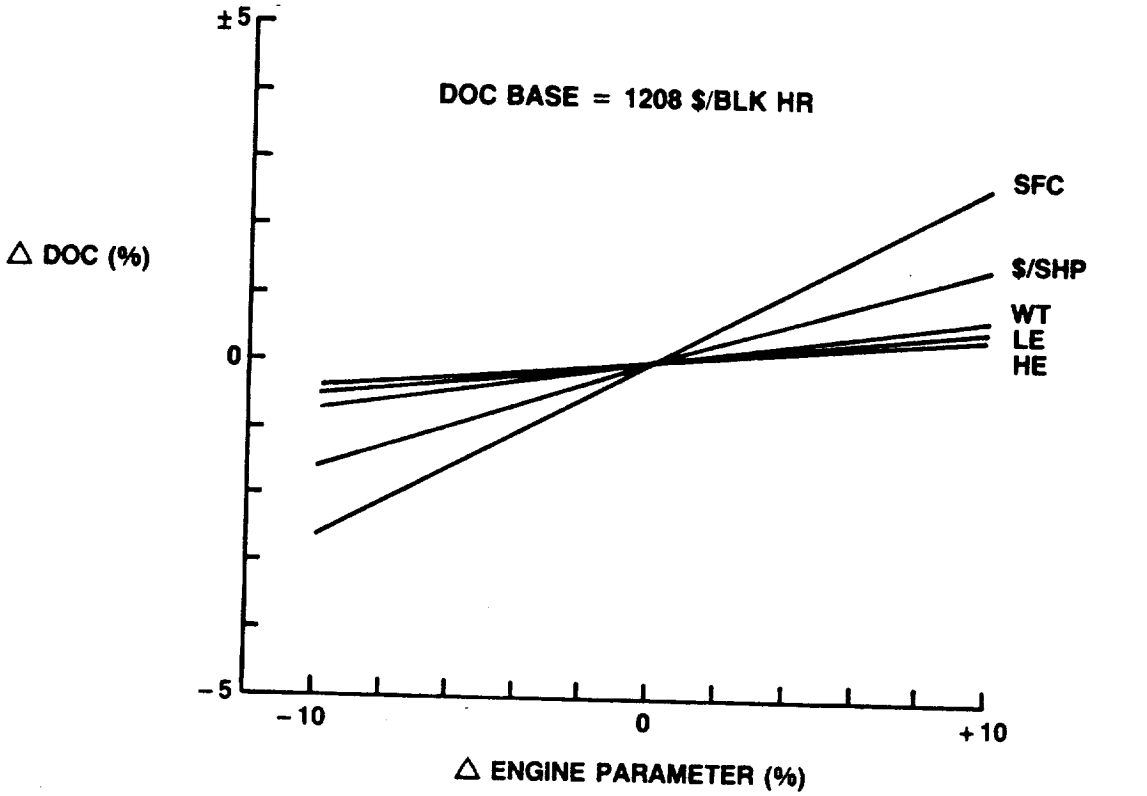

Figure 11. DOC sensitivity curves (baseline engine).

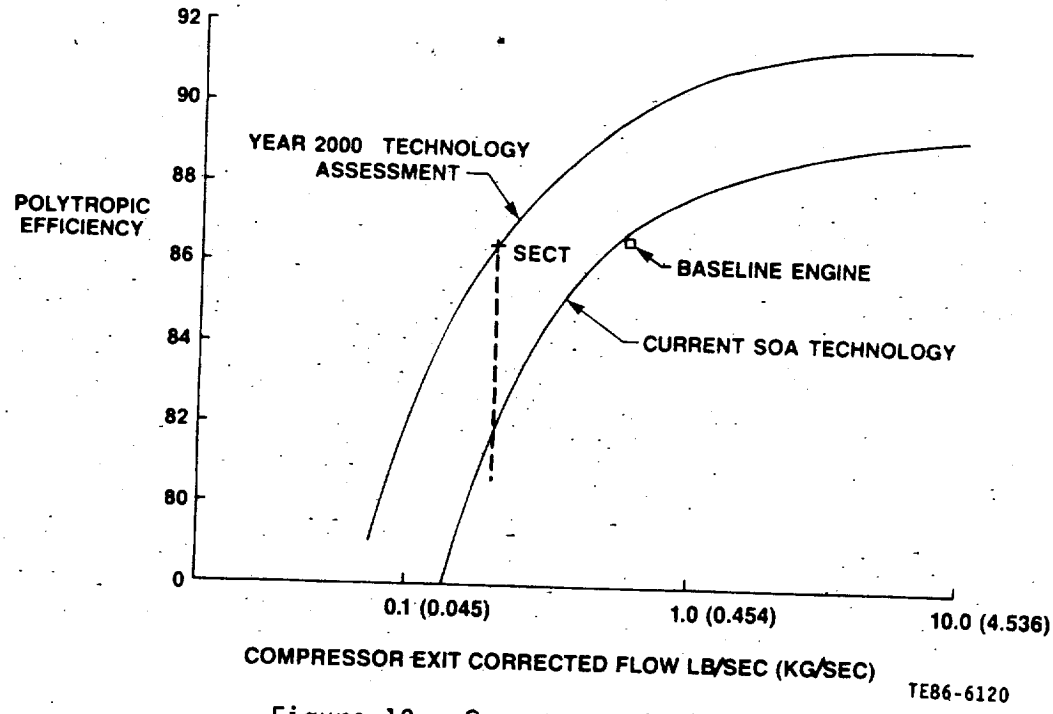

Figure 12. Compressor technology.

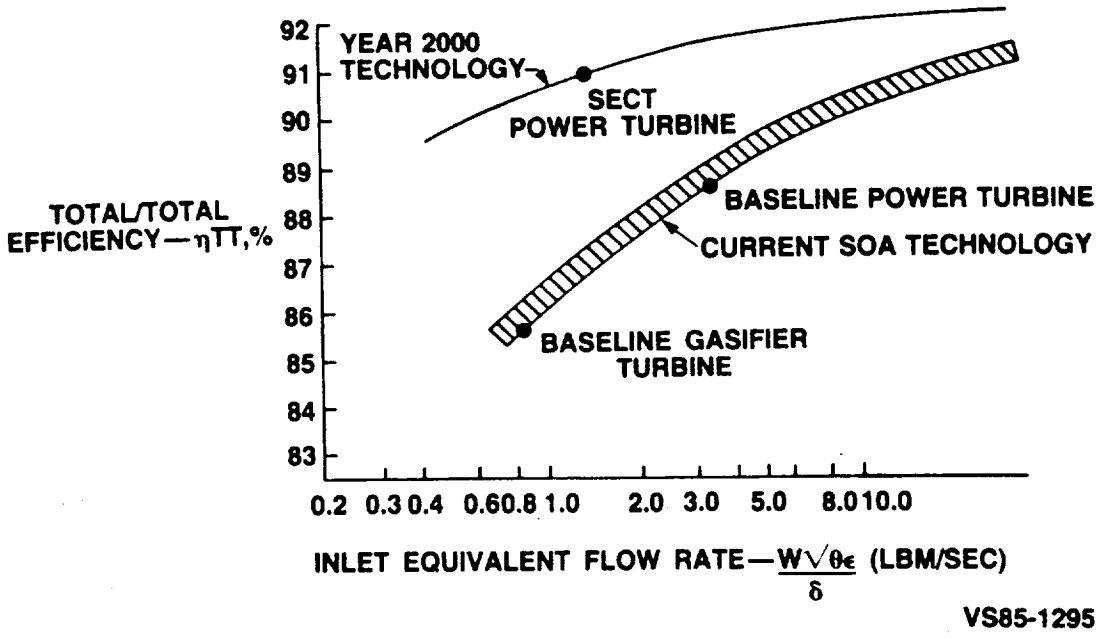

Figure 13. Comparison of SECT goal efficiency level with current axial flow turbine stage efficiency.

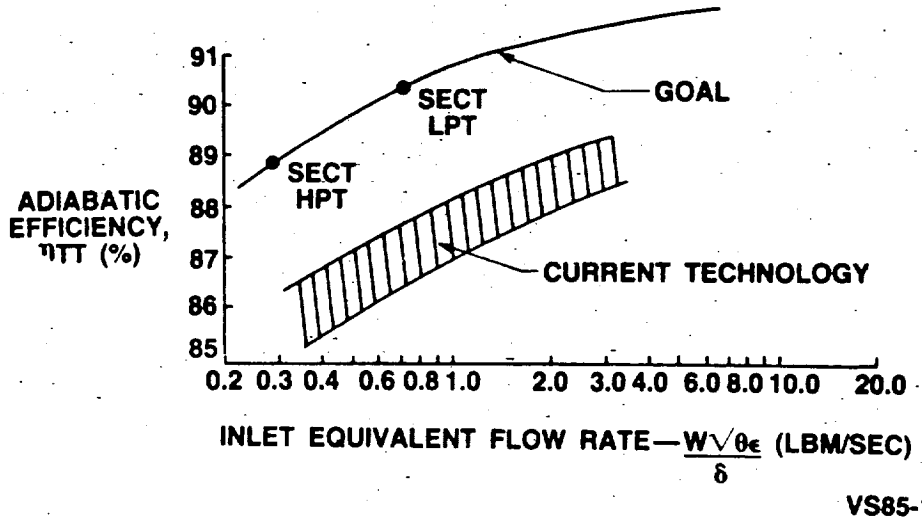

Figure 14. Current technology and SECT goal radial turbine performance.

- HIGHER CYCLE PRESSURE RATIO AND TEMPERATURE
- HIGHER THERMAL EFFICIENCY

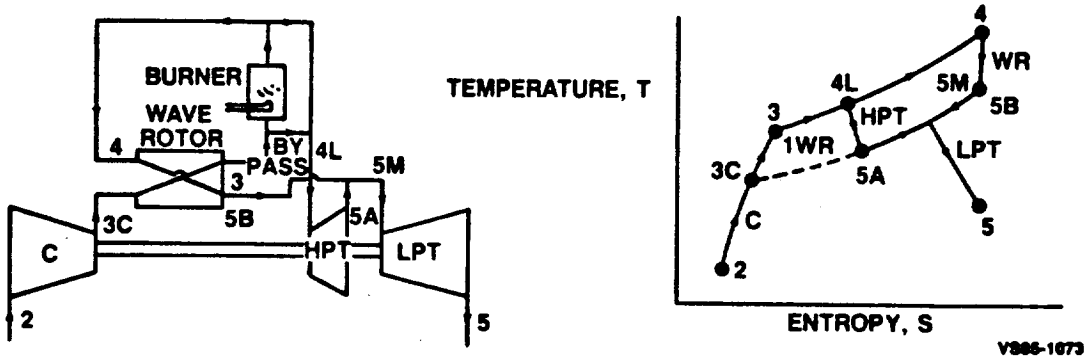

Figure 15. Wave rotor engine cycle.

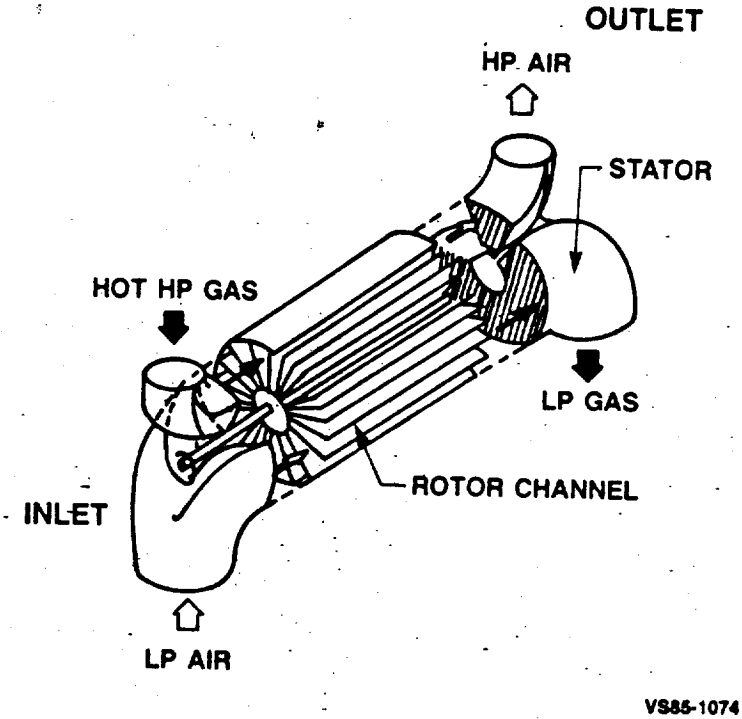

Figure 16. Wave rotor for gas turbine application.

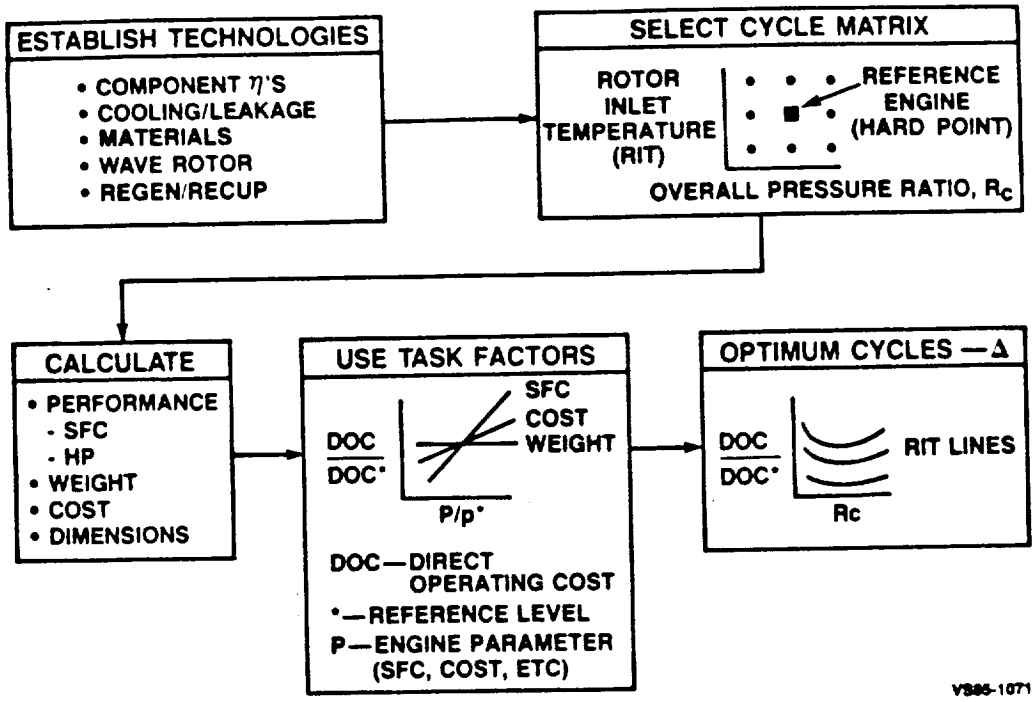

Figure 17. Cycle optimization flow chart.

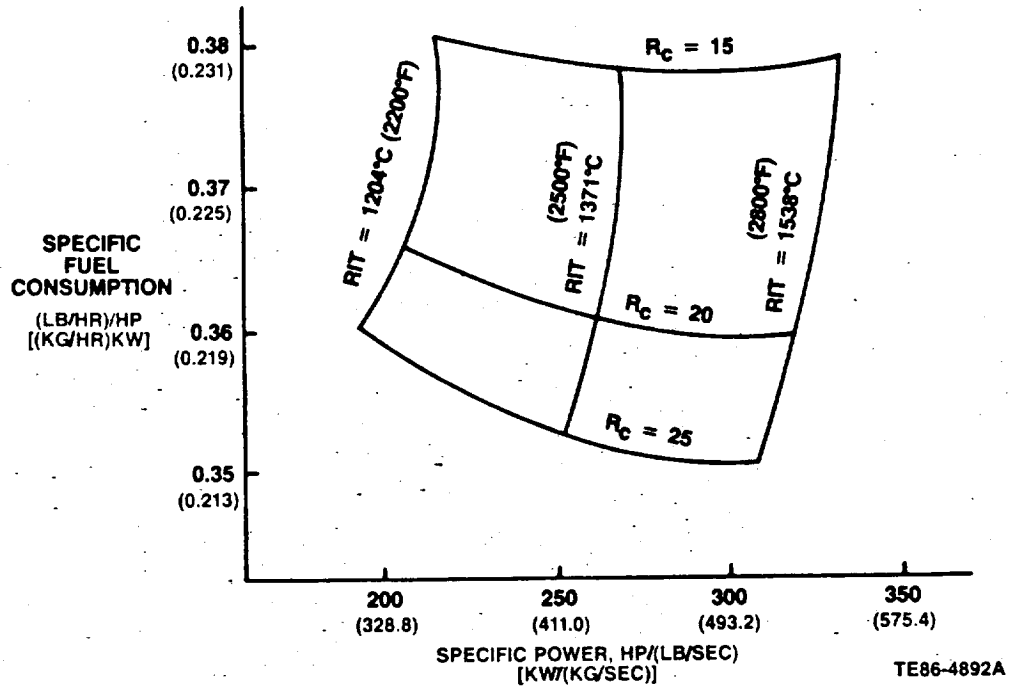

Figure 18. Concentric engine cycle optimization SFC versus specific power.

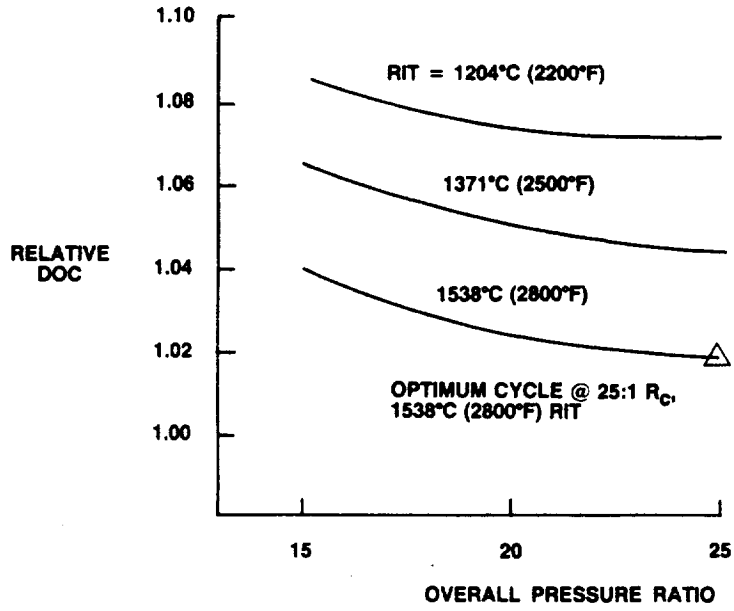

Figure 19. Concentric engine cycle optimization.

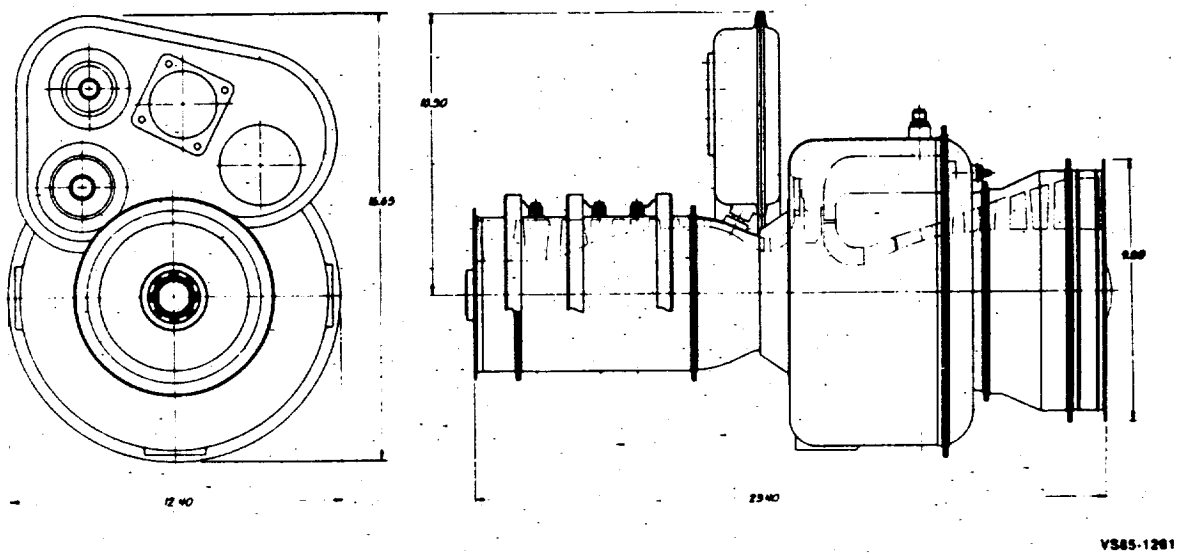

Figure 20. Concentric engine general outline.

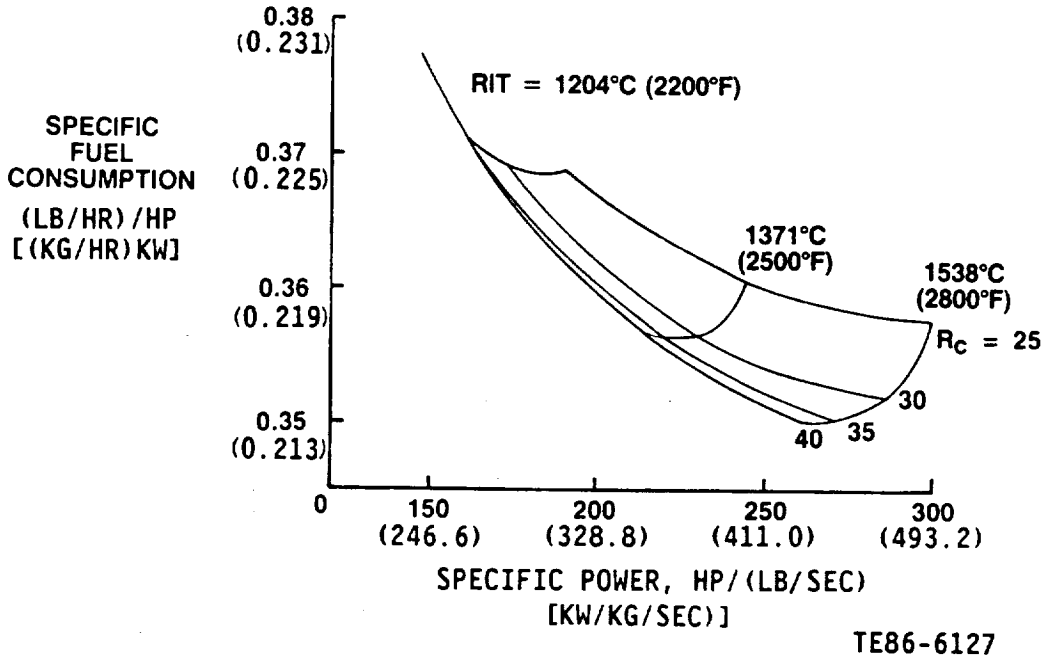

Figure 21. Nonconcentric engine cycle optimizatioon--SFC versus specific power.

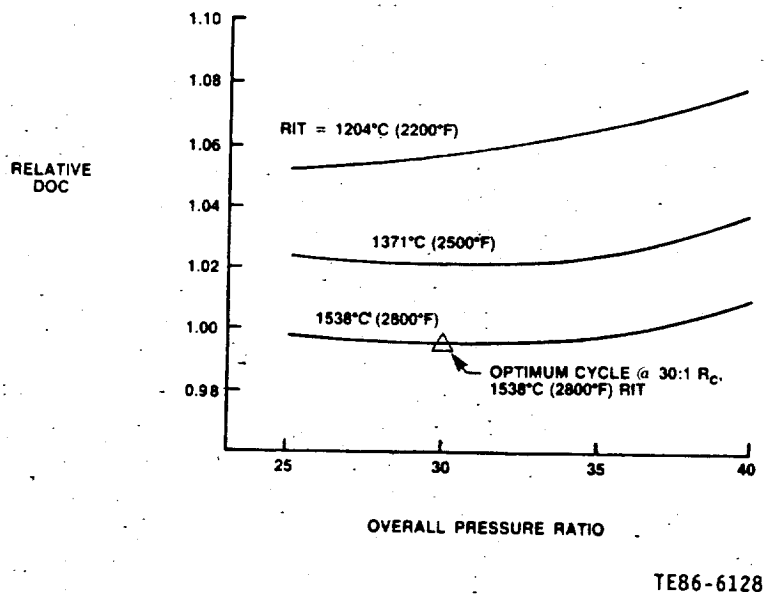

Figure 22. Nonconcentric engine cycle optimization.

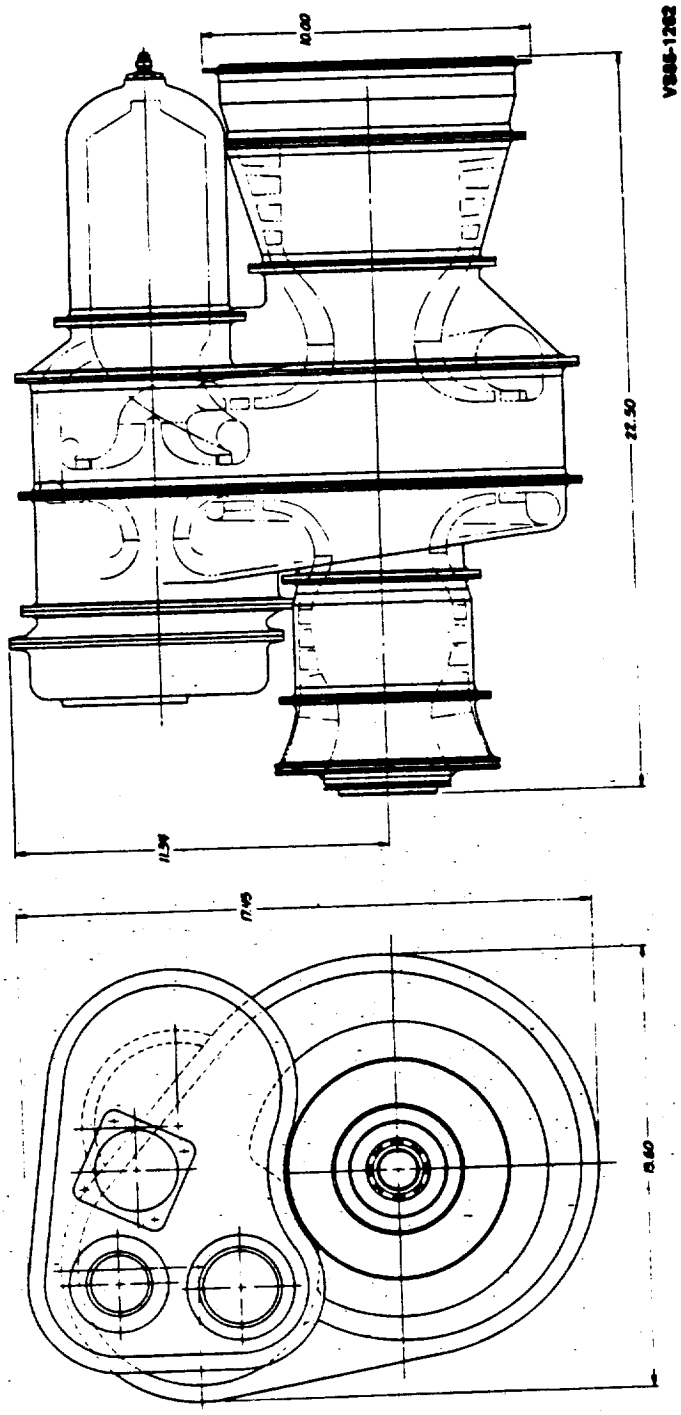

Figure 23. Nonconcentric engine general outline.

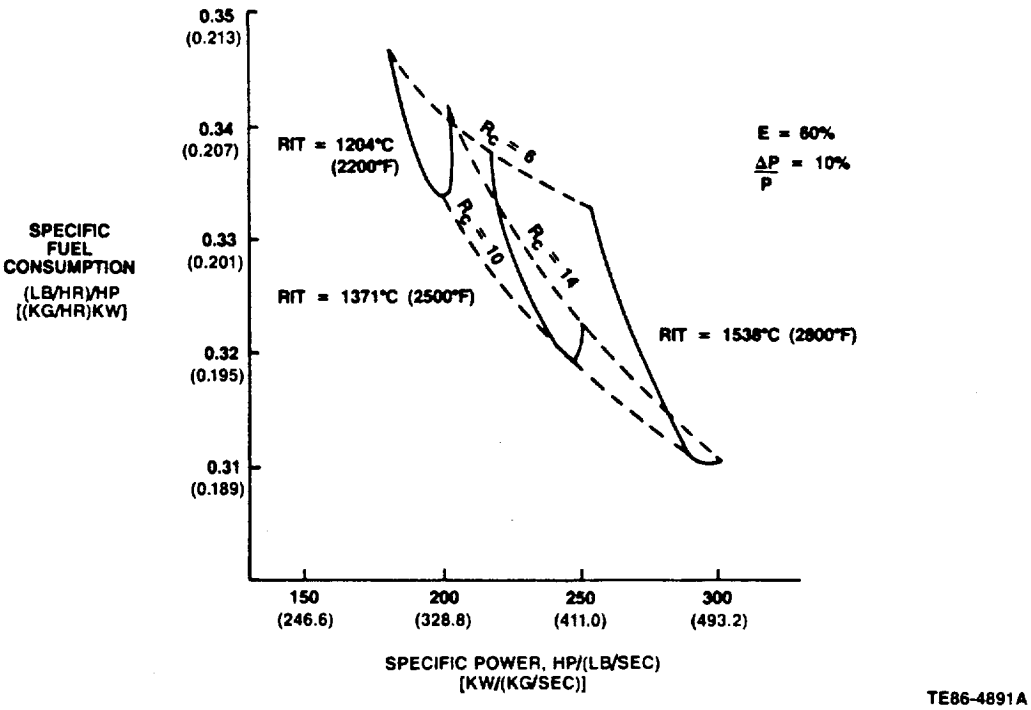

Figure 24. Recuperative engine cycle optimization--SFC versus specific power.

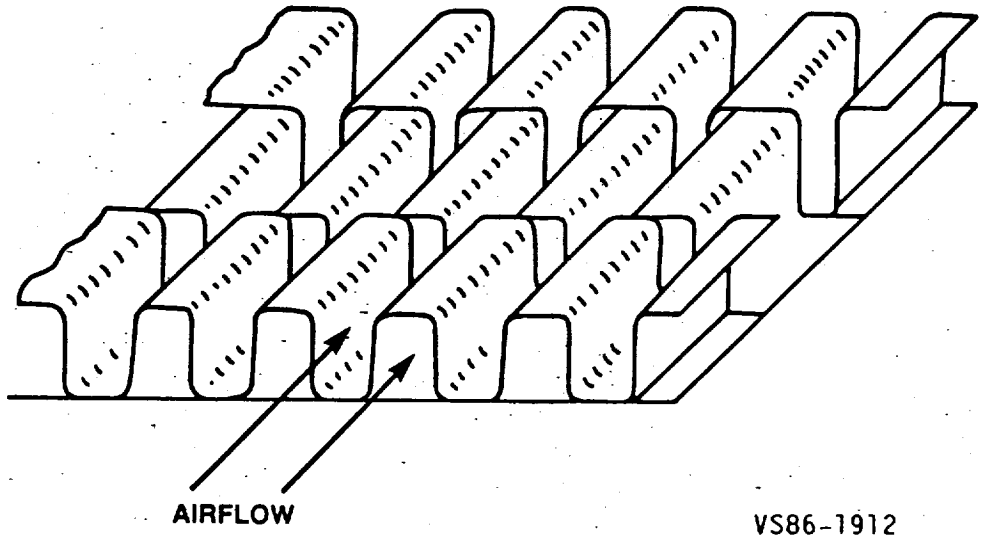

Figure 25. Offset rectangular plate-fin recuperator.

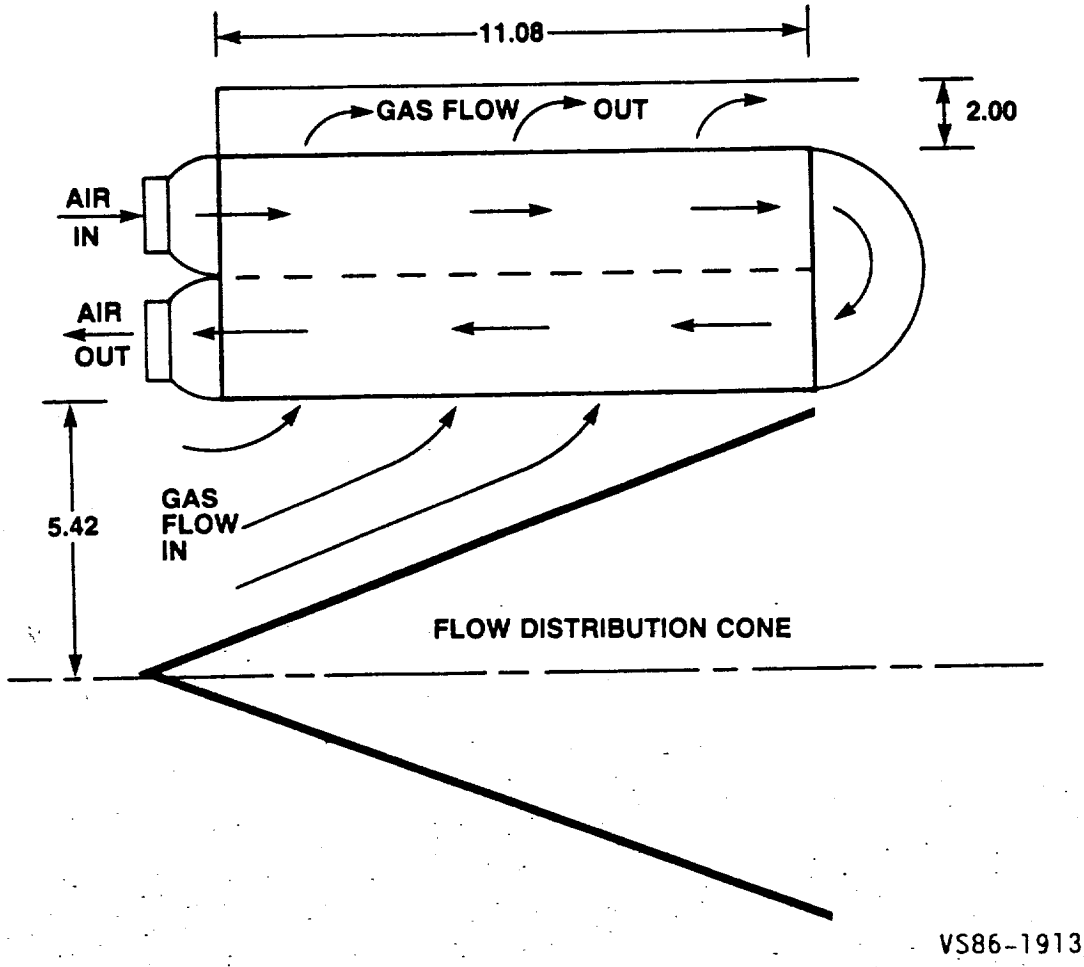

Figure 26. Two-pass cross-counterflow plate-fin recuperator.

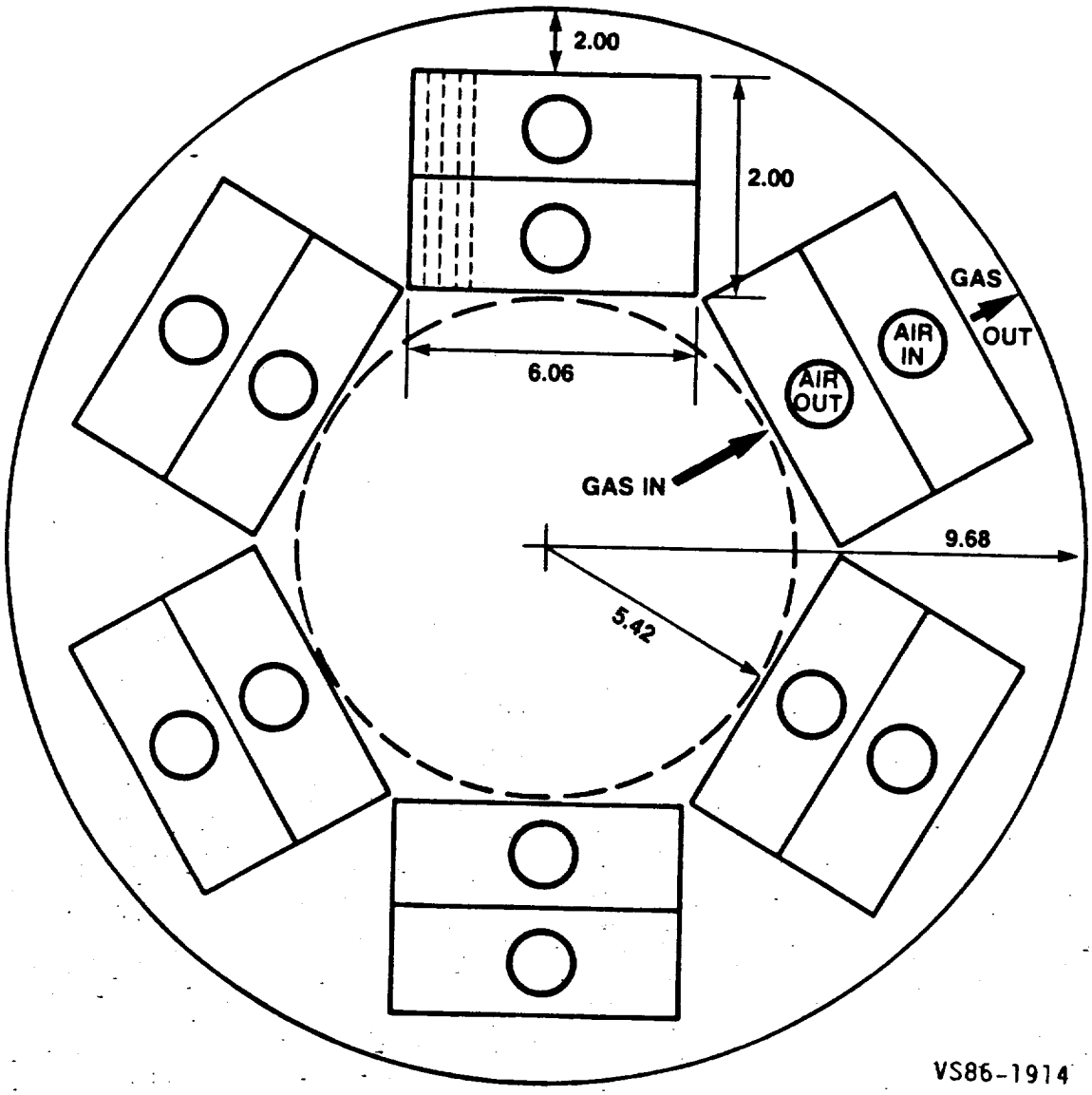

Figure 27. Annular arrangement of two-pass cross-counterflow plate-fin recuperators.

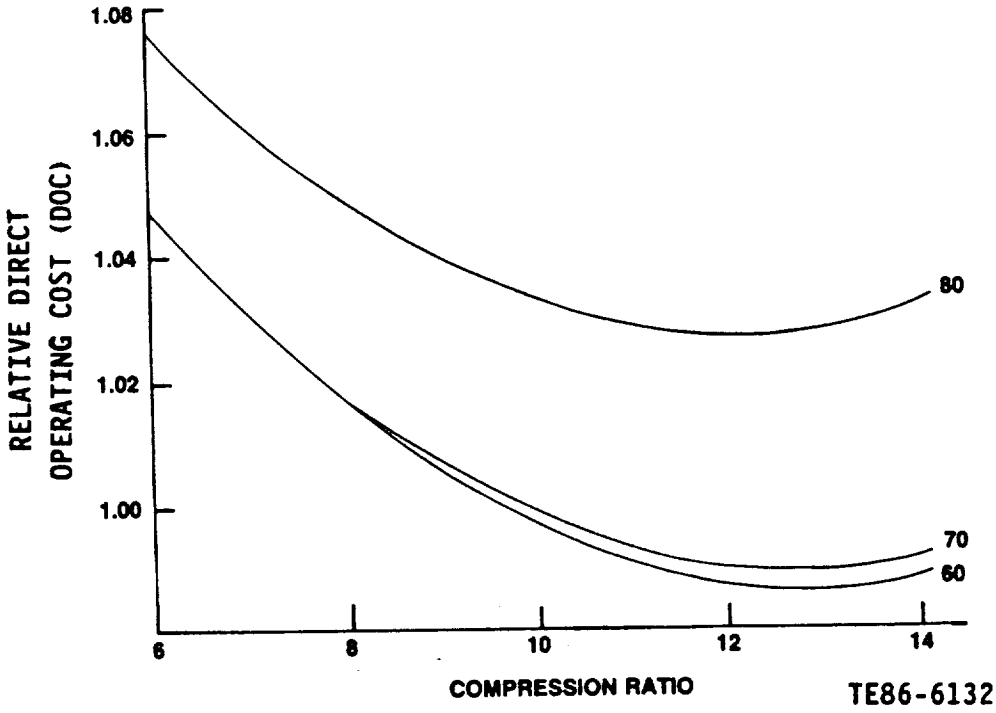

Figure 28. DOC ratio versus compression rates two-pass cross-counterplate-fin recuperator.

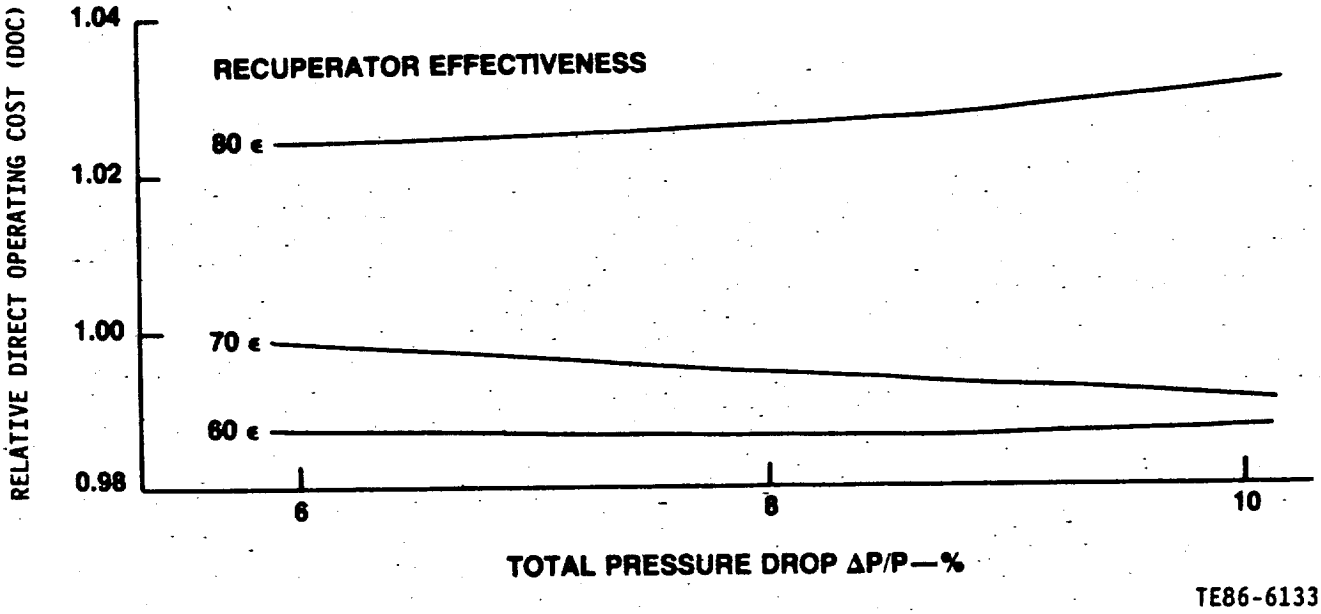

Figure 29. DOC ratio versus effectiveness of two-pass cross-counterplate-fin recuperator.

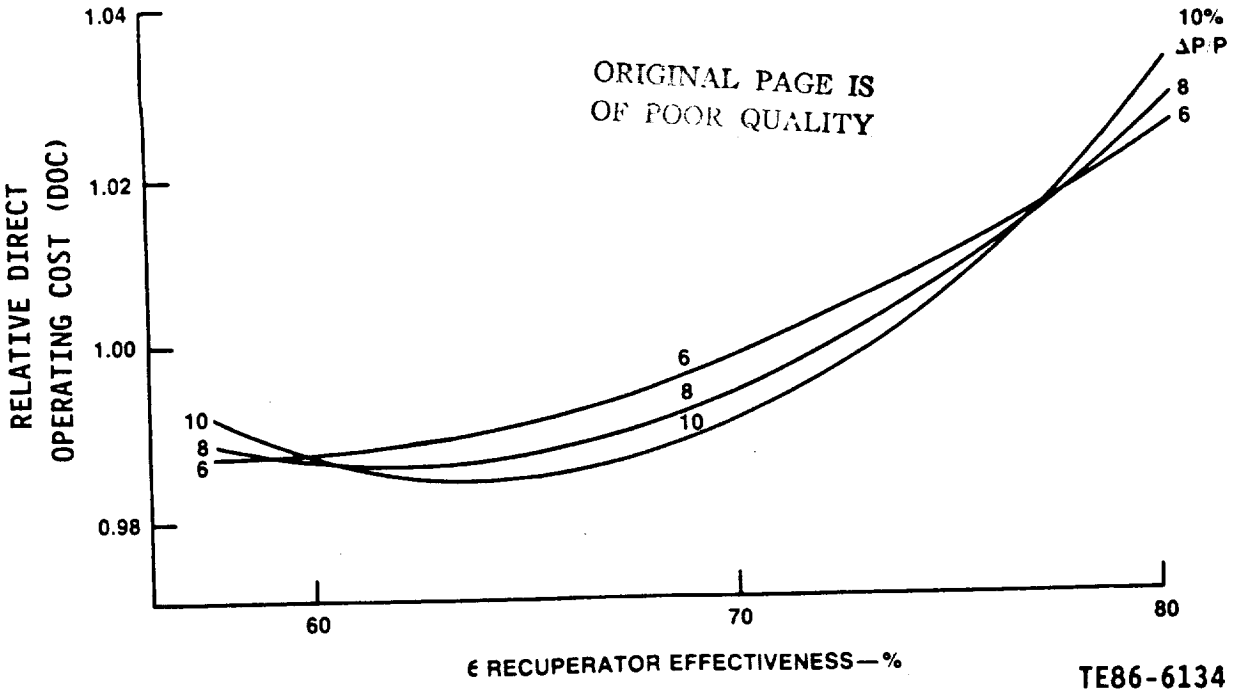

Figure 30. DOC ratio versus pressure drop of two-pass cross-counterplate-fin recuperator.

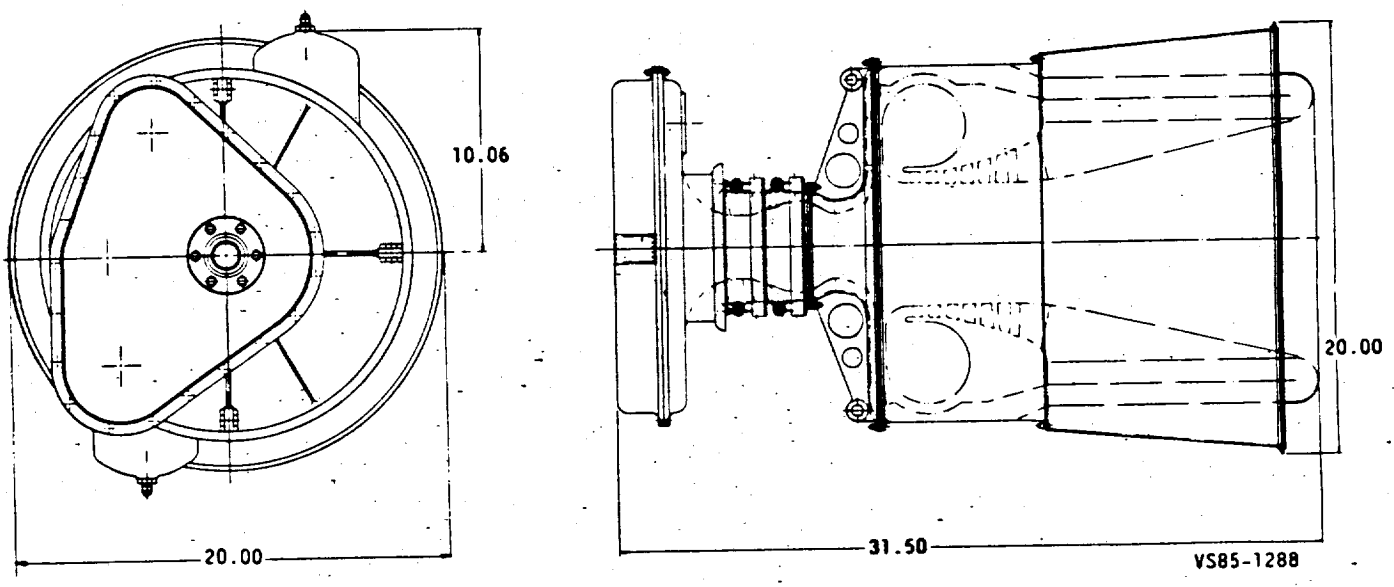

Figure 31. Recuperative engine general outline.

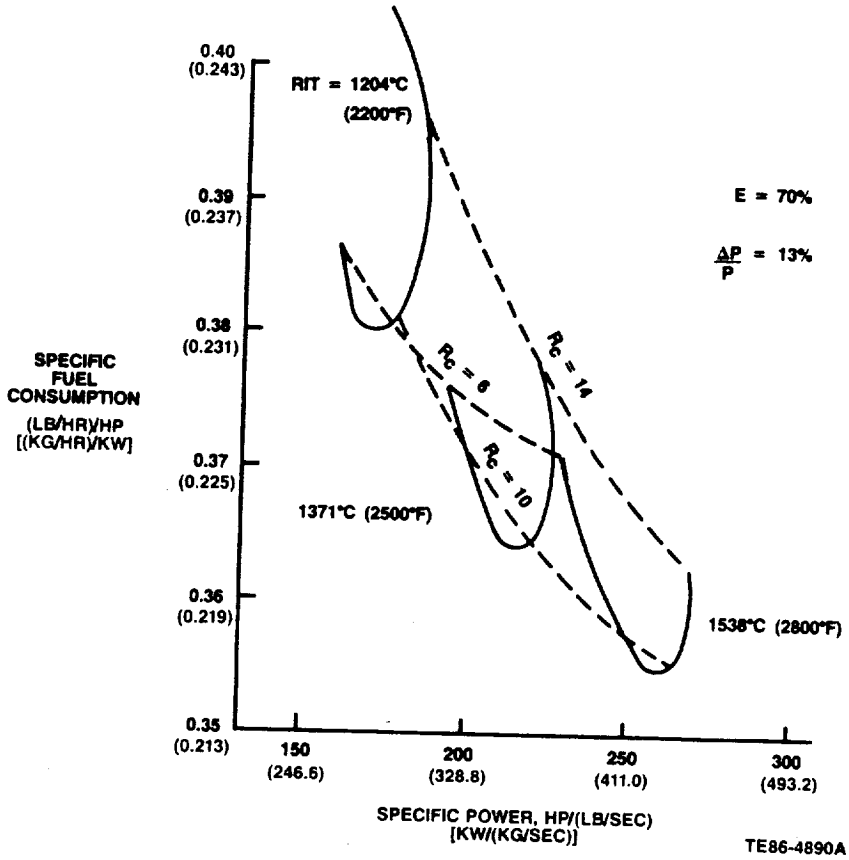

Figure 32. Regenerative engine cycle optimization--SFC versus specific power.

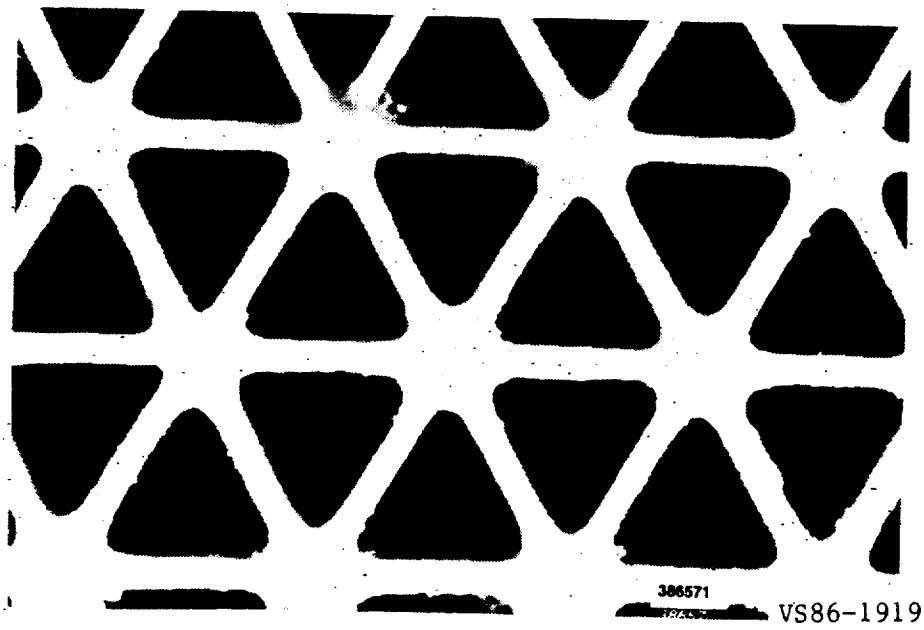

Figure 33. Extruded ceramic heat transfer matrix.

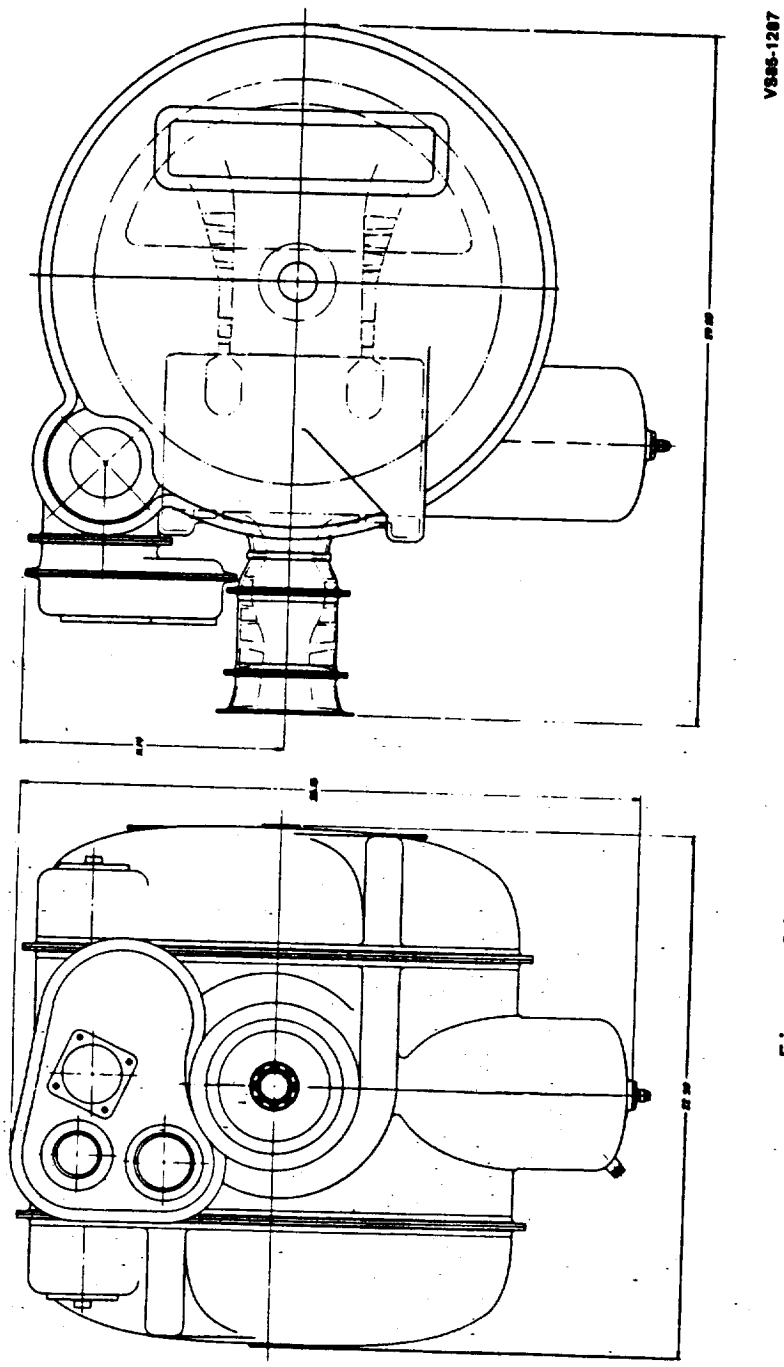

Figure 34. Regenerative engine general outline.

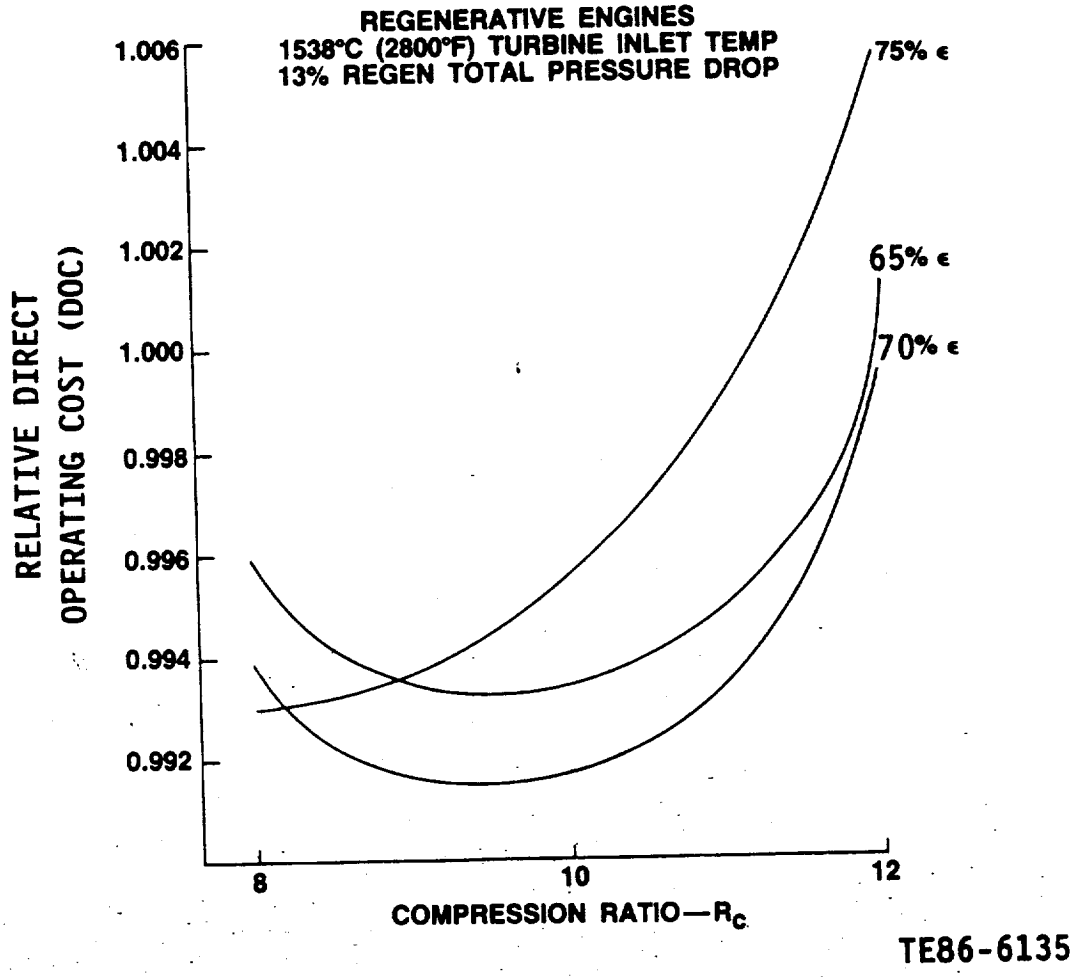

Figure 35. DOC versus compression rates of regenerative engines.

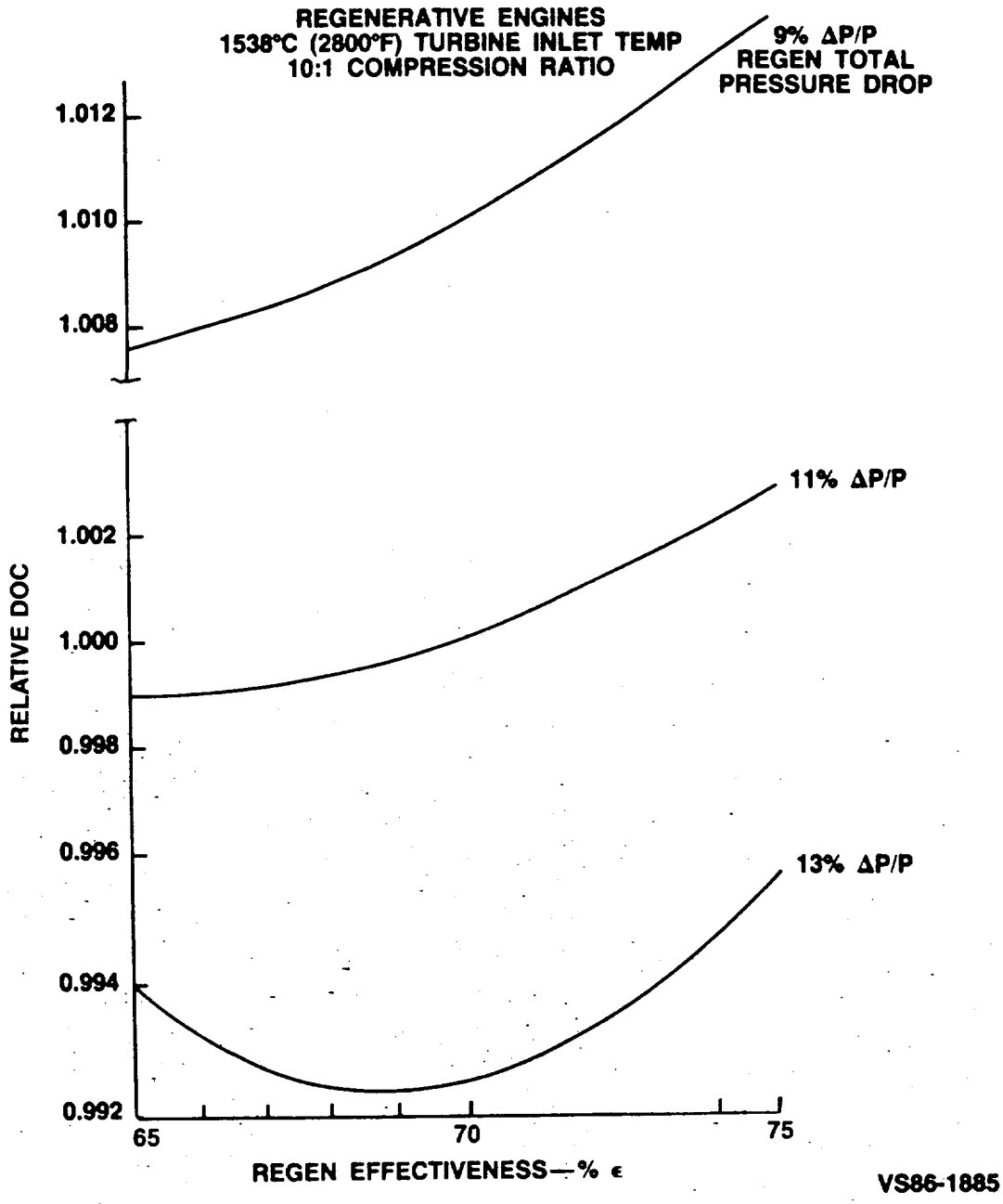

Figure 36. DOC versus regenerative effectiveness of regenerative engines.

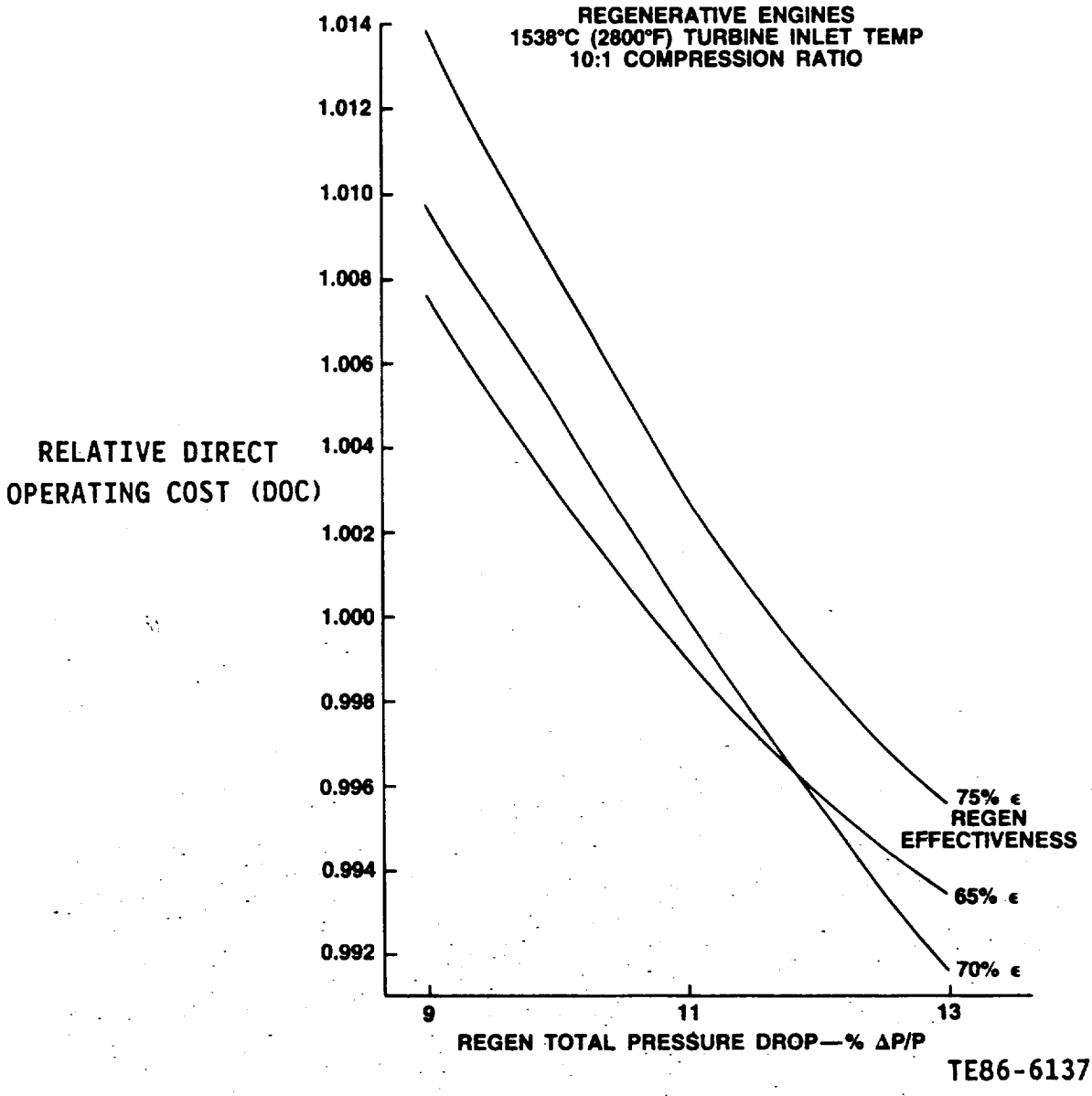

Figure 37. DOC versus regenerative total pressure drop of regenerative engines.

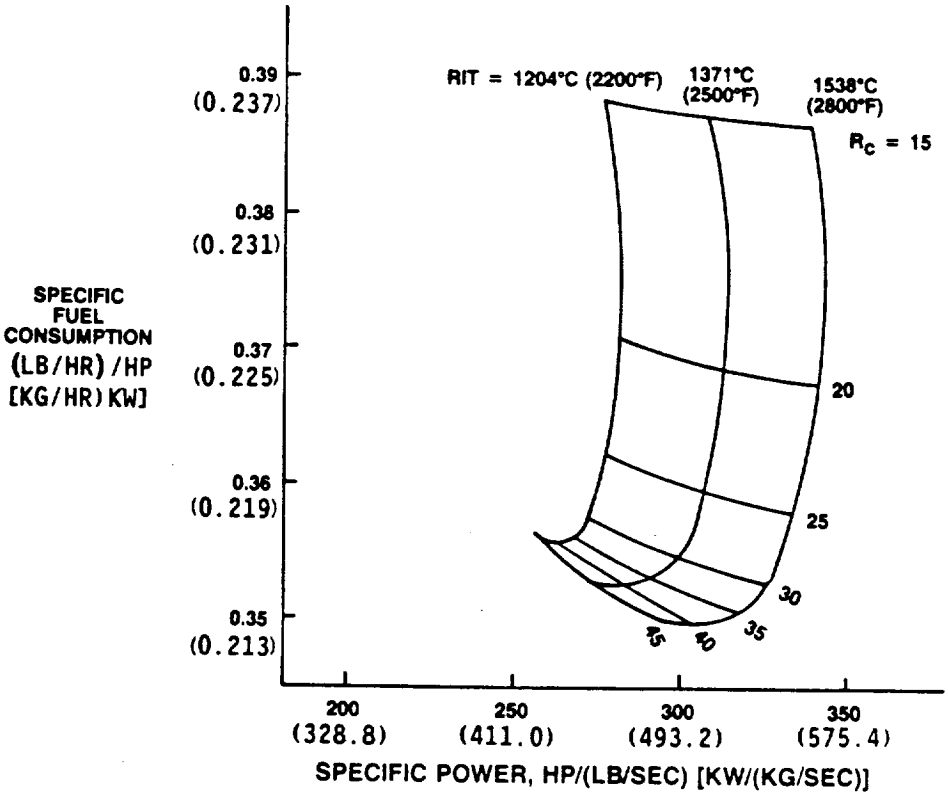

Figure 38. Wave rotor engine cycle optimization--SFC versus specific power.

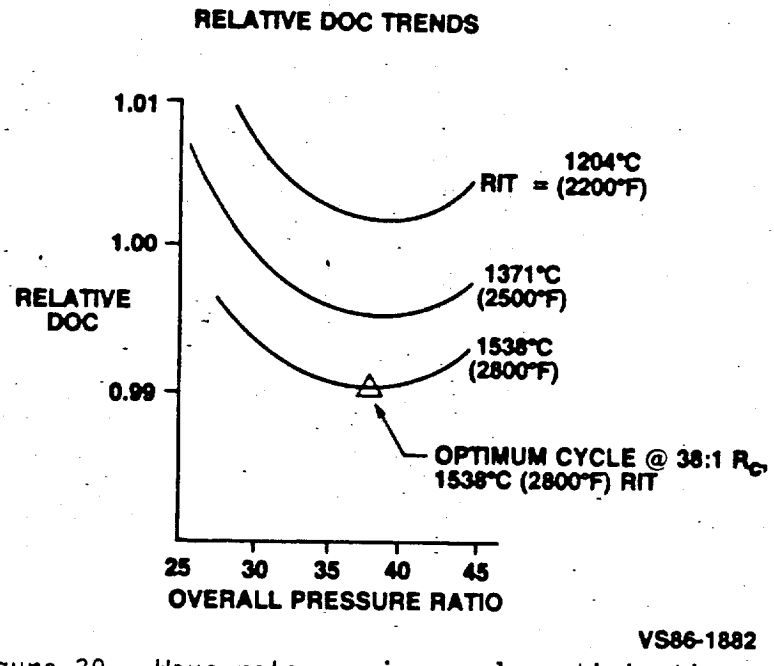

Figure 39. Wave rotor engine cycle optimization.

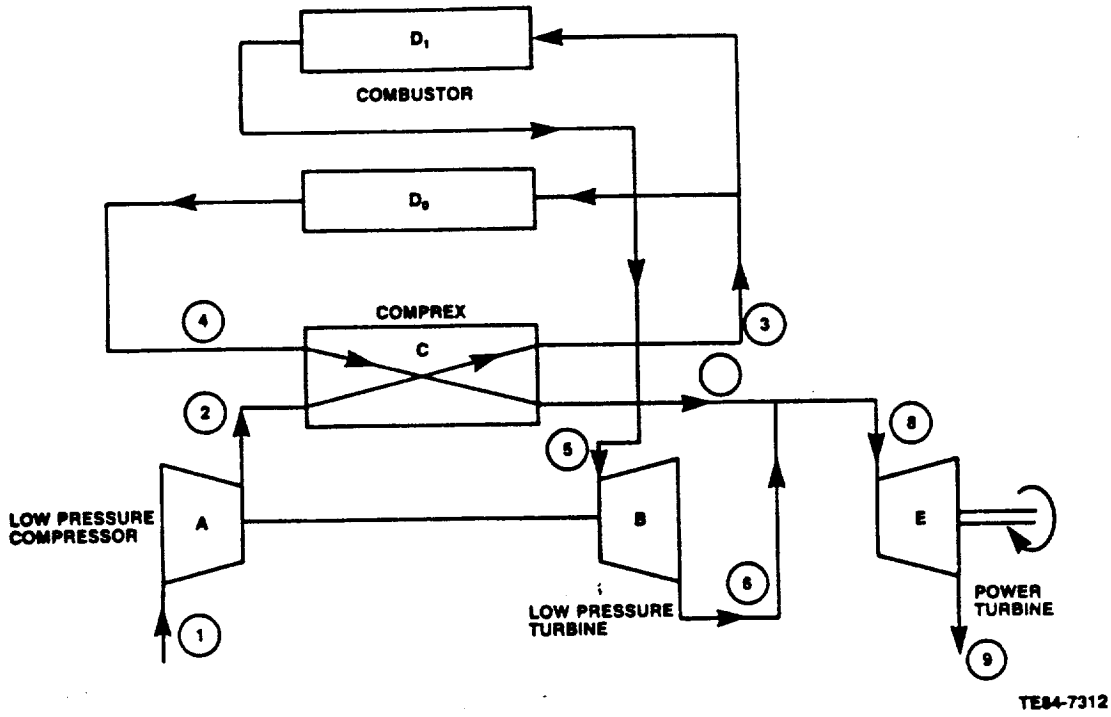

Figure 40. Possible schematic arrangement of comprex engine.

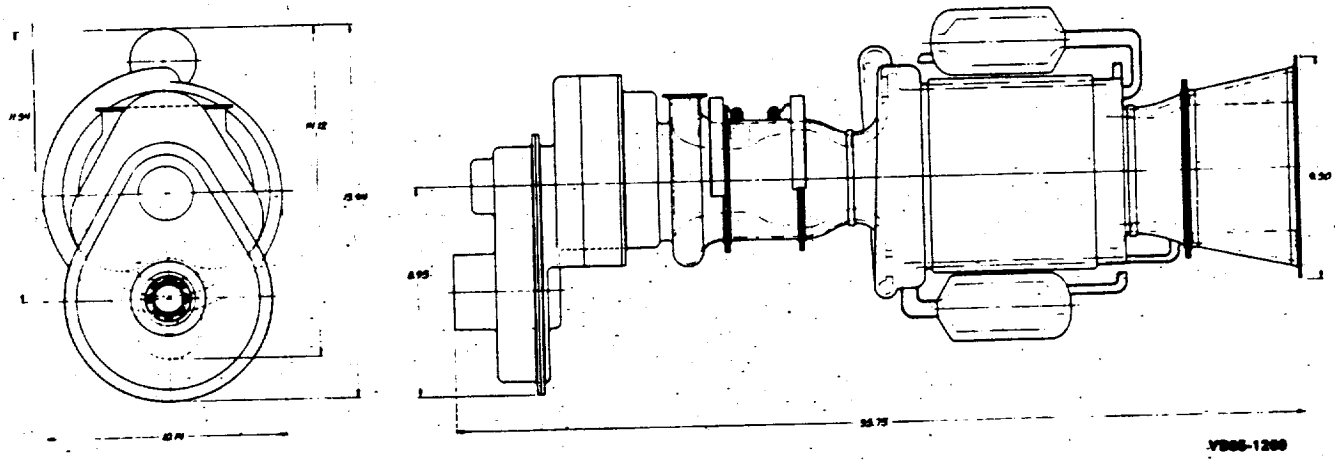

Figure 41. Wave rotor engine general outline.

ORIGINAL PAGE IS
OF POOR QUALITY

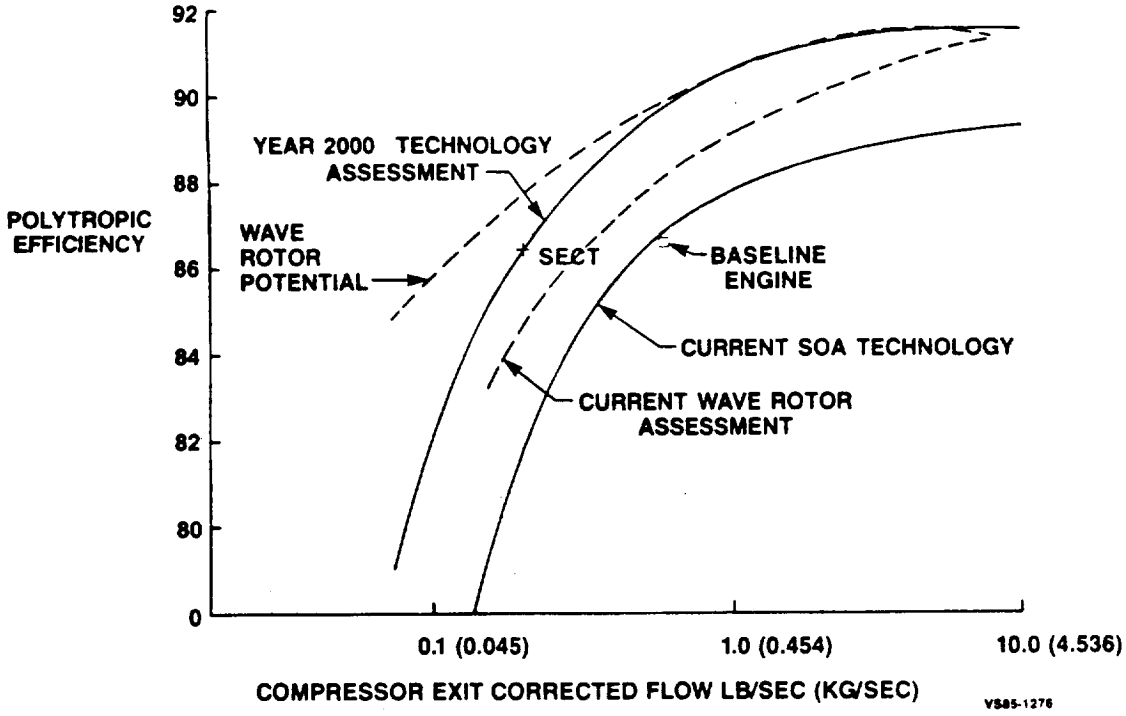

Figure 42. Compressor technology.

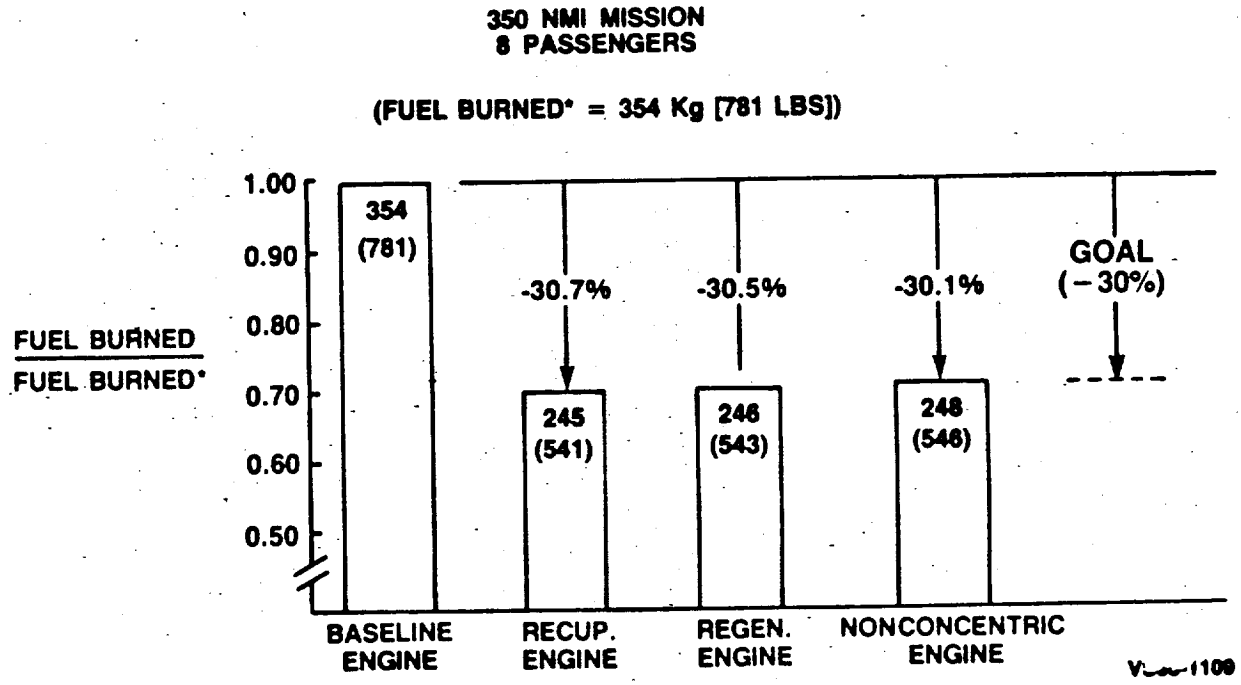

Figure 43. Fuel burned comparison.

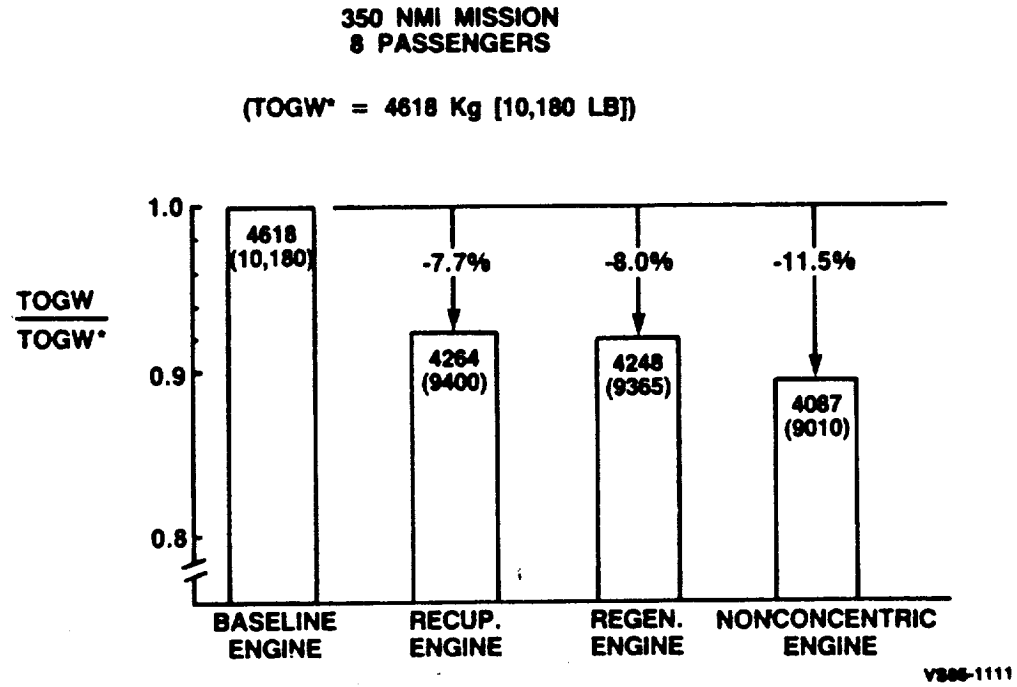

Figure 44. TOGW comparison.

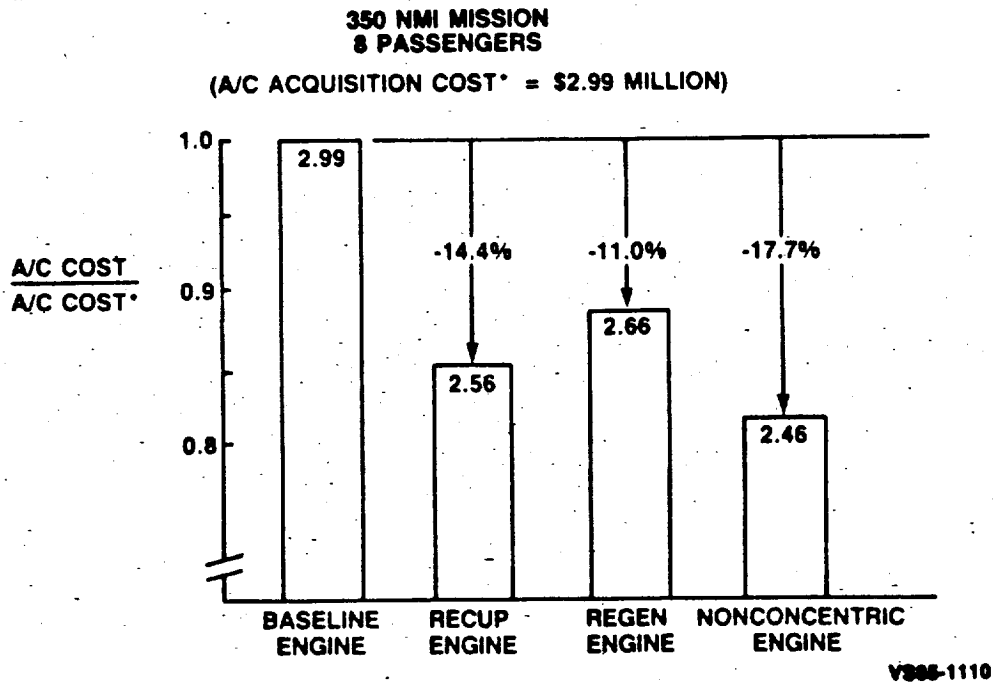

Figure 45. Aircraft acquisition cost comparison.

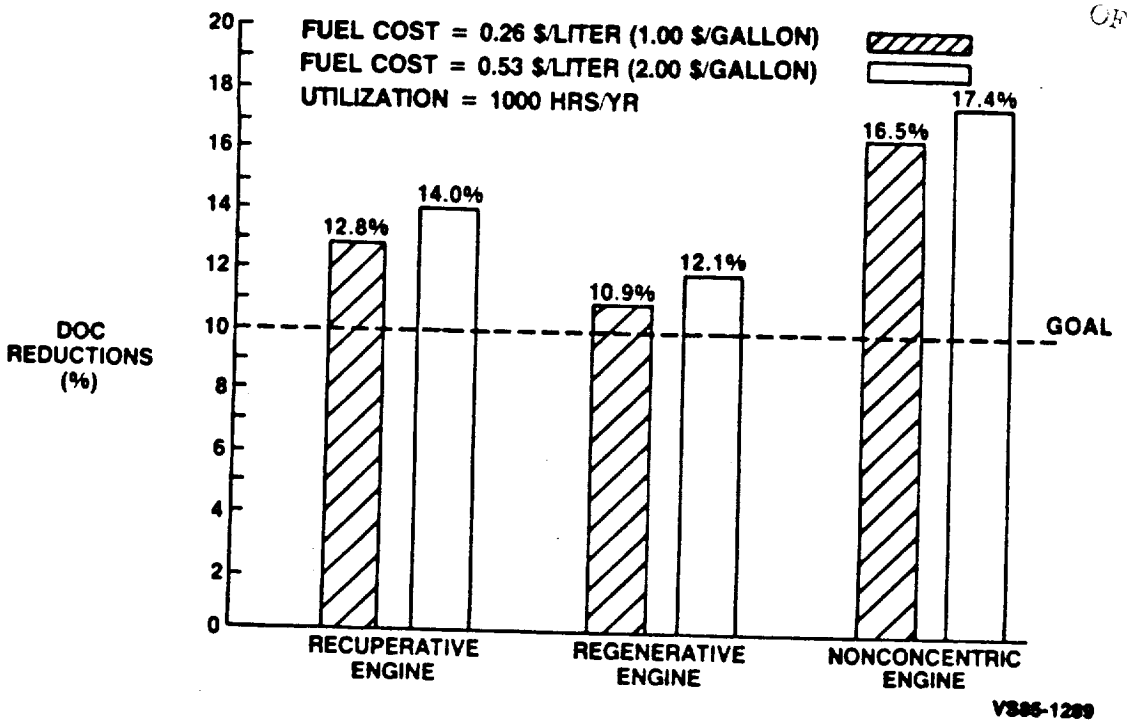

Figure 46. Percent DOC reductions (relative to baseline engine levels).

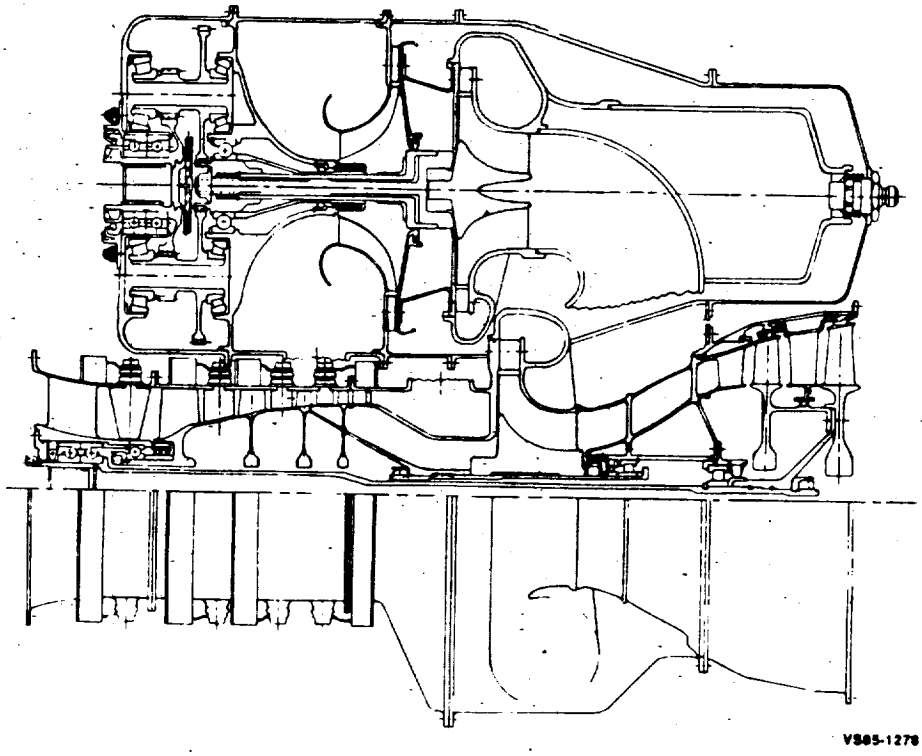

Figure 47. Nonconcentric engine general arrangement (1538°C [2800°F], 30:1 R_c).

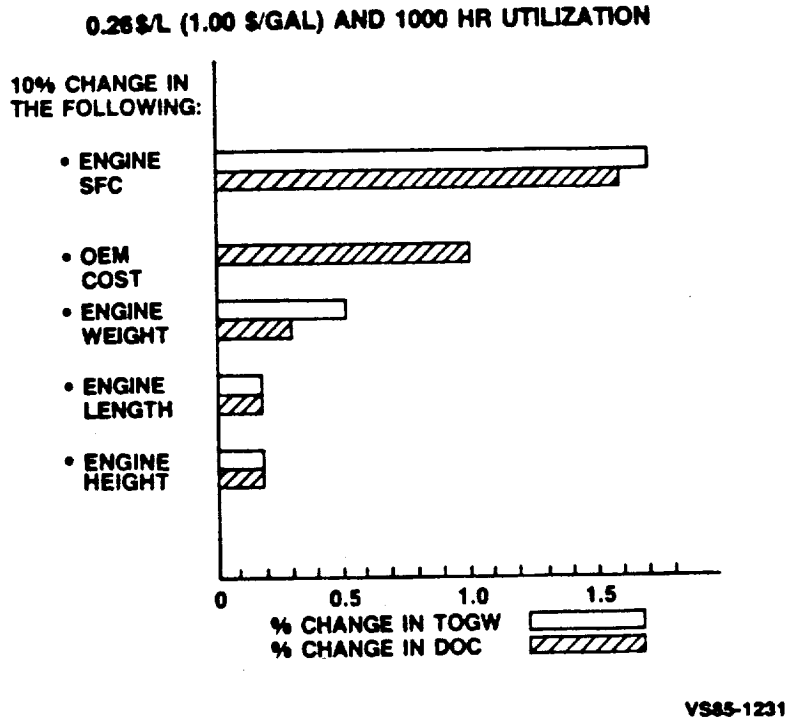

Figure 48. Nonconcentric engine sensitivity results.

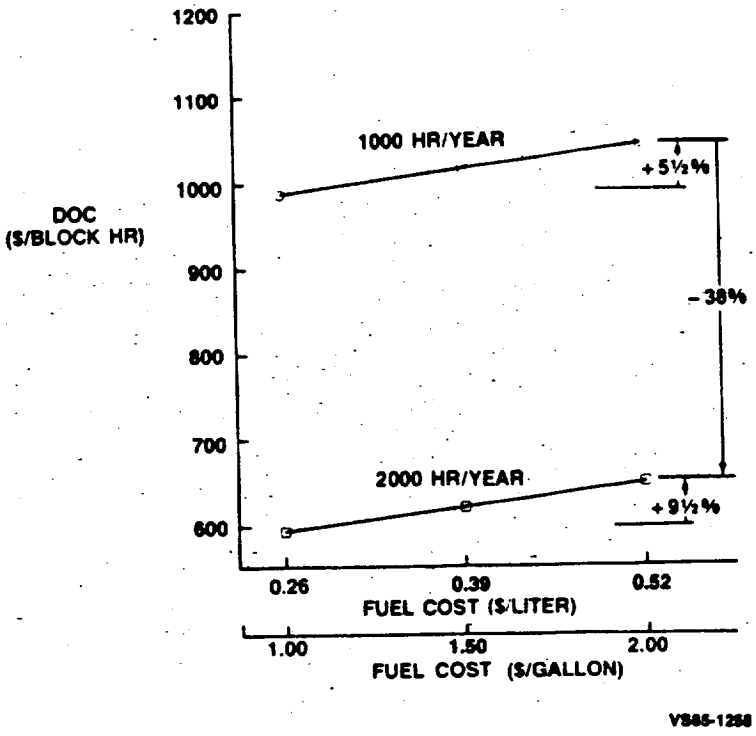

Figure 49. DOC sensitivity to fuel cost and utilization levels (nonconcentric engine).

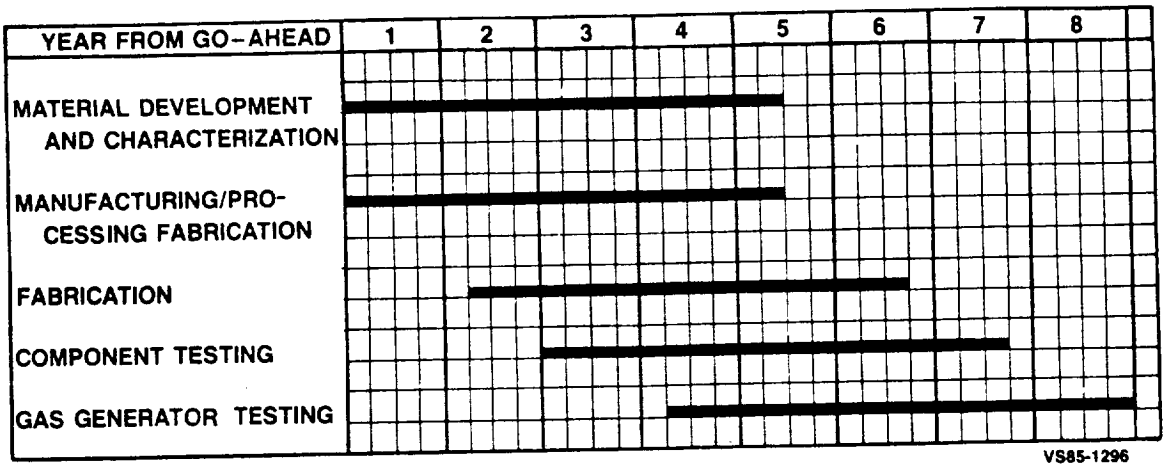

Figure 50. Ceramic HPT rotor program schedule.

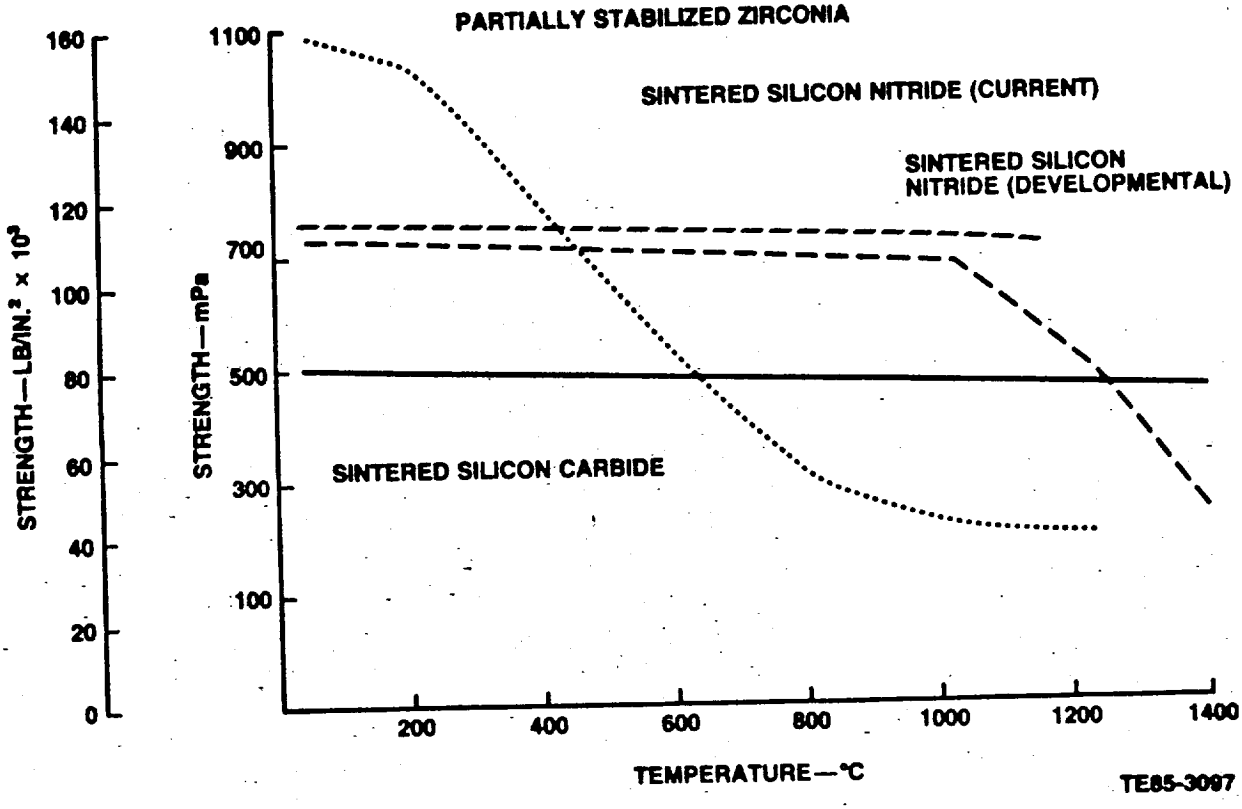

Figure 51. Flexual strength of candidate monolithic ceramic materials.

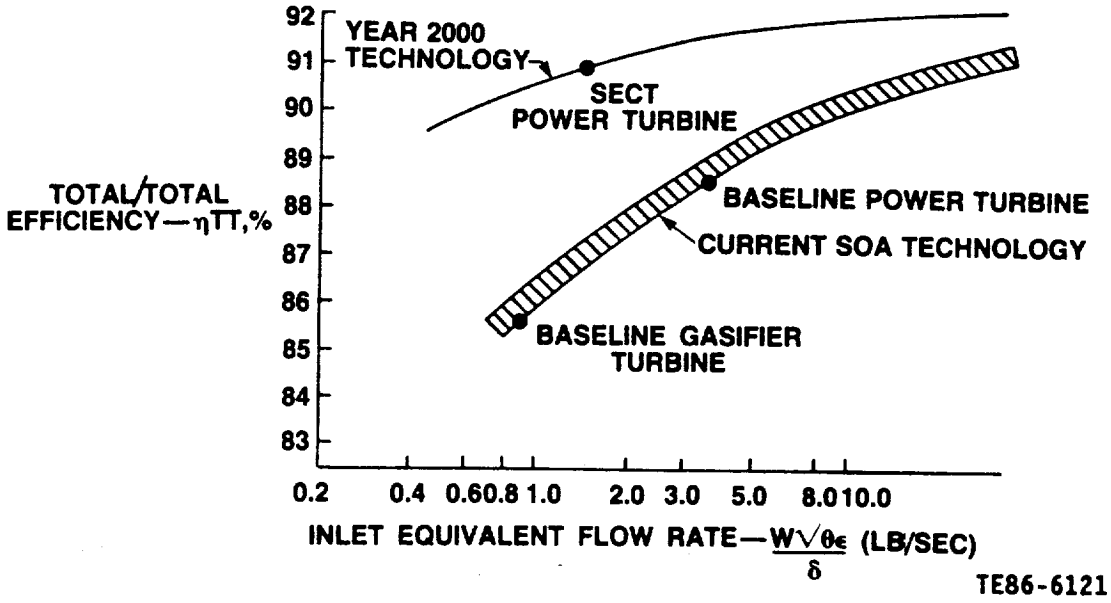

Figure 52. Comparison of SECT goal efficiency level with current axial flow turbine stage efficiency.

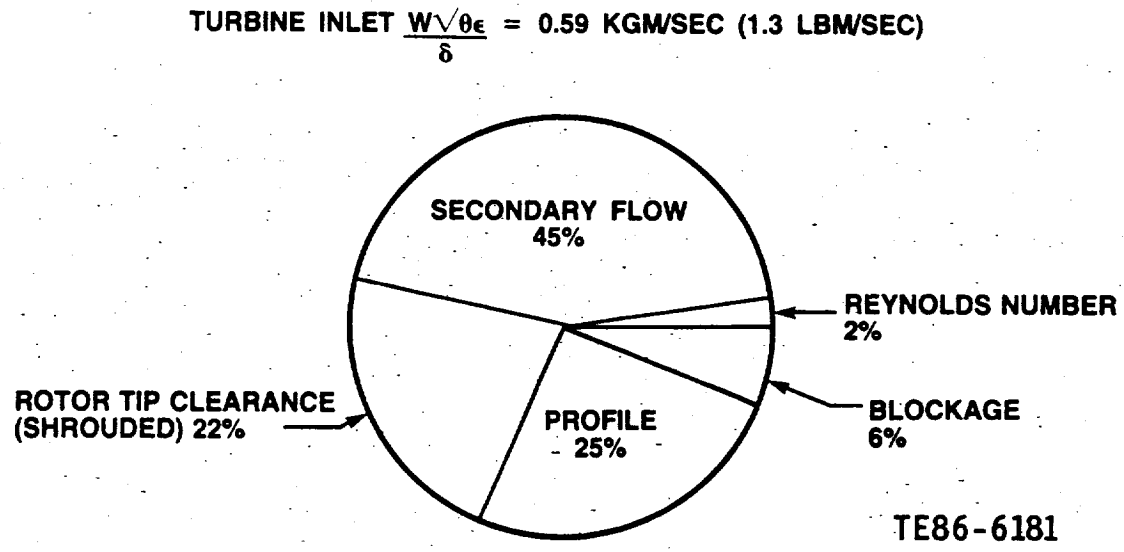

Figure 53. Loss breakdown for a small axial flow power turbine.

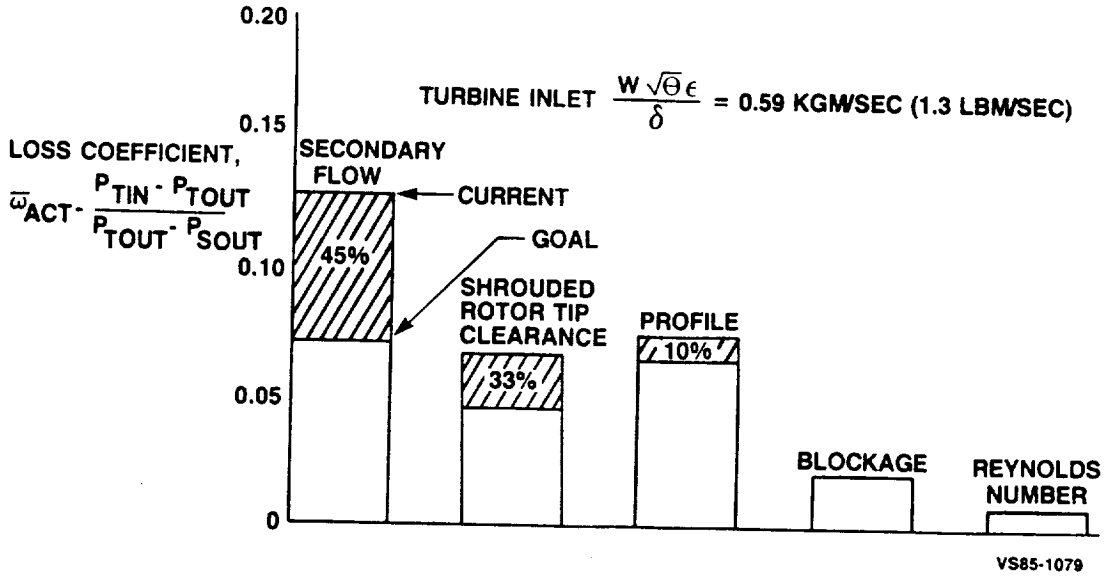

Figure 54. Small axial flow power turbine loss reductions required to meet SECT goal efficiency.

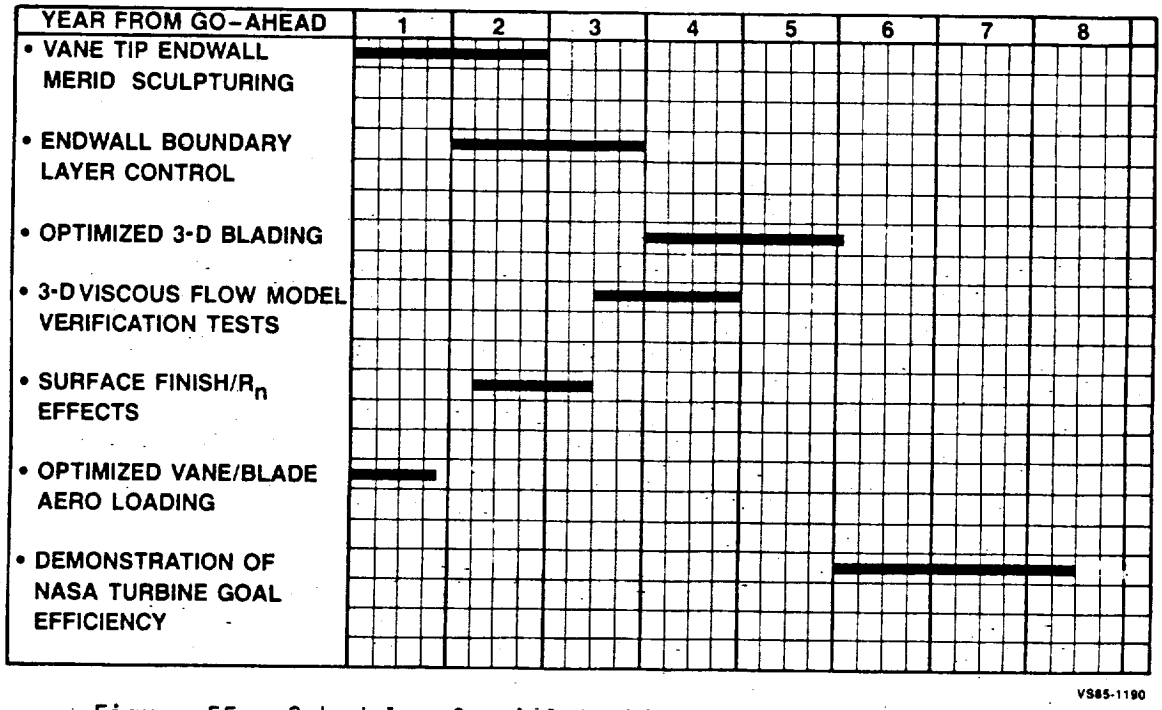

Figure 55. Schedule of axial turbine key technology programs.

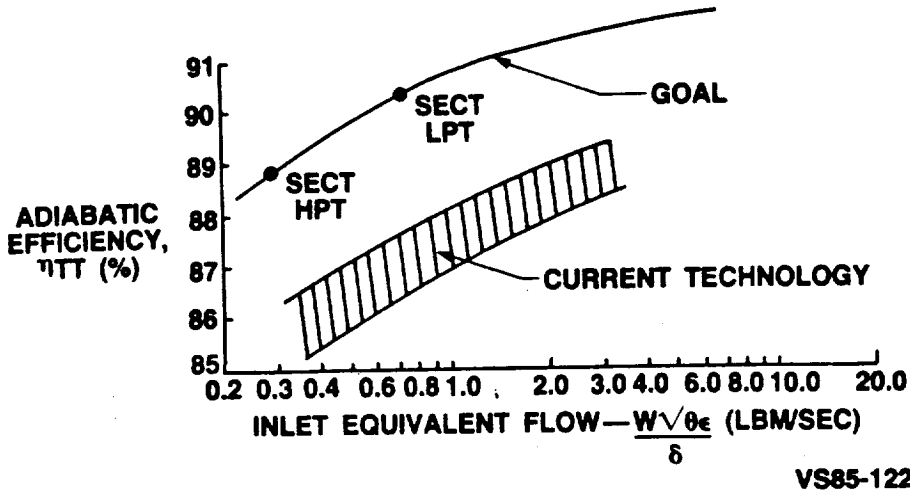

Figure 56. Current technology and SECT goal radial turbine performance.

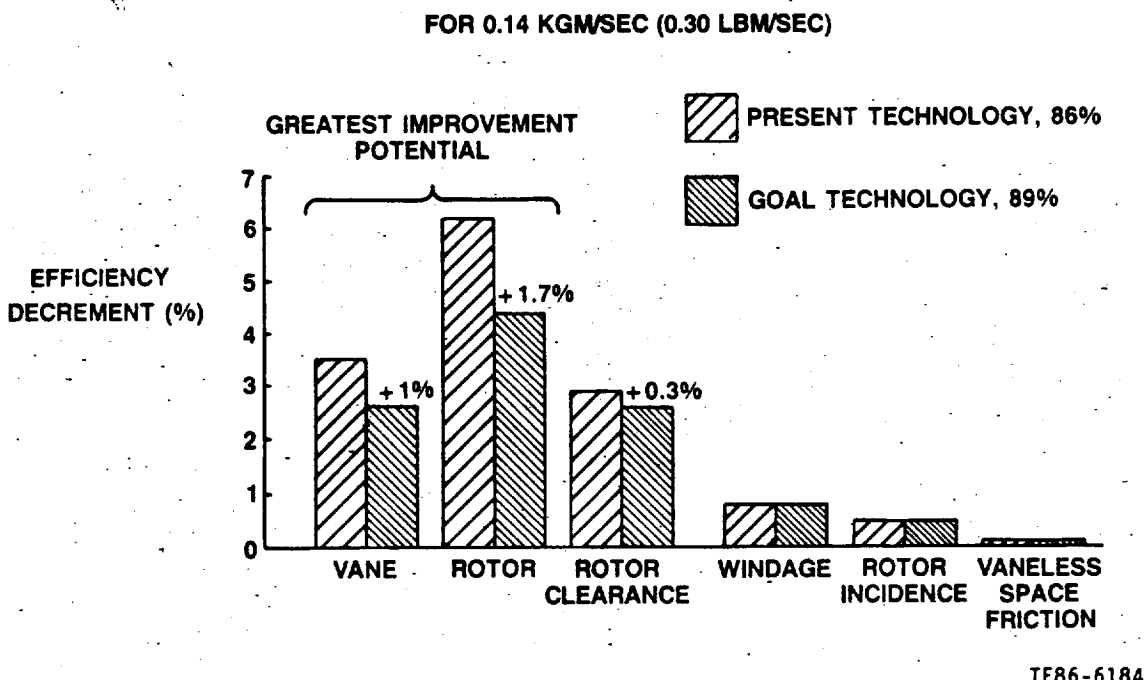

Figure 57. Small radial turbine loss breakdown.

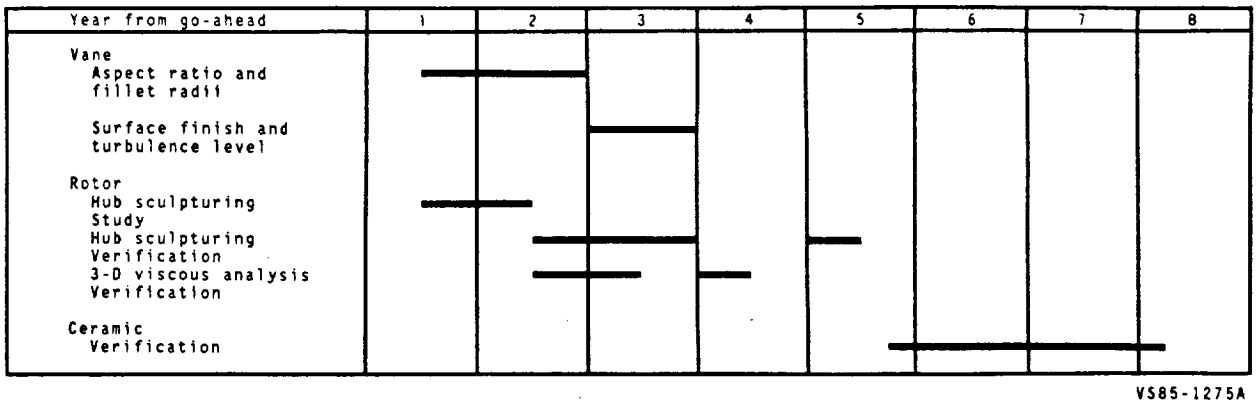

Figure 58. Radial turbine technology plan.

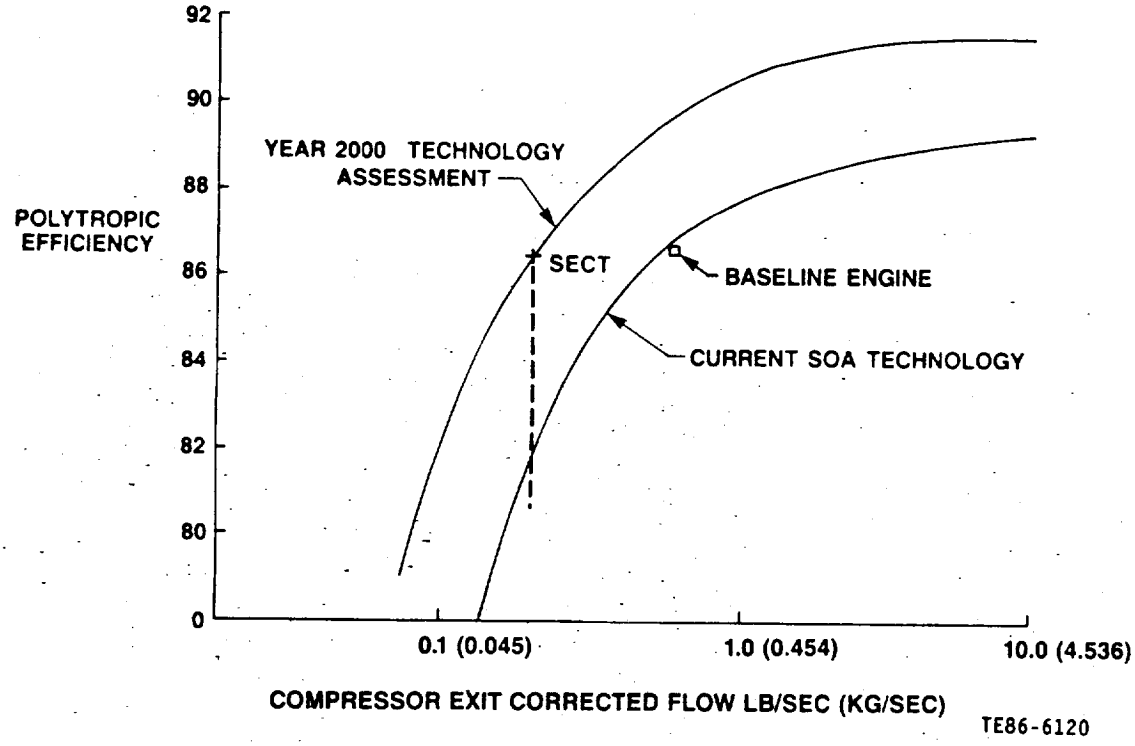

Figure 59. Compressor technology.

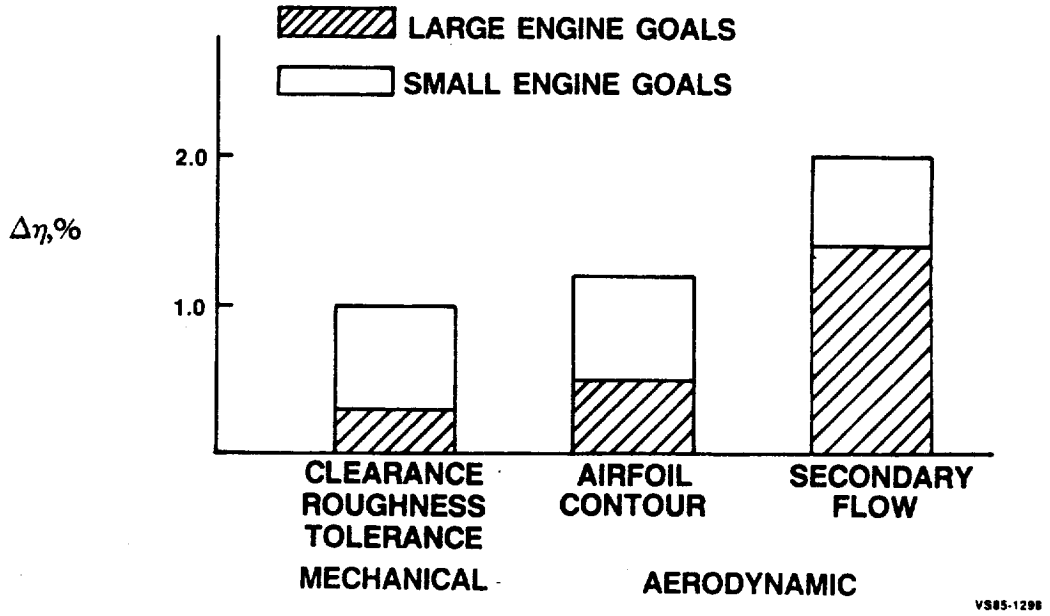

Figure 60. Efficiency improvement in small compressors.

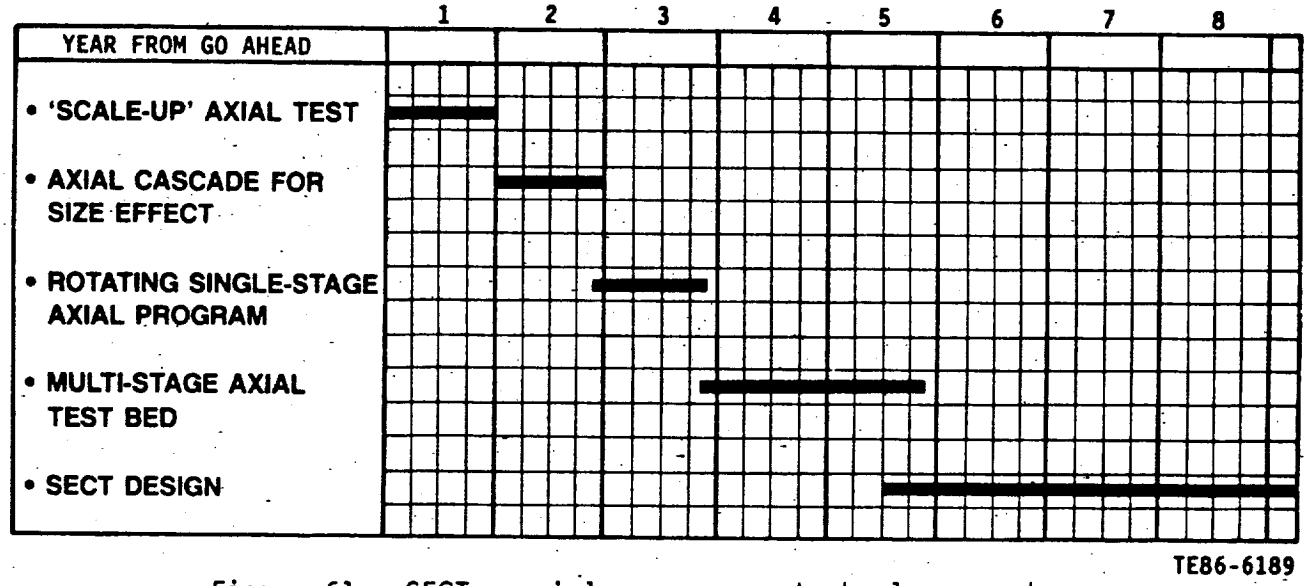

Figure 61. SECT - axial compressor technology roadmap.

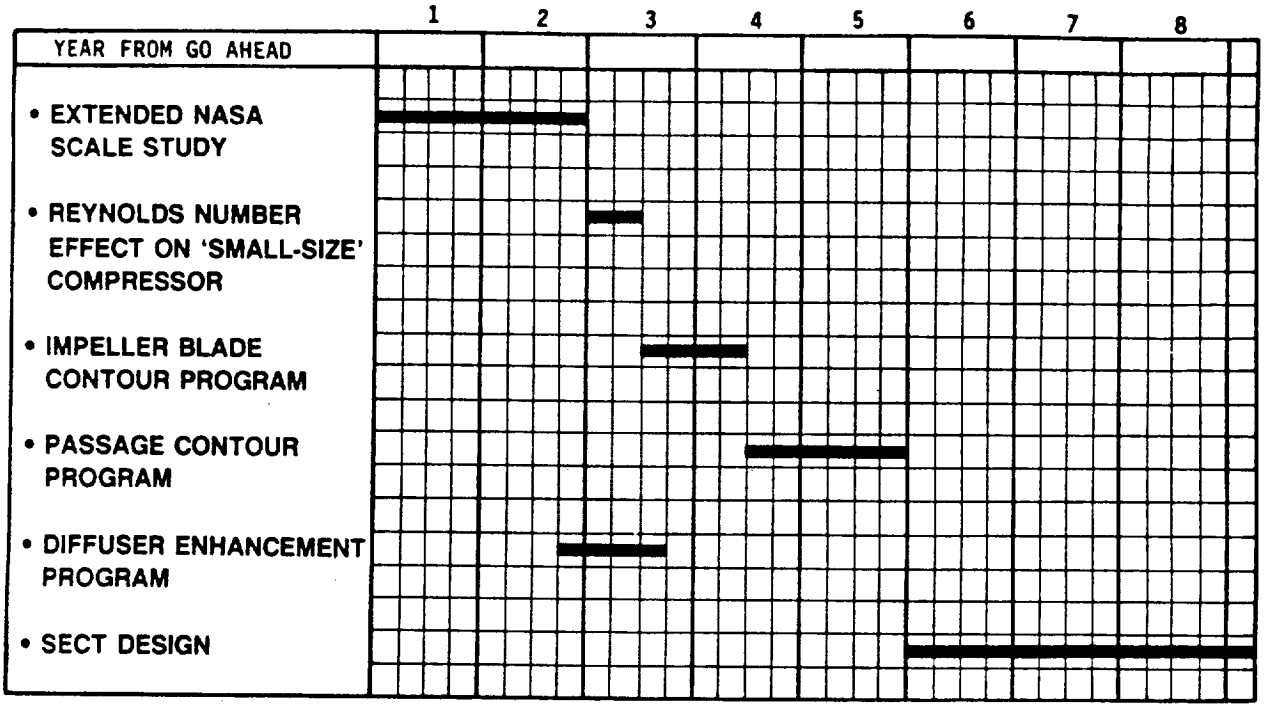

Figure 62. SECT - centrifugal compressor technology roadmap.

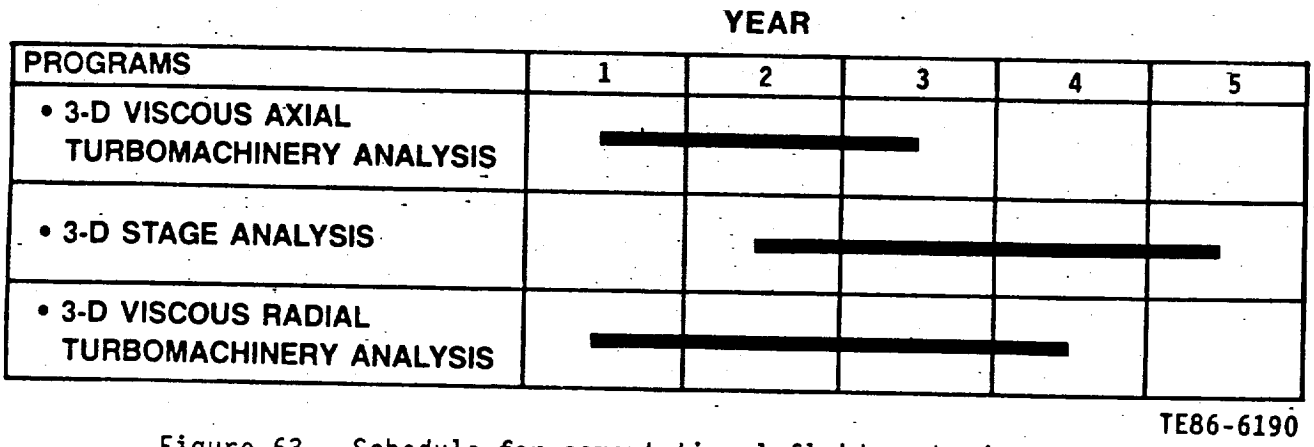

Figure 63. Schedule for computational fluid mechanics programs.

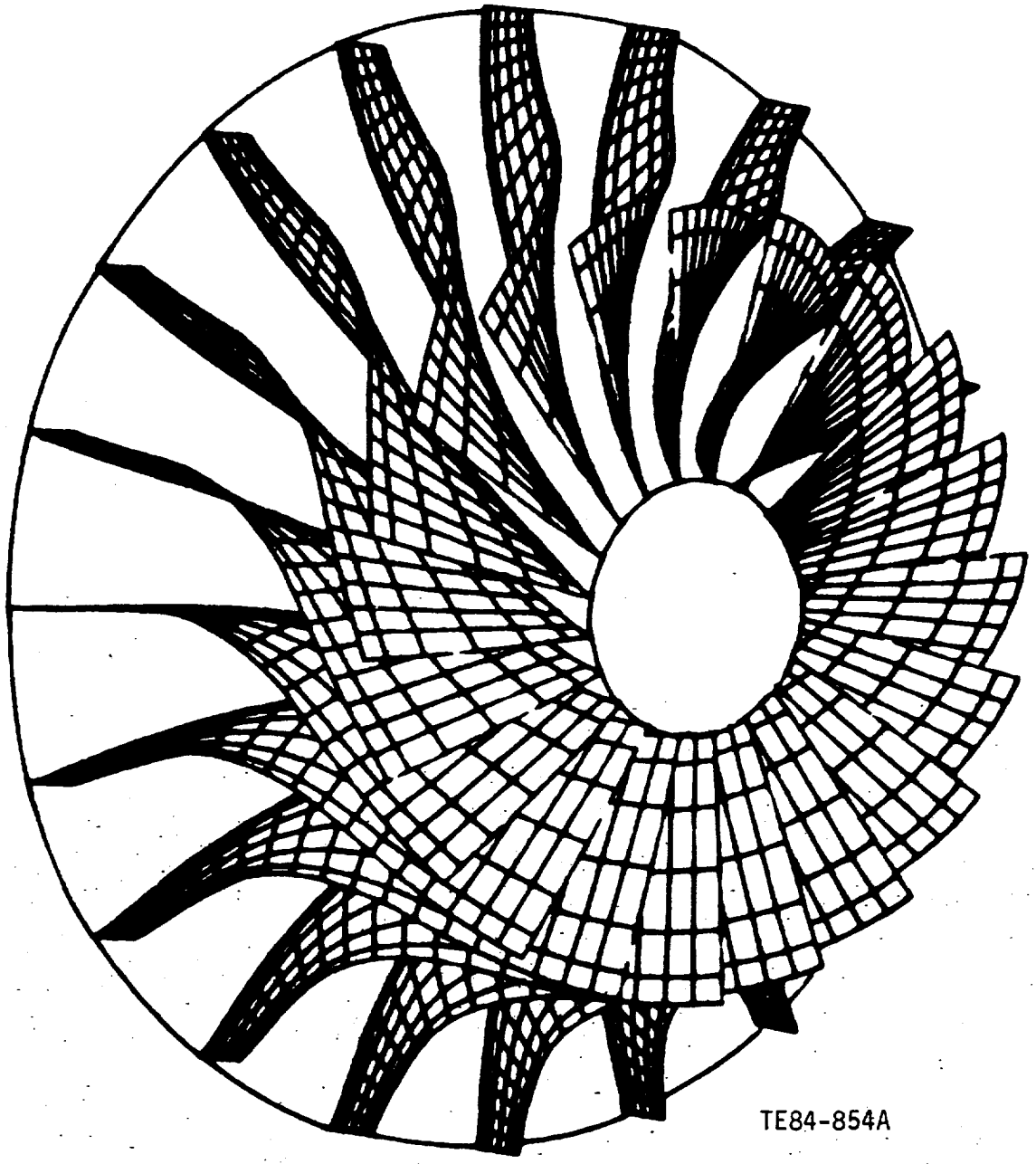

Figure 64. Schematic of Eckardt radial impeller.

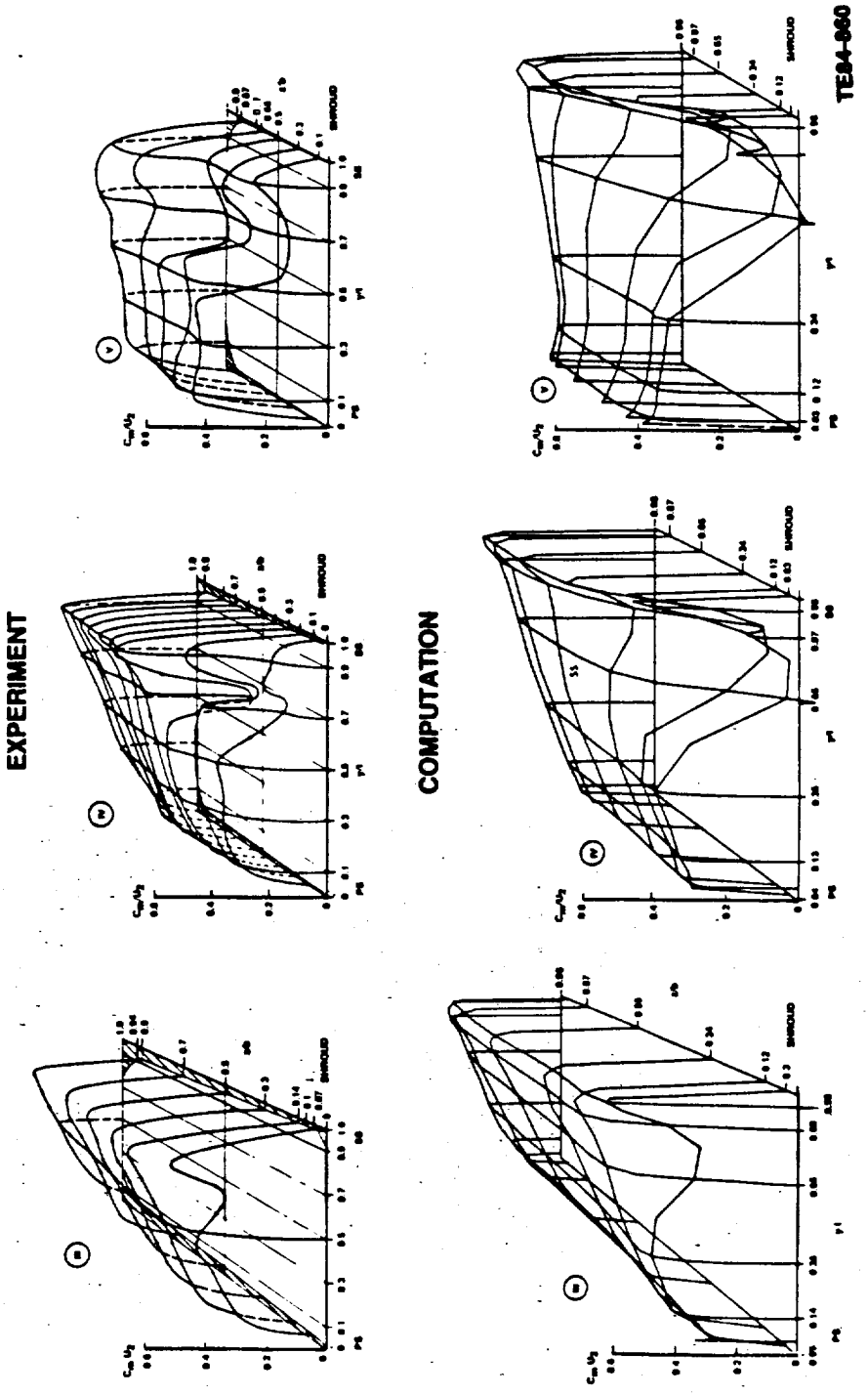

Figure 65. Comparison of calculated and measured primary velocity components at planes III through V for Eckardt.

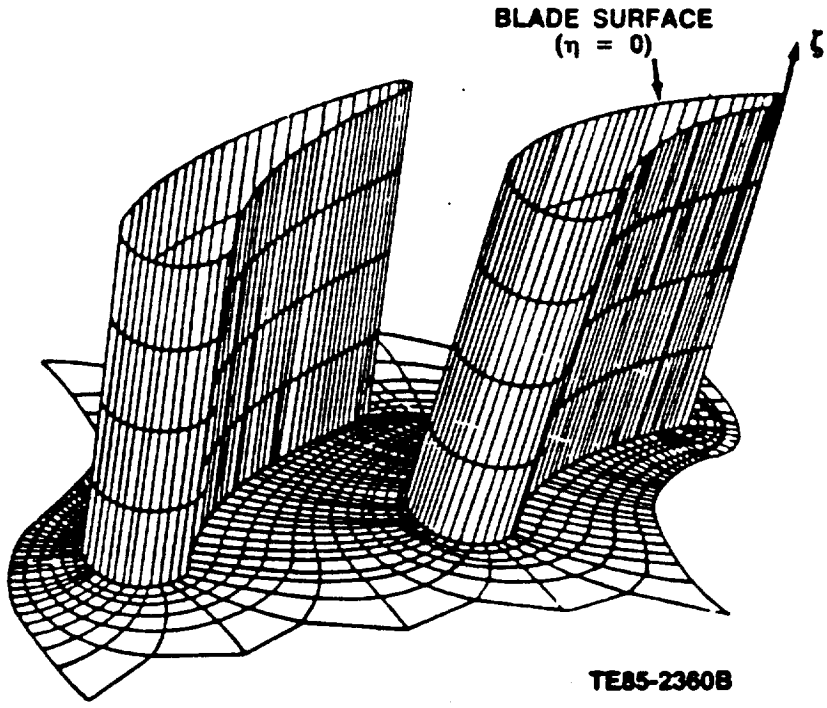

Figure 66. 3-D grid system.

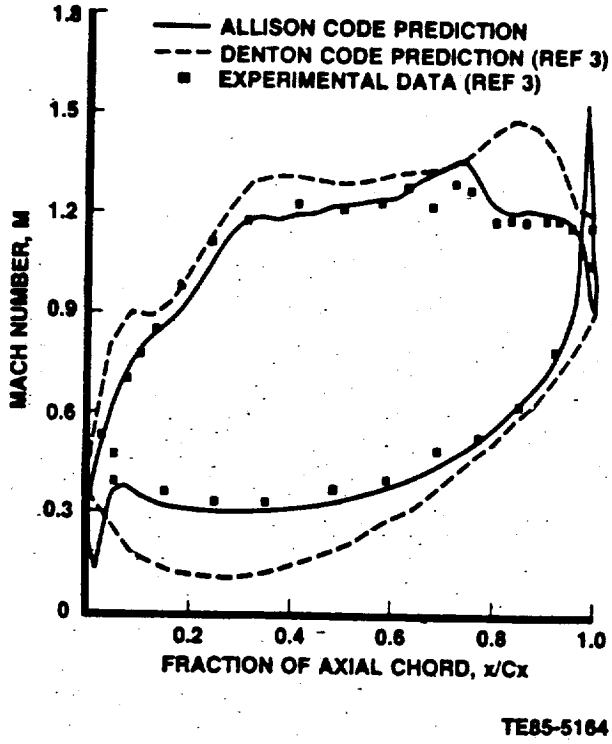

Figure 67. Calculated and experimental blade surface Mach numbers distributions for the flared endwall cascade at 8.28% span, M_2 = 1.2, i = -10 deg.

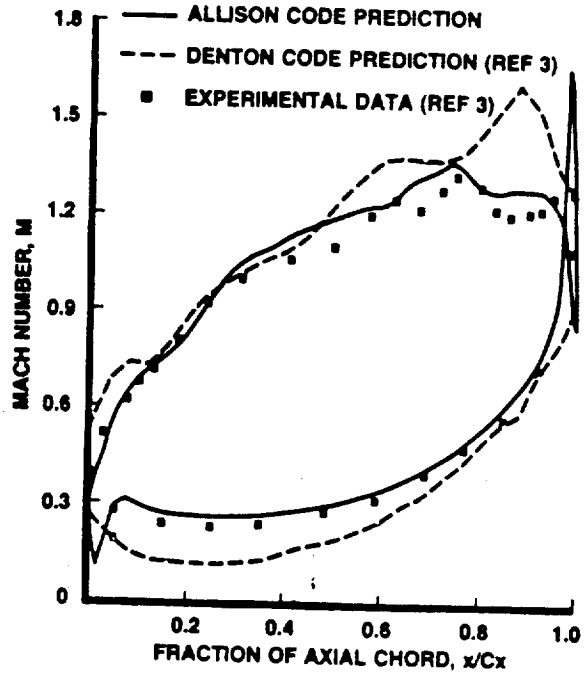

Figure 68. Calculated and experimental blade surface Mach numbers distribution for the flared endwall cascade at 48.9% span, M_2 = 1.2, γ = -10 deg.

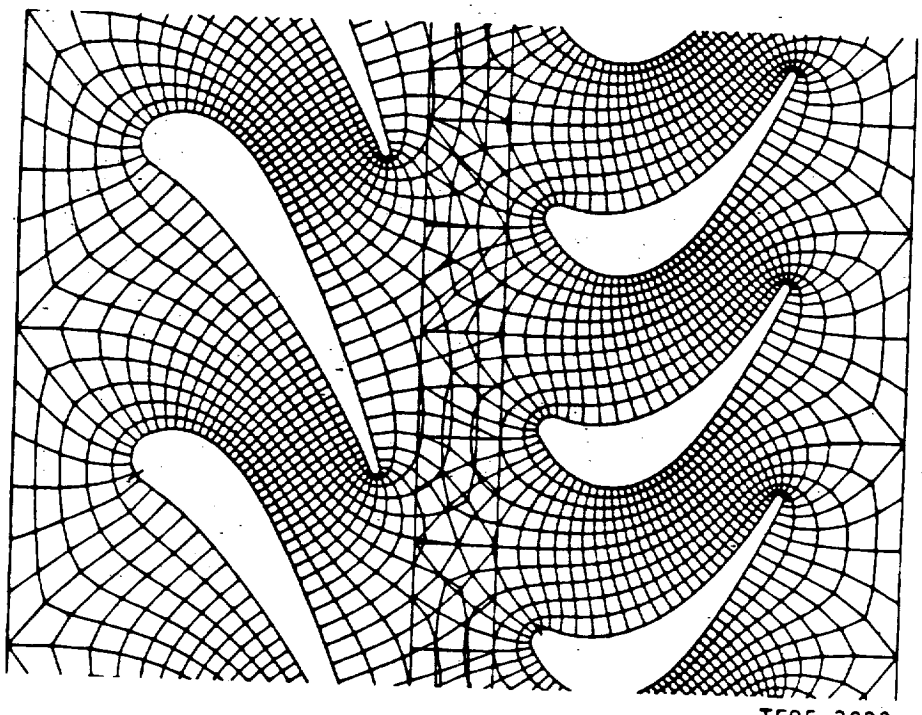

Figure 69. Overlapped grid system.

OBJECTIVES: TECHNOLOGY DEMONSTRATION FOR:

- IMPROVED DURABILITY
- LOW PATTERN FACTOR (0.12)
- LOW-SMOKE, NO CARBON DEPOSITIONS

PROGRAM YEAR	1	2	3	4	5
1. ADVANCED FUEL INJECTORS	■	■			
2. ADVANCED COOLING SCHEMES	■	■			
3. IMPROVED COMBUSTION SYSTEM			■	■	■
TOTAL PROGRAM					

TE86-6191

Figure 70. Small combustor technology plan.

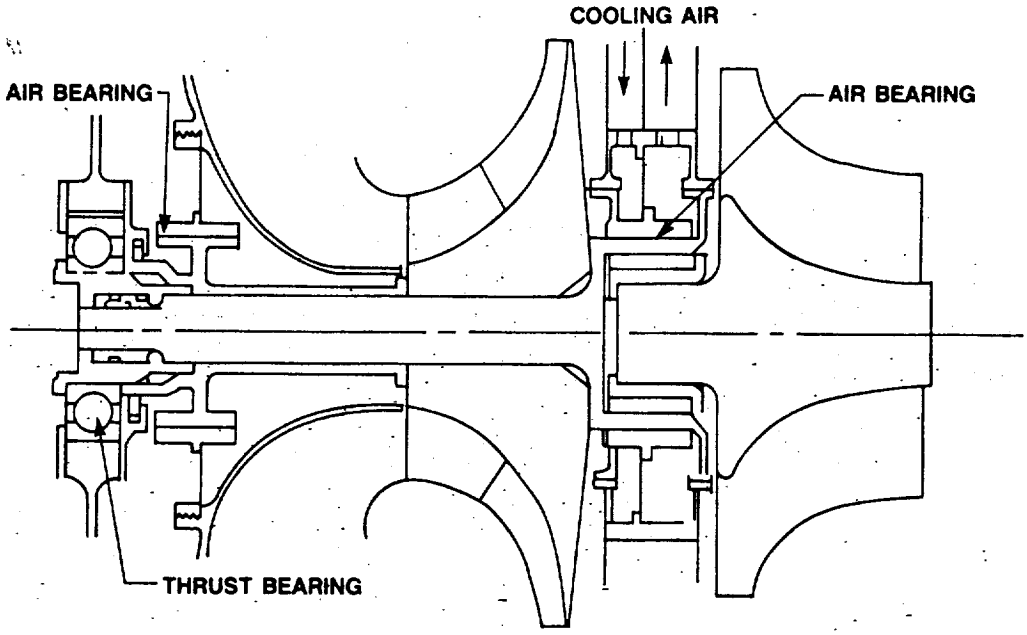

Figure 71. General arrangement of a gas generator using a rolling element bearing for thrust load and air bearings for radial loads.

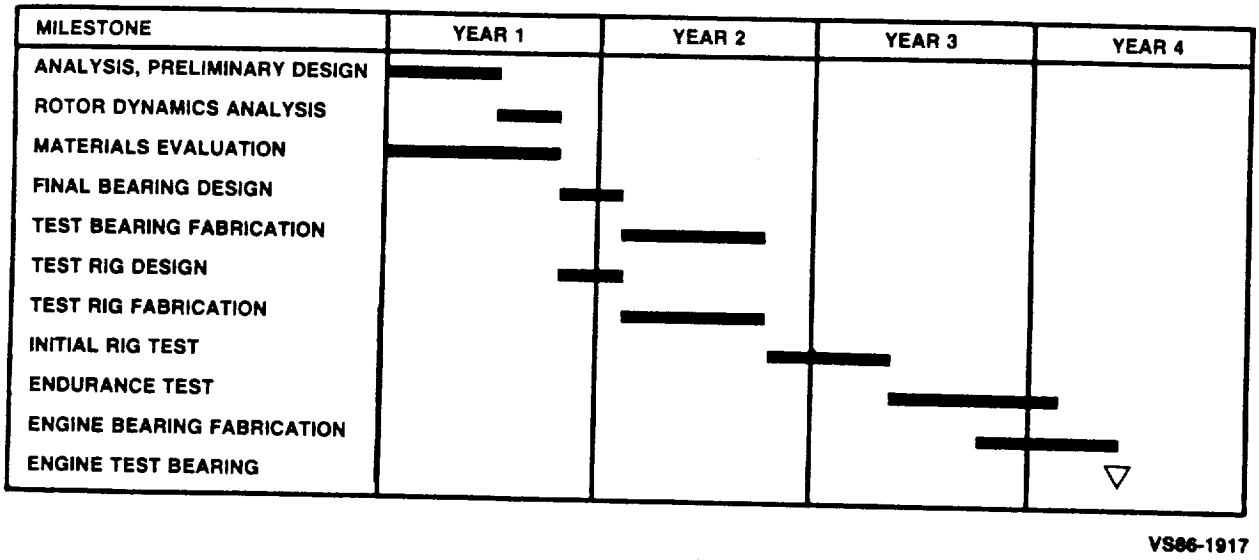

Figure 72. Technology plan for compliant foil bearings.

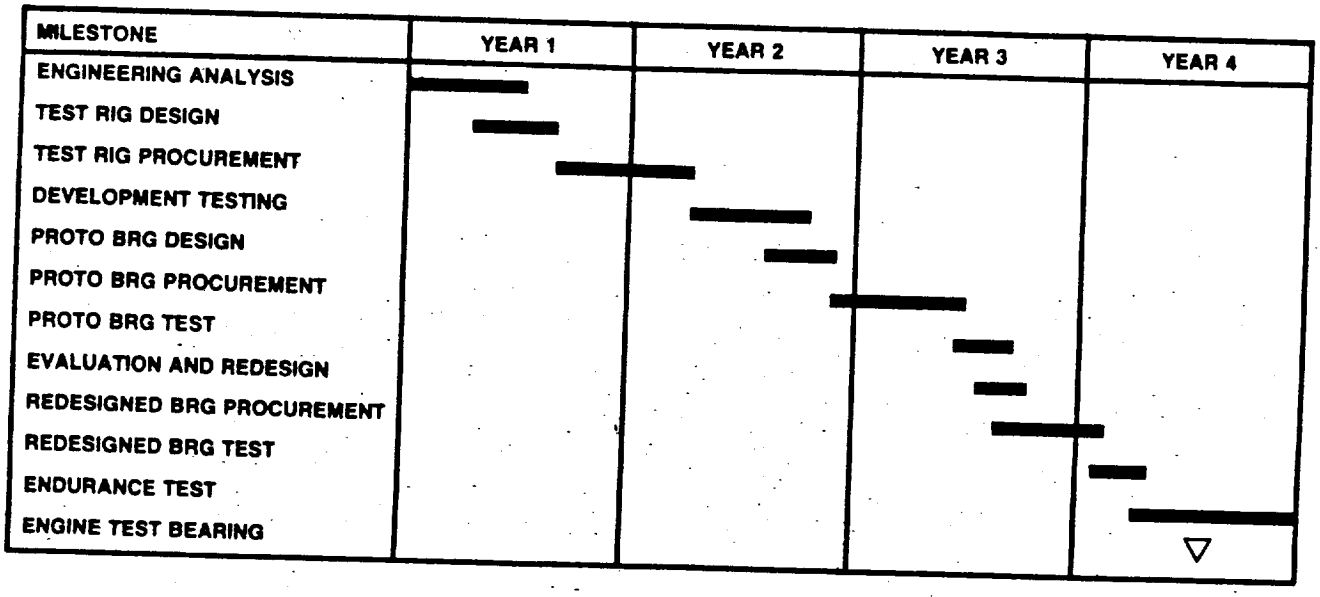

Figure 73. Technology plan for rolling element bearings.

DISTRIBUTION LIST

SECT STUDY REPORTS

NASA Lewis Research Center
21000 Brookpark Road
Cleveland, Ohio 44135

Attn:	Mail Stop
Library (2 copies)	60-3
Report Control Office	60-1
R. W. Graham	5-9
Major D. G. Kulchak	501-3
M. A. Beheim	3-9
N. T. Saunders	3-8
D. J. Poferl	3-8
D. C. Mikkelson	6-12
W. C. Strack	6-12
J. W. Gauntner	6-12
J. Eisenberg	6-12
A. J. Glassman	6-12
G. Knip	6-12
J. E. Haas	6-8
B. A. Miller	5-3
L. A. Povinelli	5-7
J. R. Wood	5-7
J. A. Ziemianski	86-1
R. C. Evans	77-6
P. T. Kerwin	77-6
T. N. Strom	77-6
P. G. Batterton	86-4
T. J. Biesiandy	86-4
G. A. Kraft	86-7
C. L. Ball	77-6
E. A. Willis	77-6
W. T. Wintucky	77-6
M. R. Vanco (5 copies)	77-6
R. W. Niedzwiecki	77-6
R. J. Roelke	77-6
F. A. Newman	77-6
R. J. Rollbuhler	77-6
J. S. Fordyce	3-5
H. R. Gray	49-1
R. L. Dreshfield	49-3
S. R. Levine	49-3
T. T. Serafini	49-3
D. E. Sokolowski	49-7
D. J. Gauntner	23-3
L. J. Kiraly	23-3
R. E. Kielb	23-3

U.S. Army Aviation Research and
Technology Activity
Propulsion Directorate
NASA Lewis Research Center
Cleveland, OH 44135

Attn:	Mail Stop
J. Acurio	77-12
G. J. Weden (5 copies)	77-12
P. L. Meitner	77-12
G. A. Bobula	77-12
G. L. Klann	6-8
W. A. Acosta	77-6
G. J. Skoch	77-6
R. G. DeAnna	77-6

NASA Headquarters
Washington, D.C. 20546
Attn: RJ/Cecil Rosen
RP/Robert Rosen
RP/John Facey
RP/Gordon Banerian

NASA Ames Research Center
Moffett Field, CA 94035
Attn: John Zuk, Mail Stop 237-11
T. L. Galloway, Mail Stop 237-11

NASA Langley Research Center
Hampton, VA 23665
Attn: Robert W. Koenig, Mail Stop 249
J. Stickle, Mail Stop 246A

Commander U.S. Army Aviation
Systems Command
4300 Goodfellow Boulevard
St. Louis, MO 63120-1798
Attn: Mr. C. Crawford
Mr. V. Edwards, DRSAV-EP

Headquarters
U.S. Army Aviation Research and
Technology Activity (AVSCOM)
NASA Ames Research Center
Moffett Field, CA 94035-1099
Attn: Dr. J. R. Carlson
Mr. W. Andre, SAVDL-AS

General Electric
Aircraft Engine Business Group
P.O. Box 6301
Evandale, OH 45215-6301
Attn: L. H. Smith, K-70

General Electric
Aircraft Engine Business Group
1000 Western Avenue
Lynn, MA 01910
Attn: L. H. King
R. Hirschkron

Garrett Turbine Engine Company
111 South 34th Street
P.O. Box 5217
Phoenix, AZ 85010
Attn: J. Howell
J. R. Switzer
M. L. Early

United Technologies Corporation
Pratt & Whitney
Engineering Division
400 Main Street
East Hartford, CT 06108
Attn: T. J. Gillespie, 162-23

United Technologies Corporation
Pratt & Whitney
Engineering Division
P.O. Box 2691
West Palm Beach, FL 33402
Attn: R. E. Davis
J. Alcorta

Sundstrand Turbomach
P.O. Box 85757
4400 Ruffin Road
San Diego, CA 92138-5757
Attn: C. Rodgers

Teledyne CAE
Turbine Engines
1330 Laskey Road
P.O. Box 6971
Toledo, OH 43612
Attn: E. H. Benstein
E. Razinsky
B. Singh

Williams International
2280 West Maple Road
P.O. Box 200
Walled Lake, MI 48088
Attn: R. C. Pampreen
D. A. Gries
R. A. Horn, Jr.

Norton - TRW
Gottard Road
Northboro, MA 01532-1545
Attn: Dr. C. L. Quackenbush

Caterpillar Tractor Company
Defense Products Department, JB7
Peoria, IL 61629
Attn: Mr. G. G. Valbert

Beech Aircraft Corporation
9709 E. Central
Wichita, KS 67201
Attn: Mr. O. Scott
Mr. C. McClure

Cessna Aircraft Corporation
P.O. Box 7704
Wichita, KS 67201
Attn: Mr. E. Kraus

Gulfstream Aerospace
P.O. Box 2206
Savannah, GA 31402
Attn: Mr. R. J. Stewart

Fairchild Aviation Company
International Airport
P.O. Box 32486
San Antonio, TX 78284
Attn: Mr. R. E. McKelvey

Bell Helicopter Textron
P.O. Box 482
Fort Worth, TX 76101
Attn: Mr. D. Karanian

Gates Learjet Corporation
P.O. Box 7707
Wichita, KS 67277
Attn: Mr. R. D. Neal

Aviation Applied Technology Directorate
U.S. Army Aviation Research and
Technology Activity (AVSCOM)
Fort Eustis, VA 23604-5577
Attn: H. Morrow, SAVDL-ATL-ATP
Mr. G. A. Elliott
Mr. E. Johnson
Mr. S. Morgan

U.S. Army Tank Automotive Command
28251 Van Dyke
Warren, MI 48397-5000
Attn: Mr. G. Cheklich
Mr. C. Mason, AMSTA-RGRT
Mr. E. Danielson

Commander Army Research Office
P.O. Box 12211
Research Park Triangle, NC 27709
Attn: Dr. R. Singleton

Naval Air Propulsion Center
P.O. Box 7176
Trenton, NJ 08628-0176
Attn: Mr. W. W. Wagner
Mr. R. Valori, PE 34

Naval Weapons Center
Code 3246
China Lake, CA 93555
Attn: Mr. G. W. Thielman

Naval Air Systems Command
Washington, D.C. 20361
Attn: Commander J. L. Murphy III
Mr. R. A. Grosselfinger, AIR-310 F

David Taylor Naval Ship R&D Center
Bethesda, MD 20084
Attn: Mr. M. Gallager, Code 1240

U.S. Marine Corps
Development and Education Command
LVT(X) Directorate, D16
Quantico, VA 22134
Attn: Carmen DiGiandomenico

Deputy Under Secretary of Defense
Research and Engineering
Research and Advanced Technology
The Pentagon
Washington, D.C. 20301
Attn: Dr. D. Dix, OUSDRE (MST)
Mr. D. Gissendanner

Department of Army, SCSRDA
Room 3E429
The Pentagon
Washington, D.C. 20301
Attn: Mr. D. R. Artis
Mr. R. Ballard

Defense Advanced Research Project
Agency
1400 Wilson Blvd.
Arlington, VA 22209
Attn: S. Sigman, Jr.
R. Williams

Wright Patterson Air Force Base
Dayton, OH 45433
Attn: Mr. Erik W. Linder, AFWAL/POTA
Mr. T. Gingrich
Lt. J. Gagliardi
Mr. E. A. Lake
Mr. W. Troha, AFWAL/POTC

U.S. Department of Energy
Office of Transportation Systems
1000 Independence Avenue, S.W.
Washington, D.C. 20585
Attn: Richard T. Alpaugh, MS 5G-046

Naval Ship Systems Engineering Station
Philadelphia, PA 19112
Attn: Mr. L. Haryslak, Code 033D
Mr. T. Bodman

U.S. Army Material Command
5001 Eisenhower Avenue
Alexandria, VA 22333
Attn: Mr. R. A. Mercure, AMCDE-SA

Allison Gas Turbine Division
General Motors Corporation
P.O. Box 420
Indianapolis, IN 46206-0420
Attn: P. C. Tramm, T21A
H. C. Mongia, T14
T. R. Larkin, T20

AVCO Lycoming
550 South Main Street
Stratford, CT 06497
Attn: H. Moellmann
L. Beatty
H. Kaehler

Boeing Vertol Company
Boeing Center
P.O. Box 16858
Philadelphia, PA 19142
Attn: D. R. Woodley

McDonald Douglas Helicopter Co.
Centinela Avenue and Teale Street
Building T 465
Culver City, CA 90230
Attn: D. Borgman

Piper Aircraft Corp.
P. O. Box 1328
Vero Beach, FL 32960
Attn: Max Bleck

Sikorsky Aircraft Division
United Technologies Corporation
N. Main Street
Stratford, CT 06602
Attn: H. Shohet

Boeing Military Airplane Co.
Research & Engineering
Wichita, KS 67210
Attn: Mr. Bert Welliver

Boeing Aerospace Company
Kent Space Center
P. O. Box 3999
Seattle, WA 98124-2499
Attn: Mr. L. Harding

Brunswick Corporation
Defense Division
3333 Harbor Blvd.
Costa Mesa, CA 92626
Attn: Mr. Richard L. Benton

General Dynamics Corporation
Convair Division
P. O. Box 85357
San Diego, CA 92138
Attn: Mr. Mark F. Dorian

Hughes Aircraft Co.
Missile Development
8433 Falbrook Avenue
Canoga Park, CA 91304
Attn: Mr. Larry Wong

Lockheed Missiles & Space Co.
Austin Division
2100 East St. Elmo Road
Austin, TX 78744
Attn: Mr. Michael Levin

Lockheed Georgia Co.
86 S. Cobb Drive
D72-16, Z399
Marietta, GA 30063
Attn: Mr. Rick Mattels

Martin Marietta Aerospace
P. O. Box 5837
Orlando, FL 32855
Attn: Mr. Victor Schilling, MP 275

McDonnel Douglas Astronautics Co.
Box 516
Bldg. 106, Level 2, Room 287
St. Louis, MO 63166
Attn: Mr. Thomas F. Schweickert

Northrop Corporation
Ventura Division
1515 Rancho Conejo Blvd.
P. O. Box 2500
Newbury Park, CA 91320
Attn: Mr. Marion Bottorff

Northrop Corporation
Hawthorne Division
One Northrop Avenue
Dept. 3810, Zone 82
Hawthorne, CA 90250
Attn: Mr. David McNally

Rockwell International Corp.
Missile Systems Division
Department 362
4405-A International Blvd.
Norcross, GA 30093
Attn: Mr. F. L. Goebel

Teledyne Ryan Aeronautical
2701 Harbor Drive
Box 80311
San Diego, CA 92138-9012
Attn: Mr. Vernon A. Corea

Hamilton Standard
Mail Stop 1-2-11
Windsor Locks, CT 06096
Attn: Mr. Fred Perkins

4. STIMS 1X ACC# 8810364 IPS-FILE ADABAS # = 19842

FICHE AVAIL	= OK	HARD COPY AVL	= OK	COPYRIGHT	= N
ORIG AGENCY	= NASA	RECEIPT TYPE	= REG	ACQUIS TYPE	= REG
DOCUMENT CLASS	= TRP	ACCESS LEVEL	= 0	ACCESS RESTR	= UNRES
LIMITATION CAT	= NONE	DOCUMENT SEC	= NC	TITLE SECURITY	= NC
SUBJECT CATGRY	= 07	SPECIAL HANDL	=	PAGE COUNT	= 00156
INC AUTHOR LST	= N	INC CNTRCT LST	= N	LANGUAGE	= EN
COUNTRY ORIGIN	= US	COUNTRY FINANC	= US	ABSTRACT PREP	= AUT
PUB DATE	= 19860300	CORP SOURCE	= G0073666		

TITLE = Small Engine Component Technology (SECT) study
TITLE SUPP = Final Report
AUTHOR = LARKIN, T. R.
CONTRACT NUM = NAS3-24542
CONTRACT NUM = DA PROJ. 1L1-61101-AH-45
SUPP RESEARCH = 535-05-01
REPORT NUM = NASA-CR-175081
REPORT NUM = NAS 1.26:175081
REPORT NUM = AVSCOM-TR-86-C-8
REPORT NUM = EDR-12422
MAJOR TERMS = GAS TURBINE ENGINES
MAJOR TERMS = RESEARCH MANAGEMENT
MAJOR TERMS = ROTARY WING AIRCRAFT
MAJOR TERMS = TECHNOLOGY ASSESSMENT
MINOR TERMS = FUEL CONSUMPTION
MINOR TERMS = LIFE (DURABILITY)
MINOR TERMS = PROPULSION SYSTEM CONFIGURATIONS
MINOR TERMS = RELIABILITY
ABST AUTHOR = Author
FORM OF INPUT = HC

ABSTRACT = The objective of this study is to identify high payoff technologies for year 2000 small gas turbine engines, and to provide a technology plan to guide research and technology efforts toward revolutionizing the small gas turbine technology base. The goal is to define the required technology to provide a 30 percent reduction in mission fuel burned, to reduce direct operating costs by at least 10 percent, and to provide increased reliability and durability of the gas turbine propulsion system. The baseline established to evaluate the year 2000 technology base was an 8-passenger commercial tilt-rotor aircraft powered by a current technology gas turbine engine. Three basic engine cycles were studied: the simple cycle engine, a waste heat recovery cycle, and a wave rotor engine cycle. For the simple cycle engine, two general arrangements were considered: the traditional concentric spool arrangement and a nonconcentric spool arrangement. Both a regenerative and a recuperative cycle were studied for the waste heat recovery cycle.

********** END OF ADABAS RECORD # 19842 **********